SPECTROSCOPIC AND MECHANISTIC STUDIES ON MANGANESE PEROXIDASE AND LIGNIN PEROXIDASE FROM THE LIGNIN-DEGRADING BASIDIOMYCETE *Phanerochaete chrysosporium*

Hiroyuki Wariishi
B.S., Tokyo Noko University, 1983
M.S., Tokyo Noko University, 1985

A dissertation submitted to the faculty of

Oregon Graduate Institute
of
Science and Technology

in partial fulfillment of the
requirements for the degree
Doctor of Philosophy
in
Biochemistry

February 1990

The dissertation "Spectroscopic and Mechanistic Studies on Manganese Peroxidase and Lignin Peroxidase from the Lignin Degrading Basidiomycete Phanerochaete chrysosporium" by Hiroyuki Wariishi has been examined and approved by the following Examination Committee:

Michael H. Gold, Thesis Advisor
Professor

Ninian J. Blackburn
Associate Professor

V. Renganathan
Assistant Professor

H. Brian Dunford
Professor at the Univ. of Alberta

ACKNOWLEDGEMENTS

I would like to take this opportunity to express my deep sense of gratitude and appreciation to Prof. M. H. Gold for his guidance, encouragement and patience during the whole course of the work. I am extremely grateful to Prof. H. B. Dunford (U. of Alberta) for his guidance to achieve the work described in Chapters 3, 6, and 9. I am grateful to Dr. K. Valli for his friendship and help rendered during the work described in Chapters 4 and 5. I am also grateful to Dr. L. Akileswaran and Dr. V. Renganathan for the help to complete the work described in Chapters 2 and 5.

I wish to thank Ms. M. Mayfield for her technical help during the initial stage of the work. I am grateful to Mr. L. Isabell for his technical assistance to operate GCMS.

I wish to thank Dr. L. Marquez and Dr. I. D. MacDonald (U. of A.) for their contribution to the work described in Chapters 3, 6, and 9. I also thank all the members in Prof. Dunford's lab. for providing a congenial and warm atmosphere in such a cold Edmonton.

I am thankful to Ms. N. Christie for her secretarial help to type this thesis and to Ms. M. Alic for her careful proof reading.

I sincerely thank all the colleagues in Prof. Gold's lab. for providing a helpful and congenial atmosphere where this work was achieved. I am extremely thankful to the faculty members in the department of Chemical and Biological Sciences for their helpful suggestions.

The financial assistance from Oregon Graduate Institute of Science and Technology is gratefully acknowledged.

DEDICATION

To my parents.

TABLE OF CONTENTS

LIST OF FIGURES

LIST OF TABLES

ABSTRACT

SPECTROSCOPIC AND MECHANISTIC STUDIES ON MANGANESE PEROXIDASE AND LIGNIN PEROXIDASE FROM THE LIGNIN DEGRADING BASIDIOMYCETE *Phanerochaete chrysosporium*

Hiroyuki Wariishi, Ph.D.
Oregon Graduate Institute of Science and Technology, 1990

Supervising Professor: Michael H. Gold

Reaction mechanisms of two extracellular lignin degrading heme enzymes, manganese peroxidase (MnP) and lignin peroxidase (LiP), were investigated.

Spectral characterization of MnP demonstrated its peroxidative catalytic cycle and the interrelationship between its five redox states. Mn^{II} acts as an obligatory reducing substrate for MnP compound II, apparently explaining the absolute Mn-dependence of this enzyme. Transient state kinetics revealed that organic acids, such as malonate, chelate Mn^{III}, thus facilitating the dissociation of Mn^{III} from the enzyme-manganese complex. The terminal organic substrates are oxidized by a freely diffusible Mn^{III}-complex. Phenolic lignin model compounds were oxidatively cleaved by either an enzymatically or chemically generated Mn^{III}-complex; furthermore, nonphenolic lignin model dimers were oxidized by the MnP system in the presence of radical mediators such as thiols, indicating that MnP is involved in lignin degradation.

The reduction of LiP compound I (LiPI) by veratryl alcohol (VAlc) was studied utilizing transient state kinetics. LiPI is reduced to native LiP via two steps with the transient formation of LiP compound II (LiPII). The pH dependence of the reduction of LiPI and LiPII dictates the overall unusually low pH optimum of the enzyme.

Two types of LiP compound III (LiPIII and LiPIII*) were spectroscopically and kinetically distinguished and characterized. LiPIII is similar to compounds III of other peroxidases. The addition of H_2O_2 to LiPIII resulted in the reversible formation of LiPIII*. Thus, LiPIII* appears to be a noncovalent complex of LiPIII and H_2O_2. LiPIII* also reacted with H_2O_2, resulting in the irreversible inactivation of the enzyme. The role of VAlc, a secondary metabolite of P. chrysosporium, was also examined. VAlc protects the enzyme against LiPIII formation by reducing LiPII, and against inactivation by reacting with LiPIII*. The latter reaction causes displacement of superoxide, thereby, converting LiPIII* to the native enzyme.

CHAPTER 1

INTRODUCTION

1.1 STRUCTURE AND DISTRIBUTION OF LIGNIN

In 1838, Anselm Payen demonstrated that treating wood with concentrated nitric acid resulted in a loss of mass. The solid fibrous residue which remained was designated as cellulose (1). The dissolved material which was referred to as "la matiere incrustante" (the incrusting material) had a higher carbon content than the fibrous residue. In 1865, Schulze used the term lignin which was derived from the Latin word for wood (lignum) (2).

Later, the development of technical pulping processes generated much interest in lignin and its reactions. In 1897, Peter Klason studied the composition of lignosulfates and suggested that lignin was chemically related to coniferyl alcohol (3).

1.1.1 Structure of Lignin

By 1940, methods based on classical organic chemistry led to the conclusion that lignin is probably composed of phenylpropane units (4-6). However, the concept of a phenylpropanoid structure failed to win

unanimous acceptance, and as late as the 1950's, some were not convinced that lignin in its native state was an aromatic substance. Finally, in 1954, Lange applied UV microscopy at various wavelengths directly on thin wood sections, demonstrating the aromatic nature of lignin (7).

The mechanism of polymer formation from phenylpropane units based on the dehydrogenation and the radical coupling theory was proposed by Freudenberg in 1952 (8). However, the initial step in understanding the structure of lignin came in the early 1930's when Erdtman found that the dehydrogenation product of isoeugenol (1-(4-hydroxy-3-methoxyphenyl)-1-propene) had the structure of phenylcoumaran (Fig. 1-1, D) (9). In 1937, Freudenberg found that the dehydrogenation of coniferyl alcohol (1-(4-hydroxy-3-methoxyphenyl)-3-hydroxy-1-propene) with ferric chloride produced products similar to those reported for isoeugenol. In 1943, he began his study on the enzymatic dehydrogenation of coniferyl alcohol (10), a process still used today to produce the synthetic lignin polymer (dehydrogenation polymer, DHP).

A detailed understanding of the structure of lignin was not possible until a pure and relatively undegraded lignin preparation could be obtained from wood. The first isolated lignin sample was called Klason lignin (11). In 1954, Bjorkman prepared milled wood lignin (MWL) (12), which is the best preparation known today and it has been widely used for structural studies.

More than two thirds of the phenylpropane units in lignin are linked by ether bonds and the rest by carbon-to-carbon bonds. Fig.

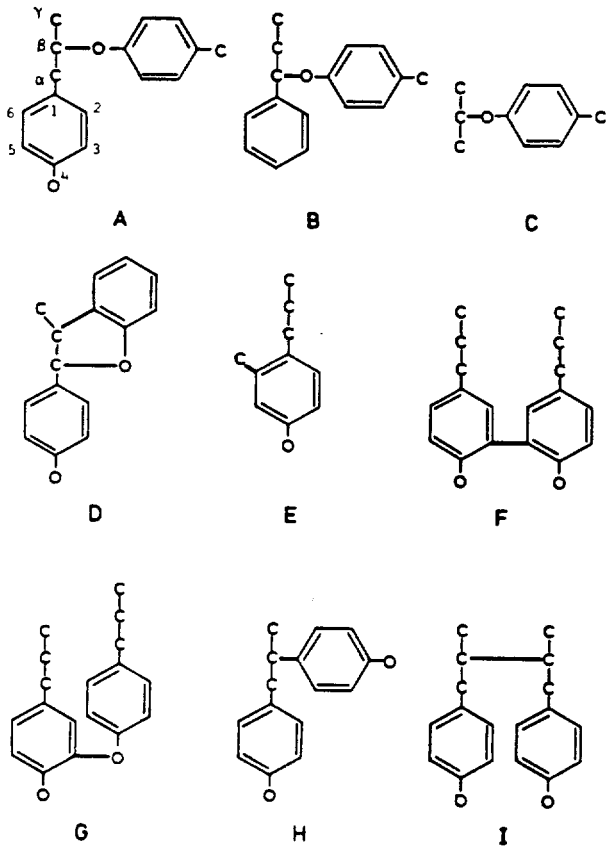

Fig. 1-1. The common linkages between phenylpropane units.

1-1 shows the principal bonds in lignin. Their proportion is presented in Table 1-1. The major functional groups of lignin consist of phenolic hydroxyl, benzylic hydroxyl, and carbonyl groups, which all have an influence upon the reactivity. Their frequency varies according to the origin of the lignins. Some typical values are shown in Table 1-2.

Freudenberg and Adler have constructed structural schemes for spruce lignin (16,17) and Nimz for beech lignin (15), in which the main units and linkage types are represented in their approximate proportions. The scheme of Adler is depicted in Fig. 1-2. However, one scheme cannot explain the entire structure of lignin. The schematic drawing shows that lignin is a complex heterogeneous and random phenylpropanoid polymer.

1.1.2 Classification and Distribution of Lignin

Lignin is found in all vascular plants and in certain primitive plant groups such as ferns and club mosses, but not in Bryophyta (true mosses) and algae (18).

The quantitative and structural analyses of isolated lignin led to studies on the heterogeneity of lignin. Lignins can be divided into several classes depending on their structural elements. Lignin normally contains three substituted cinnamyl alcohols, p-coumaryl, coniferyl, and sinapyl alcohols, (1-(4-hydroxyphenyl)-, 1-(4-hydroxy-3-methoxyphenyl)-, and 1-(3,5-dimethoxy-4-hydroxyphenyl)-3-hydroxy-1-propene). These substituted nuclei have been traditionally called

Table 1-1. Percentages of different types of bonds in lignin (MWL)

Bond Type[a]	Spruce[b]	Birch[b]			Beech[c]
		Guaiacyl	Syringyl	Total	
A Arylglycerol-β-aryl ether	48	24	36	60	} 60
B Nonphenolic benzyl aryl ether	7			7	
C Glycerolaldehyde-2-aryl ether	2			2	——
D Phenylcoumarane	10	6		6	6
E 2-, or 6-Condensed	3	1.5	1	2.5	——
F Biphenyl	10	4.5		4.5	2.3
G Diphenyl ether	4	1	5.5	6.5	1.5
H Diarylpropane	7			7	15
I β,β-Linked	2			4	5

[a] Letters **A** through **I** are defined in Fig. 1-1.

[b] Data from Ref. 13.

[c] Data from Ref. 15.

Table 1-2. Functional groups of lignin per 100 C_6C_3 units[a]

Functional Group	Spruce lignin	Birch lignin
Methoxyl	92-96	139-158
Phenolic hydroxyl (free)	15-30	9-13
Benzyl alcohol	15-20	
Noncyclic benzyl ether	7-9	
Carbonyl	20	

a Data from Ref. 13 & 14. The content may vary depending on the origin of the lignin (e.g., middle lamella or secondary wall lignin).

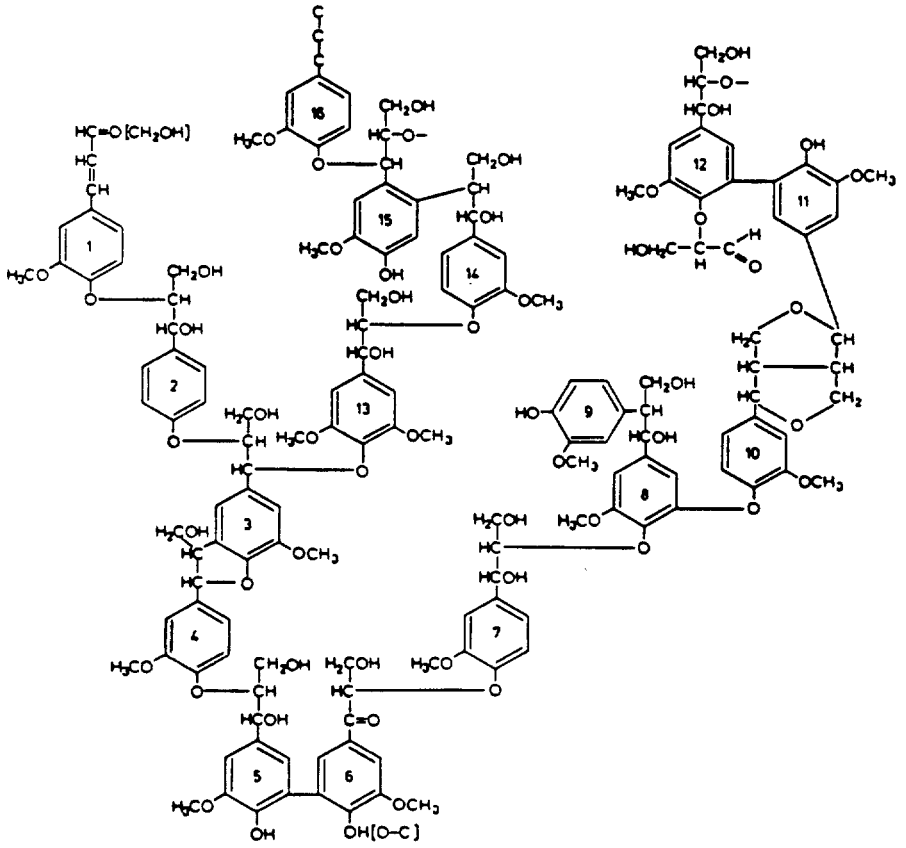

Fig. 1-2. Prominent structures of softwood lignin comprising 16 phenyl-propane units (13).

coumaryl, guaiacyl, and syringyl nuclei, respectively. These alcohols are the immediate precursors of lignin. The proportions are dependent on the plant analyzed.

So-called guaiacyl lignin which occurs in almost all conifers is composed principally of coniferyl alcohol. The ratio of coniferyl to coumaryl to sinapyl alcohols in spruce lignin has been estimated to be 80:14:6 (19). Guaiacyl-syringyl lignin, found in dicotyledonous angiosperms and a few gymnosperms, contains large amounts of coniferyl and sinapyl alcohols with only a small amount of p-coumaryl alcohol. For example, beech lignin has been found to contain a ratio of 49:46:5 of these alcohols (20). The ratio of coniferyl to sinapyl alcohol varies from 4:1 to 1:1 among angiosperm lignins (21). An additional example is compression wood, which has a high proportion of phenyl-propane units of the p-coumaryl type in addition to the normal guaiacyl units. The terms syringyl lignin and coumaryl lignin are sometimes used to denote the respective structural elements even though it is unlikely that any probably natural lignin is exclusively composed of these units.

The amount of lignin in wood can be determined gravimetrically by the Klason method. Normally conifer wood contains 26-32% lignin while the lignin content of compression wood is 35-40% (22-25). During acid hydrolysis the lignin present in angiosperms is partly dissolved and hence the gravimetric values must be corrected for acid-soluble lignin using UV spectrophotometry. Normal angiosperm wood contains 20-28% lignin (22-25).

In summary, lignin is a phenylpropanoid polymer synthesized from coniferyl, p-coumaryl, and sinapyl alcohol precursors. Free radical condensation of these alcohols, initiated by plant cell wall peroxidases (26), results in the formation of a heterogenous, amorphous, optically inactive, random and highly branched polymer containing at least 12 different interunit linkages. The most important role of lignin appears to be its contribution to the rigidity of the cell wall. Because of its resistance to degradation, lignin may also protect plants against pathogenic organisms (27). In addition, lignin minimizes water permeation across the cell walls of xylem tissue (28).

1.2 BIODEGRADATION OF LIGNIN

Lignin is the second most abundant natural polymer in the biosphere and the most abundant renewable aromatic material (14,18). Since the biodegradation of cellulose is retarded by the presence of this polymer (18,29-31), the catabolism and potential utilization of lignin are of enormous significance.

Progress in the understanding of lignin biodegradation was slow during the early stage of the research because the structure of lignin was not understood until the 1960's. Furthermore, an effective and simple assay to estimate lignin biodegradation either qualitatively or quantitatively was not developed until the 1970's. However, the first review describing lignin biodegradation was published in 1936 and

contains much valuable information showing that lignin is the most resistant polymer in plant cell walls. This review also showed that it is attacked by some microorganisms especially by basidiomycetous fungi (32). During the 1960's and 1970's biodegradation assays based on lignin model compounds and ^{14}C-lignins (^{14}C-labeled DHP or MWL) were developed (18). Model compounds are used as a substitute for the polymer in degradation studies to obtain a better understanding of the individual steps involved in lignin degradation. Radioisotopic assay techniques have been applied successfully to a wide range of lignin-related research problems, such as determination of the range of microbial taxa that are able to decompose lignin.

1.2.1 Lignin Degrading Microorganisms

Wood rotting organisms have been classified into three categories, white-rot fungi, brown-rot fungi, and soft-rot fungi, according to the color, the composition, and the histological characteristics of decayed woods. The components of wood vary depending on the species, but the major structural constituents are cellulose (50-60%), hemicellulose (5-15%), and lignin (20-35%) (33).

White-rot fungi are capable of extensively decomposing all the major structural components of wood (34). The name "white-rot" comes from the observation that wood being decayed by these organisms turns white as lignin is removed. More than a thousand species of white-rot fungi have been found and almost all belong to Basidiomycotina (35). There are also a few ascomycetes causing a white-rot type of wood

decay (35). Among the ligninolytic microorganisms, white-rot basidiomycetes are the most efficient of all known lignin degraders.

Brown-rot fungi are usually defined as wood rotting fungi that decompose and remove carbohydrate (cellulose and hemicellulose) but leave a residue of modified lignin. This lignin is typically dark brown and is almost equal in weight to the lignin in sound wood (36). Brown-rot fungi are taxonomically very similar to white-rot fungi, being mostly basidiomycetes. Analysis by numerous investigators has shown that brown-rotted lignin has a decreased methoxyl content (37,38). Brown-rot fungi also introduce other chemical modifications into the lignin polymer. More carboxyl and conjugated carbonyl groups are formed in the decayed lignin, causing the dark brown color. In addition, phenolic hydroxyl groups are introduced (38).

Soft-rot fungi attack moist wood, producing a characteristic softening of surfaces of the woody tissues (36,39,40). Most of these organisms are ascomycetes and deuteromycetes. Studies using ^{14}C-DHPs show that soft-rot fungi are able to convert all structural elements of DHPs to $^{14}CO_2$ (41). Although it seems likely that soft-rot fungi have an important role as lignin degraders in nature, laboratory culture of these organisms is still at an early stage, and essentially nothing is known about the enzymes they use to decompose lignin.

Several soil fungi belonging to Deuteromycotina that are not readily classifiable into specified decay groups are also thought to degrade lignin. Fusarium species, for example, are capable of decomposing a variety of lignin model compounds (42). However, other research using Aspergillus and other soil fungi failed to produce any

$^{14}CO_2$ from ^{14}C-DHPs over a period of two months (43). Generally it has been accepted that soil fungi can degrade lignin model dimers but not polymeric lignin. The role of soil fungi in lignin biodegradation is still unclear. They may attack fragments of degraded lignin produced by white-rot fungi.

1.2.2 Lignin Biodegradation by White-Rot Basidiomycetes

White-rot basidiomycetes are primarily responsible for the initiation of the decomposition of lignin in wood (18,29-31). Thus, much effort has been devoted towards understanding lignin biodegradation in white-rot basidiomycetes.

Compared to cellulose, lignin has relatively less oxygen and more delocalized π-electrons which can stabilize it during degradation. For this reason lignin biodegradation is thought to be an energy-requiring process. It has been suggested that the organisms obtain no net energy from lignin degradation; they merely gain access to a new source of carbohydrate. The typical white-rot fungi, Phanerochaete chrysosporium and Coriolus versicolor, do not to degrade ^{14}C-DHP to $^{14}CO_2$ in the absence of a readily utilizable growth substrate such as cellulose or glucose (44).

Initially, much work was done to understand the chemistry of the wood decayed by these fungi. Elemental and functional group analyses of white-rotted lignins provide evidence that the degradation of lignin by the white-rot fungi is an oxidative process. White-rotted lignin contains less carbon and hydrogen, and more oxygen than sound

lignin. It also shows a decrease in methoxyl groups and an increase in carbonyl and carboxyl groups (45,46). Structural analysis of lignin fragments released from decayed wood has been undertaken, and vanillin, vanillic acid, syringaldehyde, syringic acid, dimethoxybenzoquinone, methoxybenzoquinone, methoxyhydroquinone, and coniferyl alcohol were found as major fragments (47-49). The product analysis suggested that lignin degradation may occur through C-C bond cleavage at C_α-C_β linkages in propyl side chains and at alkyl-phenyl (C_α-C_1) linkages as well as through C-O bond cleavage at β-ether linkages in aryl ether structures (linkages are shown in Fig. 1-1). Recently, studies using GC-MS and ^{13}C FT-NMR indicate that aromatic ring oxidation and cleavage take place within the polymer (50). Moreover, the molecular mass of white-rotted lignin has been reported to be similar to that of sound lignin (45). Thus, white-rotted lignin is still polymeric, suggesting that the biodegradation of lignin may occur outside of the cell.

P. chrysosporium has become the model for the most current studies of lignin biodegradation. This fungus was chosen because (a) it efficiently degrades both lignin and cellulose, (b) it is thermotolerant (an optimal temperature of 38°C), (c) it produces asexual (conidia) spores prolifically — an advantage for genetic manipulation, and (d) it has been shown to form sexual fruiting structures in culture (51,52). By determining $^{14}CO_2$ released from ^{14}C-DHPs under various physiological conditions, it has been established that the ligninolytic activity in P. chrysosporium is not inducible by exogenously added lignin, but rather by the limitation of

nutrient carbon, sulfur, or nitrogen, which triggers the onset of secondary metabolism (44,53). The transition between primary and secondary metabolism has been studied. The addition of ammonium or glutamate to nitrogen starved cultures raises the concentration of intracellular glutamate (54), sharply decreases that of cAMP (55), restores primary growth (54), and stops lignin degradation (54), clearly showing that ligninolytic activity appears as a secondary metabolic process.

Under secondary metabolic conditions, P. chrysosporium synthesizes the secondary metabolite veratryl alcohol (3,4-dimethoxybenzyl alcohol, VAlc) (56). The entire pathway of VAlc biosynthesis, from phenylalanine, has been postulated (57).

Detailed studies on the catabolism of lignin by white-rot fungi present considerable obstacles since lignin is such a complex and heterogenous polymer. Therefore, simple substrates have been utilized to investigate the pathways and the reaction mechanisms involved in this process. As shown in Table 1-1, ~50% of the interphenylpropanoid linkages are arylglycerol-β-aryl ether bonds, so a variety of studies have been undertaken to examine the degradation of β-aryl ether dimers. Diarylpropane containing a β-1 type linkage also has been used in these studies. Although this structure represents a relatively minor linkage between phenylpropanoid units, this type of linkage is thought to be on the surface of the lignin bulk polymer. For example, the dimeric compounds 1-(4-ethoxy-3-methoxyphenyl)-2-(2'-methoxyphenoxy)-1,3-dihydroxypropane (58) and 1-(3,4-diethoxyphenyl)-

2-(4'-methoxyphenyl)-1,3-dihydroxypropane (59) are excellent model compounds (skeletons are shown in Fig. 1-1, **A** and **H**). They resemble structures present in lignin, and are degraded only under conditions in which lignin is also degraded (58,59). Analysis of degradation products using MS spectrometry indicated for the first time that β-ether cleavage and C_α-C_β cleavage occur (58,59). The benzaldehydes produced by these reactions via C_α-C_β cleavage are rapidly reduced by the fungus to the corresponding benzyl alcohols. Elevating the oxygen concentration increases the rate of degradation of lignin model compounds (60), which is in agreement with the results for polymer degradation (61,62).

By 1982, it had been established that the biodegradation of lignin was oxidative, extracellular, non-specific with regard to substrate, and a secondary metabolic activity. It had also been concluded through the degradative experiments using polymeric lignin (47-50) and dimeric model compounds (58,59,63-67) that the important mechanisms of lignin degradation are C_α-C_β cleavage and β-ether cleavage for non-phenolic compounds and alkyl-phenyl cleavage for phenolic compounds and that side chain cleavage and ring opening reactions may occur simultaneously in lignin polymer.

1.2.3 Lignin Degradation by Activated Oxygen Species

Lignin and lignin model compounds were shown to be degraded by the white-rot fungi, yet no corresponding enzyme had been identified. At this time, Hall suggested that an activated oxygen species may be the depolymerizing reagent (68), since 100% oxygen atmosphere

enhances lignin degradation. Immediately, the possible involvement of hydroxyl radical (·OH) (69-71) and singlet oxygen ($^1O_2$) (72) was suggested. Subsequent investigations have discounted involvement of $^1O_2$ (70,73,74). The degradation products formed by ·OH from various lignin model dimers were very similar to those formed by the fungus (but some were not identical), and ·OH scavengers inhibited the reaction systems in both ·OH and in vivo cultures (70). However, no direct evidence for the involvement of ·OH in lignin biodegradation has been provided; EPR experiments failed to detect ·OH in ligninolytic cultures of P. chrysosporium (75).

H_2O_2 was detected in ligninolytic fungal cultures and the addition of exogenous catalase inhibits lignin degradation (69,70,76). H_2O_2 itself is not a strong enough oxidant to cause C-C or C-O bond cleavage, but one-electron reduction or oxidation of H_2O_2 generates ·OH and superoxide ($O_2^{-}\cdot$), respectively. These radicals are strong oxidants and are well known to be involved in a variety of biological reactions. H_2O_2 is also known to act as a cosubstrate for peroxidases. Study of the role of H_2O_2 on lignin biodegradation in white-rot fungi led to the finding of ligninolytic peroxidases a year later.

1.3 ENZYMES INVOLVED IN LIGNIN BIODEGRADATION

The relationship between ligninolytic activity and Bavendamm's reaction has been known for 60 years. Bavendamm showed that most

white-rot fungi, which are capable of degrading lignin, produce a colored zone around mycelium on agar plates containing tannin and that the colorization is caused by phenol oxidases secreted by the fungi (77). Kirk (78) and Sundman (79) have reconfirmed that the ligninolytic activity of wood-rotting fungi and the positive Bavendamm's test are almost parallel with only a few exceptions. It seemed to be reasonable, therefore, to consider that phenol oxidases are related to lignin degradation. The correlation between phenol oxidase and ligninolytic activity is supported by genetic studies. Phenol oxidase negative mutants of P. chrysosporium, which are in fact regulatory mutants, lost the ability to degrade lignin (80,81). These mutants were also unable to degrade lignin model compounds and did not produce VAlc (81).

Traditionally, three distinct types of enzymes have been considered as phenol oxidases (36). Tyrosinase uses oxygen to oxidize monophenols, yielding o-diphenols or o-quinones. They can also oxidize catechols to o-quinones. This enzyme, however, has a relatively narrow substrate specificity and is found intracellularly, so that tyrosinase has not been considered to be a key enzyme in nonspecific oxidation of lignin. Laccase catalyzes the oxidation of a large variety of phenolic compounds by abstraction of an electron and a hydrogen ion from the phenolic hydroxyl group to form phenoxy radicals. The free radicals produced by the enzyme undergo disproportionation or polymerization via radical coupling. Laccase uses oxygen as an electron acceptor which is ultimately reduced to water.

Peroxidases perform the same reaction as laccase, but use hydrogen peroxide rather than oxygen as the cosubstrate.

Since laccase is abundant in extracellular fluid of many white-rot fungi and since it is relatively easy to isolate, numerous attempts have been made to degrade lignin and model compounds using purified laccase.

1.3.1 Laccase

Most white-rot basidiomycetes produce extracellular laccases (EC 1.10.3.2). Laccase apparently has a role in sexual fruiting (82) and in lignin degradation. Work with various phenolic lignin model dimers and purified laccase shows that certain degradative reactions occur, particularly with syringyl models (83-87). Condensation reactions were predominant with guaiacyl type models. When the isolated lignin (MWL) was treated with laccase, polymerization through radical coupling was observed as a major consequence of one-electron oxidation. A small amount of depolymerization also occurred (88,89). Only a trace amount of 2,6-dimethoxy-1,4-benzoquinone was identified from depolymerized fragments (88). Thus, it is now thought that some modification of lignin may be caused by laccase (35); however, the primary effect is further polymerization (88-91). Other roles for laccase have been suggested. It may act to detoxify low-molecular-mass phenols released during lignin degradation (90), and it may produce a specific chemical transformation required for further degradation by other enzymes (92). Furthermore, laccase has been

shown not to oxidize nonphenolic lignin related compounds (83,85,86). Normally, lignin contains only 15-20% free phenolic hydroxyl groups in its phenylpropanoid units (Table 1-2), so lignin might be a poor substrate for laccase.

Finally, a few of the best lignin degrading fungi lack the ability to produce laccase. For example, P. chrysosporium belongs to the minority of white-rot fungi that produce no detectable laccase. However, apparently all white-rot fungi secrete enzymes capable of oxidizing phenols. Simple color tests are used to determine whether these are the laccase type or the peroxidase type (93).

1.3.2 Peroxidases Involved in Lignin Degradation

It was well known that P. chrysosporium had phenol oxidase activity, but no one had found an extracellular laccase from this fungus. Studies on activated oxygen species from this fungus led to the discovery of extracellular hydrogen peroxide in the culture medium (69,70,76). H_2O_2 can be detected in the medium just before P. chrysosporium begins to degrade lignin and the rate of H_2O_2 production is nearly parallel with ligninolytic activity (76). These findings generated speculation on the involvement of H_2O_2 requiring enzyme(s) or of peroxidase(s) in ligninolytic fungal culture medium.

In 1983, Gold's and Kirk's groups simultaneously announced the discovery in P. chrysosporium of an extracellular H_2O_2-requiring enzyme involved in lignin degradation (94-97). This enzyme is currently referred to as lignin peroxidase (LiP) or ligninase.

Subsequently, a second enzyme involved in lignin degradation, which is now referred to as manganese peroxidase (MnP), was isolated in Gold's laboratory (98). Both enzymes exist as a series of isozymes. The major isozymes of LiP and MnP have been isolated and purified to homogeneity from the extracellular culture medium of P. chrysosporium and have been characterized as heme enzymes (98-105).

LiP catalyzes the oxidation of nonphenolic lignin model compounds which are also oxidized by the fungus (29-31,58-60,63-67,106). P. chrysosporium had been shown to decolorize polymeric dyes under ligninolytic conditions (107). Subsequent studies indicated that MnP catalyzes the decolorization of dyes and it also oxidizes a variety of phenolic monomers (98,104,105,108). More detailed LiP and MnP reaction mechanisms will be reviewed in the following sections (1.5.1 and 1.5.2). The discovery of these enzymes, the major catalysts in the lignin degradation system, initiated the reexamination of the physiology of lignin degradation in various white-rot basidiomycetes, including P. chrysosporium.

LiP activity has been found only under secondary metabolic conditions and recently has been detected in other white-rot fungi, including Phlebia radiata (109), Panus tigrinus (110), C. versicolor (111,112), Pleurotus ostreatus, and Bjerkandera adusta (30). LiP has not been detected in Fomes lignsus, Tramates cingulata (30), and Lentinus edodes (113). However, L. edodus shows MnP activity under ligninolytic conditions (113). De novo synthesis of VAlc has recently been found in C. versicolor (114) and P. radiata (30). The relation

between LiP and VAlc is not well understood but it seems likely that LiP-producing fungi also are capable of biosynthesizing VAlc.

Although ligninolytic activity was once reported not to be inducible, the addition of VAlc to cultures of P. chrysosporium raises the ligninolytic activity and the level of LiP (102,115-117). Recent studies have confirmed that exogenously added excess lignin also increases the extent of lignin degradation and the level of LiP production (116,118). This is probably due to saturation of the lignin degradation system of P. chrysosporium with lignin; the more lignin is added to the culture, the more is degraded (116,118). The association of VAlc with lignin degradation and secondary metabolism deserves further study.

1.3.3 H_2O_2-generating Enzymes

The discovery of extracellular H_2O_2 in ligninolytic cultures of P. chrysosporium and the H_2O_2 requirement for LiP and MnP activities demanded a clarification of the origin of H_2O_2. Earlier, several intracellular enzymes were reported to be able to generate H_2O_2. These are fatty acyl-coenzyme A oxidase (120), glucose-1-oxidase (121), and glucose-2-oxidase (122). However, the fungus has a strong intracellular catalase activity under secondary metabolic conditions (123,124). Extracellular MnP has been demonstrated to produce H_2O_2 in the presence of NAD(P)H, glutathione, dithiothreitol, or dihydroxyfumaric acid (DHF) as an electron donor (104,105,108,125). Surprisingly, Kuwahara reported that intact ligninolytic cultures of P.

chrysosporium can produce extracellular NAD(H) and NADP(H) (126). The mechanism of H_2O_2 production from O_2 and NADH by MnP is thought to be the same as that by horseradish peroxidase (HRP) (127,128). The HRP reaction system has been reported to generate one mole of H_2O_2 at the expense of one mole of NADH, suggesting a very energy-consuming reaction. It is not known how the fungus generates the reduced coenzymes extracellularly.

A new extracellular enzyme, glyoxal oxidase, has been demonstrated in ligninolytic cultures of P. chrysosporium (129). The enzyme oxidizes glyoxal, methyl glyoxal, and several other α-hydroxy carbonyl and dicarbonyl compounds coupled to the reduction of O_2 to H_2O_2. Both glyoxal and methyl glyoxal were identified in the extracellular culture medium under ligninolytic conditions (129).

Another H_2O_2-producing enzyme, veratryl alcohol oxidase, was recently identified in the extracellular culture medium of the white-rot basidiomycete Pleurotus sajor-caju (130). The enzyme oxidizes various nonphenolic aromatic alcohols to the corresponding aldehydes via a two-electron oxidation with concomitant reduction of O_2 to H_2O_2. The physiological function of this enzyme is still unclear. Further study is required to understand the role of the enzyme in lignin biodegradation. The distribution of the enzyme among the white-rot fungi is also unknown, but similar enzyme activity has been reported with the basidiomycete Polystictus versicolor (131) and with the deuteromycete Fusarium sp. (132).

White-rot basidiomycetes could be classified into several groups, according to their extracellular ligninolytic enzymes (Table 1-3). Of course this classification requires further physiological and genetic studies. The fungi classified into groups 1 and 2 have been said to be strong lignin degraders. Two extracellular peroxidases, LiP and MnP, along with an H_2O_2-generating system appear to be the major components in the P. chrysosporium lignin degradative system.

1.4 HEME PEROXIDASES

Heme proteins are found in all organisms from the prokaryotes to humans. They are involved in photosynthesis, respiratory and microsomal electron transfer, and the utilization and metabolism of oxygen and peroxides. While a large number of heme proteins participate in these processes, they naturally fall into three functionally distinct groups; electron carriers (cytochromes), reversible oxygen binders (globins), and heme enzymes. Each group has unique functions, but they all share at least one common and important structural feature. They contain an iron porphyrin prosthetic group.

Heme enzymes can be categorized into three types: peroxidases, oxygenases, and oxidases. Peroxidases catalyze the heterolytic cleavage of the RO-OH bond (R = H or alkyl group) and store both oxidizing equivalents of the peroxide molecule within the enzyme active center for utilization in the oxidation of a variety of organic

Table 1-3. Classification of white-rot basidiomycetes

Group	Extracellular Secretion				Fungus	Ref.
	LiP	MnP	Laccase	VAlc		
1	+	+	-	+	*P. chrysosporium*	29-31
2	+	+	+	+	*C. versicolor*	111,114 133,134
					P. radiata	30,109
3	-	+	+(?)	-(?)	*L. edodus*	113

and inorganic compounds. Oxygenases cleave the O–O bond of molecular oxygen and then insert either one or both O_2-derived oxygen atoms into aliphatic or aromatic compounds. Those that insert one oxygen atom are called monoxygenases and those that insert two, dioxygenases. Oxidases carry out the 4-electron reduction of O_2 to H_2O and serve as the terminal oxidase in respiratory electron transport.

Early in the biochemical research on lignin peroxidase (LiP) and manganese peroxidase (MnP), both enzymes were shown to contain a single ferric protoporphyrin IX prosthetic group (Fig. 1-3) per enzyme molecule and to require H_2O_2 for their catalytic activities (98-101,104,105). Much early effort was devoted to clarifying whether these enzymes were peroxidases or oxygenases. Subsequent spectroscopic studies have shown that the enzymes are distinct from P_{450} oxygenase, share some properties with globins, and are true peroxidases (see sections 1.5.1 & 1.5.2). Finally, the research on lignin degradation merged with the field of heme peroxidase biochemistry. Biochemical studies on LiP and MnP have been performed to understand (i) the reaction mechanisms of the enzymes with lignin and lignin model compounds based on product analysis, (ii) the catalytic mechanisms of the enzymes based on spectroscopic and kinetic techniques, and (iii) the regulation of the enzymes in the fungus based on physiological and genetic approaches.

1.4.1 General Properties of Peroxidases

Peroxidases catalyze the oxidation of a variety of organic and inorganic compounds by hydrogen peroxide or organic hydroperoxides.

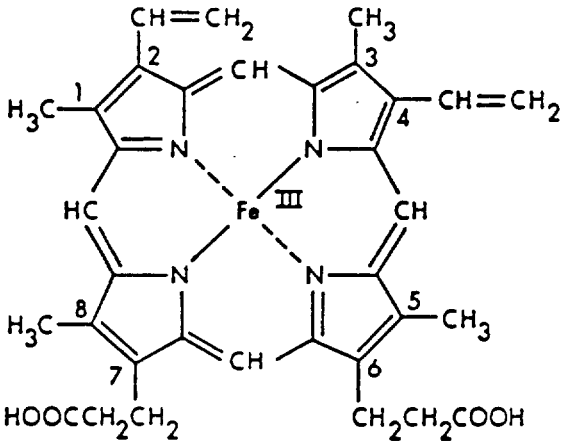

Fig. 1-3. Ferric protoporphyrin IX (ferric heme).

Peroxidases have been among the most extensively investigated enzymes since the beginnings of enzymology (135,136).

The peroxidases are ubiquitous in the plant and animal kingdoms. Horseradish roots are one of the richest sources and its peroxidase has been designated as horseradish peroxidase (HRP) (EC 1.11.1.7). HRP is the most intensively studied peroxidase. Other well studied plant peroxidases are turnip peroxidase (TuP) and Japanese radish peroxidase (JRP) (137). All the peroxidases purified so far from plants contain a ferric protoporphyrin IX prosthetic group (Table 1-4).

Peroxidases from animal sources, however, show a wider variation in the nature of their prosthetic groups. They normally contain prosthetic groups different from protoporphyrin IX (Table 1-4). Glutathione peroxidase is unique among known peroxidases in that it contains one atom of selenium per sub-unit and is apparently a non-heme enzyme (147).

In addition to the higher plant and animal sources, peroxidases are also found in fungi, algae, bacteria, and microorganisms. These peroxidases, chloroperoxidase (CPO) isolated from a fungus, bromoperoxidase (BPO) from marine algae, and cytochrome c peroxidase (CCP) from aerobically grown yeast, contain ferriprotoporphyrin IX as a prosthetic group (Table 1-4).

Diverse physiological functions have been reported for the peroxidases. Myeloperoxidase (MPO) of leucocytes is involved in the phagocytic process (148). Thyroid peroxidase (ThP) might be involved

Table 1-4. Some properties of peroxidases

Enzyme	M.W.	Prosthetic group	Origin	Ref.
Plant peroxidase				
HRP	40,500	Ferriprotoporphyrin IX	Root of horseradish	137
TuP	~43,000	Ferriprotoporphyrin IX	Root of Turnip	137
JRP	~55,500	Ferriprotoporphyrin IX	Root of Japanese radish	137
Animal peroxidase				
LPO	76,500	Derivative of mesoheme IX	Bovine Milk	138
MPO	149,000	Two atoms of porphyrin bound iron	Mammalian leukocyte	139,140
ThP	62,000	Not ferriprotoporphyrin IX	Hog thyroid	141
Others				
CPO	40,200	Ferriprotoporphyrin IX	Caldariomyces fumago (Mold)	142,143
BPO	55,000x2	Ferriprotoporphyrin IX	Penicillus capitatus (Marine algae)	144
CCP	34,100	Ferriprotoporphyrin IX	Yeast	145,146

in the biosynthesis of the hormones thyroxine and triiodothyronine (149-151). The early stage of prostaglandin biosynthesis has recently been shown to be catalyzed by prostaglandin H synthase (152). Spectral features of this synthase have been attributed to the heme-enzyme complex (153,154). Studies on the biosynthesis of the halogen-containing compound caldariomycin in C. fumago led to the isolation of CPO (138,142,143). CPO and BPO have unique abilities to effectively oxidize inorganic chloride and bromide ions, respectively (142-144). CCP has an extremely high specific activity towards ferrocytochrome c (145,146). Compared with these peroxidases, much less information has been accumulated on the physiological roles of plant peroxidases. They have been suggested to be involved in lignification (26,128,129). The function of HRP in the horseradish is not totally clear, but in vitro the enzyme oxidizes a wide range of organic substrates, with a particularly high activity toward phenols and araomatic amines (137,155,156). A plausible hypothesis concerning all peroxidases is that they were first used by primordial organisms in their defense mechanism against oxidation by toxic oxygen compounds and that later, once survival from oxidation was firmly established, more specialized functions evolved (148).

LiP and MnP contain ferriprotoporphyrin IX prosthetic groups (98-105), sharing this structural feature with the plant peroxidases. Among the plant peroxidases, HRP is the most extensively studied enzyme, so it is the best peroxidase model for the spectroscopic characterization of LiP and MnP.

1.4.2 Native Ferric Peroxidase

Native HRP contains a ferriprotoporphyrin IX prosthetic group (Fig. 1-3). The oxidation state of iron in the heme has been confirmed to be Fe^{III} by Mössbauer, electron paramagnetic resonance (EPR) and resonance Raman spectroscopic studies (137,157). The four pyrrole nitrogen atoms provide ligands in coordination positions 1 through 4 for the ferric ion. Coordination position 5 (the back side of the heme plane shown in Fig. 1-3) is known to be occupied by an imidazole group of a histidine residue (158), which is referred to as the proximal histidine. Coordination position 6 (the facing side of the plane) is normally vacant in the peroxidases (159) and this side of the heme plane is referred to as the distal side. In contrast, the 6th position of metmyoglobin is occupied by water (159).

The number of unpaired electrons present in a transition metal ion is a function of its oxidation state, coordination number, and field strength of its ligands (137,155,160). For the native HRP, which is a penta-coordinate species, there could be two opposing influences on the ligand field strength. The absence of a sixth ligand would decrease the d-orbital splitting; however, coordination of the fifth ligand could be strong, pulling the iron out of the porphyrin plane to form a distorted square pyramidal complex. The experimental observation was that the Fe^{III} of the native HRP at room temperature has a mixed spin state of high spin, S=5/2, with intermediate spin, S=3/2 (161,162). Resonance Raman spectroscopic studies recently suggested a temperature-sensitive coordination

equilibria. For example, the predominant pentacoordinate state of CCP at 290 K changes to hexacoordinate at 9 K, whereas in HRP, the predominant high-spin five coordinate species converts to a pure intermediate spin state upon lowering temperature from 290 to 9 K (163).

The primary amino acid sequence of HRP is known (164). It confirmed the presence of the proximal histidine and demonstrated that the active site occurred in a hydrophobic region of the amino acid sequence (164,165). The histidine and arginine residues were found on the distal side (164). Amino acid sequences of the other peroxidases have been studied, indicating that the distal and proximal histidines and the distal arginine are conserved among almost all heme peroxidases (166,167).

It has been established that the heme iron of the native HRP is in the high spin, S=5/2, probably mixed with a small part of intermediate spin, S=3/2, pentacoordinate, ferric state with histidine coordination as the fifth ligand (161,162,165). Therefore, HRP and most plant peroxidases can be distinguished spectroscopically from cytochrome P_{450} (oxygenase) whose heme iron has a cysteinate as the fifth ligand (168), from cytochrome $\underline{b}_5$ (electron carrier) whose heme iron is a ferric low-spin (169), from oxy- and deoxymyoglobin (oxygen binder) whose heme iron is in the ferrous state (170), and from metmyoglobin whose heme iron is hexacoordinate (159).

1.4.3 Catalytic Mechanism of Peroxidase

The enzymes in the peroxidase family have many common mechanistic features. The central feature of this mechanism is the formation of a

spectrally distinct intermediate, compound I, by the action of an oxidizing substrate such as hydrogen peroxide or organic peroxyacids on the native enzyme (137,155,156). HRP compound I (HRPI) was first detected by Theorell in 1941, and it was proposed to be an enzyme-substrate complex (171). Later, many studies have demonstrated that it is an oxidized derivative of the enzyme (172). Compound I contains two oxidizing equivalents above the native ferric enzyme. Thus, it is formally an Fe^{5+} form of the enzyme. Electron donating substrates (reducing substrates) reduce HRPI to the native ferric enzyme in two steps via the formation of a second intermediate, HRP compound II (HRPII). HRPII contains one oxidizing equivalent above the native ferric enzyme (172) and is therefore a formal Fe^{4+} form of the enzyme. It appears that all members of the peroxidase family form similar one- and two-electron oxidized intermediates, and there has been much effort directed at identifying the chemical nature of these oxidized enzyme species.

Magnetic susceptibility measurements of HRPI and HRPII showed that they contain three and two unpaired electrons, respectively (173,174). For compound II this is consistent with a low-spin ferryl peroxidase. The formulation of compound II as a ferryl type of structure is now widely accepted, and the existence of Fe^{IV}-porphyrin was first demonstrated by cyclic voltammetry (175). Many spectroscopic techniques have been applied to deduce the structure of compound II as a ferryl type structure. Mössbauer spectroscopy which provides information on the electron configuration of iron indicates

that the iron in HRPII is a low-spin (S=1) Fe^{IV} species (176). A ferryl group in both HRPII and ferryl myoglobin was also shown by NMR study (177). The clear evidence for Fe^{IV}=O complex in both HRPII and ferryl myoglobin was provided using resonance Raman spectroscopy on the basis of ^{18}O isotope exchange experiments (178-180). All these data indicate that compound II is a low-spin hexacoordinate species in which the central metal ion is oxidized above ferric to the ferryl, Fe^{IV}=O, state.

The location of the oxidized sites in compound I is more difficult to determine. The existence of three unpaired electrons in compound I can be explained in several ways (181): (i) Fe^{V}-spin 3/2, (ii) Fe^{IV}-spin 1 + a radical, (iii) Fe^{III}-spin 1/2 + a biradical, (iv) Fe^{III}-spin 3/2 + peroxide or an oxidized porphyrin, (v) Fe^{III}-spin 5/2 and Fe^{III}-spin 1/2 + peroxide. All of these proposals are consistent with the magnetic susceptibility results, but each conflicts with data from other sources. For example, proposal (i) does not explain the similarities in the Mössbauer spectra of compounds I and II, which also suggests the Fe^{IV} oxidation state of iron in compound I (176). For the same reason, proposals (iii)-(v) are not likely. Proposal (ii) fits the Mössbauer results, but no clear evidence for the existence of the free radical signal had been provided by EPR spectroscopic studies. In 1965, the first evidence of an EPR free radical signal at g = 2.003 for HRPI at 98 K was reported, but its spin concentration was very low relative to the concentration of compound I (182). Later, another EPR study of HRPI

described an asymmetric signal for compound I at g = 1.995 below 40 K. Although the spin concentration of the signal was approximately 1% of the concentration of compound I, a titration of HRP with H_2O_2 demonstrated that the signal intensity was proportional to the amount of compound I and the signal intensity and optical absorbance decayed simultaneously (183). The low signal intensity was suggested to be due to the nearby fast-relaxing ferryl iron. Finally the nature of the π-cation radical of the porphyrin ring has been identified. The identification was proposed by Dolphin and coworkers based on the spectral comparison of the enzyme compound I and synthetic porphyrin π-cation radicals (184,185). In addition, they further characterized the electronic absorption spectra into two classes and assigned them to porphyrin radicals with different ground states (184,186). There has been widespread acceptance that compound I of peroxidases, except CCP which contains a protein centered radical (188,189), contains a porphyrin π-cation radical and the central iron is in the ferryl, Fe^{IV}=O, state. The Fe^{IV}=O distance in both HRPI and HRPII has been recently reported to be the same, 1.64Å (187).

Fig. 1-4 gives the electronic absorption spectra of native HRP, HRPI, and HRPII, showing that they are spectrally distinguishable. The peak at ~400 nm is referred to as the Soret band and is characteristic for heme proteins. The reduced intensity of the Soret band of HRPI is due to its π-cation radical nature (184), and the peak at 650 nm to an A_{2u} type ground state (184,186). CCPI has been shown to

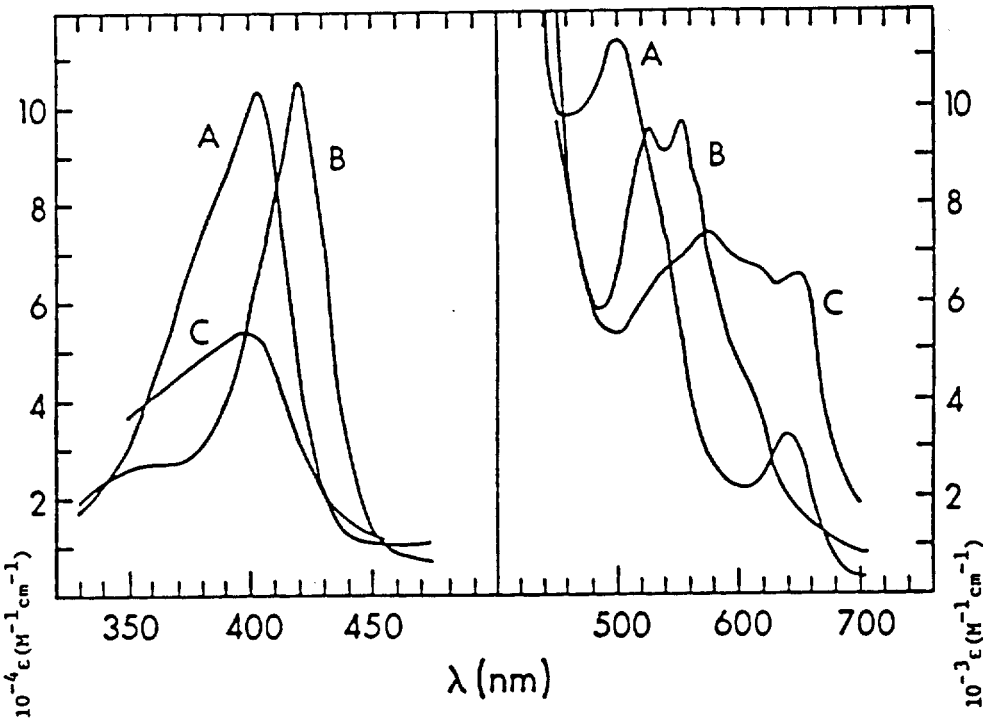

Fig. 1-4. **Electronic absoption spectra of native HRP, HRPI, and HRPII.** A, native HRP; B, HRPI; C, HRPII (137).

contain a protein-centered radical with an Fe^{IV}=O form and its spectral features are similar to that of HRPII (188,189), supporting the porphyrin π-cation radical nature of HRPI.

The normal peroxidative catalytic cycle is represented by the following:

$$HRP + H_2O_2 \xrightarrow{k_1} HRPI + H_2O \qquad [1\text{-}1]$$

$$HRPI + AH_2 \xrightarrow{k_2} HRPII + \cdot AH \qquad [1\text{-}2]$$

$$HRPII + AH_2 \xrightarrow{k_3} HRP + \cdot AH + H_2O \qquad [1\text{-}3]$$

where AH_2 is a reducing substrate and ·AH a free radical product. Thus, a single two-electron oxidation of the enzyme is followed by two single-electron reductions. The sum of reactions 1-3, above, is:

$$H_2O_2 + 2AH_2 = 2\cdot AH + 2H_2O \qquad [1\text{-}4]$$

There are several possible fates for the free radical product, depending upon its chemistry. It may dimerize, react with another substrate molecule, or attack another species causing cooxidation. It may reduce molecular oxygen to superoxide or it may be scavenged by molecular oxygen to form a peroxy radical. The above scheme can be represented as a modified type of ping pong kinetics (155):

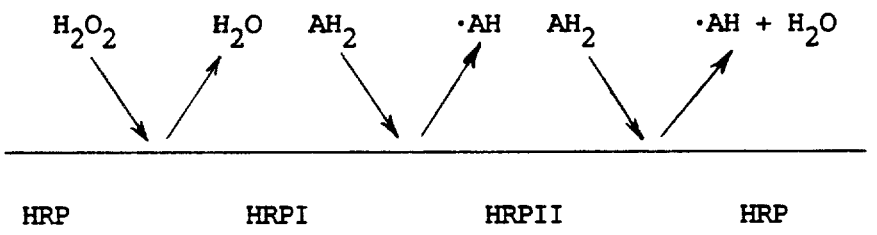

[1-5]

Each step of the peroxidative catalytic cycle (Eqs. 1-3) has been well characterized using transient state kinetic techniques and product analyses. The formation of compound I normally obeys second order kinetics and the rate constant for HRPI formation with H_2O_2 has been reported to be 1.8×10^7 M^{-1} s^{-1} (k_1) (190).

The formation of compound I involves an electron push-pull mechanism for the heterolytic cleavage of the O-O bond of hydrogen peroxide (191,192). Positive distal groups provide the pull and a deprotonated proximal histidine provides the push. In this mechanism, a distal group should accept the proton from the α-oxygen atom of H_2O_2. The heme linked ionization groups involved in the formation of compound I have been extensively studied (193-195). The ionization-controlling amino acid residue is still not clear, but either the distal His or Asp has been suggested. On the basis of a low pKa value, ~2.5 (193), if His is the controlling group, then a large shift from the normal pKa value has occurred. Asp has a lower pKa value at 3.9. However, studies on the crystal structure of CCP suggested the involvement of His in compound I formation (191,285).

The overall process which involves formation of HRPI, the transfer of a hydrogen ion and a hydroxyl ion, the cleavage of O-O

bond, formation of an Fe-O bond and subsequent rearrangement within the enzyme, is extraordinarily efficient with an activation energy of 14.6 kJ mol^{-1} (196).

The reduction of compound I to the ferric native enzyme by a reducing substrate usually occurs via compound II through the formation of free radicals of bivalent electron donors. In most cases, the reaction of HRPII with various reducing substrates is rate-determining and its second order rate constant (k_3) is 10-100 times smaller than that of HRPI (k_2) (197-202).

The redox potentials of HRPI and HRPII have been determined, based on the equilibrium data coupled with the K_2IrCl_6/K_3IrCl_6 system. E_0' (compound I/compound II) was determined to be 0.94 V and E_0'(compound II/native) to be 0.96 V at pH 6.53 (203). Thus, the redox potential cannot explain the higher reactivity of HRPI over HRPII.

Two possible mechanisms for the reduction of compound I have been proposed. From the studies on the nature and location of inhibitor damage to HRP, based mainly upon reactions of substituted hydrazines, the ferryl oxygen atom and most of the heme of HRPI are believed to be inaccessible to reducing substrate (204-208). The higher reactivity of compound I may be because the porphyrin π-cation radical is exposed at a peripheral site (208) and this peripheral site may be sterically available to large organic substrates. In another proposal the reducing substrate, typically a phenol, is considered as a hydrogen donor (209,210), in which a proton is accepted by a distal group, probably the imidazole side chain of the distal His, and the electron

is transferred simultaneously to the heme (155,208). The latter mechanism accounts for the fact that a proton is taken up by the enzyme upon the reduction of HRPI to HRPII, and that a distal group of pKa ~5.1 plays an important role in HRPI reactions (155,211). Thus, both proposals have the common feature of electron transfer to the porphyrin ring. Whether the ferryl oxygen atom is directly accessible or inaccessible to reducing substrate is still unclear.

There is a heme linked ionization corresponding to a pKa value of 8.6 which is of crucial importance to the catalytic activity of HRPII. When the group is deprotonated, HRPII is totally inactive (137). During the reduction of HRPII to native HRP, water is a leaving group with the oxygen atom coming from Fe^{IV}=O. The simplest and most plausible mechanism is that one proton is supplied by the distal group of pKa 8.6 and the other by the hydrogen-donor reducing substrate (210). The distal group might be His. Detailed studies on the reaction mechanisms of compounds I and II are continuing.

1.4.4 Ferrous Enzyme and Compound III

The reduction of native HRP by dithionite (hydrosulfite) results in the formation of ferrous HRP (137). Although ferrous HRP is not a part of the normal peroxidatic cycle, it can be used to mimic a part of the cycle. Ferrous HRP reacts rapidly with H_2O_2 to form HRPII, which resembles the reaction of native HRP with H_2O_2 to form HRPI. Furthermore, there is interest in the reactivity of the ferrous enzyme. For example, HCN, CO, NO, or O_2 binding to ferrous enzyme

mimics the complex formation of ferrous myoglobin and hemoglobin. CO binding to ferrous HRP has been studied and both the association and dissociation rates of CO are small for HRP compared to myoglobin and hemoglobin (212).

Another oxidation state of the enzyme was found when a large excess H_2O_2 was added to native ferric HRP (175). This intermediate was designated as compound III (HRPIII). O_2 binding to ferrous HRP was found to form oxyperoxidase, resembling oxymyoglobin and oxyhemoglobin (213). Later, oxyperoxidase was shown to be the same as HRPIII (214,215). Titrimetric experiments showed that HRPIII was at a three-equivalent oxidized state above ferric HRP (216-219). Thus, compound III is a formal Fe^{+6} form of the enzyme.

It is now well known that compound III is formed through three reaction paths: (i) oxygen binding to ferrous enzyme (213-215), (ii) superoxide binding to native ferric enzyme (220,221), and (iii) the reaction of ferryl enzyme (compound II) with H_2O_2 (173,222,223). The formation of compound III from native enzyme in the presence of excess H_2O_2 occurs via reaction (iii) (175, 222). Compound III can be regarded as a resonance hybrid with the contributing structure represented as $Fe^{II}-O_2 \leftrightarrow Fe^{III}-O_2^{-\cdot}$ (137,155,156). It has been widely accepted that HRPIII is relatively inert, mainly because it is not a part of the peroxidatic cycle. However, it has been shown to have chemical reactivity towards iodoacetic acid (224,225). Compound III is less reactive with electron donors than compound II, and in the absence of such donors compound III is less stable than compound II (218).

HRPIII undergoes a spontaneous decay to the ferric enzyme without forming detectable intermediates (216,218) and during its decay superoxide is released (226). Therefore, O_2 is activated when it combines with the ferrous enzyme to form HRPIII. Likewise, H_2O_2 is oxidized to superoxide when it reacts with ferryl enzyme to form HRPIII. The physiological role of compound III is not clear, but its formation might be involved in activated oxygen species formation.

The interrelationship between five redox forms of a peroxidase is summarized in Fig. 2-7. All of the oxidized states are fairly stable under suitable experimental conditions. The reaction paths, 3 → 5 → 4 → 3, indicate one catalytic cycle of the enzyme. These redox states and reaction paths are almost universal among the family of peroxidases.

1.5 SUMMARY OF RESEARCH

At the time that the research described in this thesis was begun, both LiP and MnP had been purified to homogeneity and partially characterized. LiP had been more extensively studied since many reactions observed with lignin model compounds in ligninolytic culture of P. chrysosporium are catalyzed by this enzyme. The following sections (1.5.1 and 1.5.2) review the work on the spectroscopic properties and reaction mechanisms of LiP and MnP, which had been studied in several

laboratories before the present research work was begun. Section 1.5.3 summarizes the present work.

1.5.1 Lignin Peroxidase

LiP was identified from the extracellular culture medium of ligninolytic P. chrysosporium as the enzyme catalyzing the H_2O_2-dependent oxidation of nonphenolic lignin model compounds (94-97). The enzyme was purified to electrophoretical homogeneity by a combination of anion exchange chromatography and gel filtration (98-101) and was shown to contain one mole of ferriprotoporphyrin IX prosthetic group per mole of enzyme, to have molecular mass of 41-42,000 with a single polypeptide chain, and to be glycosylated (98-101). The enzyme is present as a series of isozymes (101-103) with pIs ranging from 3.2 to 4.0. The characterization of the enzyme has been focused on the major isozyme of LiP, LiP isozyme 2 (101) or H8 (102), and this isozyme has been used for the present study.

The electronic absorption spectrum of native LiP is characteristic of a high-spin ferric protein, with Soret and visible maxima at 408, 500, and 632 nm (99), similar to those of HRP and metmyoglobin. Like HRP, the ferric LiP forms typical low-spin hexacoordinate complexes with CN^- and N_3^- (99), with spectra distinct from those of P_{450} low-spin complexes (168). The spectrum of the reduced enzyme is typical of high-spin pentacoordinate ferrous heme (99). The ferrous enzyme forms a complex with CO which has a spectrum typical of peroxidases. This spectrum probably rules out a cysteinate fifth

ligand as is found in cytochrome P_{450} (168). These spectral data are summarized in Table 1-5.

The EPR spectrum of native LiP is also typical of high-spin ferric heme (245). The g values are essentially identical to those of aquometmyoglobin but differ somewhat from those of HRP and CCP for which a large rhombic component is observed. The similarities between LiP and aquometmyoglobin suggested that LiP may have a more axial heme symmetry as compared with the other peroxidases. Resonance Raman studies (227-229) indicate that native LiP is a high-spin ferric enzyme and is predominantly pentacoordinate at ambient temperature and also confirm that the reduced enzyme is a high-spin pentacoordinate ferrous species. These spectral characteristics indicate that the fifth ligand to the heme iron in LiP is probably a histidine as found for other plant peroxidases (137,155). All the spectral data indicate that the heme environment of LiP is similar to a peroxidase rather than a P_{450} type oxygenase.

Finally, the product analyses on the oxidation of diarylpropane type lignin model dimers by LiP/H_2O_2 under aerobic and anaerobic conditions using $^{18}O_2$ and $H_2{}^{18}O$ clearly showed that oxygen incorporation during the oxidative cleavage at C_α-C_β in propyl side chains resulted from the addition of molecular oxygen to carbon-centered radicals (230,231). These studies demonstrated that the essential mechanism of LiP is not an oxygenase but rather a peroxidase mechanism.

Table 1-5. Electronic absorption spectral maxima of LiP, MnP, and HRP

System	Absorption Maxima (nm)				Ref.
Ferric, native					
LiP, pH 4.5	408	500		632	99
MnP, pH 4.5	406	502		632	104
HRP, pH 6.0	403	500		641	137
Ferric, low spin					
CN^--LiP	423		540		99
CN^--MnP	421		546		104
CN^--HRP	422		539		137
N_3^--LiP	418		540	575	99
N_3^--MnP	417		542	580	104
N_3^--HRP	416		534	565	137
Ferrous					
LiP	435		556		99
MnP	433		554		104
HRP	437		556		137
Ferrous CO					
CO-LiP	420		535	568	99
CO-MnP	423		541	570	104
CO-HRP	423		541	575	137

Electronic absorption spectral data for the oxidized intermediates of LiP are compared with those of HRP in Table 1-6. The primary reaction product of peroxidases with the oxidizing substrate H_2O_2 is compound I. Spectral characteristics of LiP compound I (LiPI) are similar to those of HRPI, indicating that it contains two oxidizing equivalents above the native ferric enzyme and that the two equivalents reside in the Fe^{IV}=O state of the iron and a porphyrin π-cation radical (232). Reduction of LiPI by one equivalent of reducing substrate yields LiP compound II (LiPII) with spectral characteristics similar to HRPII (99,137,232), suggesting an Fe^{IV}=O structure for LiPII. Resonance Raman evidence also indicates an Fe^{IV}=O nature for LiPII (229). Finally, addition of excess H_2O_2 to LiP yields compound III (232). A similar intermediate is formed by adding oxygen to ferrous LiP (101). These spectral features of the oxidized intermediates of LiP indicate the peroxidatic nature of the enzyme.

The recent nucleotide sequences of cDNAs encoding several LiP isozymes indicate that the proximal and distal histidine and the distal arginine are conserved (233-235), suggesting a similar reaction mechanism for LiP and other peroxidases.

LiP catalyzes the oxidation of veratryl alcohol (VAlc) to veratraldehyde (VAld). Since this reaction can be easily followed at 310 nm where VAld absorbs strongly, it is the standard assay for this enzyme (99,100). HRP cannot catalyze this oxidation because VAlc does not have a free phenolic hydroxyl group. LiP has an extremely low pH optimum (~2.5) for a peroxidase (236,237). Although the peroxidative

Table 1-6. Absorption maxima (nm) of oxidized intermediates of LiP and HRP

Peroxidase	Compound I	Compound II	Compound III[a]	Ref.
LiP	408, 550, 608, 650	420, 525, 556	419, 543, 578	99
HRP	400, 557, 622, 650	420, 527, 554	413, 546, 583	155

[a] Two types of LiP compound III have recently been characterized and designated as LiPIII and LiPIII* (Chapter 8 and Ref. 263). The values in the Table are for LiPIII*.

nature of LiP has been demonstrated, the mechanism for VAlc oxidation is not clear. The stoichiometry of VAlc oxidation by LiP indicates that one mole of VAld is formed at the expense of one mole of H_2O_2. Furthermore, the failure to detect a substrate free radical has been reported (236). These observations were thought to be consistent with a single step two-electron oxidation or with rapid one-electron oxidations in two steps at the enzyme active site by direct oxygenation (236). However, peroxidases normally catalyze two steps one-electron oxidations to form substrate free radicals (137,155,156).

Since VAlc is a secondary metabolite of the fungus, the oxidation of this substrate probably has special significance. Several possible roles for VAlc have been suggested. These include acting as an inducer of LiP synthesis (102) and acting as a radical mediator (238,239).

LiP catalyzes the H_2O_2-dependent oxidation of a wide variety of nonphenolic lignin model compounds to yield numerous products (Fig. 1-5) (29-31,67,99-101,106,230,231,240-247). Aromatic substrate oxidation by LiP was of great interest due to the diversity and complexity of the reaction products. All of these reactions are now explained by a mechanism involving the initial one-electron oxidation of the substrate to form an aryl cation radical followed by a series of nonenzymatic reactions to yield the final products (101,230,231, 240,248,249). Fig. 1-6, for example, illustrates the mechanism for the oxidative cleavage of a diarylpropane dimeric lignin model compound (231). In this pathway the oxidized form of the enzyme in

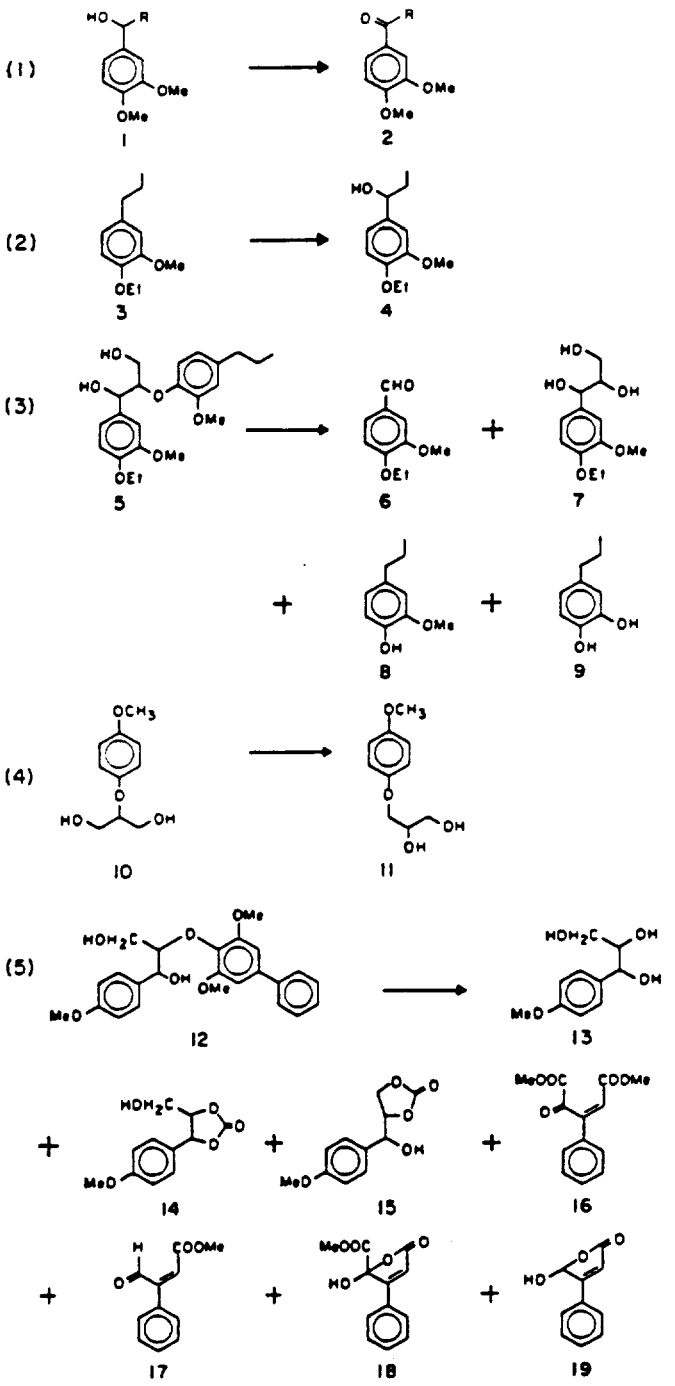

Fig. 1-5. **Reactions catlyzed by lignin peroxidase.** Me = $-CH_3$, Et = $-C_2H_5$.

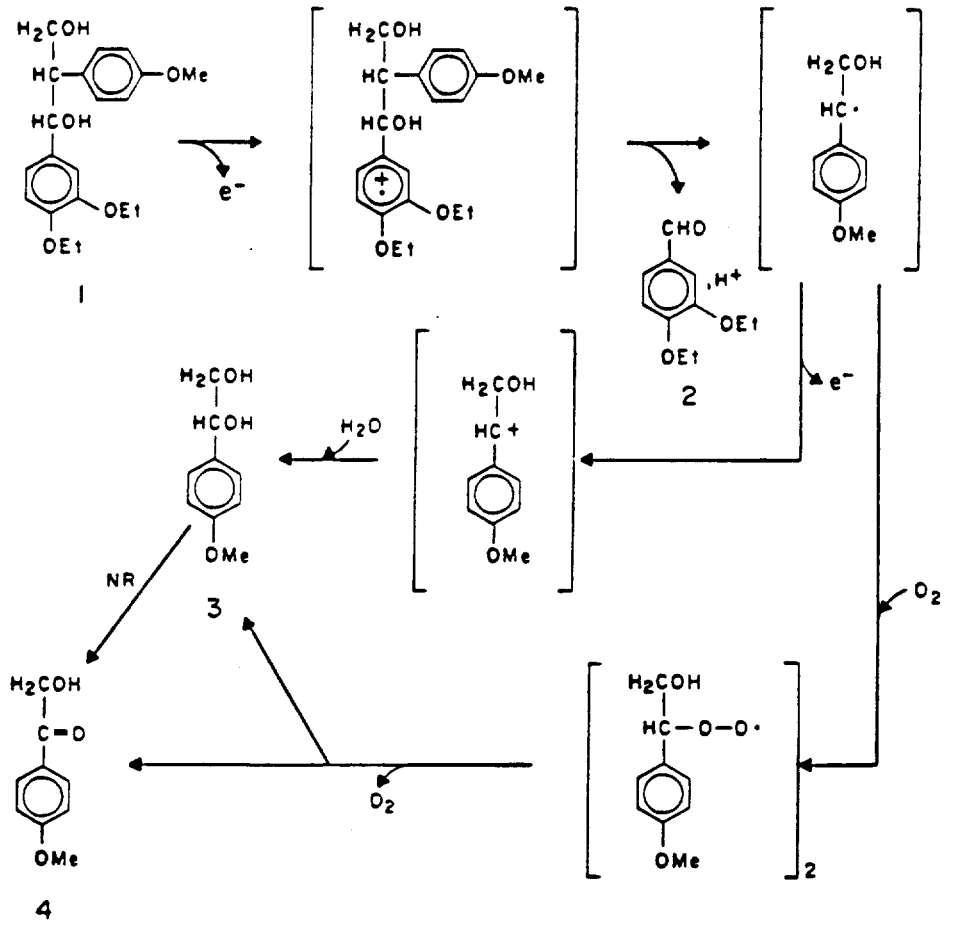

Fig. 1-6. Mechanism of C_α–C_β cleavage by lignin peroxidase (231). NR = no reaction.

turn oxidizes the diarylpropane to form an aryl cation radical. Direct EPR evidence for the formation of aryl cation radicals by LiP has been presented (249). The unstable aryl cation radical undergoes a radical cleavage at C_α-C_β to form the benzaldehyde and C_6C_2 benzylic radical intermediate. EPR evidence for such carbon-centered radical intermediates has also been presented (240). The benzylic radical intermediate is attacked preferentially by molecular oxygen under aerobic conditions and the resulting peroxy radical would decompose to form phenylglycol and phenylketol. In the absence of O_2, however, the benzylic radical is oxidized most probably by the enzyme to the corresponding cation which is subsequently attacked by H_2O yielding phenylglycol. These pathways are consistent with $^{18}O_2$ and $H_2{}^{18}O$ incorporation experiments (231) and with EPR experiments (240).

Thus, the key reaction of LiP with the aromatic substrates is a one-electron oxidation of the substrate to an aryl cation radical and this is partially dependent on the redox potential of the aromatic ring. Strong electron withdrawing groups such as benzylic carbonyls suppress the formation of aryl cation radicals (245) while electron donating alkoxyl groups tend to activate aryl cation radical formation (241).

Ring-opening reactions have also been suggested to occur during the oxidation of lignin by P. chrysosporium (49,50). The first direct evidence for this reaction in the fungal cultures was reported using β-aryl ether dimer (250) and VAlc (251) as substrates. The rational design of substrate has allowed the study of side chain cleavage, β-

ether cleavage, and rearrangement as well as ring-opening reactions, shown in reaction 5 of Fig. 1-5. The mechanisms were described in detail and these reactions can also be explained by the initial formation of aryl cation radicals (243,244,246,247). Oxidative aromatic cleavage had heretofore been thought to be solely catalyzed by dioxygenases; however, in the LiP-catalyzed reaction, ring cleavage is initiated by a one-electron oxidation.

1.5.2 Manganese Peroxidase

Under ligninolytic conditions P. chrysosporium is capable of decolorizing various polymeric dyes (107). Subsequent studies led to the discovery of a peroxidase activity different from LiP in extracellular culture medium of P. chrysosporium (98,104). The enzyme, manganese peroxidase (MnP), catalyzes H_2O_2-dependent decolorization of organic dyes and oxidation of phenols and amines only in the presence of manganese (II) (98,104,105). Certain organic acids such as lactate stimulated this reaction (104,105,108).

MnP has been purified to electrophoretic homogeneity by a combination of anion exchange chromatography, affinity chromatography, and gel filtration (98,104,105). MnP exists as a series of isozymes with pIs ranging to 4.2 to 4.9, contains one iron protoporphyrin IX prosthetic group, and is a glycoprotein of molecular mass ~46,000 with a single polypeptide chain (98,102-105). The characterization of the enzyme had been done on the major isozyme referred to as MnP isozyme 1 in our laboratory and this isozyme also has been used for the present study.

Electronic absorption maxima for MnP and various liganded forms of the enzyme are shown in Table 1-5. The spectrum of native MnP is characteristic of a high-spin ferric heme protein similar to HRP and metmyoglobin. Spectra of liganded MnP showing typical low-spin hexa-coordinate complexes are also similar to those of HRP complexes but distinct from P_{450} type oxygenases (104). The reduced form of MnP and its complex with CO show spectra similar to those of the other peroxidases but clearly different from those of P_{450} (104,168).

The EPR spectrum of native MnP is typical of high-spin ferric heme, with g values 5.79 and 2.00 (105,252). These features are essentially identical to those of high-spin aquometmyoglobin and LiP (227) and are somewhat different from CCP and HRP for which a large rhombic component appears to be present (137). Thus, it was suggested that MnP may have a more axial heme symmetry as compared with the other peroxidases. The rhombic character of the EPR spectrum of HRP may arise from an intermediate-spin species (161,162).

As with ferrous HRP, identification of the fifth ligand as an N-bonded species has been achieved from the investigation of EPR spectrum of ferrous heme NO adducts (253). EPR spectra of ^{14}NO- and ^{15}NO-adducts of ferrous MnP were compared with those of HRP and the presence of a proximal histidine ligand was confirmed from the pattern of superfine splitting of the NO signals centered at g = 2.005 (252).

The appearance of the Fe^{II}-His stretch in the resonance Raman spectrum at ~240 cm^{-1} and its apparent lack of deuterium sensitivity suggest that the N proton of the proximal histidine is more strongly

hydrogen-bonded than that of globins and that this imidazole ligand may be described as having a comparatively strong anionic character (252). This would help to stabilize the higher oxidation states of compounds I and II. Resonance Raman studies also indicate that native MnP is a high-spin ferric enzyme which is predominantly pentacoordinate at ambient temperature (252). These spectral characteristics suggest the peroxidative nature of MnP.

Most importantly, it has been demonstrated that MnP oxidizes Mn^{II} to Mn^{III} and that the Mn^{III} produced, in turn, oxidizes organic substrates (104,105,108). Thus, the manganese ion participates in the reaction as a redox couple rather than acting as an enzyme-binding activator. This is supported by experimental results, demonstrating that the MnP/Mn^{II}/H_2O_2 system separated from the organic substrate by a semipermeable membrane was capable of oxidizing the substrate by the diffusible Mn^{III} generated by the enzyme (108). Mn^{III} formation was spectroscopically confirmed. Mn^{III} has been known to form spectrally characteristic complexes with pyrophosphate and lactate (104,105,108). The enzyme activity was stimulated by α-hydroxy acids such as lactate (104,108) and tartrate (105), which has been suggested to reflect stabilization of Mn^{III} in aqueous solution (104,108). Since manganese is the reducing substrate, the enzyme was designated as manganese peroxidase (104,105,108).

The nucleotide sequences of cDNAs encoding MnP isozymes have been recently determined and confirm the presence of a proximal and distal histidine and a distal arginine (254,255). This suggests a similar

reaction mechanism for MnP and other peroxidases.

As described above (Section 1.3.3), MnP appears to function not only as a phenol oxidizing enzyme but also as an NADH, DHF (dihydroxyfumarate), and thiol oxidizing enzyme. In the latter reactions, H_2O_2 was produced from molecular oxygen (105,108). From these experiments, Kuwahara et al. concluded that the function of MnP is the production of H_2O_2 from NADH and O_2 (126,127). However, it is not known how the fungus may generate the reduced coenzymes extracellularly.

Including NADH oxidation, the specificity for the oxidation of organic substrates by the MnP/Mn^{II} system is similar to that of HRP; however, MnP is very unique as a peroxidase because of its dependency on Mn^{II}. In fact, Mn^{II} is the real substrate for the enzyme.

1.5.3 Present study

The biochemical and physiological studies on P. chrysosporium have demonstrated that two extracellular heme enzymes, LiP and MnP, along with a H_2O_2-generating system appear to be the major components of its lignin degradative system. Spectroscopic evidence indicated the peroxidase nature of both enzymes. Furthermore, the peroxidative catalytic cycle has been shown to be the LiP reaction mechanism.

Much less information had been accumulated on the reaction mechanism for MnP. MnP had been shown to require H_2O_2 for its activity and to catalyze one electron oxidation of Mn^{II} to Mn^{III}, which is consistent with the mechanism for the peroxidative catalytic cycle. Yet, the peroxide-oxidized intermediates and the catalytic mechanism of MnP had not been elucidated.

The spectral characterization of the oxidized states of MnP compounds I, II, and III is presented in Chapter 2 (and Ref. 256). Interrelationships among the five redox states of MnP and its peroxidative catalytic cycle are shown. Mn-dependency of the enzyme is clearly explained by the observation that Mn^{II} acts as an obligatory substrate for MnP compound II, allowing the enzyme to complete its catalytic cycle.

To characterize the reaction mechanism further, transient state kinetics were utilized. This work is presented in Chapter 3 (and Ref. 257). Kinetic analyses demonstrated that the reaction of Mn^{II} with MnPI and MnPII exhibits a binding interaction and that organic acids such as lactate facilitate the dissociation of Mn^{III} from the enzyme to form a stable Mn^{III}-organic acid complex. These experiments also confirmed that Mn^{II} serves as an obligatory substrate for MnPII.

Since ~15-20% of phenylpropanoid units of native lignin are free phenols (Table 1-2), it has been assumed that the oxidation of these phenolic units by the MnP system results in polymeric degradation. However, the oxidation of simple phenols does not model the oxidative reactions involved in the cleavage of the lignin polymer. Chapter 4 (and Ref. 258) describes a study of the oxidation of the phenolic diarylpropane lignin model dimer, 1-(3,5-dimethoxy-4-hydroxyphenyl)-2-(4'-methoxyphenyl)-1,3-dihydroxypropane by either MnP/Mn^{II} or chemically prepared Mn^{III} complex. The phenolic dimer was effectively oxidized by both oxidants to form a phenoxy radical. This was followed by alkyl-phenyl cleavage, C_α-C_β cleavage, and benzyl

oxidation. Oxygenated products were formed through the attack of oxygen on carbon-centered radicals or of water on carbonium ions.

Chapter 5 (and Ref. 259) describes the oxidation of nonphenolic lignin model compounds by MnP in the presence of thiols. Either enzymatically or chemically prepared Mn^{III} oxidizes the thiol to a thiyl radical. The latter in turn abstracts hydrogen from nonphenolic models to cause β-aryl ether bond cleavage. Thus, this reaction demonstrates the novel, thiol-mediated oxidation of nonphenolic lignin model compounds by the MnP system.

Initial characterization of the formation and reaction of the oxidized intermediates LiPI, LiPII, and LiPIII suggest that the oxidation states and catalytic cycle of LiP are similar to HRP (232). Nevertheless, the mechanism for the oxidation of VAlc had not been elucidated. The reactivity of LiPI with VAlc at the unusually low pH optimum (<3.0) was studied utilizing a stopped-flow rapid scan technique and the results are presented in Chapter 6 (and Ref. 260). Spectrally pure LiPI was obtained at low pH for the first time because it is unstable under these conditions. A low pH optimum of LiP catalysis is dictated by pH dependence of the reduction of LiPI and LiPII rather than that of the formation of LiPI. Kinetic analysis clearly shows that the reduction of LiPI by VAlc occurs in two steps via the transient formation of LiPII. This observation is consistent with one-electron oxidation of VAlc to an aryl cation radical by LiPI and by LiPII.

LiP has a typical peroxidative catalytic cycle, but with several unique features. Although LiP has an unusually low pH optimum as a peroxidase, the rate of LiPI formation is independent of pH from 2.5-8.0 (261,262). The key catalytic action of LiP is the initial formation of an aryl cation radical rather than a phenoxy radical (231,248,249). In addition, the ready formation of a LiPIII species occurs with considerably less H_2O_2 than is required with other peroxidases. Chapters 7-9 describe work on LiP compound III, the formation, conversion, reactivity, and mechanisms.

In Chapter 7 (and Ref. 262), the reaction of native LiP with H_2O_2 is studied. In the presence of excess H_2O_2, compound III species formed through the transient formation of LiPI and LiPII (260), are inactivated to a spectroscopically featureless form of the enzyme. During this inactivation process, the addition of VAlc caused the rapid conversion of compound III species back to native LiP via a single step with the release of superoxide. This observation suggested that a possible role of VAlc, the secondary metabolite of the fungus, was to protect the enzyme against the H_2O_2-dependent inactivation.

Chapter 8 (and Ref. 263) describes the further characterization of the formation and conversion of compound III species. Compound III was prepared via three different reactions; ferrous LiP + O_2, ferric LiP + $O_2^{\cdot-}$, and ferryl LiP (LiPII) + H_2O_2 followed by treatment with catalase. In the absence of H_2O_2, each LiPIII is more stable and less reactive than other oxidized intermediates at the catalytic pH. Every

LiPIII spontaneously reverted to ferric LiP via a single step, releasing superoxide quantitatively. Addition of H_2O_2 to these LiPIII preparations resulted in the formation of another intermediate LiPIII*. Spectral analysis suggested that the conversion of LiPIII to LiPIII* is reversible. Kinetic analysis revealed that the inactivation is mainly the second order reaction of LiPIII* with H_2O_2. Addition of VAlc caused the rapid reversion of LiPIII* to ferric LiP with the release of a quantitative amount of superoxide. In contrast, addition of VAlc did not influence the stability of LiPIII. The results also indicated that VAlc was not oxidized during the rapid reversion of LiPIII* to native LiP.

Chapter 9 reports the reactions of LiPII and LiPIII with H_2O_2 utilizing transient state kinetics. The rapid scan spectra clearly showed that LiPII reacts with H_2O_2 to form LiPIII* via the transient formation of LiPIII. Moreover, the results indicated not only the intermediate formation of LiPIII but a kinetically detectable LiPII-peroxide complex. The formation of LiPIII* from LiPIII is kinetically confirmed to be a reversible reaction.

In summary, the research involved the further characterization of the reaction mechanism for both MnP and LiP, implicating the clarification of the peroxidative catalytic mechanism for MnP and of the mechanism for the novel, thiol-mediated oxidation of nonphenolic lignin model compounds by the MnP system; the discovery of LiPIII*, a unique enzyme intermediate; and the suggestion of a possible role of

VAlc, the secondary metabolite of the fungus, in LiP reactions. Effective oxidation of a phenolic lignin model compound by the MnP system suggested that MnP is a lignin-degrading enzyme rather than a H_2O_2-producing enzyme. Furthermore, although more research is required, a possible involvement of LiP III* in lignin biodegradation as a generator of an activated oxygen species is suggested.

The experiments in Chapters 3, 6, and 9 were a collaborative effort with Prof. H. B. Dunford's Lab at the Univ. of Alberta.

CHAPTER 2

SPECTRAL CHARACTERIZATION OF THE OXIDIZED STATES AND THE CATALYTIC CYCLE OF MANGANESE PEROXIDASE*1

2.1 INTRODUCTION

Lignin is a complex, optically inactive and random phenylpropanoid polymer that comprises 20-30% of woody plants (14). Since the biodegradation of cellulose is retarded by the presence of lignin (18), the catabolism and potential utilization of this polymer are of enormous significance. White-rot basidiomycetes are primarily responsible for the initiation of the decomposition of lignin in wood (18). Recent studies have shown that when cultured under ligninolytic conditions, the white rot basidiomycete Phanerochaete chrysosporium

---

*1 The contents of this chapter have been published;
Manganese Peroxidase from the Basidiomycete Phanerochaete chrysosporium: Spectral Characterization of the Oxidized States and the Catalytic Cycle.
H. Wariishi, L. Akileswaran and M. H. Gold (1988) Biochemistry **27**, 5365-5370 (Ref. 256)

produces at least two extracellular heme peroxidases (98-100,104) which are important components of the ligninolytic system. Lignin peroxidase (LiP)[*2] (ligninase) has been studied extensively (29-31, 106). Recently, a second extracellular enzyme, manganese peroxidase (MnP), has been identified (98), purified, and partially characterized (104,105,108). This peroxidase is an H_2O_2-dependent heme glycoprotein of M_r = 46,000, with an iron protoporphyrin IX prosthetic group. The enzyme oxidizes a variety of dyes, phenols, and amines (98,104,105, 108). Electronic absorption (104,105), EPR, and resonance Raman spectral evidence (252) suggest that the heme iron in the native protein is in the high-spin, pentacoordinate, ferric state, with histidine coordinated as the fifth ligand.

Most importantly, recent experiments have demonstrated that MnP oxidizes Mn^{II} to Mn^{III}, and that the Mn^{III} produced, in turn, oxidizes organic substrates (104,105,108). In order to more fully understand the mechanism of MnP, we have prepared all of the oxidation states of the enzyme using H_2O_2 and organic peroxides as oxidants. In addition, we have reduced the oxidized states of the enzyme coupled with the oxidation of selected substrates. These experiments indicate that the

---

[*2] Abbreviations:
CAT, catalase; CCP, cytochrome c peroxidase; CPO, chloroperoxidase; EPR, electron paramagnetic resonance; HRP, horseradish peroxidase; LiP, lignin peroxidase; LPO, lactoperoxidase; mCPBA, m-(chloroper-oxy)benzoic acid; MnP, manganese peroxidase; pNPBA, p-(nitroperoxy)benzoic acid; SA, syringic acid.

oxidized states of MnP are similar to those of HRP (137,155) and LiP (232). These experiments also indicate that although Mn^{II} and a variety of phenols are capable of reducing MnP compound I to compound II, only Mn^{II} is capable of efficiently reducing compound II to the native enzyme.

2.2 EXPERIMENTAL PROCEDURES

2.2.1 Enzyme Preparation

MnP was purified from the extracellular medium of acetate-buffered, agitated cultures of P. chrysosporium as previously described (101,104). The purified protein was electrophoretically homogeneous and had an RZ value (A_{407}/A_{280}) of ~6.15 and a millimolar extinction coefficient at 406 nm of 129.3 (104). The homogeneous enzyme was dialyzed exhaustively against buffers, prepared from water that had been purified initially by deionization and then by triple glass distillation.

2.2.2 Spectral Analyses

MnP-catalyzed oxidation of organic substrates was determined in 1 ml reaction mixtures containing 50 mM Na-lactate, 50 mM Na-succinate, pH 4.5, $MnSO_4$ (0.1 mM), H_2O_2 (0.1 mM), gelatin (3 mg/ml), substrate (0.1 mM), and enzyme (1 μg). Phenolic substrates were dissolved in dimethylformamide and diluted at least 100-fold in triply distilled

water to 10 mM. Electronic absorption spectra were recorded on a Shimadzu UV-260 spectrophotometer at room temperature with a spectral band width of 1.0 nm and cuvettes of 1-cm light path. Compounds I, II, and III of MnP were prepared by adding 1, 2, and 250 equivalents of H_2O_2 to the enzyme in 20 mM sodium succinate, pH 4.5. These intermediates were also obtained when the enzyme was oxidized in sodium lactate, pH 4.5.

mCPBA and pNPBA were dissolved in 2-methyl-2-propanol and diluted 100-fold in triply distilled water to a final concentration of 5 mM. One or 25 equivalents of these oxidants were then added to the enzyme as described. Phenolic substrates, ferric sulfate, ferrous sulfate, manganese sulfate, and ferrocyanide were each added as aqueous solutions to the oxidized enzymes as described.

The ferrous enzyme was prepared (99,104) under anaerobic conditions by purging the native enzyme with scrubbed argon in a septum-fitted cuvette, after which $Na_2S_2O_4$ (160 equivalents) was added anaerobically. The ferrous oxy complex (Compound III) was generated by purging the ferrous enzyme with O_2 gas above the solution (101).

2.2.3 Chemicals

Cumene hydroperoxide and H_2O_2 (30% solution) were obtained from Sigma. mCPBA, pNPBA, and all phenolic substrates except guaiacyl glycerol-β-guaiacyl ether (I) were obtained from Aldrich. I was synthesized as previously described (65). All other chemicals were reagent grade. Buffers were prepared in triply distilled water.

2.3 RESULTS

2.3.1 Spectral Characteristics of MnP Compounds I, II, and III

The absorption spectrum of the native enzyme (104) (Fig. 2-1, Table 2-1) had a Soret maximum at 406 nm with visible bands at 502 and 632 nm. Upon the addition of one equivalent of H_2O_2, the intensity of the Soret band was reduced to ~40% that of the native enzyme with no apparent shift in the wavelength maximum. The visible region showed a broad absorption with peaks at 558, 608 and 650 nm (Fig. 2-1, Table 2-1). The characteristics of the spectrum in Fig. 2-1 are similar to those of HRP compound I (137,155) and LiP compound I (232). The addition of two equivalents of H_2O_2 produced a spectrum similar to that of HRP compound II (137,155) with absorption maxima at 420, 528 and 555 nm (Fig. 2-2, Table 2-1). However, the extinction of the Soret maximum (420 nm) was only ~ 65% of that of the native enzyme.

The oxidation of MnP by several organic peroxides was also investigated. The addition of one equivalent of mCPBA or pNPBA led to the formation of a MnP compound I intermediate (Table 2-1). However, 25 equivalents of these organic peroxides were required to produce a compound II spectrum. Excess cumene hydroperoxide (500 equivalents) did not result in the oxidation of MnP. MnP compound I spontaneously reverted to compound II with a $t_{1/2}$ of ~60 minutes at pH 4.5. At this pH, compound II spontaneously reverted to the native enzyme with a $t_{1/2}$ of ~120 minutes. Half lives were estimated from the plot of the logarithm of absorbance against time. MnP compounds I and II could

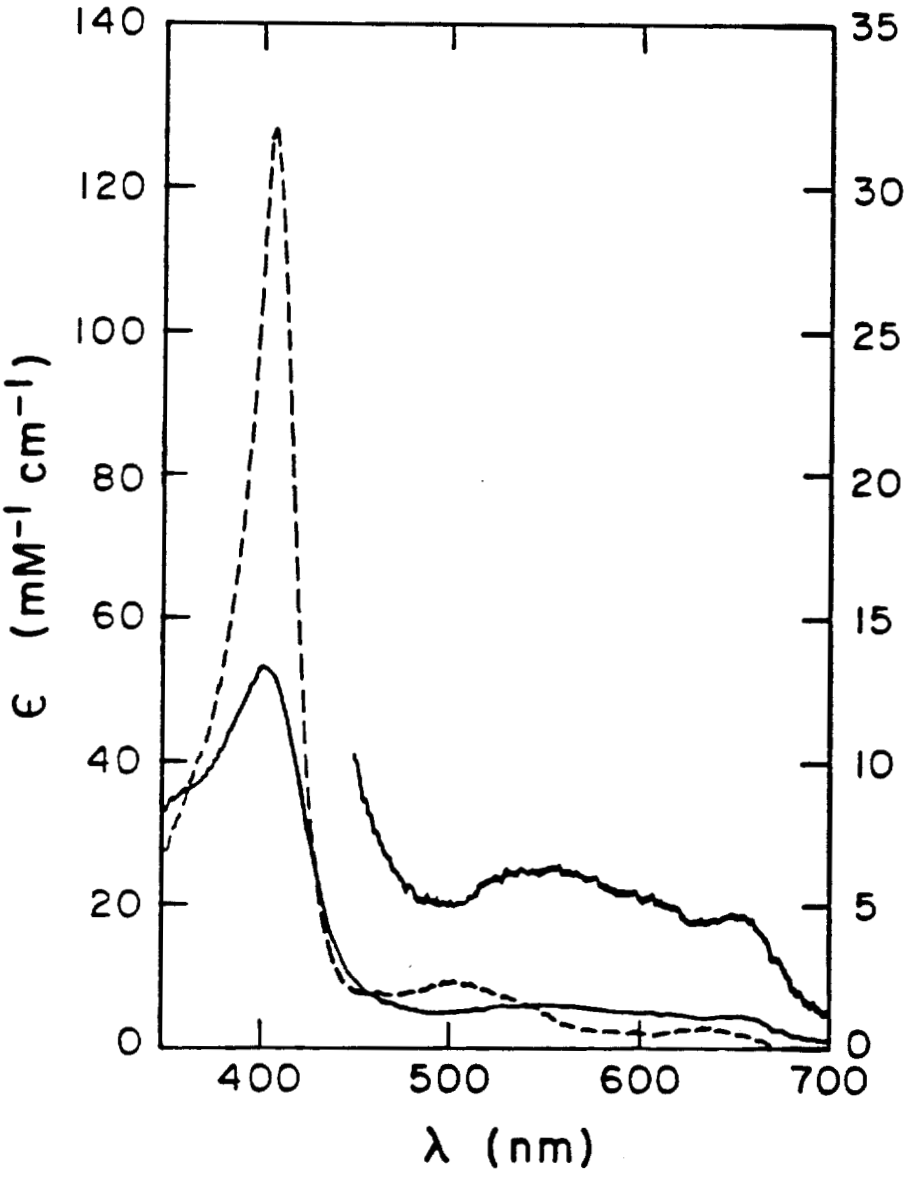

Fig. 2-1. **Electronic absorption spectrum of the native enzyme (- - -) and of MnP compound I (——).** To produce compound I, one equivalent of H_2O_2 was added to the native enzyme (1.25 μM) in 1 ml of 20 mM Na-succinate, pH 4.5. Other procedures were as described in the text.

Table 2-1. Oxidation states of manganese peroxidase

Enzyme species	Absorption maxima (nm) [ε ($mM^{-1}cm^{-1}$)]				
Ferric[a]	406 [129.3]	502 [9.9]			632 [3.4]
Ferrous[a]	435 [108.5]		556 [17.5]	590 [sh][b]	
Compound I	407 [53.4]		558 [6.4]	617 [sh]	650 [4.7]
Compound II[a]	420 [82.6]	528 [9.9]	555 [10.0]		
Compound III	417 [115.7]		545 [11.6]	579 [9.0]	
Ferrous + O_2	411 [104.0]		540 [8.9]	580 [6.9]	
pNPBA or mCPBA oxidized	407 [54]		558 [6.4]	617 [sh]	650 [4.8]

[a] Data from Ref. 104.

[b] sh = shoulder.

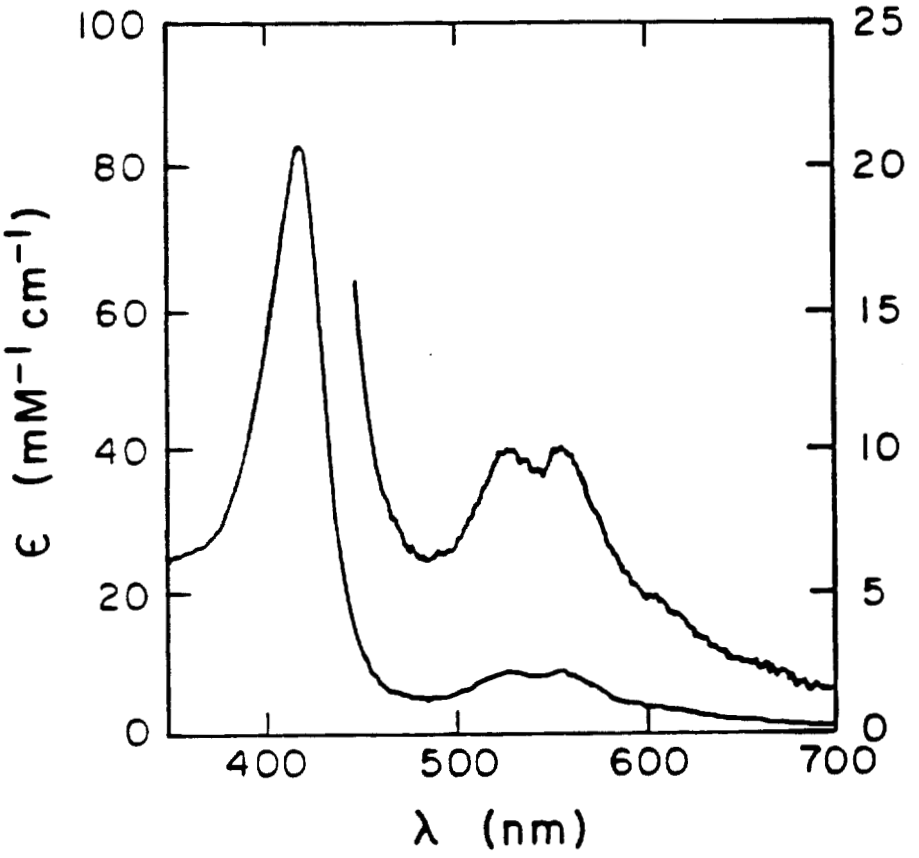

Fig. 2-2. **Electronic absorption spectrum of MnP compound II.** Two equivalents of H_2O_2 were added to the native enzyme (1.25 μM) in 1 ml of 20 mM Na-succinate, pH 4.5. Other procedures were as described in the text.

also be prepared at pH 3.0 and 6.0. However, compound I was comparatively unstable at pH 3.0, reverting to compound II with a $t_{1/2}$ of ~5 minutes. Both oxidized intermediates were approximately as stable at pH 6.0 as at pH 4.5.

The addition of excess H_2O_2 (250 equivalents) to the native enzyme or to MnP compound II led to the formation of MnP compound III. The absorption maxima of this intermediate were at 417, 545 and 579 (Fig. 2-3A, Table 2-1). Reduction of the native ferric enzyme to the ferrous form followed by purging with O_2 led to the formation of the equivalent ferrous oxy form of MnP. The absorption spectrum of this intermediate had maxima at 411, 540 and 580 nm (Fig. 2-3B, Table 2-1).

2.3.2 Reduction of MnP Compounds I and II

The extinction coefficients at 430 nm for the native enzyme, compound I and compound II were 25.0, 27.5 and 64.5 mM^{-1} cm^{-1}, respectively; therefore, the reduction of MnP compounds I and II could be followed at this wavelength. The addition of one equivalent of either syringic acid (SA) or Mn^{II} to compound I resulted in its rapid reduction to MnP compound II. A variety of other phenols and amines including p-cresol, guaiacol, vanillyl alcohol, 4-hydroxy-3-methoxy-cinnamic acid, isoeugenol, I, ascorbic acid, and o-dianisidine, were also able to reduce MnP compound I to MnP compound II. Subsequent addition of a second equivalent of SA or the phenols listed above to MnP compound II produced by the reduction of MnP compound I did not reduce compound II to the native enzyme (Fig. 2-4A). In contrast, the

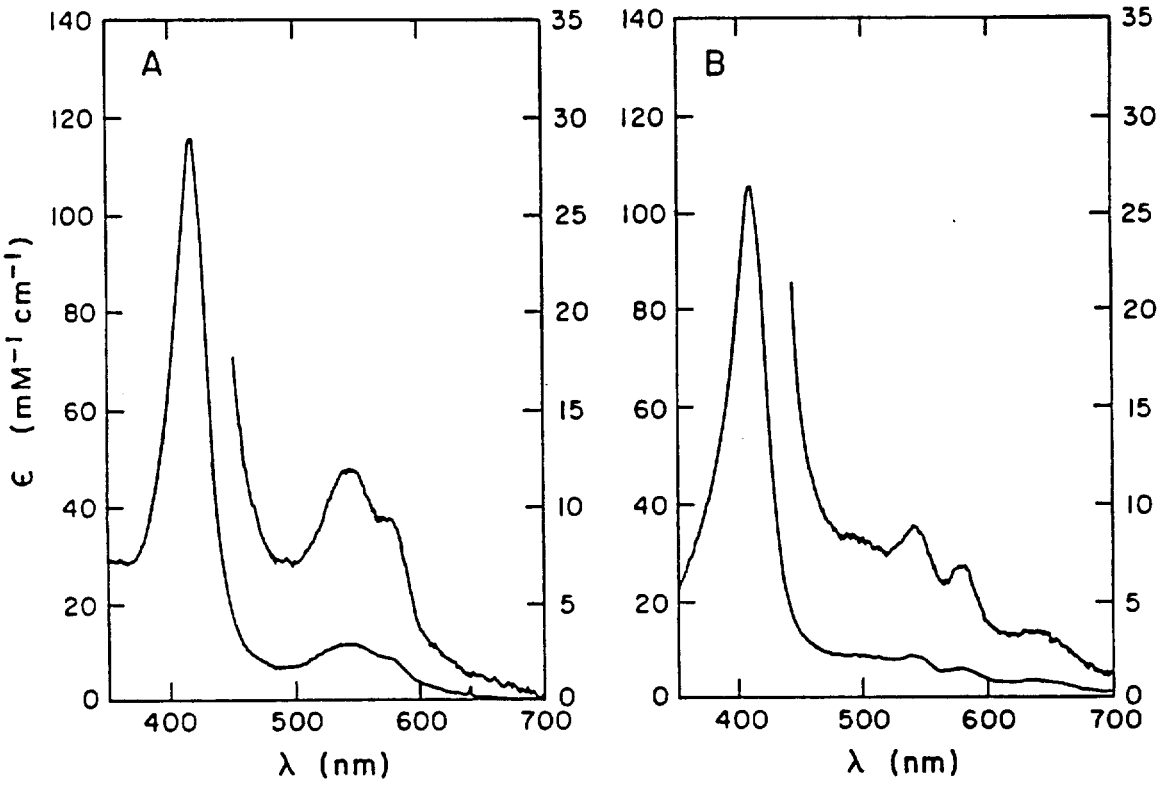

Fig. 2-3. **Electronic absorption spectrum of MnP compound III.** (A) 250 equivalents of H_2O_2 were added to the native enzyme (1.25 μM) in 1 ml of 20 mM Na-succinate, pH 4.5. (B) The ferrous oxy complex was prepared by adding molecular oxygen to the ferrous enzyme. The latter was prepared by reducing the native enzyme with sodium dithionite as described in the text.

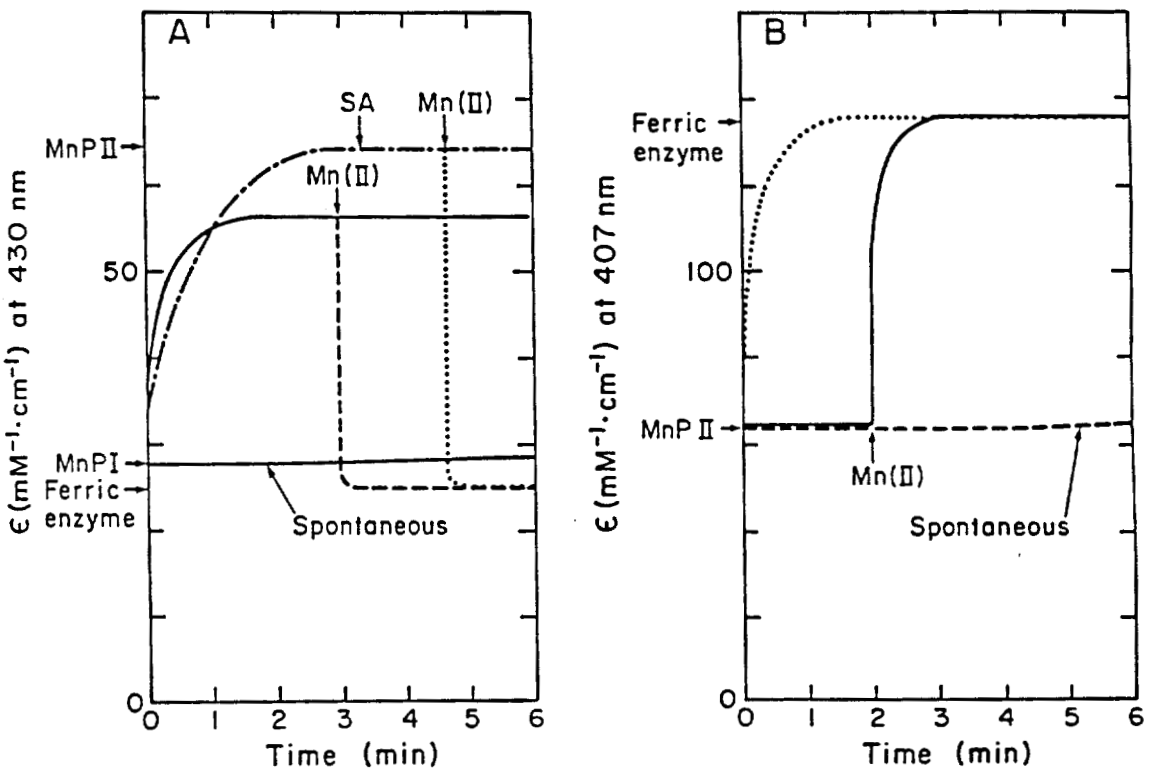

Fig. 2-4. **Reduction of MnP compounds I and II.** (A) MnP compound I was prepared by adding one equivalents of pNPBA to the native enzyme as described in the text. Reduction of MnP compounds I and II was followed at 430 nm. Addition of one equivalent of syringic acid (SA) (-·-) or of Mn^{II} (——) led to the conversion of compound I to compound II. Addition of a second equivalent of SA did not result in the reduction of compound II. In contrast, the addition of a second equivalent of Mn^{II} (---,···) resulted in the reduction of compound II. (B) MnP compound II was prepared directly by adding two equivalent of H_2O_2 to the native enzyme. Conversion of compound II to the native enzyme was followed at 407 nm. Addition of one equivalent of Mn^{II} (···) resulted in the reduction of compound II. Addition of SA (——) had no effect.

addition of a second equivalent of Mn^{II} to compound II produced via the reduction of compound I resulted in the rapid reduction of MnP compound II to the native enzyme (Fig. 2-4A).

To clarify the role of Mn^{II} in the reduction of MnP compound II, this enzyme intermediate was obtained directly by oxidizing the native enzyme with two equivalents of H_2O_2. The reduction of MnP compound II to the native enzyme was then followed by monitoring the increase in absorbance at 407 nm. The addition of one equivalent of SA to MnP compound II generated directly did not result in any spectral shift (Fig. 2-4B), indicating that MnP compound II is not readily reduced by this substrate. Likewise, addition of one equivalent of the other organic substrates listed above had no effect on MnP compound II. In contrast, the addition of Mn^{II} resulted in the rapid reduction of MnP compound II to the native enzyme (Fig. 2-4B).

2.3.3 Role of Manganese in MnP Catalytic System

Fig. 2-5A shows that the one-electron substrate ferrocyanide was able to reduce MnP compound I to MnP compound II. Subsequent addition of a second equivalent of ferrocyanide generated the native enzyme (Fig. 2-5A). Ferrous sulfate gave the same result as ferrocyanide. However, Fe^{II} could not replace Mn^{II} as a redox coupler during the oxidation of phenols by MnP (104,108). Fig. 2-5B shows that in the presence of Fe^{II}, the enzyme had little effect on guaiacol, whereas the subsequent addition of Mn^{II} to the system resulted in the immediate oxidation of guaiacol as monitored at 420 nm.

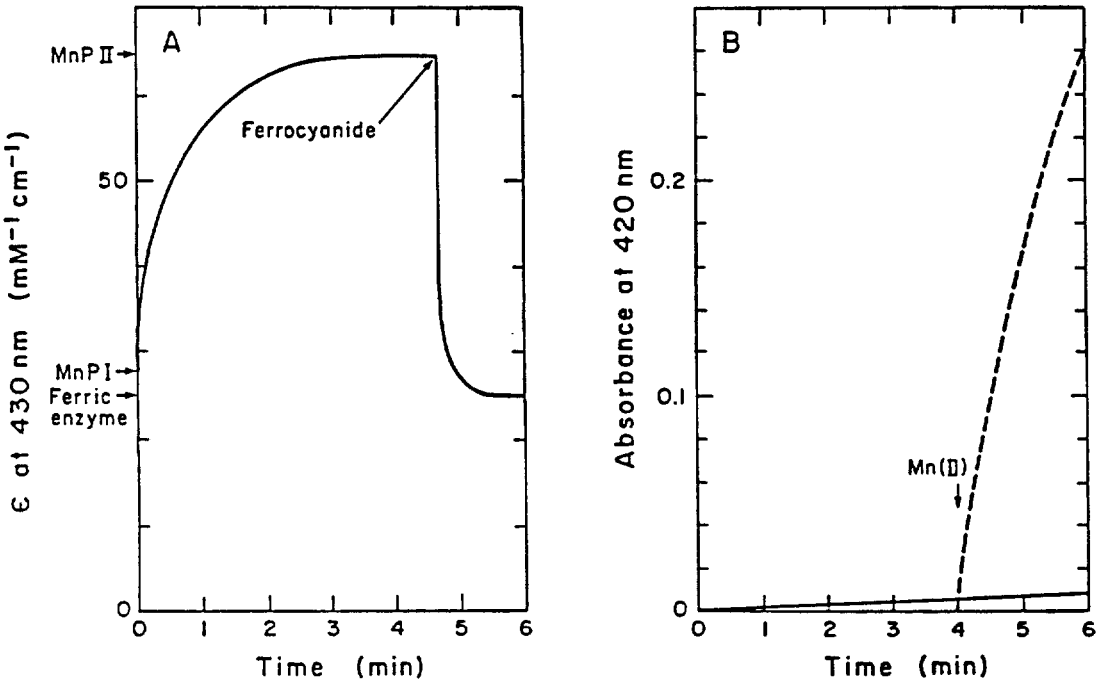

Fig. 2-5. **Reduction of MnP compounds I and II by ferrocyanide.** (A) Reduction of MnP compounds I and II was followed at 430 nm. The addition of one equivalent of ferrocyanide reduced compound I to compound II. The addition of a second equivalent of ferrocyanide reduced compound II to the native enzyme. (B) Oxidation of guaiacol by MnP was followed at 420 nm. Initial reaction mixtures (——) (1 ml) contained enzyme (1 μg), guaiacol (0.1 mM), H_2O_2 (0.1 mM), and ferrocyanide (0.1 mM). After 4 min. Mn^{II} (0.1 mM) was added to the reaction and the oxidation of guaiacol was monitored (- - -).

To further confirm the role of Mn^{III} as a redox coupler in this system, we examined the direct effect of Mn^{III} and Fe^{III} on the oxidation of the aromatic amine o-dianisidine and the phenol guaiacol. Fig. 2-6 shows that Mn^{III} oxidized both o-dianisidine and guaiacol, and that the rate of oxidation was dependent on the concentration of the metal ion. In contrast, Fe^{III} was not able to oxidize these substrates.

2.4 DISCUSSION

Manganese peroxidase is a heme-containing enyzme isolated from the extracellular medium of ligninolytic cultures of the white-rot basidiomycete P. chrysosporium (98,104,105,108). The enzyme requires H_2O_2 as a cosubstrate and oxidizes a variety of phenols, amines and organic dyes (104,105,108). While the enzyme was originally isolated as a H_2O_2-requiring, Mn^{II}-dependent enzyme (98), recent studies (104, 105,108) have demonstrated that the enzyme oxidizes Mn^{II} to Mn^{III} and that the Mn^{III} then acts as an obligatory redox coupler, oxidizing various organic substrates. The prosthetic group of MnP is iron protoporphyrin IX (104). In this respect, MnP resembles other fungal and plant peroxidases (137,264). Previous studies using electronic absorption (104), EPR, and resonance Raman spectroscopy (252) indicate that the iron in the native protein is in the high-spin, ferric, pentacoordinate state with histidine coordinated as the fifth ligand.

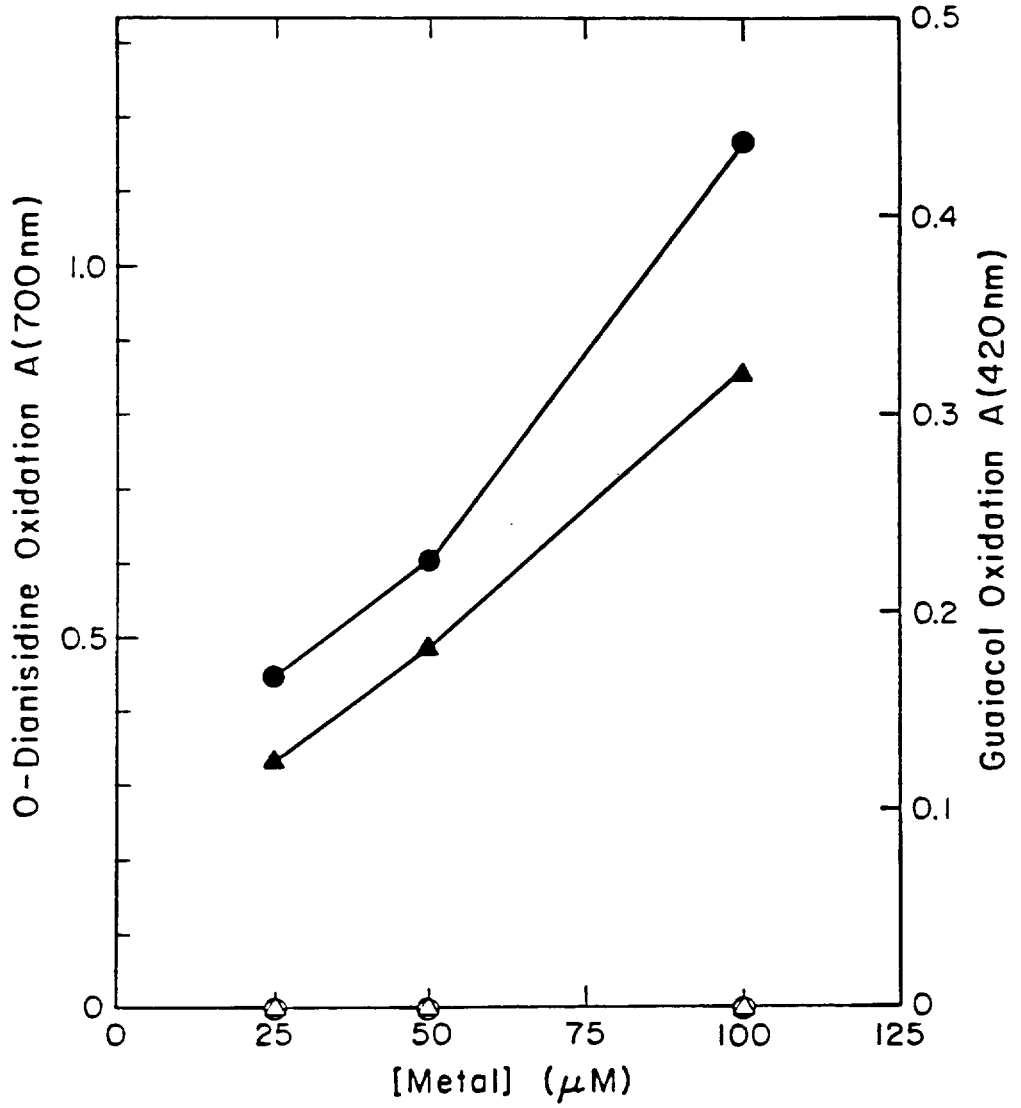

Fig. 2-6. **Oxidation of o-dianisidine and guaiacol by Mn^{III}-lactate.** o-Dianisidine oxidation ΔA/min in the presence of Mn^{III} (●) or Fe^{III} (○) and guaiacol oxidation ΔA/min in the presence of Mn^{III} (△) or Fe^{III} (▲) were followed at 700 and 420 nm, respectively. Reaction mixtures contained substrate (0.1 mM) and either Mn^{III} acetate or ferric sulfate at the concentrations indicated in 50 mM Na-lactate, pH 4.5.

2.4.1 MnP Compound I

The primary reaction product of peroxidases with H_2O_2 is the oxidized intermediate compound I. This intermediate accepts both oxidizing equivalents of H_2O_2 and is thus in the formal Fe^V oxidation state (155,264,265); i.e., it contains two additional oxidizing equivalents over the native ferric enzyme (171). Mössbauer (176) and electron-nuclear double resonance (Endor) (266) spectral studies indicate an [Fe^{IV}=O] state of the heme iron for HRP compound I; and thus only one oxidizing equivalent is present at the iron center. In HRP, the second oxidizing equivalent is stored as a porphyrin π-cation radical (176,184,266).

The electronic absorption spectrum obtained on the addition of one equivalent of H_2O_2 to native MnP has a Soret maximum at 407 nm with reduced intensity relative to the native enzyme and additional maxima at 558 and 650 nm (Fig. 2-1, Table 2-1), and thus, this appears to be a compound I species. The absorption maxima for several peroxidase compound I species are compared in Table 2-2. The spectral characteristics of MnP compound I are most similar to those of HRP compound I and LiP compound I. The reduced Soret intensity suggests the π-cation radical nature of the MnP compound I porphyrin ring (155). Furthermore, the absence of absorbance in the 680-nm region suggests that this Fe^{IV}=O porphyrin π-cation radical has an A_{2u}-type or HRP-type electronic ground state (184-186,267).

Table 2-2. Absorption maxima (nm) of oxidized intermediates of several peroxidases

Peroxidase[a]	Compound I	Compound II	Compound III	Ref.
MnP	407, 558, 605, 650	420, 528, 555	417, 545, 579	This work
LiP	408, 550, 608, 650	420, 525, 556	419, 543, 578	232
HRP	400, 557, 622, 650	420, 527, 554	413, 546, 583	137
CPO	367, 545, 610, 688	438, 542, 571	432, 555, 586	267 277
LPO	410, 562, 600, 662	433, 537, 568	428, 551, 590	278

[a] Abbreviations: MnP, manganese peroxidase; LiP, lignin peroxidase; HRP,horseradish peroxidase; CPO, chloroperoxidase; LPO, bovine lactoperoxidase.

2.4.2 MnP Compound II

One-electron reduction of HRP compound I by a peroxidase substrate results in the formation of compound II (137,155). This intermediate has a formal oxidation state of IV. Mössbauer (176) and resonance Raman (178-180,268-270) spectroscopy indicate an Fe^{IV}=O structure for HRP compound II. Recent resonance Raman evidence also suggests an Fe^{IV}=O structure for LiP compound II (229). As with HRP compound II and LiP compound II, the Soret maximum of MnP compound II is red-shifted to 420 nm and the visible maxima are at 528 and 555 nm (Fig. 2-2, Table 2-2). In contrast to HRP compound II, the intensity of the Soret maximum of MnP compound II is reduced to ~65% of that of the native enzyme. Under the conditions used for the production of MnP compound II (Fig. 2-2), with no substrate other than H_2O_2 present, the second equivalent of H_2O_2 probably reduces compound I to compound II and presumably is oxidized in turn to $HO_2\cdot/O_2^{-}\cdot$.

2.4.3 Effect of Organic Peroxide on Compound I Formation

HRP is oxidized to compound I by such organic peroxides as methyl and ethyl hydroperoxide and pNPBA (271). Lignin peroxidase (232) is also oxidized to compound I by mCPBA. The addition of one equivalent of either pNPBA or mCPBA oxidizes MnP to compound I (Table 2-1). However, it requires ~25 equivalents of either mCPBA or pNPBA to oxidize native MnP to MnP compound II, suggesting that neither organic peroxide is particularly effective at reducing MnP compound I to compound II.

2.4.4 MnP Compound III

The addition of excess H_2O_2 converts HRP to compound III (137,155,156). The absorption maxima of HRP compound III are at 413, 546, and 583 nm (Table 2-2). The absorption spectrum of the ferrous oxy species of HRP, produced by the addition of oxygen to ferrous HRP (137,272), is very similar to that of HRP compound III. HRP compound III contains four oxidizing equivalents over the ferrous state of the enzyme (137,216). These studies suggest that HRP compound III is either a ferric superoxide complex ($Fe^{III}O_2^{-\cdot}$) or a ferrous oxy complex ($Fe^{II}O_2$) (137,264) (Fig. 2-7). The addition of excess H_2O_2 to native MnP yields an intermediate with absorption maxima at 417, 545 and 579 nm (Fig. 2-3A, Table 2-2). MnP compound III may also be formed by the addition of O_2 to the ferrous enzyme (Fig. 2-3B, Table 2-1). The amount of H_2O_2 required to produce MnP compound III (~250 equivalents) is similar to that required to produce HRP compound III (137) but considerably more than that required to produce LiP compound III (232).

2.4.5 Catalytic Cycle of MnP

The oxidation of phenols and other organic substrates by MnP is dependent on Mn^{II} (98,104). Apparently the enzyme first oxidizes Mn^{II} to Mn^{III}, which subsequently oxidizes the organic substrates (104,105, 108). In order to elucidate the role of Mn^{II} in the mechanism of the enzyme, we examined the ability of Mn^{II} and various phenols to reduce the oxidized states, compounds I and II of MnP. The catalytic cycles

of HRP and LiP follow the path: native enzyme → compound I → compound II → native enzyme. In the process, compound I is reduced back to the native enzyme via two one-electron steps (155,156,232). A similar pathway has been found for MnP. Addition of one equivalent of Mn^{II} rapidly reduces MnP compound I to compound II. A second equivalent of Mn^{II} rapidly reduces MnP compound II to the native ferric form (Fig. 2-4A) with the oxidation of Mn^{II} to Mn^{III} as previously shown (104, 108). Similarly, MnP compound I is reducible by phenolic substrates. The addition of one equivalent of syringic acid or p-cresol reduces MnP compound I to MnP compound II, albeit at a slower rate (Fig. 2-4A). However, the addition of a second equivalent of either of these phenols to the MnP compound II so formed does not lead to its reduction to the native enzyme (Fig. 2-4A). In contrast, the addition of one equivalent of Mn^{II} to MnP compound II formed by the reduction of MnP compound I, rapidly reduces MnP compound II to the native enzyme (Fig. 2-4A).

MnP compound II was prepared directly by the addition of two equivalents of H_2O_2 to the native enzyme. As shown in Fig. 2-4B, the addition of one equivalent of Mn^{II} to MnP compound II rapidly reduces this intermediate to the native enzyme. In contrast, the addition of one equivalent of SA to MnP compound II has no effect. Multiple equivalents of phenols do reduce MnP compound II; however, the conversion is very slow. For example, the $t_{1/2}$ for conversion of MnP compound II to the native enzyme by one equivalent of Mn^{II} is <10 seconds, while the $t_{1/2}$ for the conversion of MnP compound II to the

native enzyme by 20 equivalents of SA or guaiacol is 72 and 160 seconds, respectively. Thus, it appears that the enzyme cannot efficiently complete its catalytic cycle in the absence of Mn^{II}. This explains the absolute Mn^{II} requirement for enzymatic activity.

The one-electron reductant, ferrocyanide, is also capable of reducing the oxidized states of MnP. Addition of one equivalent of ferrocyanide reduces MnP compound I to MnP compound II. Subsequent addition of a second equivalent of ferrocyanide reduces MnP compound II to the native enzyme (Fig. 2-5A). This titration confirms that MnP compound I is reduced back to the native enzyme via two single electron steps. Although ferrocyanide is able to reduce the oxidized states of MnP, the Fe^{III} formed in the reaction cannot oxidize the phenolic substrates, as shown in Figs. 2-5b and 2-6. This is predicted by the relative redox potentials of Fe^{III} and the phenolic substrates (see below).

All of these results indicate the interrelationship between the redox states of the enzyme as depicted in Fig. 2-7. Formally, peroxidases can exist in five redox states from 2+ to 6+ (156). Earlier, we observed the native ferric and ferrous forms of the enzyme (104). Together with the spectral characterization of compounds I, II, and III reported here, we have now demonstrated all five oxidation states of the enzyme. In addition, we have shown that both Mn^{II} and phenols are able to reduce MnP compound I to MnP compound II, although the rate of reduction with Mn^{II} is faster; however, only Mn^{II} can efficiently reduce MnP compound II to the native enzyme.

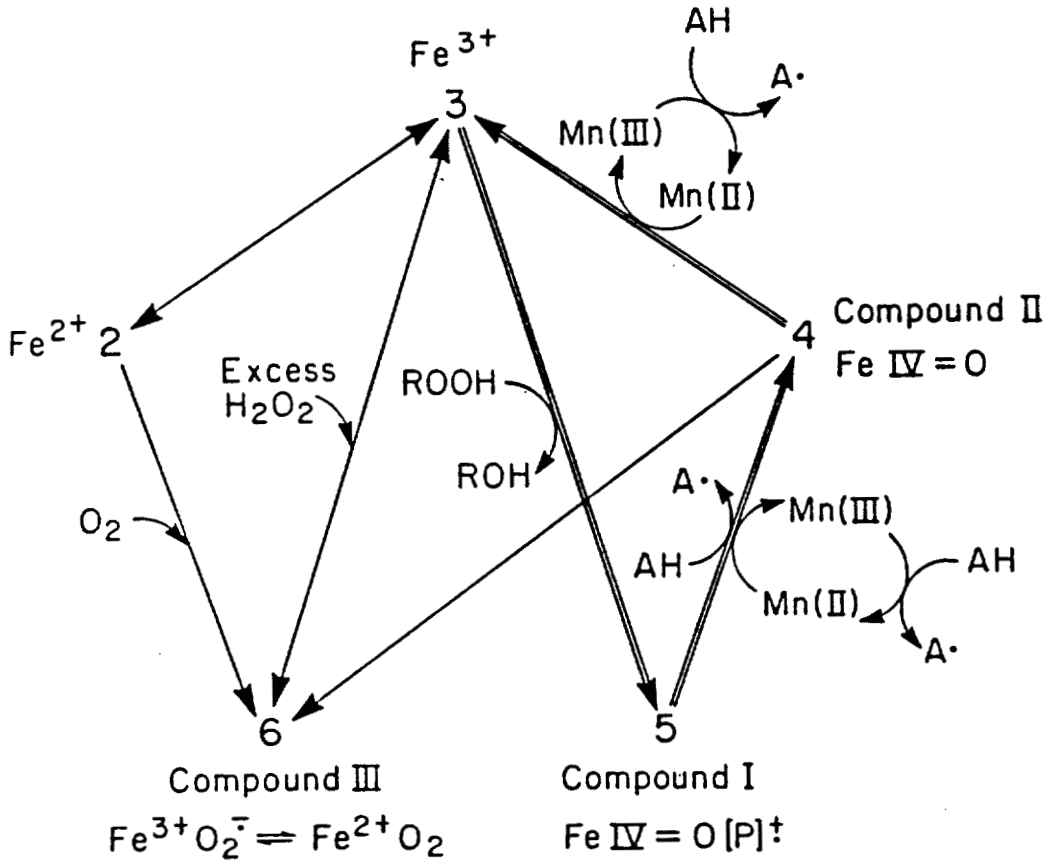

Fig. 2-7. **Interrelationships among the five oxidation states of MnP.** Reaction paths 3 → 5 → 4 → 3 indicate one catalytic cycle of the enzyme. AH = organic substrate.

In previous work, Glenn et al. demonstrated that MnP cannot oxidize Co^{II} or Ni^{II} (108). The oxidation/reduction potentials for Co^{III}/Co^{II}, Mn^{III}/Mn^{II}, and $[Fe(CN)_6]^{3-}/[Fe(CN)_6]^{4-}$ are approximately 1.8, 1.5, and 0.36 volts, respectively (273), suggesting that, solely based on thermodynamics, the oxidation/reduction potentials for MnP compounds I and II are sufficient to allow both oxidized states to oxidize the terminal substrate, guaiacol, with an oxidation reduction potential of 0.75 volts (274). Thus, other factors must hamper the oxidation of guaiacol by MnP compound II. Guaiacol and the other organic substrates may not have ready access to the catalytic center of MnP compound II. As described above, the two oxidizing equivalents carried by HRP compound I and presumably by MnP compound I reside in an Fe^{IV}=O center and a porphyrin π-cation radical. In the conversion of compound I to compound II, the porphyrin π-cation radical is reduced back to a normal porphyrin. This suggests that the porphyrin radical is exposed as a peripheral site as recently suggested (208) and this peripheral site may be sterically available to both larger phenols and amines as well as to Mn^{II} and Fe^{II}. In contrast, the Fe^{IV}=O center in MnP compound II may be partially buried and only fully available to the Fe^{II} and Mn^{II} ions.

To our knowledge, this fungal peroxidase is the only known enzyme system which utilizes freely diffusible Mn^{II}/Mn^{III} as an obligatory redox couple. This arrangement has several advantages. Most importantly, the redox potential of Mn^{II}/Mn^{III} falls between those of the

enzyme's oxidized states and the terminal phenolic substrates. In addition, the complexes formed by Mn^{III} and α-hydroxy acids such as lactate (104) are stable, yet have a high redox potential (275,276). Finally, both Mn^{II} and Mn^{III} are soluble and relatively stable oxidation states in aqueous medium. Our present results appear to account for the manganese dependence of this unique manganese peroxidase.

CHAPTER 3

TRANSIENT STATE KINETICS AND REACTION MECHANISM OF MANGANESE PEROXIDASE[*1]

3.1 INTRODUCTION

Lignin is a heterogeneous and random phenylpropanoid polymer that comprises 20-30% of woody plants (14). White-rot basidiomycetes are primarily responsible for the initiation of the decomposition of lignin in wood (29-31). When cultured under ligninolytic conditions the white-rot fungus Phanerochaete chrysosporium secretes two extracellular heme peroxidases which, along with an H_2O_2-generating system (30) appear to be major components of its lignin degradative system. These peroxidases, manganese peroxidase (MnP)[*2] and lignin peroxidase

---

[*1] The contents of this chapter have been published; Manganese Peroxidase from the Lignin-degrading Basidiomycete Phanerochaete chrysosporium: Transient State Kinetics and Reaction Mechanism. H. Wariishi, H. B. Dunford, I. D. MacDonald, and M. H. Gold (1989) J. Biol. Chem. **264**, 3335-3340 (Ref. 257)

(LiP), have been purified to homogeneity and characterized (98-101, 103,104). MnP is a glycoprotein of M_r ~46,000 with one iron protoporphyrin IX prosthetic group (104,105). The enzyme catalyzes the H_2O_2- and Mn^{II}-dependent oxidation of a variety of phenols, amines, and dyes (104,105,108). Electronic absorption (104,108), EPR, and resonance Raman spectral evidence (252) indicate that the heme iron in the native protein is in the high spin, pentacoordinate, ferric state with histidine coordinated as the fifth ligand.

It has also been demonstrated that MnP oxidizes Mn^{II} to Mn^{III} and that the Mn^{III} produced, in turn, oxidizes the organic substrates (104,105,108,256). Thus, the Mn ion participates in the reaction as a redox couple rather than acting as an enzyme-binding activator. Our initial optical spectral characterization of the oxidized intermediates MnPI, MnPII, and MnPIII (256) indicated that the oxidation states and catalytic cycle of MnP are similar to *HRP* and *LiP* as shown below.

$$\mathrm{MnP} + \mathrm{H_2O_2} \xrightarrow{k_1} \mathrm{MnPI} + \mathrm{H_2O} \qquad [3\text{-}1]$$

$$\mathrm{MnPI} + \mathrm{Mn^{II}} \xrightarrow{k_2} \mathrm{MnPII} + \mathrm{Mn^{III}} \qquad [3\text{-}2]$$

$$\mathrm{MnPII} + \mathrm{Mn^{II}} \xrightarrow{k_3} \mathrm{MnP} + \mathrm{Mn^{III}} \qquad [3\text{-}3]$$

$$\mathrm{Mn^{III}} + \mathrm{AH} \xrightarrow{k_4} \mathrm{Mn^{II}} + \mathrm{A}\cdot \qquad [3\text{-}4]$$

These experiments also demonstrated that although Mn^{II} and a variety of phenols are capable of reducing MnPI to MnPII (eq. 3-2), only Mn^{II} is capable of reducing MnPII to the native enzyme (eq. 3-3). Herein, we utilize transient state kinetics to determine the rate of formation of MnPI and the rate of reduction of MnPI and MnPII using Mn^{II} or p-cresol as reducing substrates. Values of k_1, k_2 and k_3 were measured directly and reactions were conducted under pseudo-first-order conditions with excess substrate, which facilitated data analysis.

3.2 EXPERIMENTAL PROCEDURES

3.2.1 Enzyme Preparation

Manganese peroxidase was purified from the extracellular medium of acetate-buffered agitated cultures of P. chrysosporium as described (98,99,104) except that the medium contained 0.1% Tween 80 and 6-fold concentrated trace elements (102,279), and benzyl alcohol (6 mM) was added on day 3. Cultures were harvested when maximal MnP activity was observed (day 5 or 6).

---

*2 Abbreviations:
MnP, manganese peroxidase; LiP, lignin peroxidase; MnPI, MnPII and MnPIII, manganese peroxidase compounds I, II and III; HRP, HRPI and HRPII, horseradish peroxidase and its compounds I and II; AH organic reducing substrate; m-CPBA, m-chloroperoxybenzoic acid; p-NPBA, p-nitroperoxybenzoic acid.

The purified protein was electrophoretically homogeneous and had an RZ (A_{406}/A_{280}) value of 6.1. Enzyme concentrations were determined at 406 nm using an extinction coefficient of 129 mM^{-1} cm^{-1} (5). The homogeneous enzyme was dialyzed exhaustively against glass-distilled, filtered water before use.

3.2.2 Kinetic and Spectral Analyses

Kinetic measurements were conducted using the Photal (formerly Union Giken) RA 601 Rapid Reaction Analyzer equipped with a 1-cm observation cell and interfaced with a digital computer system (Sord M200 Mark III). One reservoir contained enzyme in water, at a concentration of 1.0 μM after mixing, while the other reservoir contained the substrate (H_2O_2, Mn^{II} or p-cresol) and buffer. All experiments were performed at (25 $\pm$ 0.5)°C in 20 mM sodium lactate buffer or otherwise as indicated in the text. The pH was varied from 3.12 to 8.29. MnPI was prepared by adding 0.9 equiv. H_2O_2 to native MnP. MnPII was obtained by the successive addition of 1.0 equiv. ferrocyanide and 0.9 equiv. H_2O_2. All enzyme samples were freshly prepared for each experiment. The substrate concentrations were at least 10 times in excess to maintain pseudo-first-order kinetics. The pseudo-first-order rate constants were determined by a nonlinear least squares computer analysis of the exponential traces. Experiments were conducted with stable solutions of native MnP, MnPI or MnPII (13) placed in the stopped-flow apparatus, for the direct determination of k_1, k_2 or k_3. Electronic absorption spectra were recorded on a

Shimadzu UV-260 at room temperature with a spectral band width of 1.0 nm and cuvettes of 1-cm light path.

3.2.3 Chemicals

H_2O_2 (30% solution) and peracetic acid (40%) were obtained from BDH Chemicals and FMC Corp., respectively. Other organic peroxides and p-cresol were purchased from Aldrich. All other chemicals were of reagent grade. Solutions were prepared using deionized water obtained from the Milli Q System (Millipore). The concentration of H_2O_2 was determined by the HRP assay (280).

3.3 RESULTS

3.3.1 Spectral Characteristics

Spectra of native MnP, MnPI and MnPII in the Soret region (256) are compared in Fig. 3-1. Isosbestic points between native MnP and MnPI occur at 426 and 358 nm, between native MnP and MnPII at 417 nm, and between MnPI and MnPII at 397 nm. In our previous work (256) MnPII was prepared by adding 2 equivalents of H_2O_2 to the native enzyme. In the present study, with the successive addition of stoichiometric amounts of ferrocyanide and H_2O_2, the absorbance of the MnPII Soret peak was 10% higher than the value we obtained previously, but had the identical λ_{max} at 420 nm.

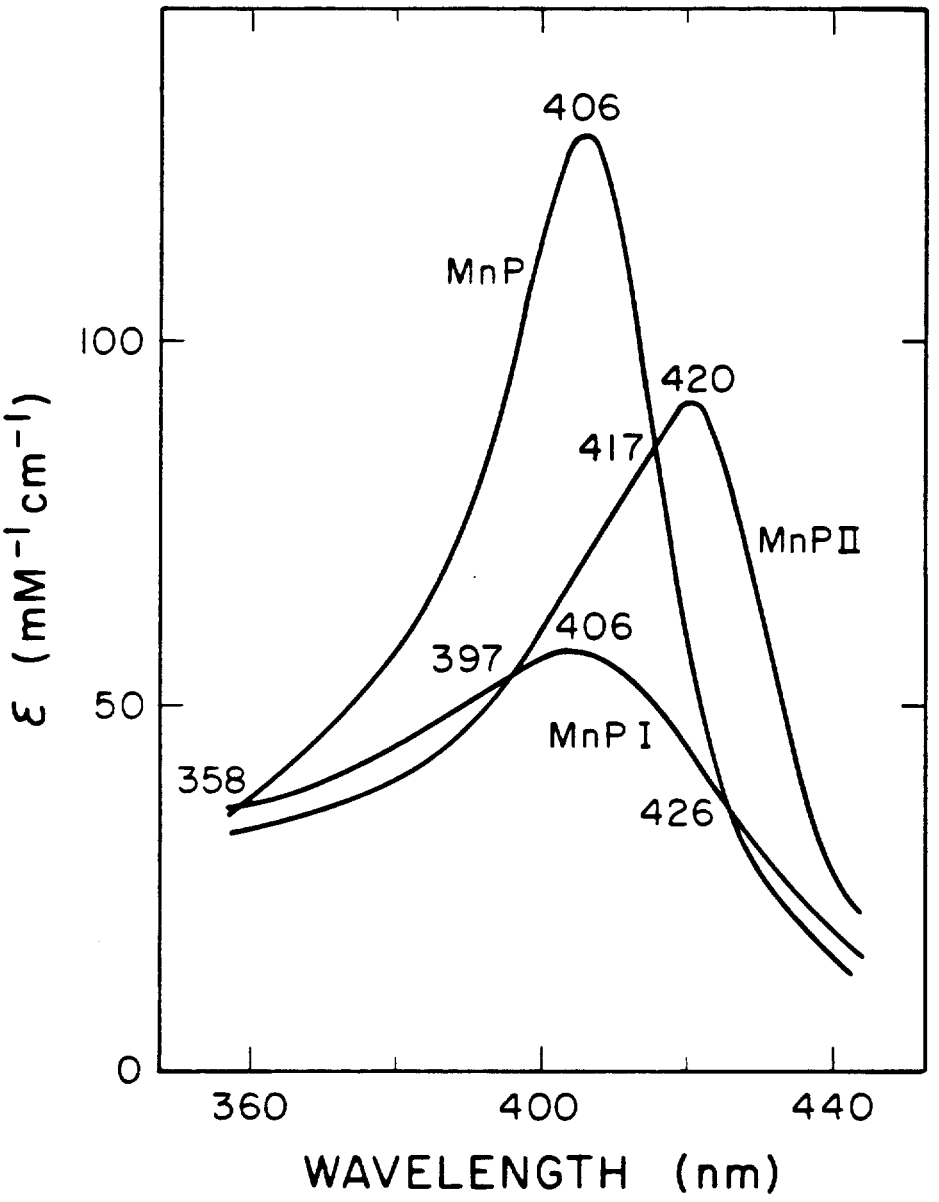

Fig. 3-1. **Electronic absorption spectra of native MnP, of MnPI and of MnPII in the Soret region.** Spectra were recorded in 20 mM Na-lactate buffer, pH 4.5 at room temperture. To produce MnPI, 1 equiv. of H_2O_2 was added to the native enzyme (5 μM). MnPII was obtained by the successive additions of 1 equiv. each of ferrocyanide and H_2O_2 to the native enzyme. The indicated numbers are the wavelength maxima of the Soret peaks and the isosbestic points in the Soret region.

3.3.2 Formation Rate of MnP Compound I

The rate of compound I formation was determined by measuring absorbance change at 397 nm, the isosbestic point between MnPI and MnPII. Thus, the possible subsequent conversion of MnPI to MnPII did not interfere with the rate measurement. All kinetic traces were of a single exponential character (Fig. 3-2, inset). The observed rate constants (k_{obs}) were linearly proportional to the H_2O_2 concentration from 20 to 100 times in excess. The plot of k_{obs} vs. H_2O_2 concentration (Fig. 3-2) passed through the origin within experimental error, indicating that the formation of MnPI was irreversible. The second order rate constant (k_{1app}) was found to be $(2.0 \pm 0.1) \times 10^6$ $M^{-1}s^{-1}$ (Fig. 3-2). A plot of log k_{1app} vs. pH is shown in Fig. 3-3. The formation of MnPI exhibited no pH dependence over the pH range 3.12 to 8.29. This value did not change significantly when the reaction was conducted in the presence of high ionic strength buffers. MnP activity is stimulated significantly by α-hydroxy acids such as lactate or citrate (98,104,108,256) presumably because these acids chelate the Mn^{III} generated during the reaction. Therefore, as predicted the same rate of formation of MnPI was observed in citrate, succinate or phosphate buffer (Fig. 3-3). The second order rate constants for MnP compound I formation with H_2O_2 and various organic peroxides are listed in Table 3-1.

3.3.3 Activation Energy for MnPI Formation

Using H_2O_2 as the substrate the rate of MnP compound I formation was measured over the temperature range of 3.5 to 34.0°C. The

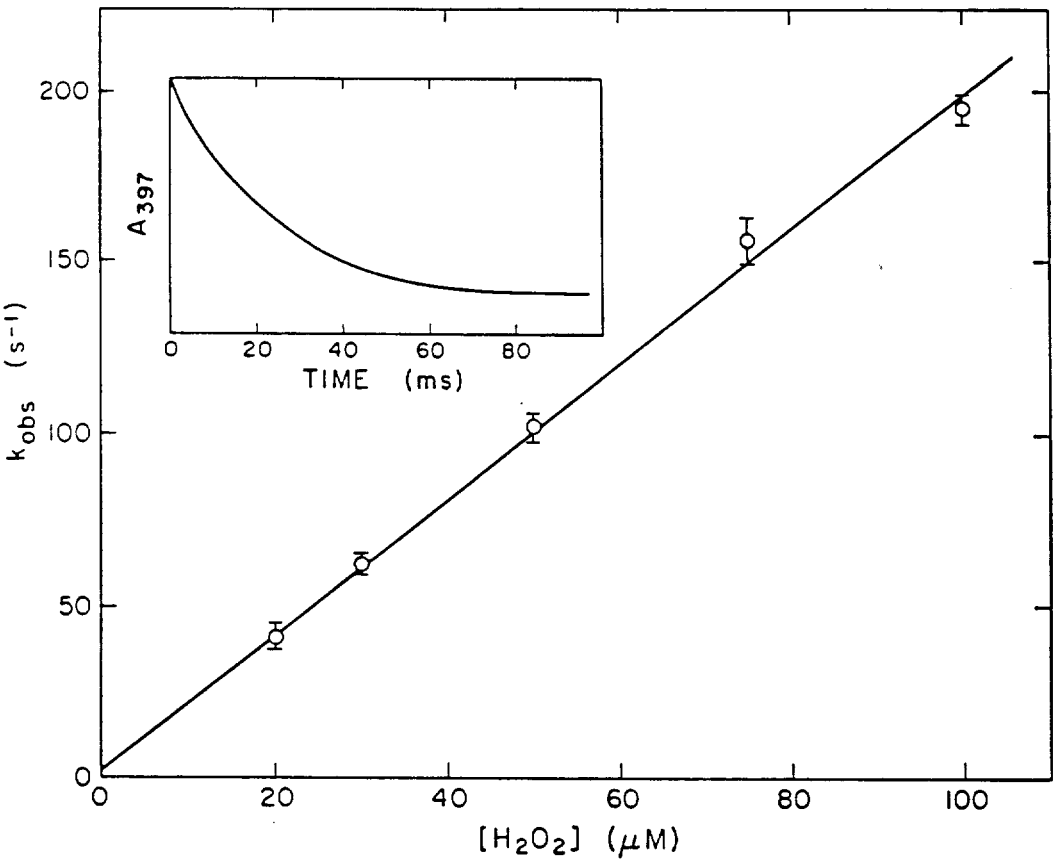

Fig. 3-2. **Plot of k_{obs} vs. H_2O_2 concentration for the reaction of native MnP with H_2O_2.** One syringe contained MnP (1 μM after mixing) and the other syringe contained H_2O_2 in lactate buffer, pH 4.5 (0.02 M after mixing). The inset shows a typical exponential trace (20 μM H_2O_2) from which k_{obs} was determined. The decrease in absorbance at 397 nm (the isosbestic point between MnPI and MnPII) was measured. Each determination of k_{obs} is the mean of 6 traces.

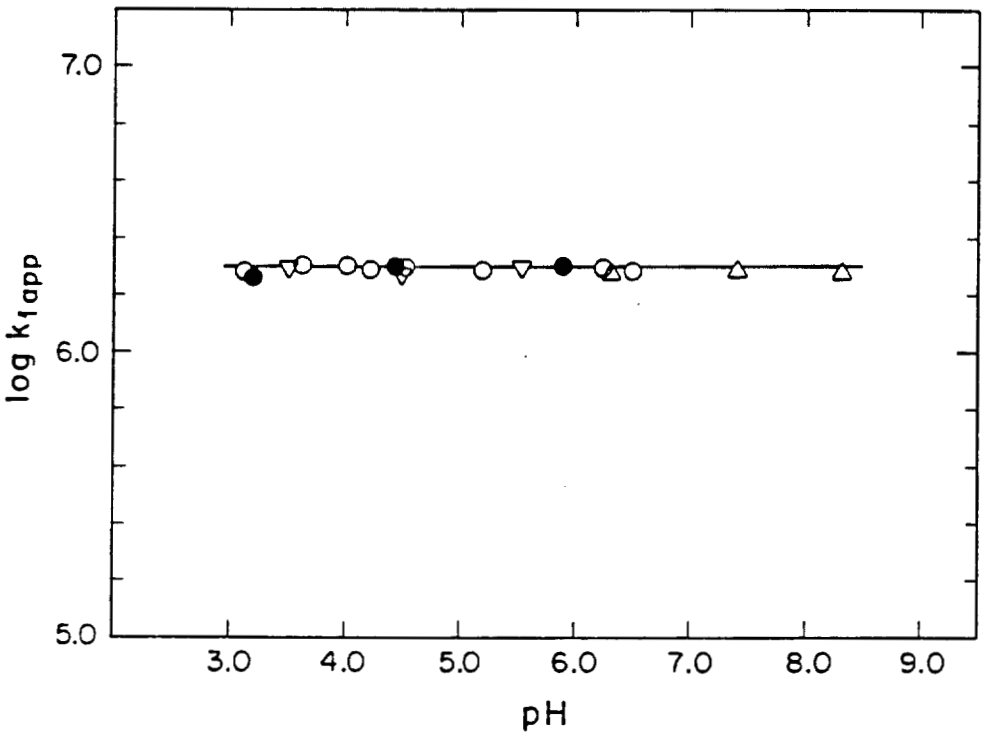

Fig. 3-3. **The pH dependence of MnPI formation.** Experiments were conducted as described in Fig. 3-2. k_{1app} was obtained from the slope of the plot, k_{obs} vs $[H_2O_2]$. Each k_{obs} was calculated from a trace of the change in absorbance at 397 nm (Fig. 3-2 inset). Buffers used were sodium lactate (μ = 0.02) (○); sodium succinate (μ = 0.02) (▽); potassium phosphate (μ = 0.02) (△); and sodium lactate (μ = 0.1) (●). For the latter buffer, K_2SO_4 was added to adjust the ionic strength to 0.1.

Table 3-1. Rate of peroxidase compound I formation with various peroxides[a]

Peroxide	Rate constant ($M^{-1}s^{-1}$)
Hydrogen peroxide	$(2.0 \pm 0.1) \times 10^6$
Peracetic acid	$(9.7 \pm 0.2) \times 10^5$
m-Chloroperoxybenzoic acid	$(9.5 \pm 0.2) \times 10^4$
p-Nitroperoxybenzoic acid	$(5.9 \pm 0.1) \times 10^4$

[a] k_{1app} was obtained from the slope of the plot of k_{obs} vs. [peroxide]. k_{obs} was determined as described in Fig. 3-2.

temperature dependence of the second order rate constants is presented as an Arrhenius plot (Fig. 3-4). The activation energy calculated from the slope of the plot was (4.9 ± 0.1) kcal mol^{-1} or (20.7 ± 0.5) kJ mol^{-1}.

3.3.4 Reduction of MnP Compound I

The reduction of MnPI to MnPII was followed at 417 nm, the isosbestic point between native MnP and MnPII (Fig. 3-1). Pseudo-first-order conditions were employed using an excess of reducing substrate, p-cresol or Mn^{II} (as $MnSO_4$) at pH 4.51, the pH optimum for MnP activity (104,105,108).

A linear dependence of k_{obs} on p-cresol concentration was observed between 0-1.0 mM (Fig. 3-5). The second order rate constant, k_{2app}, for the reaction of MnPI with p-cresol, calculated from the slope of the plot in Fig. 3-5, was found to be (1.8 ± 0.2) × 10^3 M^{-1} s^{-1}.

In contrast, with Mn^{II} as the reducing substrate, the plot of k_{obs} vs. [Mn^{II}] leveled off at high Mn^{II} concentrations (Fig. 3-6). This behavior can be described by a simple binding interaction between reactants according to equations 3-5 and 3-6 (Appendix A),

$$\text{MnPI} + \text{Mn}^{\text{II}} \underset{}{\overset{K_1}{\rightleftharpoons}} \text{MnPI} - \text{Mn}^{\text{II}} \xrightarrow{k_5} \text{MnPII} + \text{Mn}^{\text{III}} \qquad [3\text{-}5]$$

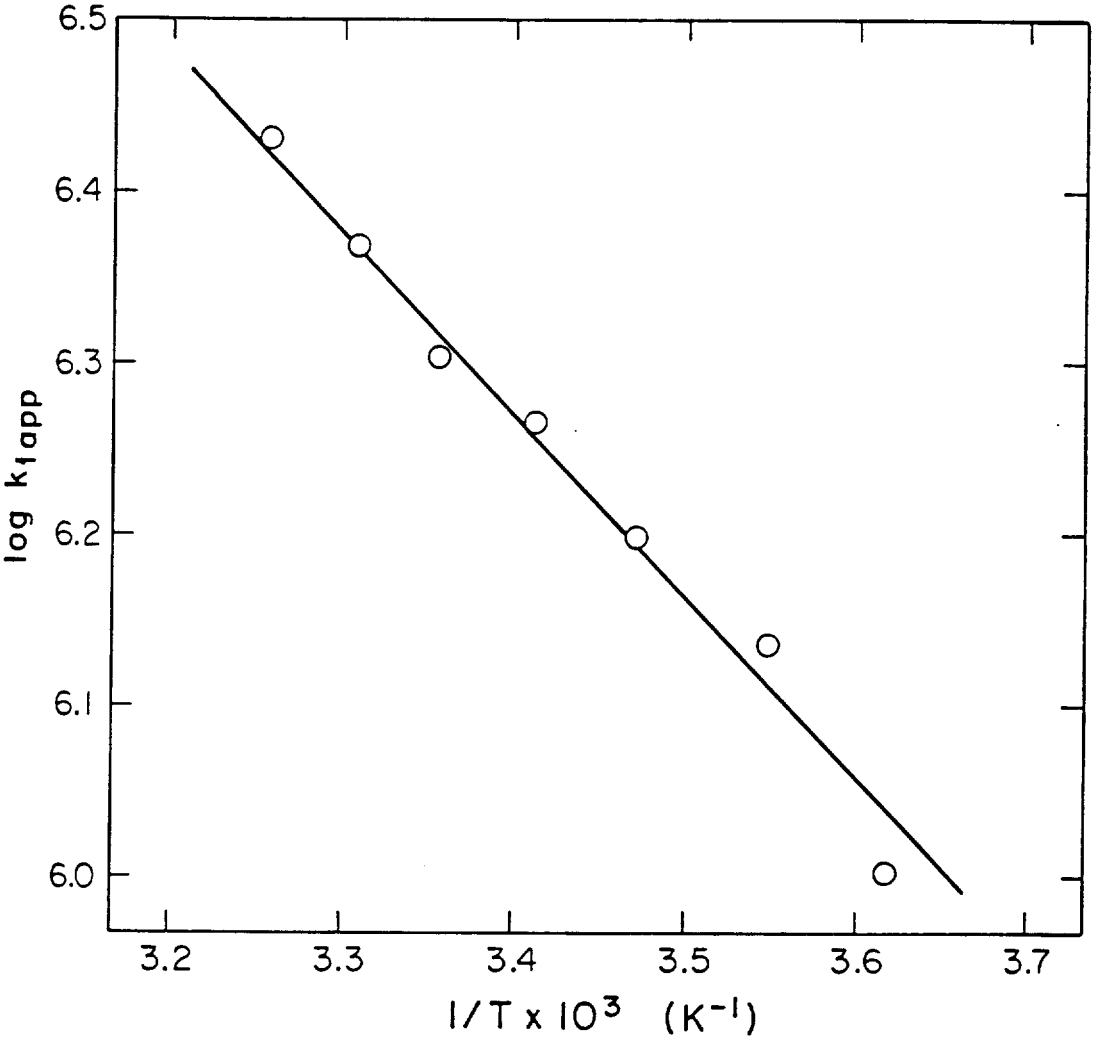

Fig. 3-4. **Arrhenius plot for MnP compound I formation.** Values of $k_1$app were obtained as in Fig. 3-3. The temperature was varied from 3.5 to 34.0°C. The buffer used was 20 mM Na-lactate, pH 4.5.

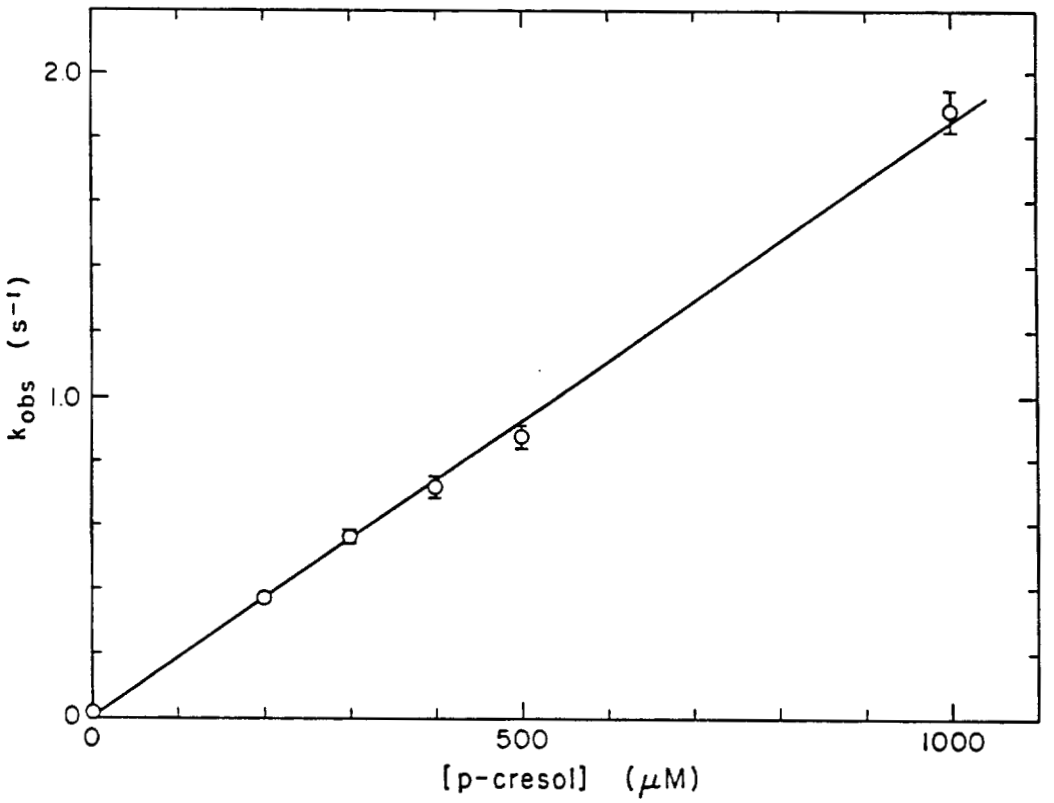

Fig. 3-5. **Reaction of MnPI with p-cresol.** One drive syringe contained MnPI in H_2O and the other syringe contained p-cresol in Na-lactate buffer, pH 4.51 (μ = 0.02 after mixing). k_{obs} was determined from the exponential change in absorbance at 417 nm (the isosbestic point between native MnP and MnPII) as a function of time. The linear plot of k_{obs} vs. p-cresol concentration indicates that any complex between compound I and p-cresol is too short-lived to detect under these experimental conditions.

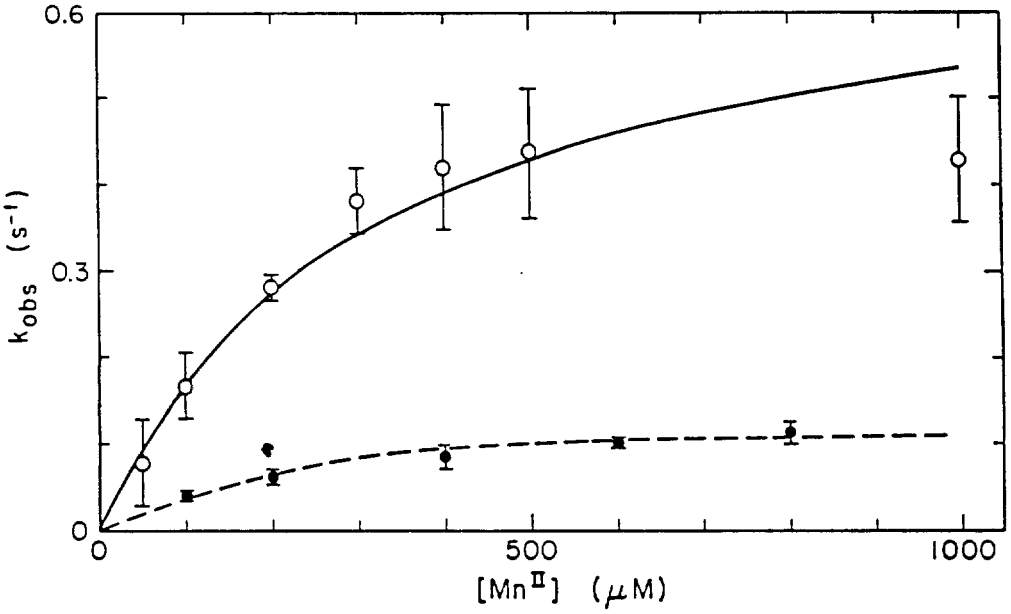

Fig. 3-6. **Reaction of MnPI with Mn^{II}.** Experimental conditions were as in Fig. 3-5, except that Mn^{II} was the reducing substrate. The buffers used were 20 mM Na-lactate (pH 4.51) (———) and 20 mM Na-succinate, pH 4.49 (– – –). The plot of k_{obs} vs. Mn^{II} concentration was a nonlinear least squares fit of the data. Eq. 3-6 in the text was used for the curve fit.

$$k_{5\ obs} = \frac{k_5}{1 + \frac{K_1}{[Mn^{II}]}} \qquad [3\text{-}6]$$

where k_5 is a first order rate constant (s^{-1}) and K_1 is an apparent dissociation constant (M) given by eq. 3-7.

$$K_1 = \frac{[MnPI]\ [Mn^{II}]}{[MnPI - Mn^{II}]} \qquad [3\text{-}7]$$

The constants, k_5 and K_1, were calculated from equation 6 using a non-linear least squares fit to the data. The calculated curve is shown in Fig. 3-6; k_5 and K_1 were determined to be (0.7 ± 0.1) s^{-1} and (3.3 ± 0.8) × 10^{-4} M, respectively. The reduction of MnPI by Mn^{II} was also performed in Na-succinate (μ = 0.02 M) at pH 4.49 where saturation kinetics were again observed (Fig. 3-6). With this buffer which cannot chelate Mn^{III} readily (8,11), values of k_5 and K_1 were (0.13 ± 0.01) s^{-1} and (2.3 ± 0.2) × 10^{-4} M, respectively. The curve fit computed from equation 3-6 is also shown in Fig. 3-6. Finally, when the reaction was conducted in citrate buffer (μ = 0.02 M) at pH 4.42, the values for k_5 and K_1 were similar to those found with lactate buffer.

3.3.5 Redution of MnP Compound II

Reduction of MnPII to native MnP was followed at 420 nm at pH 4.51 under pseudo-first-order conditions with reducing substrate, p-cresol or Mn^{II} in excess. With p-cresol as the reducing substrate a linear relationship between k_{obs} and substrate concentration (0-10 mM) was observed (data not shown). The second order rate constant (k_{3app}) for the reaction of MnPII with p-cresol was calculated to be 9.5 ± 0.5 $M^{-1}s^{-1}$. This is an extremely small value for a peroxidase compound II reduction. The initial rate of substrate oxidation in a reaction mixture consisting of 1.0 μg/mL enzyme, 0.1 mM phenolic substrate and excess H_2O_2 would be approximately 1×10^{-3} nmol min^{-1} μg^{-1}. With such a slow rate of reduction of MnPII the catalytic cycle of the enzyme would be stopped. This explains why MnP requires Mn^{II} to complete its catalytic cycle (256).

With Mn^{II} as the reducing substrate for MnPII, saturation kinetics were observed. This reaction can be described by equations 3-8 to 3-10 which are analogous to equations 3-5 to 3-7 (Appendix B).

$$\text{MnPII} + Mn^{II} \underset{}{\overset{K_2}{\leftrightarrows}} \text{MnPII} - Mn^{II} \overset{k_8}{\rightarrow} \text{MnP} + Mn^{III} \qquad [3\text{-}8]$$

$$k_{8\ obs} = \frac{k_8}{1 + \frac{K_2}{[Mn^{II}]}} \qquad [3\text{-}9]$$

$$K_2 = \frac{[MnPII]\,[Mn^{II}]}{[MnPII - Mn^{II}]} \qquad [3\text{-}10]$$

Using equation 3-9 and the same nonlinear least squares analytical method, the first order rate constant (k_8) and dissociation constant (K_2) were found to be $(0.14 \pm 0.01)\ s^{-1}$ and $(4.4 \pm 0.8) \times 10^{-4}$ M. The fit of the calculated curve to the data is shown in Fig. 3-7. Table 3-2 summarizes the kinetic parameters obtained from these transient state kinetic studies on the reductions of MnPI and MnPII.

3.4 DISCUSSION

Manganese peroxidase is a heme-containing enzyme isolated from the extracellular medium of ligninolytic cultures of the white-rot basidiomycete P. chrysosporium (98,104,105,108). In the presence of Mn^{II}, the enzyme catalyzes the H_2O_2-dependent oxidation of a variety of amines, organic dyes and phenols including phenolic lignin model compounds (31,98,104,105,108,256). The catalytic activity is dramatically stimulated by α-hydroxy acids such as lactate and citrate and it has been suggested that α-hydroxy acids complex Mn^{III}, thus stabilizing its high redox potential (104,108,256). Recent studies (104,105,108,256) have shown that the enzyme oxidizes Mn^{II} to Mn^{III} and that the Mn^{III} acts as an obligatory redox couple, oxidizing

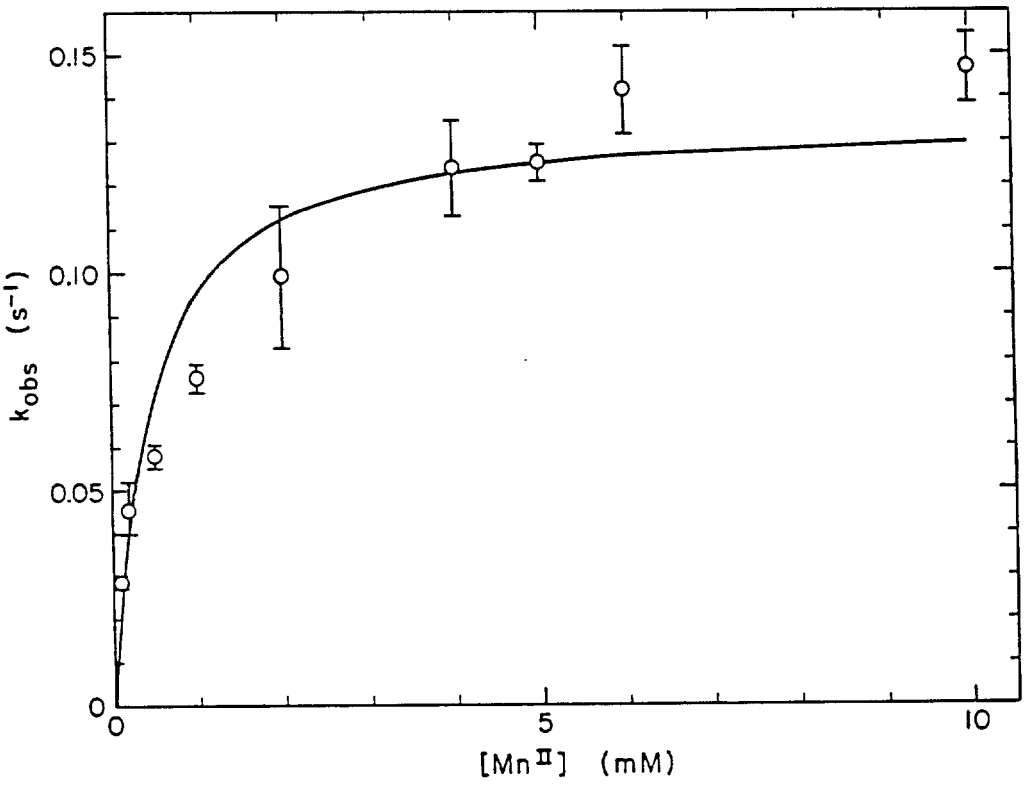

Fig. 3-7. **Reaction of MnPII with Mn^{II}.** MnPII was prepared by the successive addition of 1.0 equiv. of ferrocyanide and 0.9 equiv. of H_2O_2 to native MnP in water. Mn^{II} in Na-lactate, pH 4.5 (μ = 0.02 after mixing) was added to the enzyme and the exponential change in absorbance was measured at 420 nm as a function of time. k_{obs} was determined from a mean of 4-6 experimental traces. The plot of k_{obs} vs. Mn^{II} concentration is a nonlinear least squares fit of the data. Eq. 3-9 in the text was used for the curve fit.

Table 3-2. Parameter values for the reactions of MnPI and MnPII

Oxidized enzyme	Substrate	Second order rate constant $(M^{-1}s^{-1})^a$	First order rate constant $(s^{-1})^b$	Apparent dissociation constant $(M)^c$
MnPI	Mn^{II}	-----	0.7 ± 0.1	$(3.3 \pm 0.8) \times 10^{-4}$
		-----	0.13 ± 0.01[d]	$(2.2 \pm 0.2) \times 10^{-4}$[d]
	p-cresol	$(1.8 \pm 0.2) \times 10^{3}$	-----	-----
MnPII	Mn^{II}	-----	0.14 ± 0.01	$(4.4 \pm 0.8) \times 10^{-4}$
	p-cresol	9.5 ± 0.5	-----	-----

[a] Given as k_{2app} and k_{3app} in the text

[b] Given as k_5 and k_8 in the text

[c] Given as K_1 and K_2 in the text

[d] The data obtained in succinate buffer

various organic substrates. The prosthetic group of MnP is iron protoporphyrin IX (104,252). In this respect MnP resembles other fungal and plant peroxidases. Recently we were able to prepare the oxidized intermediates of MnP, compounds I, II and III, in the presence of stoichiometric amounts of H_2O_2 (104,256). Each of these intermediates has spectral characteristics similar to those of HRP (137) and lignin peroxidase (232). In addition, titration of MnPI with ferrocyanide demonstrated that MnPI was reduced back to the native enzyme via two single electron steps (256) with MnPII as an intermediate. Furthermore, we demonstrated that although both Mn^{II} and phenols are able to reduce MnPI to MnPII, only Mn^{II} is capable of efficiently reducing MnPII to the native enzyme (256). These findings indicate that the catalytic cycle of MnP is similar to that of HRP and LiP as shown in equations 3-1 through 3-3, and they explain the absolute dependence of the catalytic activity on Mn^{II}. To understand more fully the mechanism of MnP and the role of Mn^{II} and α-hydroxy acids in the catalytic cycle, the transient state kinetics of MnPI formation and of MnPI and MnPII reductions were studied at the pH optimum (4.5) and under pseudo-first-order conditions with substrate in excess.

3.4.1 Formation of MnP Compound I

The primary reaction product of peroxidases with H_2O_2 is the oxidized intermediate compound I. This intermediate accepts both oxidizing equivalents of H_2O_2 and thus contains two oxidizing

equivalents above the native enzyme (137,176,184). The electronic absorption spectrum of MnPI, Soret maximum at 406 nm with reduced intensity (Fig. 3-1) (256) and additional maxima at 558 and 650 nm (256) is very similar to that of HRP (137) and LiP (232,260). The reduced Soret intensity suggests the π-cation radical nature of the MnP compound I porphyrin ring (155,184). The activation energy for MnPI formation (4.9 kcal mol^{-1}) is also in the same range as that of other peroxidases: 3.5 kcal mol^{-1} for HRP (196), 5.9 kcal mol^{-1} for LiP (261) and 2.9 and 5.4 kcal mol^{-1} for turnip peroxidase isoenzymes P_1 and P_7, respectively (281).

The pH dependence of the formation rate of compound I has been studied with a variety of peroxidases. These studies indicate that peroxidases possess a distal ionizable group which controls the pH dependence of compound I formation. Its pK value has been reported to be in the range of 3.0-5.3 (104,193,278,282-284). Based on the crystal structure of cytochrome c peroxidase, Poulos and Kraut (285) proposed that the distal histidine serves as an acid base catalyst participating in the heterolytic cleavage of H_2O_2. Although MnPI is similar to other peroxidases in its spectral features and activation energy of formation, the second order rate constant for MnPI formation using H_2O_2 as the substrate (k_1) is independent of pH over the range 3.12-8.29 (Fig. 3-3). This may account for the decreased rate of MnPI formation. k_1 was found to be 2.0×10^6 $M^{-1}s^{-1}$, which is 5-10 times smaller than for most other peroxidases (137,278,283,284). The same pH independence was observed for LiPI formation, which also has a

smaller k_1 value (260,261). Since either ionic strength or nitrate or acetate have been reported to shift the apparent pK of HRP (193,286), k_1 for MnPI formation was also determined at higher ionic strength. However, no effect was observed in lactate buffer with added K_2SO_4 (μ = 0.1 M) (Fig. 3-3). Similarly, no effect of ionic strength was seen with LiPI formation (261). Furthermore, the value of k_1 was essentially unchanged in succinate and phosphate buffers, indicating that α-hydroxy acids have no effect on MnPI formation (Fig. 3-3). The pH independence of MnPI and LiPI formation is interesting in view of the cDNA sequence of MnP (254,255) and LiP (233-235). In both proteins the distal histidine as well as adjacent residues including the distal arginine are conserved. If as proposed (285) the distal ionizable group in HRP and CCP is the distal histidine, then the pK of the relevant histidine must be significantly shifted in MnP and LiP. This might occur if the histidine were in a hydrophobic pocket, yet still accessible to H_2O_2. It is also possible that another ionizable group is responsible for the pH dependence of peroxidase compound I formation. The decreased second order rate constants for MnPI formation observed with organic peroxides are probably due to steric constraints.

3.4.2 Interaction of MnPI and MnPII with Manganese

The reduction of MnPI and MnPII (equations 3-2 and 3-3) was investigated using p-cresol and Mn^{II} as reducing substrates. To assure single turnover conditions, 0.9 molar equivalent of H_2O_2 was

added to generate MnPI. The reduction of MnPI was measured at 417 nm, the isosbestic point between MnPII and MnP. Therefore, this was a direct assay of the conversion of MnPI to MnPII since any subsequent reduction of MnPII to the native enzyme would not contribute any error to the rate constant (k_{obs}) determination. The plot of k_{obs} vs. p-cresol concentration was linear with zero intercept (Fig. 3-5), indicating that second order kinetics were obeyed.

The reduction of MnPII was followed at 420 nm. The use of only 0.9 equiv. of H_2O_2 and 1.0 equiv. of ferrocyanide to generate MnPII assured a single turnover. Since native MnP, the product of MnPII reduction, does not react with phenolic substrates, there can be no interference from a subsequent reaction. Therefore, the rate of MnPII reduction could be measured at the Soret optimum for MnPII (420 nm). The plot of k_{obs} vs. p-cresol concentration for the reduction of MnPII also showed a linear slope with zero intercept (data not shown). However, k_3 was extremely small (Table 3-2), which apparently explains why the enzyme cannot complete its catalytic cycle efficiently in the absence of Mn^{II} (104,108,256).

When Mn^{II} was used as the reducing substrate for the reduction of both MnPI and MnPII, the plots of k_{obs} vs. Mn^{II} concentration were nonlinear (Fig. 3-6 and 3-7). Nonlinear saturation responses have been observed previously in the reactions of HRPI and HRPII with p-cresol (200,201) and p-aminobenzoic acid (203). This was attributed to a binding interaction between the enzyme and substrate followed by the enzyme reduction; the same explanation is offered for our present

results. The apparent dissociation constants for native MnP complexes were determined from difference spectra between native MnP and MnP plus substrate in lactate buffer at pH 4.5: K_D ~ 4.5 μM for Mn^{II} and ~120 μM for p-cresol (data not shown). These data for the native enzyme are in accord with our findings for MnPI and MnPII, where Mn^{II} forms a complex with the enzyme, which affects the observed kinetics, whereas p-cresol does not.

3.4.3 Role of Organic Acid in MnP Catalytic Action

The reduction of MnPI with Mn^{II} was dependent on the buffer used; k_3 was >5 times larger in lactate and citrate than in succinate. In contrast, the dissociation constants K_1 are approximately the same in either buffer (Table 3-2). This suggests that α-hydroxy acids act to facilitate the dissociation of the enzyme-Mn complex by chelating Mn^{III}. A similar buffer effect was seen for the reduction of MnPII; however, in succinate buffer the rate was too small to obtain accurate values (data not shown). It is also likely that α-hydroxy acids act by stabilizing the Mn^{III} at a high redox potential (108,256). If the stimulation of enzyme activity by α-hydroxy acids occurs in part by accelerating the dissociation of the enzyme-manganese complex, then productive Mn-enzymes are implied. The possibility of non-productive complexes with HRP compounds has been discussed (201).

3.4.4 Manganese as Diffusible Redox Couple

The addition of Mn^{II} and p-cresol to MnPI led to a rate of reduction which was the sum of the individual rates in the presence of a single reducing substrate. This relationship was demonstrated with various concentrations of reducing substrates, indicating that Mn^{II} does not act as an enzyme-binding activator and that the reaction with both substrates present probably does not occur via a ternary complex.

Although the spectral characteristics of the oxidized intermediates of MnP and its catalytic cycle are similar to those of other peroxidases, this enzyme has some unusual properties. Mn^{II} is the preferred substrate especially for MnPII and in the absence of Mn^{II} the enzyme apparently cannot complete its catalytic cycle. The enzyme uses freely diffusible Mn^{II}/Mn^{III} as a redox couple (108,256). The potential of this redox couple falls conveniently between those of the enzyme's oxidized states and the terminal organic substrates (108,256). The Mn^{III}-lactate complex generated is able to oxidize a variety of organic compounds including lignin substructures (31,104,108,256). The effect of α-hydroxy acids apparently occurs via interaction with Mn^{III}. These Mn^{III}-α-hydroxy acid complexes are stable (108,256), yet have a high redox potential (275). Furthermore, the present results suggest that α-hydroxy acids help to facilitate the dissociation of Mn^{III} from the manganese-enzyme complex.

CHAPTER 4

OXIDATIVE CLEAVAGE OF A PHENOLIC DIARYLPROPANE LIGNIN MODEL DIMER BY MANGANESE PEROXIDASE*1

4.1 INTRODUCTION

Lignin is a complex heterogeneous and random phenyl propanoid polymer which constitutes 20-30% of woody plants (14). Since the biodegradation of cellulose is retarded by the presence of lignin (18,29-31), the catabolism and potential utilization of this polymer are of enormous significance. White-rot basidiomycetous fungi are primarily responsible for the initiation of the decomposition of lignin in wood (18,29-31). When cultured under ligninolytic conditions, the white rot basidiomycete Phanerochaete chrysosporium produces two extracellular heme peroxidases (98-101,104) which, along

---

*1 The contents of this chapter have been published; Oxidative Cleavage of a Phenolic Lignin Model Dimer by Manganese Peroxidase from Phanerochaete chrysosporium. H. Wariishi, K. Valli, and M. H. Gold (1989) Biochemistry **28**, 6017-6023 (Ref. 258)

with an H_2O_2-generating system (30), appear to be the major components of its lignin degradative system. The structure and mechanism of lignin peroxidase have been studied extensively (29-31,98-101,103,106, 232). Manganese peroxidase (MnP)*2 has also been purified and characterized (98,104,105,108). This enzyme exists as a series of isozymes (pI 4.2-4.9), contains one iron protoporphyrin IX prosthetic group, and is a glycoprotein of M_r ~46,000 (98,103-105,108). A cDNA encoding an MnP isozyme has recently been isolated and the nucleotide sequence has been determined (254,255). MnP catalyzes the H_2O_2- and Mn^{II}-dependent oxidation of a variety of phenols, amines, and organic dyes (98,104,105,108,256), and its catalytic activity is stimulated by various organic acids such as lactate (98,104,108).

Electronic absorption, EPR, and resonance Raman spectral evidence (31,104,108,252,256) indicates that the heme iron in the native enzyme is in the high-spin pentacoordinate ferric state with histidine coordinated as the fifth ligand. Spectral and kinetic evidence (256,257) indicates that the H_2O_2-oxidized states (compounds I and II) and the catalytic cycle of MnP are similar to those of lignin and horseradish peroxidases. Most importantly, it has been demonstrated

---

*2 Abbreviations:
MnP, manganese peroxidase; BSTFA, N,O-bis(trimethylsilyl) trifluoroacetamide; GCMS, gas chromatography mass spectrometry; TMS, tri-methylsilyl; MS, mass spectrum; FT-NMR, Fourier transform nuclear magnetic resonance.

that MnP oxidizes Mn^{II} to Mn^{III} and that Mn^{III} in turn oxidizes theorganic substrates (104,105,108,256). Transient state kinetic analysis (257) has confirmed that Mn^{II}/Mn^{III} acts as a redox couple rather than as an enzyme binding activator. Kinetic (257) and spectroscopic evidence (104,108,256) indicates that organic acids such as lactate chelate Mn^{III}, thereby facilitating its release from the manganese-enzyme complex. In addition, chelation by organic acids also stabilizes the Mn^{III} at a relatively high redox potential (0.9-1.2 V) (275,289). Preliminary studies on the substrate specificity of the enzyme system have also been reported (98,104,105,108). These studies have utilized simple phenols, aromatic amines, and dyes. Since 15-20% of the phenylpropanoid units of native lignin are free phenols (14), it has been assumed that the oxidation of these phenolic units by MnP results in polymeric degradation. Herein, we report the mechanism of oxidative cleavage of a free phenolic lignin substructure by MnP. These results imply a role for the enzyme in the degradation of lignin.

4.2 EXPERIMENTAL PROCEDURES

4.2.1 Enzyme Preparation

Manganese peroxidase isozyme 1 was purified from the extracellular medium of an acetate-buffered agitated culture of *P. chrysosporium* strain OGC101 (290) as previously reported (104,257).

The purified enzyme was electrophoretically homogeneous and had a pI of 4.9.

4.2.2 Enzyme Reactions

Model compound oxidations were carried out at 37°C for 30 minutes in 1 ml of 50 mM sodium lactate, pH 4.5 (citrate, malonate, or oxalate were substituted for lactate as indicated), containing MnP (5 μg), substrate (0.2 mM), and $MnSO_4$ (0.5 mM). Reactions were initiated by adding H_2O_2 (0.2 mM).

4.2.3 ^{18}O Incorporation Experiments

For experiments conducted under $^{18}O_2$, reaction vessels contained enzyme, $MnSO_4$, 50 mM Na-lactate, and substrate in one compartment and H_2O_2 in the other. The vessels were evacuated, flushed with scrubbed argon (3x), and equilibrated with $^{18}O_2$ (95%, Monsanto Research Corp.) as previously described (98,231) after which the contents were mixed.

For experiments conducted in $H_2{}^{18}O$, reaction mixtures were enriched with $H_2{}^{18}O$ (60%) and incubated under 100% O_2 or argon as previously described (231).

4.2.4 Oxidation of Diarylpropane I by Mn^{III}-Malonate Complex

Mn^{III}-malonate complex (4 mM stock solution) was prepared by dissolving Mn^{III}-acetate (Aldrich) in 0.1 M sodium malonate immediately prior to use. Reaction mixtures (1.6 ml) contained substrate (I) (0.2 mM), Mn^{III}-malonate (0.2 or 2.0 mM) in 50 mM Na-

malonate buffer, pH 4.5. Reactions were carried out for 5 minutes at room temperature. The reaction mixtures were saturated with NaCl, extracted with EtOAc (3x 1 ml), dried over Na_2SO_4, evaporated with N_2 and analyzed either directly or following derivatization (BSTFA: pyridine 2:1 v/v). GCMS was performed at 70 eV on a VG Analytical 7070E mass spectrometer fitted with an HP 5790A GC and a 25-m fused silica column (DB-5, J & W Science). ^{1}H-NMR spectra were determined with a JEOL FX90Q-FT-NMR with chemical shifts expressed as parts per million (δ) downfield from an internal standard of tetramethylsilane.

4.2.5 Preparation of Compounds

1-(3,5-Dimethoxy-4-hydroxyphenyl)-2-(4-methoxyphenyl)-1,3-dihydroxypropane (I) was synthesized by the condensation of o-benzyl syringaldehyde and the methyl ester of methoxyphenyl acetic acid followed by reduction of the resultant methyl ester and debenzylation as previously described (291). MS (m/z) (tri TMS ether) 550 (M^+, 0.8%), 535 (1.2), 485 (9.9), 385 (5.8), 327 (100), 297 (11.2), 223 (27.5), 134 (26.0). ^{1}H NMR ($CDCl_3$) δ 3.05-3.12 (C_β 1H, m), 3.74-3.77 (C_γ 2H, m), 3.80 (Ar(B) OCH_3 3H, s), 3.83 (Ar(A)OCH_3 6H, s), 4.90 (C_α 1H, d), 6.47 (Ar(B) 2H, s), 6.89 (Ar(B) 2H, d), 7.17 (Ar(A) 2H, d).

1-(3,5-Dimethoxy-4-hydroxyphenyl)-2-(4'-methoxyphenyl)-1-oxo-3-hydroxypropane (II) was prepared by the oxidation of I using one equivalent of 2,3-dichloro-5,6-dicyano-1,4-dibenzoquinone in dioxane (room temperature, 16 hours) (292). MS (m/z) (di TMS ether) 476 (M^+, 3.3%), 461 (6.2), 386 (10.0), 342 (26.1), 253 (100), 223 (7.9), 134 (20.6).

2,6-Dimethoxy-1,4-benzoquinone (**III**) was prepared from 2,6-dimethoxyphenol in nitric acid (50% in EtOH) (40°C, 5 hours) as previously described (293).

2,6-Dimethoxy-1,4-dihydroxybenzene (**IV**) was prepared by the reduction of **III** using sodium dithionite in water. MS (m/z) (di TMS ether) 314 (M^+, 100%), 299 (11.8), 284 (87.3), 269 (3.9), 254 (30.2), 224 (5.0), 112 (7.2).

1-(4-Methoxyphenyl)-1-oxo-2-hydroxyethane (**V**), 1-(4-methoxyphenyl)-1,2-dihydroxyethane (**VI**), and 1-(3,4-diethoxyphenyl)-2-(4-methoxyphenyl)-1,3-dihydroxypropane (**VII**) were prepared as previously reported (59). **V**: MS (m/z) (TMS ether) 238 (M^+, 2.2%), 223 (38.2), 207 (19.2), 149 (2.5), 135 (100), 121 (12.5). **VI**: MS (m/z) (di TMS ether) 312 (M^+, 1.3%), 297 (9.3), 222 (6.2), 209 (100), 150 (5.9), 117 (14.8).

Syringaldehyde (**VIII**): MS (m/z) (TMS ether) 254 (M^+, 42.1%) was obtained from Aldrich and recrystallized before use. All other chemicals were reagent grade.

4.3 RESULTS

4.3.1 Oxidation of the Phenolic Diarylpropane (I) by MnP

As shown in Fig. 4-1, the phenolic diarylpropane **I** was oxidized by MnP under aerobic conditions to yield seven identifiable products. The diarylpropanone **II**, benzoquinone **III**, hydroquinone **IV**, phenylketol

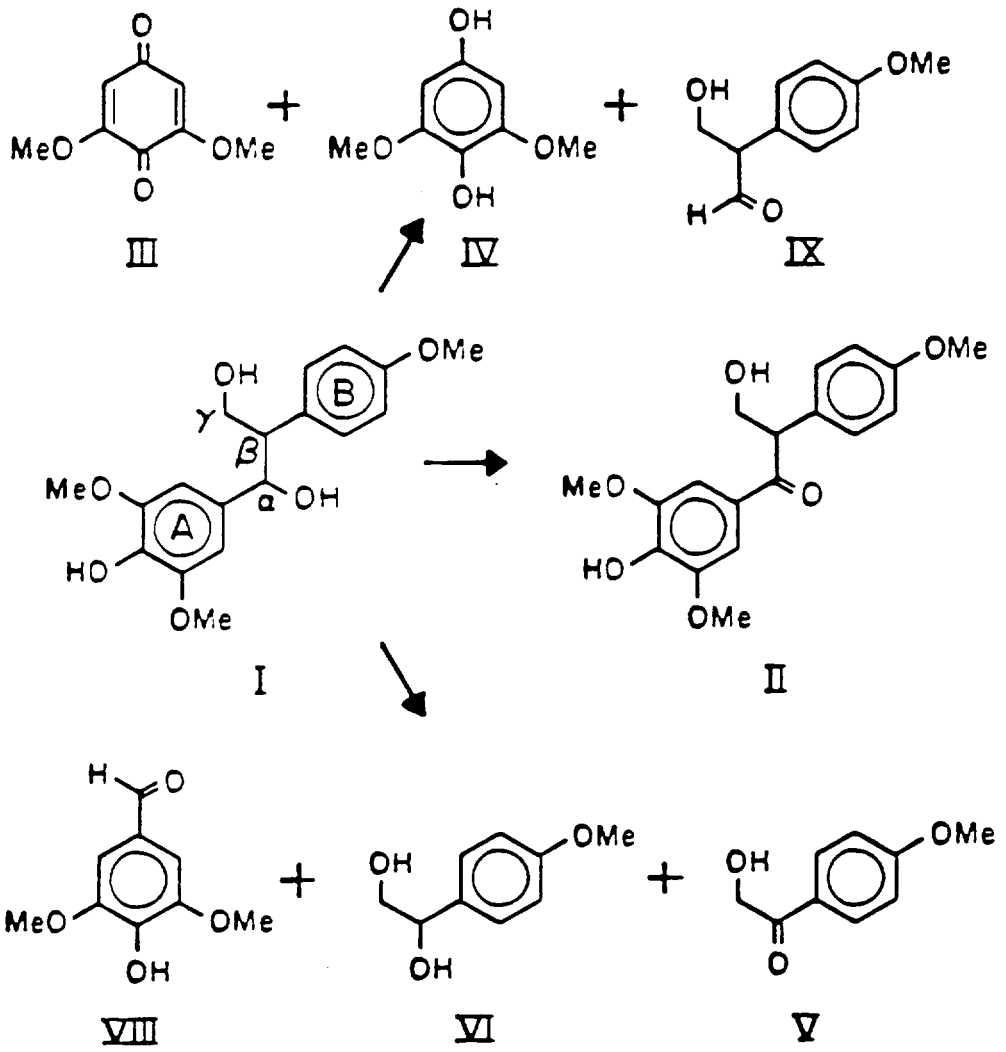

Fig. 4-1. **Structures of the substrate I and manganese peroxidase-produced products II-VI,VIII and IX identified in these studies.** Reactions were conducted and products isolated and analyzed as described in the text.

V, phenylglycol **VI**, and syringaldehyde **VIII** were identified by comparison of their retention times on GC and by comparison of their MS spectra with those of chemically synthesized standards. GCMS data alone indicated the occurrence of 2-(4-methoxyphenyl)-3-hydroxy-propanal **IX**, and the unsaturated carbonyls 1-(3,5-dimethoxy-4-hydroxy-phenyl)-2-(4-methoxyphenyl)-1-oxo-2-propene **X** and 2-(4-methoxyphenyl)-2-propene-1-al **XI**: **IX**, MS (m/z) (TMS ether) 252 (M^+, 37.5%), 237 (5.4), 223 (50.8), 222 (100), 192 (11.4), 162 (30.0), 148 (8.8), 134 (72.2), 121 (86.5); **X**, MS (m/z) (TMS ether) 386 (M^+, 62.0), 371 (11.3), 355 (17.5), 253 (100), 241 (10.0), 133 (35.1); **XI**, MS (m/z) 162 (M^+, 54.6%), 133 (100%), 118 (10.2). The formation of similar α,β unsaturated carbonyls during mass spectrometric analysis has been reported (86). In order to confirm that the α,β unsaturated carbonyl **X** could be derived from the diarylpropanone **II**, the latter was purified preparatively by TLC using solvent systems a: (benzene: acetone, 1:1) and b: (chloroform:methanol, 95:5), silylated and analyzed by GCMS as above. In addition to **II**, a trace amount of **X** was observed.

The propanal **IX** was also purified from the reaction mixture by TLC without derivatization using solvent systems a and b and analyzed by direct inlet-mass spectrometry. **IX**, MS (m/z) 180 (M^+, 30.3%), 162 (11.5), 133 (13.4), 121 (100), 91 (6.9), 78 (13.5), 77 (12.2). When this underivatized fraction was analyzed by GCMS, a peak corresponding to the α,β unsaturated carbonyl **XI** was seen, indicating that H_2O was

readily lost during thermal treatment in the GC.

Yield of products (Table 4-1) was determined using the GC with FID detection and 4,4'-dimethoxybenzhydrol as an internal standard. When the enzyme-catalyzed reaction was conducted under anaerobic conditions, the phenylketol product (**V**) was not detected and approximately twice as much phenylglycol **VI** was obtained. Identical products were found when the reaction was conducted in lactate, citrate, malonate, or oxalate buffers. No products were obtained when the reaction was conducted in the absence of either enzyme, H_2O_2, or Mn^{II}.

MnP could not catalyze the oxidation of either the phenylglycol **VI** or the nonphenolic diarylpropane **VII** under similar conditions in lactate, citrate, malonate or oxalate buffers.

4.3.2 Oxidation of Monomeric Phenols by MnP

MnP readily catalyzed the quantitative conversion of 2,6-dimethoxy-1,4-dihydroxybenzene **IV** to 2,6-dimethoxy-1,4-benzoquinone **III** (Table 4-1). When syringaldehyde **VIII** was used as the substrate, the benzoquinone **III** and a trace of the hydroquinone were found as oxidation products (Table 4-1). The presence of oxygen did not affect the products obtained from substrates **IV** and **VIII**. The oxidation of syringaldehyde **VIII** was considerably slower than the oxidation of syringic acid under the same conditions (data not shown).

Table 4-1. Yield of products from the oxidation of I.

Substrate	Oxidant	Conditions[a]	Products[b] (mole % of starting substrate)							
			I	II	III	IV	V	VI	VII	IX
I	MnP/Mn^{II}	O_2	14	36	11	2.1	1.6	2.6	1.8	8
I	MnP/Mn^{II}	Ar	12	38	12	2.4	0	5.0	2.0	10
IV	MnP/Mn^{II}	O_2	--	--	82	10	--	--	--	--
VIII	MnP/Mn^{II}	O_2	--	--	8.0	T[c]	--	--	83	--
I	Mn^{III}	O_2	18	42	6.5	3.2	1.4	2.8	2.5	7

[a] O_2 = aerobic, under 100% molecular oxygen; Ar = anaerobic, under argon.

[b] Products were identified and quantitated as described in the text.

[c] T = Trace.

4.3.3 ^{18}O Studies

Fig. 4-2 and Table 4-2 show the anisyl aldehyde ion fragment for the phenylketol **V** formed under a variety of conditions. **V** formed under $^{16}O_2$ and in $H_2{}^{16}O$ exhibited a fragment ion peak at m/z 135. When **V** was formed under $^{18}O_2$ and in $H_2{}^{16}O$, 88% incorporation of ^{18}O occurred at the carbonyl position. When **V** was formed under $^{16}O_2$ and in $H_2{}^{18}O$, ^{18}O was not incorporated. Fig. 4-3 and Table 4-2 show the anisyl alcohol ion fragment for the phenylglycol **VI** formed under a variety of conditions. **VI** formed under $^{16}O_2$ and in $H_2{}^{16}O$ exhibited a fragment ion peak at m/z 209. When **VI** was formed under argon and in $H_2{}^{18}O$, 89% incorporation of ^{18}O was found at the 1 position. In contrast, under $^{16}O_2$ and in $H_2{}^{18}O$, only 42% incorporation of ^{18}O was detected at the 1 position of **VI**. Finally, when **VI** was formed under $^{18}O_2$ but in $H_2{}^{16}O$, approximately 28% incorporation of ^{18}O was found at the 1 position. In all cases the M+4 fragment ion was not detected, indicating that only a single atom of oxygen was incorporated into products **V** and **VI**. Table 4-2 also shows the ^{18}O content of the benzoquinone **III** and hydroquinone **IV** products. The benzoquinone and hydroquinone each contained ~one atom of ^{18}O when those products were formed in $H_2{}^{18}O$ under either aerobic or anaerobic conditions. In contrast, when either **III** or **IV** was formed under $^{18}O_2$ but in $H_2{}^{16}O$, no significant oxygen incorporation was detected. ^{18}O incorporation was not detected for the diarylpropanone **II**, syringaldehyde **VIII**, or the phenylpropanal **IX**.

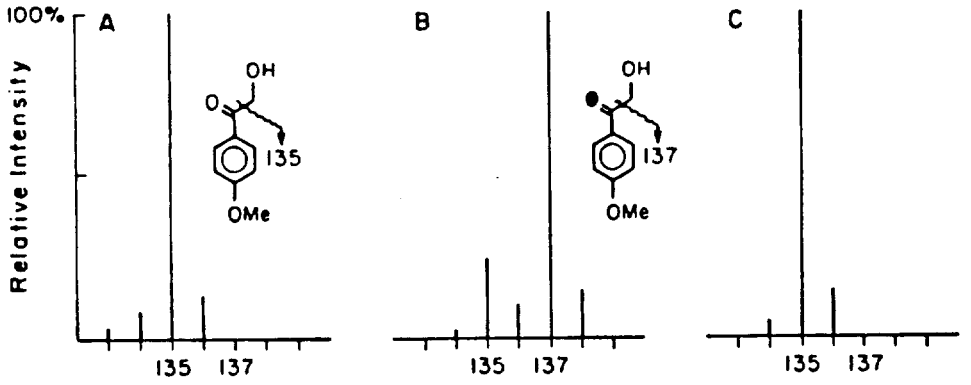

Fig. 4-2. **Portion of the MS of the phenylketol V showing the anisyl aldehyde radical fragment ion region.** (A) Product formed during the oxidation of I under $^{16}O_2$ and $H_2{}^{16}O$. (B) Product formed under $^{18}O_2$ in $H_2{}^{16}O$. (C) Product formed under $^{16}O_2$ and $H_2{}^{18}O$. (●) Oxygen derived from O_2.

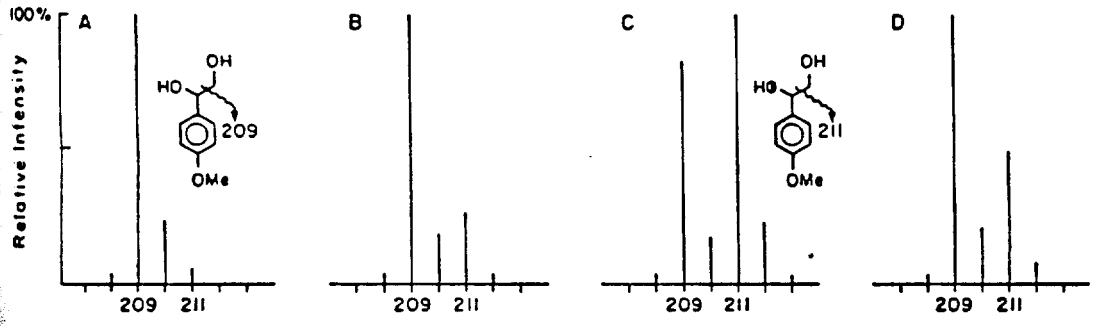

Fig. 4-3. **Portion of the MS of the TMS ether derivative of the phenylglycol VI showing the anisyl alcohol radical fragment ion regions.** (A) Product formed during the oxidation of I under $^{16}O_2$ in $H_2{}^{16}O$. (B) Product formed under $^{18}O_2$ in $H_2{}^{16}O$. (C) Product formed under argon and in $H_2{}^{18}O$. (D) Product formed under $^{16}O_2$ and $H_2{}^{18}O$. (◑) Oxygen derived from H_2O.

Table 4-2. Incorporation of ^{18}O (%) into products during the oxidation of the diarylpropane **I**.

Products	m/z	Conditions		
		$^{18}O_2/H_2{}^{16}O$	$Ar/H_2{}^{18}O$	$^{16}O_2/H_2{}^{18}O$
III	168/170	2.5 [a]	83.4	76.6
IV	314/316	2.2	86.6	78.5
V	135/137	88.8	ND [b]	0
VI	209/211	28.4	89.3	42.7

[a] % incorporation of ^{18}O = (^{18}O content of product / ^{18}O content of the O_2 or H_2O in the reaction mixture) x 100. Products **IV**, **V**, and **VI** were silylated derivatives. Products were isolated, silylated, and analyzed as described in the text.

[b] ND = **V** was not detected when the reactions were conducted under anaerobic conditions.

4.3.4 Oxidation of I by Mn^{III}

The phenolic diarylpropane I was oxidized by chemically prepared Mn^{III} (in the presence of malonate, lactate, citrate, or oxalate). Table 4-1 shows the yields produced when 10 equiv. Mn^{III} was added to I in Na-malonate, pH 4.5. The products were identical to those produced by the enzyme system. Only trace amounts of oxidation products were formed when 1 equiv. of Mn^{III} was used.

4.4 DISCUSSION

As shown in equations 4-1 through 4-4, spectral and kinetic studies indicate that Mn^{II}/Mn^{III} acts as an obligatory redox couple in the MnP catalytic mechanism (104,108,256).

$$MnP + H_2O_2 \rightarrow MnPI + H_2O \qquad [4\text{-}1]$$

$$MnPI + Mn^{II} \rightarrow MnPII + Mn^{III} \qquad [4\text{-}2]$$

$$MnPI + AH \rightarrow MnPII + A\cdot \qquad [4\text{-}2']$$

$$MnPII + Mn^{II} \rightarrow MnP + Mn^{III} \qquad [4\text{-}3]$$

$$Mn^{III} + AH \rightarrow Mn^{II} + A\cdot \qquad [4\text{-}4]$$

These experiments have demonstrated that although Mn^{II} and a variety of phenols are capable of reducing the oxidized enzyme intermediate, manganese peroxidase compound I (MnPI) (eq. 4-2, 4-2'), only Mn^{II} is capable of reducing manganese peroxidase compound II (MnPII) at a

kinetically significant rate (eq. 4-3) (256,257). These results indicated that in the absence of Mn^{II}, the enzyme cannot complete its catalytic cycle. Kinetic analysis also indicated that certain organic acids such as lactate and malonate facilitate the release of Mn^{III} from its complex with the oxidized enzyme intermediates MnPI and MnPII by forming an Mn^{III}-organic acid complex (257). These Mn^{III}-organic acid complexes are relatively stable, yet have a high redox potential (~1.0 v) (108,275,289). Studies on the oxidation of a variety of organic compounds by Mn^{III} have been reported (108,275,294) although several of those reactions were conducted under nonphysiological conditions (e.g., organic solvents, high temperature).

Previous work has shown that MnP is capable of oxidizing monomeric phenols (104,105,108); however, the oxidation of these simple substrates does not model the oxidative reactions involved in the cleavage of the lignin polymer. Since the mechanism of the MnP-catalyzed oxidation of phenolic lignin substructures had not been examined thoroughly, a study of the oxidation of the phenolic diarylpropane I was undertaken. This particular dimer was chosen because during its oxidation, ring condensation via radical coupling is inhibited by the presence of a methoxy group at the 5 position of ring A (Fig. 4-1).

The phenolic diarylpropane I was readily oxidized by MnP to produce a variety of products (Fig. 4-1, Table 4-1). Alkyl phenyl bond cleavage produced the benzoquinone **III**, hydroquinone **IV**, and the phenylpropanal **IX**. C_α-C_β bond cleavage produced syringaldehyde **VIII**,

the phenylketol **V**, and the phenylglycol **VI**. Finally, C_α oxidation yielded the diarylpropanone **II**. Exogenously added syringaldehyde was oxidized by MnP to produce the benzoquinone **III**. The nonphenolic substrates **VI** and **VII** were not oxidized by MnP under these conditions, suggesting that the critical step in the MnP-catalyzed reaction is the oxidation of the phenol to a phenoxy radical by enzyme-generated Mn^{III}. In addition, **I** was oxidized by chemically prepared Mn^{III} to produce identical products. Identification of these oxidation products in addition to the results of ^{18}O incorporation studies suggest several mechanisms for the MnP-catalyzed oxidation of **I**.

4.4.1 Mechanism of C_α-C_β Bond Cleavage of the Diarylpropane **I**

Oxidation of **I** to a phenoxy radical **I'** by enzyme-generated Mn^{III} would result in C_α-C_β bond cleavage, giving rise to a quinone methide and a C_6-C_2 radical (Fig. 4-4). The quinone methide would undergo rearrangement to yield syringaldehyde **VIII**. Subsequently, **VIII** would be oxidized by Mn^{III} to form the corresponding phenoxy radical (Fig. 4-4). Radical rearrangement would result in a cyclohexadienyl radical which also would be oxidized by Mn^{III} to form the corresponding cation (295). The cation is susceptible to attack by water to yield the quinone **III** and formaldehyde. One atom of ^{18}O from water is incorporated into the benzoquinone (Table 4-2) as predicted by this pathway. Syringic acid is oxidized by MnP to produce a quinone **III** and hydroquinone **IV**; however, no evidence for its formation was obtained in this study. The C_6-C_2 radical would be scavenged by O_2 under aerobic

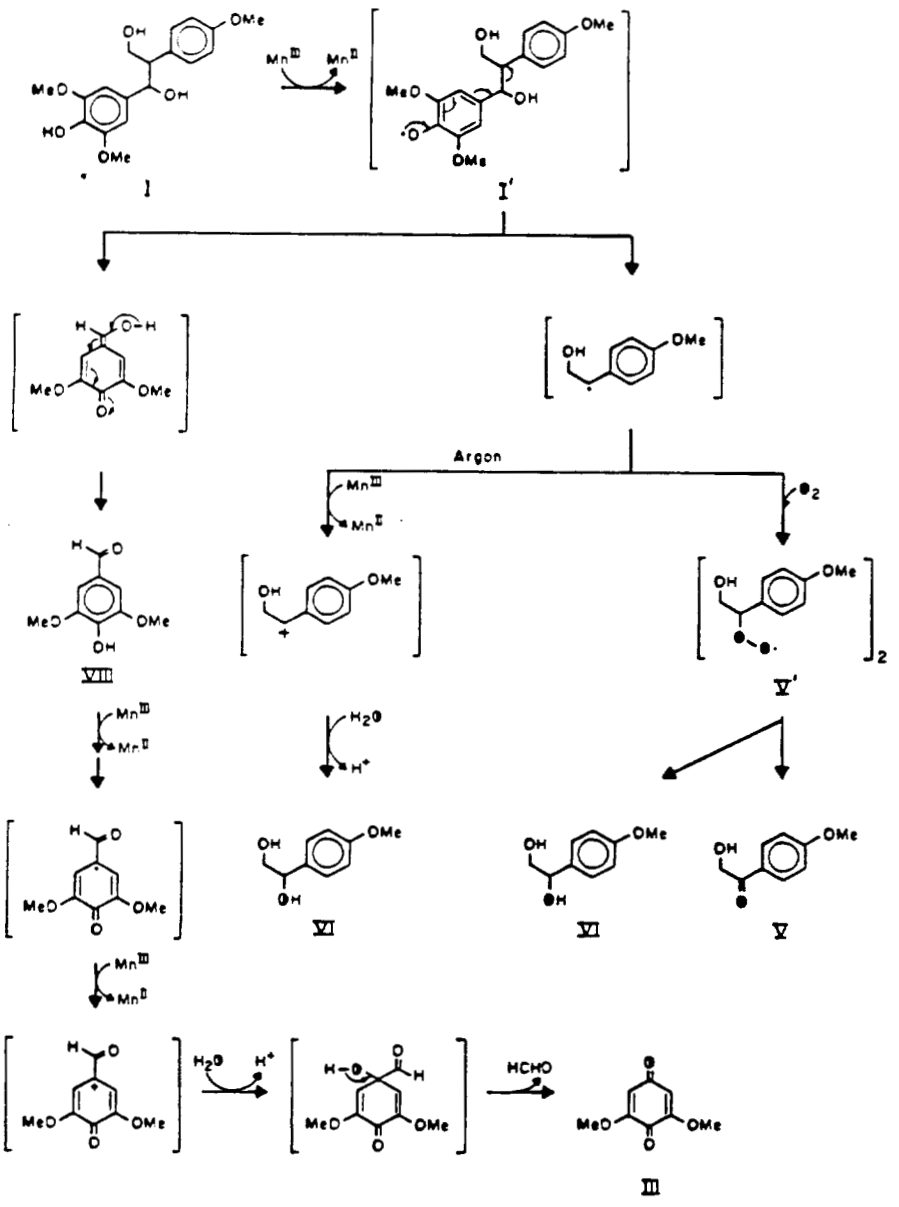

Fig. 4-4. **Proposed pathways for the C_α–C_β cleavage of the substrate I by manganese peroxidase.** (●) Oxygen derived from O_2. (◑) Oxygen derived from H_2O.

conditions to form a hydroperoxy radical **V'**. The hydroperoxy radical **V'** could decompose via a tetroxide intermediate as described previously (231,296) to form the phenylketol **V** and phenylglycol **VI** (Fig. 4-4). The observations that the phenylketol **V** was formed only under aerobic conditions and that one atom of molecular oxygen was incorporated into **V** support this mechanism. The observation of 28% incorporation of ^{18}O from $^{18}O_2$ at the 1 position of the phenylglycol **VI** also supports this mechanism. Alternatively, homolytic cleavage of the hydroperoxide radical **V'** could lead to the formation of the phenylketol **V**. Under anaerobic conditions, the C_6-C_2 radical would be oxidized by Mn^{III} to a carbonium ion, which would be attacked by H_2O to yield the phenylglycol **VI**. The oxidation of a benzylic radical to a benzyl cation by Mn^{III} has been reported (295). The observations (Table 4-2) that one atom of oxygen from water was incorporated into the phenylglycol under anaerobic conditions but that only 43% incorporation of oxygen from water occurred at the 1 position of the phenylglycol **VI** under aerobic conditions, where both pathways are operative support these dual mechanistic pathways. The ratio of phenylketol **V** and phenylglycol **VI** formed was found to be 1:1.6 (MnP oxidation) and 1:2 (Mn^{III} oxidation) (Table 4-2). In addition, only 28% incorporation of ^{18}O from $^{18}O_2$ into the glycol **VI** under aerobic conditions was observed. These observations suggest that even under aerobic condtions, the C_6-C_2 radical may be attacked by Mn^{III} at a significant rate.

4.4.2 Mechanism of Alkyl Phenyl Cleavage

Oxidation of I by enzyme-generated Mn^{III} would yield the phenoxy radical I'. The alternative resonance form of I', a cyclohexyldienyl radical (Fig. 4-5), would be oxidized by Mn^{III} to form the corresponding cation (I") (295). Attack by H_2O would yield the triol intermediate which readily cleaves at the alkyl-phenyl bond to produce the phenylpropanal **IX** and the hydroquinone **IV**. The latter is readily oxidized by Mn^{III} to produce the quinone **III**. The observation (Table II) that one atom of ^{18}O from water is incorporated into both the quinone **III** and hydroquinone **IV** supports this mechanism. The hydroquinone **IV** is readily oxidized by MnP to form the quinone **III** (Table 4-1). A phenoxy radical is an intermediate in that reaction (296).

4.4.3 Mechanism of C_α Oxidation

Finally, loss of an α-proton by the cation intermediate I" (Fig. 4-5) would result in a quinone methide which rearranges to form the diarylpropanone **II**. In this case, as predicted, no incorporation of ^{18}O from molecular oxygen or water was seen.

Thus, the phenolic lignin model diarylpropane I is oxidatively cleaved by MnP-generated Mn^{III}. In all of the oxidative mechanisms described in the present study, the initial formation of a phenoxy radical is followed by radical rearrangements and other nonenzymatic reactions. The reactions described herein are similar but not identical to those reported previously with laccase-catalyzed

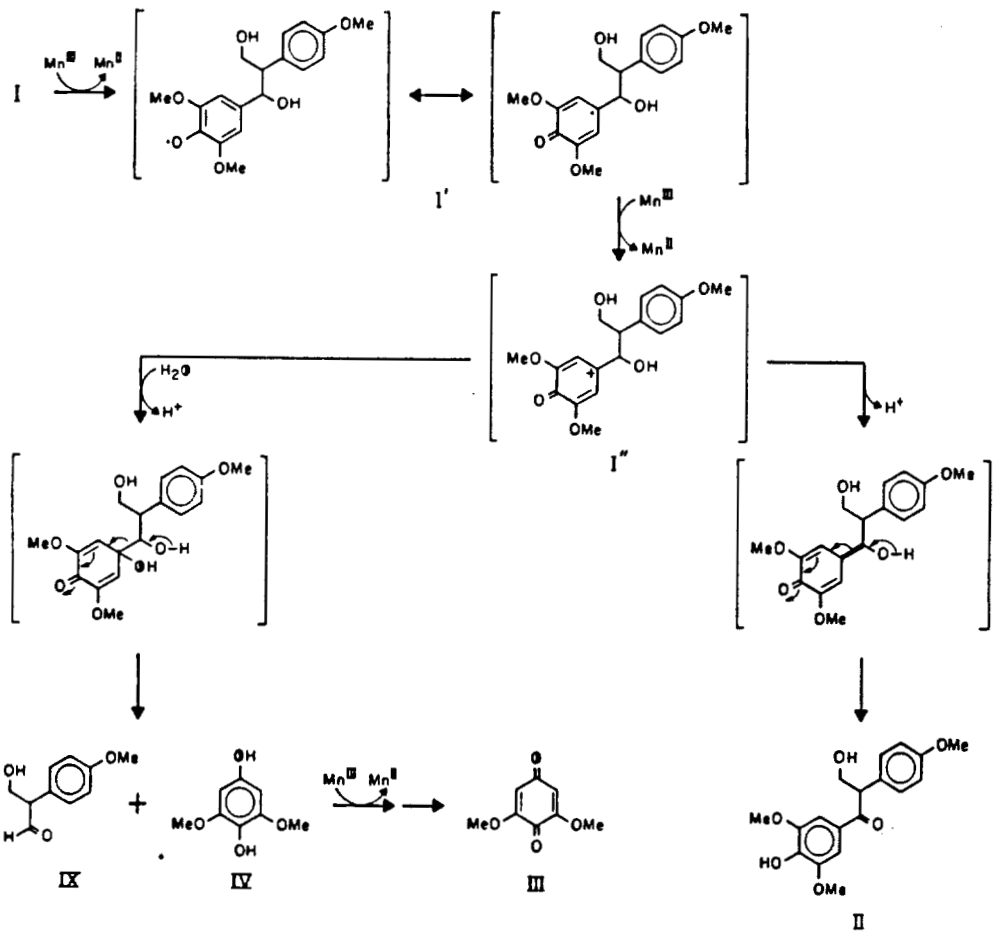

Fig. 4-5. Proposed pathways for alkyl phenyl cleavage and C_α oxidation of I by manganese peroxidase.

reactions (84-86,298). The MnP system apparently differs from laccase due to the ability of Mn^{III} to readily oxidize carbon-centered radicals to the corresponding cations which are subsequently attacked by H_2O.

As we reported earlier, MnP preferentially oxidizes Mn^{II} to Mn^{III} and the Mn^{III} in turn oxidizes phenolic substrates. This system is advantageous because the Mn^{III} chelated by organic acids can diffuse from the enzyme and oxidize the relatively inaccessible, insoluble lignin polymer. The results reported herein indicate some of the oxidative mechanisms which are likely to be involved in the MnP-catalyzed oxidation of lignin. The oxidation of diols and ketols (294,299,300) and olefins (294,301,302), by Mn^{III} complexes has been reported previously.

CHAPTER 5

THIOL-MEDIATED OXIDATION OF NONPHENOLIC LIGNIN MODEL COMPOUNDS BY MANGANESE PEROXIDASE*1

5.1 INTRODUCTION

Lignin, the most abundant renewable aromatic polymer, constitutes 20-30% of woody plants (14). Since the biodegradation of cellulose is retarded by the presence of lignin, the catabolism and utilization of this polymer are of enormous significance (18,29-31). White-rot basidiomycetous fungi are primarily responsible for the initial decomposition of lignin in wood (18,29-31). When cultured under ligninolytic conditions the white-rot basidiomycete Phanerochaete chrysosporium produces two heme peroxidases (29-31,98-101,104) which along with an H_2O_2 generating system (30) appear to be the major

---

*1 The contents of this chapter have been published; Thiol-mediated Oxidation of Nonphenolic Lignin Model Compounds by Manganese Peroxidase of Phanerochaete chrysosporium. H. Wariishi, K. Valli, V. Renganathan, & Gold, M.H. (1989) J. Biol. Chem. **264**, 14185-14191 (Ref. 259)

components of its lignin degradative system. The structure and mechanism of lignin peroxidase have been studied extensively (29-31, 99-101,103,106). Manganese peroxidase (MnP)*2 has also been purified and characterized (31,98,103-105,108). The enzyme exists as a series of isozymes (102,103), contains one iron protoporphyrin IX prosthetic group (104), and is a glycoprotein of M_r ~46,000 (98,104,105). MnP catalyzes the H_2O_2- and Mn^{II}-dependent oxidation of a variety of phenols, amines, and organic dyes (98,104,105,108,256).

Electronic absorption (98,104,256), EPR, and resonance Raman spectral evidence (252) indicates that the heme environment of native MnP has features which are similar to those of other plant peroxidases (137). The nucleotide sequence of a cDNA encoding an MnP isozyme has been determined and confirms the presence of a proximal and distal histidine at the active center of the enzyme (254,255). In addition, spectral and kinetic evidence (257,257) indicates that the H_2O_2-oxidized states (compounds I and II) and the catalytic cycle of MnP are similar to those of lignin and horseradish peroxidases (137,232). Most importantly, it has been demonstrated that MnP oxidizes Mn^{II} to

---

*2 Abbreviations:
BSTFA, N,O-bis(trimethysilyl)trifluoroacetamide; DDQ, 2,3-dichloro-5,6-dicyano-1,4-dibenzoquinone; Cys, cysteine; DTE, dithioerythritol; DTT, dithiothreitol; GCMS, gas chromatography mass spectrometry; GSH, glutathione; HRP, horseradish peroxidase; MnP, manganese peroxidase.

Mn^{III} and that the Mn^{III} in turn oxidizes monomeric phenols (104,105, 108,256) and phenolic lignin dimers (258) via the formation of a phenoxy radical. Transient state kinetic analysis (257) has confirmed that Mn^{II}/Mn^{III} acts as a redox couple rather than as an enzyme binding activator.Chelation by certain organic acids such as lactate and malonate stabilizes the Mn^{III} at a high redox potential (0.9-1.2 V) facilitating the oxidation of organic substrates (275,289).

The one-electron oxidation of phenols (104,258,294) and thiols (294,303,304) to phenoxy or thiyl radicals by Mn^{III} and other transition metals has been well studied. In contrast, Mn^{III} complexes with organic acids such as malonate apparently are not capable of easily oxidizing most nonphenolic lignin model compounds such as veratryl alcohol under normal physiological conditions (31,98,104,258). In contrast, a recent report by Forrester et al. (305) claims that nonphenolic lignin model compounds are oxidized directly by Mn^{III}-pyrophosphate in the presence of glutathione via the initial formation of aryl cation radicals. However, since the mechanism of Forrester et al. (305) appeared unlikely, we have reexamined the oxidation of nonphenolic lignin models by MnP-generated and chemically prepared Mn^{III} in the presence of thiols. Herein, we demonstrate that in this system, Mn^{III} oxidizes thiols to thiyl radicals which in turn react with the lignin models to form carbon-centered radicals. The latter undergo a variety of reactions to yield the final products.

5.2 EXPERIMENTAL PROCEDURES

5.2.1 Enzyme Preparation

MnP isozyme 1 was purified from the extracellular medium of an acetate-buffered agitated culture of P. chrysosporium strain OGC 101 (290) as previously reported (104,257). The purified enzyme was electrophoretically homogeneous and had a pI of 4.9.

5.2.2 Enzyme Reactions

Aromatic compound oxidations were carried out at 37°C for 30 minutes in 1 ml of 50 mM sodium malonate (pH 4.5) containing aromatic substrate (0.2 mM), GSH (5.0 mM) (DTE, DTT, or Cys were substituted where indicated), $MnSO_4$ (0.5 mM) and enzyme (5.0 μg) under anaerobic conditions or as indicated. Anaerobic conditions were obtained as described (98,231,258). Reactions were initiated by adding H_2O_2 (0.2 mM).

5.2.3 Oxidation of Aromatic Substrates by Mn^{III}-Malonate Complex in the Presence of GSH

Mn^{III}-malonate complex (4 mM stock solution) was prepared by dissolving Mn^{III}-acetate (Aldrich) in 0.1 M sodium malonate immediately prior to use. Mn^{III}-malonate showed absorption maxima at 270 and 460 nm. Reaction mixtures (1.6 ml) contained aromatic substrate (0.2 mM), GSH (5.0 mM) and Mn^{III}-malonate (2.0 mM) in 50 mM Na-malonate buffer, pH 4.5. Reactions were carried out at 37°C for five minutes under anaerobic conditions.

5.2.4 γ-Irradiation

Reaction mixtures (1.0 ml) contained aromatic substrate (0.2 mM) and GSH (5.0 mM) in 10 mM Na-phosphate buffer (pH 7.2). Samples were irradiated under anaerobic conditions for 6 hours with a ^{137}Cs γ-ray source (21.2 Krads/hr).

5.2.5 Product Analyses

Upon completion of the reactions, mixtures were acidified to pH 3.0 with HCl, extracted with chloroform (2 × 2 mL), dried over Na_2SO_4, evaporated with N_2 and analyzed either directly or following derivatization (BSTFA:pyridine 2:1 v/v). Products were identified by comparison of their retention times on GC and by comparison of their MS spectra with those of chemically synthesized standards. GCMS was performed at 70 eV on a VG Analytical 7070E mass spectrometer fitted with an HP5790A GC and a 25-m fused silica column (DB-5, J&W Science). The temperature was programmed from 80 to 320°C at 10°C/min. Quantitative analysis of substituted benzaldehyde products was carried out by HPLC (HP LiChosphere 100 RP-18 column) using a solvent gradient system from 5% MeOH in H_2O to 100% MeOH.

5.2.6 Kinetic and Spectral Analyses

Veratryl alcohol oxidations were carried out in 2 ml of 50 mM Na-malonate (pH 3.1-6.1), containing veratryl alcohol (0.1 mM), enzyme (2 μg), $MnSO_4$ (0.1 mM), and GSH (5.0 mM). Reactions were initiated by adding H_2O_2 (0.1 mM) using a microsyringe, conducted under argon or

air as indicated, and monitored at 310 nm. Lactate, oxalate, or pyrophosphate replaced malonate, and DTT, DTE, or Cys replaced GSH where indicated.

Mn^{II}-malonate oxidations were carried out in 2 ml of 50 mM Na-malonate, pH 4.5, containing $MnSO_4$ (0.1 mM), enzyme (2 μg), GSH (0-5.0 mM) and H_2O_2 (0.1 mM) under anaerobic conditions. Mn^{III}-malonate formation was monitored at 270 nm.

5.2.7 Chemicals and Preparation of Compounds

H_2O_2 and the reduced thiols GSH, DTT, DTE, and Cys were obtained from Sigma. 3,4-Dimethoxybenzyl alcohol (veratryl alcohol) (**I**), 4-methoxybenzyl alcohol (anisyl alcohol) (**II**), and benzyl alcohol (**III**), the corresponding aldehydes veratraldehyde (**IV**), anisaldehyde (**V**), and benzaldehyde (**VI**), 4-hydroxy-3-methoxybenzyl alcohol (vanillyl alcohol) (**VII**), and the corresponding aldehyde vanillin (**VIII**) were all obtained from Aldrich. All other chemicals were reagent grade.

1,2-Bis(3,4-dimethoxyphenyl)-1,2-dihydroxyethane (**IX**) was prepared from veratraldehyde (**IV**) via a benzoin condensation as described previously (306): a) veratraldehyde/KCN in 80% EtOH, reflux 6 hr; b) $NaBH_4$ in EtOH, rt, 16 hr. 1,2-Bis(4-methoxyphenyl)-1,2-dihydroxyethane (**X**) and 1,2-bis-phenyl-1,2-dihydroxyethane (**XI**) were prepared by the reduction of anisoin and benzoin, respectively (307). MS m/z (**IX**) (di TMS ether) 478 (M^+, 0.3%), 463 (5), 239 (100), 147 (2), 73 (18); MS m/z (**X**) (di TMS ether) 393 (M-15, 4%), 209 (100), 147 (2), 73 (16); MS m/z (**XI**) (di TMS ether) 343 (M-15, 4%), 179 (100), 163 (6), 147 (15), 73 (48).

1-(4-Ethoxy-3-methoxyphenyl)-2-(4'-hydroxymethyl-2'-methoxyphenoxy)-1,3-dihydroxypropane (**XII**) was prepared as described previously (241,308). 1-(4-Ethoxy-3-methoxyphenyl)-2-(4'-hydroxymethyl-2'-methoxyphenoxy)-1-oxo-3-hydroxypropane (**XIII**) was prepared by the oxidation of **XII** using one equivalent of DDQ in dioxane (room temperature, 16 hours) (292). MS m/z (**XII**) (tri TMS ether) 594 (M^+, 3%), 368 (1), 297 (4), 253 (100), 225 (4); MS m/z (**XIII**) (di TMS ether) 520 (M^+, 17%), 505 (4), 295 (11), 252 (10), 179 (100), 149 (39), 147 (12), 73 (57).

1-(4-Ethoxy-3-methoxyphenyl)-2-(4'-formyl-2'-methoxyphenoxy)-1,3-dihydroxypropane (**XIV**) was prepared as follows: a) The formyl group of methyl(4-formyl-2-methoxyphenoxy)acetate was protected by forming the dimethyl acetal derivative using methyl orthoformate and p-toluene sulfonic acid (308). b) The dimethyl acetal derivative was condensed with 4-ethoxy-3-methoxybenzaldehyde (241,308). c) Reduction with $LiAlH_4$ in THF, rt, followed by treatment with HCl yielded **XIV**. 1-(4-Ethoxy-3-methoxyphenyl)-2-(4'-formyl-2'-methoxyphenoxy)-1-oxo-3-hydroxypropane (**XV**) was prepared by the oxidation of **XIV** with DDQ (292). MS m/z **XIV** (di TMS ether) 520 (M^+, 6%), 505 (1), 458 (3), 279 (2), 253 (100), 225 (3), 223 (2), 209 (6), 147 (4), 73 (35). MS m/z (**XV**) (di TMS ether) 446 (M^+, 2%), 431 (5), 428 (4), 325 (16), 253 (29), 209 (21), 179 (89), 152 (24), 151 (25), 73 (100).

1-(4-Ethoxy-3-methoxyphenyl)-1,3-dihydroxypropane (**XVI**) was prepared by the condensation of 4-ethoxy-3-methoxybenzaldehyde and ethyl bromoacetate in benzene with zinc powder (reflux, 30 min.), followed

by treatment with 10% H_2SO_4 in benzene (0°C) and by reduction with $LiAlH_4$ in THF (-30°C, 1 hr.) (309). 1-(4-Ethoxy-3-methoxyphenyl)-2,3-dihydroxypropane (**XVII**) and 1-(4-ethoxy-3-methoxyphenyl)-1,2-dihydroxypropane (**XVIII**) were prepared as previously described (64). MS m/z (**XVI**) (di TMS ether) 370 (M^+, 11%), 355 (2), 327 (4), 279 (6), 253 (100). MS m/z (**XVII**) (di TMS ether) 370 (M^+, 10%), 280 (35), 267 (10), 239 (4), 223 (3), 205 (72), 147 (60), 117 (100). MS m/z (**XVIII**) (di TMS ether) 370 (M^+, 4%), 355 (5), 253 (100), 237 (6), 225 (7), 147 (25). The isomers **XVI**, **XVII**, and **XVIII** could be reproducibly separated by capillary GC and showed retention times of **XVI**, 12.6 min; **XVII**, 13.0 min; **XVIII**, 12.0 min. 1-(4-Ethoxy-3-methoxyphenyl)-1-oxo-3-hydroxypropane (**XIX**) was prepared by the oxidation of **XVI** with DDQ. MS m/z (**XIX**) (TMS ether) 296 (M^+, 89%), 281 (100), 253 (26), 223 (19), 206 (83), 179 (97), 151 (66).

5.3 RESULTS

5.3.1 Oxidation of Aryl Alcohols by the MnP/Mn^{III}/Thiol System

As shown in Table 5-1, veratryl alcohol (**I**) anisyl alcohol (**II**), and benzyl alcohol (**III**) were oxidized almost quantitatively by MnP/Mn^{II} in the presence of GSH under anaerobic conditions to yield the corresponding aldehydes **IV**, **V**, and **VI** and coupled dimers **IX**, **X**, and **XI**. No products were obtained when the reactions were carried out in the absence of enzyme, GSH, Mn^{II}, or H_2O_2. Identical products were

Table 5-1. Products obtained from the oxidation of substituted benzyl alcohols[a]

Oxidant	substrate	Vald[c]	Aald[c]	Bald[c]	Coupled dimers		
		IV	V	VI	IX	X	XI
MnP/Mn^{II}/GSH	veratryl alcohol	96			T[b]		
	anisyl alcohol		95			T	
	benzyl alcohol			90			T
Mn^{III}/GSH	veratryl alcohol	92			T		
	anisyl alcohol		91			T	
	benzyl alcohol			95			T
GSH/γ-irrad.	veratryl alcohol	85			T		
	anisyl alcohol		83			T	
	benzyl alcohol			80			T

[a] Reactions were conducted under anaerobic conditions as described in the text. When the reactions were conducted under aerobic conditions, the same products were obtained but the yields were ~50% of those under anaerobic conditions.

[b] T = trace

[c] Vald, Aald, and Bald; veratraldehyde, anisaldehyde, and benzaldehyde, respectively.

obtained if lactate or oxalate replaced the malonate buffer or if DTT, DTE, or Cys replaced the glutathione. Under aerobic conditions the same products were obtained and no veratryl alcohol ring cleavage was observed.

In the presence of thiol, under anaerobic conditions, chemically prepared Mn^{III}-malonate was also capable of oxidizing these substituted benzyl alcohols to the corresponding aldehyde and coupled dimer products (Table 5-1).

When the Mn^{III}-malonate or Mn^{III}-pyrophosphate reaction was carried out in the absence of thiol at either pH 4.5 or pH 3.0, no products were observed.

In order to test the possibility that Mn^{III}-generated thiyl radicals (294,303,304) were involved in the oxidation of the benzyl alcohols **I**, **II**, and **III**, we examined the oxidation of **I**, **II**, and **III** in a γ-irradiation system consisting of substrates, GSH, and buffer. The generation of thiyl radicals from thiols by γ-irradiation has previously been well studied (310,311). As shown in Table 5-1, when the alcohols were irradiated in the presence of GSH under anaerobic conditions, the same aldehyde and coupled dimer products were obtained. Furthermore, in the absence of GSH, γ-irradiation did not lead to oxidation of the substrates.

Since the formation of the coupled dimer (**IX**) was negligible, the initial rate of veratryl alcohol oxidation could be followed spectrophotometrically by measuring the rate of formation of veratraldehyde at 310 nm (99-101) (Table 5-2). Under anaerobic conditions GSH, DTE

Table 5-2. Effect of thiols and organic acids on the oxidation of veratryl alcohol by manganese peroxidase[a]

Thiol	Organic acid	Initial rate (μmole min^{-1} mg^{-1})	
		Anaerobic	Aerobic
GSH	malonate	6.7	3.0
DTE	malonate	5.9	2.2
DTT	malonate	5.1	2.5
Cys	malonate	1.3	0.5
GSH	lactate	4.5	2.2
GSH	oxalate	1.1	0.5
GSH	succinate	0.01	0.0
GSH	pyrophosphate[b]	1.4	0.6

[a] Reactions were conducted as described in the text.

[b] 50 mM Na-pyrophosphate was dissolved in 50 mM Na-succinate buffer, pH 4.5.

and DTT were all effective thiols. However, activity was considerably reduced when cysteine was used as the thiol. In the presence of GSH, both malonate and lactate were effective as Mn^{III} chelators. Activity was considerably reduced when oxalate or pyrophosphate were substituted for malonate. Very low activity was detected in succinate buffer, confirming that succinate is unable to form an Mn^{III} complex (289). With all thiols and organic acids used, the initial rate of veratraldehyde formation was ~2-fold greater under anaerobic conditions than under aerobic conditions.

5.3.2 Oxidation of Thiol by Mn^{III}

As shown in Fig. 5-1A, Mn^{III}-malonate was effectively reduced by GSH in the absence of substituted benzyl alcohols. Addition of 10 equiv. of GSH to Mn^{III}-malonate resulted in the rapid formation of a featureless spectrum between 250-500 nm, characteristic of Mn^{II} organic acid complexes (Fig. 5-1A) (104,108). In contrast, in the absence of thiol, less than 1% of the Mn^{III}-malonate was reduced upon addition of 10 equiv. of veratryl alcohol (data not shown). Furthermore, Fig. 5-1B shows that in the absence of veratryl alcohol, Mn^{III}-malonate accumulation in the enzyme system is suppressed by the addition of thiol. The kinetic curve obtained in the presence of 1.0 mM GSH (Fig. 5-1B) suggests that there is an initial burst of Mn^{III}-malonate followed by a plateau when the rate of Mn^{III} formation approximately equals the rate of Mn^{III} reduction. After Mn^{III}-malonate was reduced by DTT (1,4-dimercapto-2,3-dihydroxybutane), the

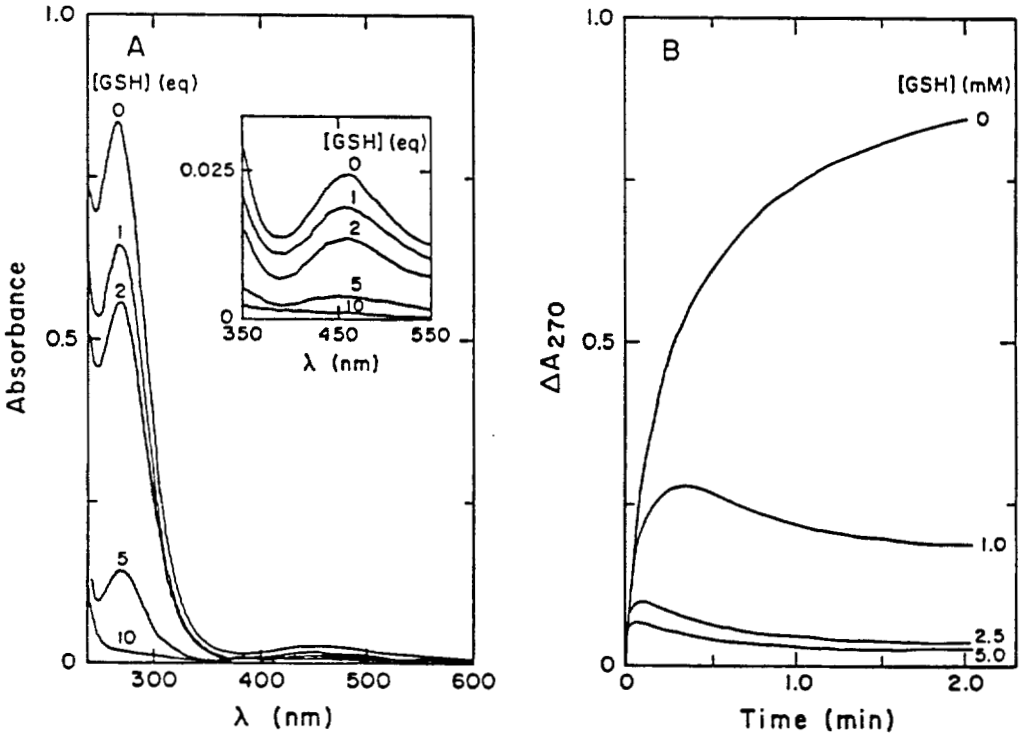

Fig. 5-1. **Reduction of Mn^{III}-malonate by GSH.** (A) Reaction mixtures contained Mn^{III}-malonate (0.1 mM) in 50 mM Na-malonate buffer, pH 4.5, to which the indicated equivalents of GSH were added. Spectra were recorded 10 s after the addition of GSH. (B) Accumulation of Mn^{III}-malonate in the presence of various amounts of GSH. Reaction mixtures contained Mn^{II} (0.1 mM), GSH (as indicated), MnP (5.0 μg) in 50 mM Na-malonate buffer, pH 4.5. Reactions were initiated by adding 0.1 mM H_2O_2 and conducted under anaerobic conditions. Mn^{III}-malonate formation was monitored at 270 nm.

mixtures were extracted with chloroform, derivatized, and analyzed by GCMS. The MS spectrum of the products demonstrated the formation of 4,5-dihydroxy-1,2-dithiane which contains an intramolecular disulfide bond. MS (m/z) (di TMS ether) 296 (M^+, 13%), 203 (8), 180 (59), 147 (25), 116 (100), 101 (24), 73 (92). These results indicate that the Mn^{III}-malonate is capable of effectively oxidizing the thiol to a thiyl radical which subsequently undergoes radical coupling to form an intramolecular disulfide bond.

The pH dependence from pH 3.1-6.1 for the oxidation of veratryl alcohol by MnP/Mn^{II}/GSH is shown in Fig. 5-2. Activity increased with increasing pH. Fig. 5-2 also shows the pH dependence of the lignin peroxidase-catalyzed oxidation of veratryl alcohol (237). Here, activity increased with decreasing pH.

5.3.3 Oxidation of β-Aryl Ether Lignin Model Compounds

As shown in Fig. 5-3, the non-phenolic β-vanillyl alcohol ether (**XII**) was oxidized by the MnP/Mn^{II}/GSH system under anaerobic conditions to yield the dimeric ketone (**XIII**), the β-vanillin ether dimer (**XIV**), the phenylpropane-1,3-diol (**XVI**), the phenylpropane-1-oxo-3-ol (**XIX**), vanillyl alcohol (**VII**), and vanillin (**VIII**). The isomers of **XVI**, the phenylpropane-2,3-diol (**XVII**), and the phenylpropane-1,2-diol (**XVIII**) were not found.

The MnP/Mn^{II}/GSH system also oxidized the nonphenolic β-vanillin dimer (**XIV**) under anaerobic conditions to yield the dicarbonyl dimer (**XV**), the phenyl propane-1-oxo-3-ol (**XIX**), and vanillin (**VIII**) (Fig.

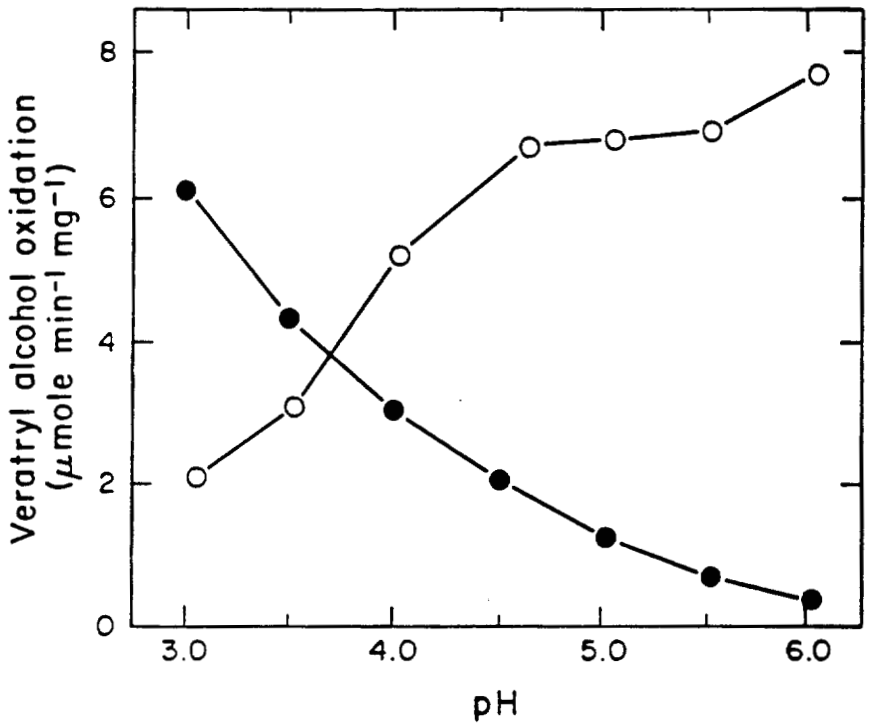

Fig. 5-2. **pH Profile for veratryl alcohol oxidation by MnP in the presence of GSH (○) and by lignin peroxidase (●).** For MnP, reaction mixtures contained enzyme (1 μg/ml), Mn^{II} (0.1 mM), veratryl alcohol (0.1 mM), GSH (5.0 mM), and H_2O_2 (0.1 mM) in 50 mM Na-malonate buffer, pH 3.1-6.1. Reactions were conducted under anaerobic conditions. The profile for lignin peroxidase was previously obtained in our laboratory (232).

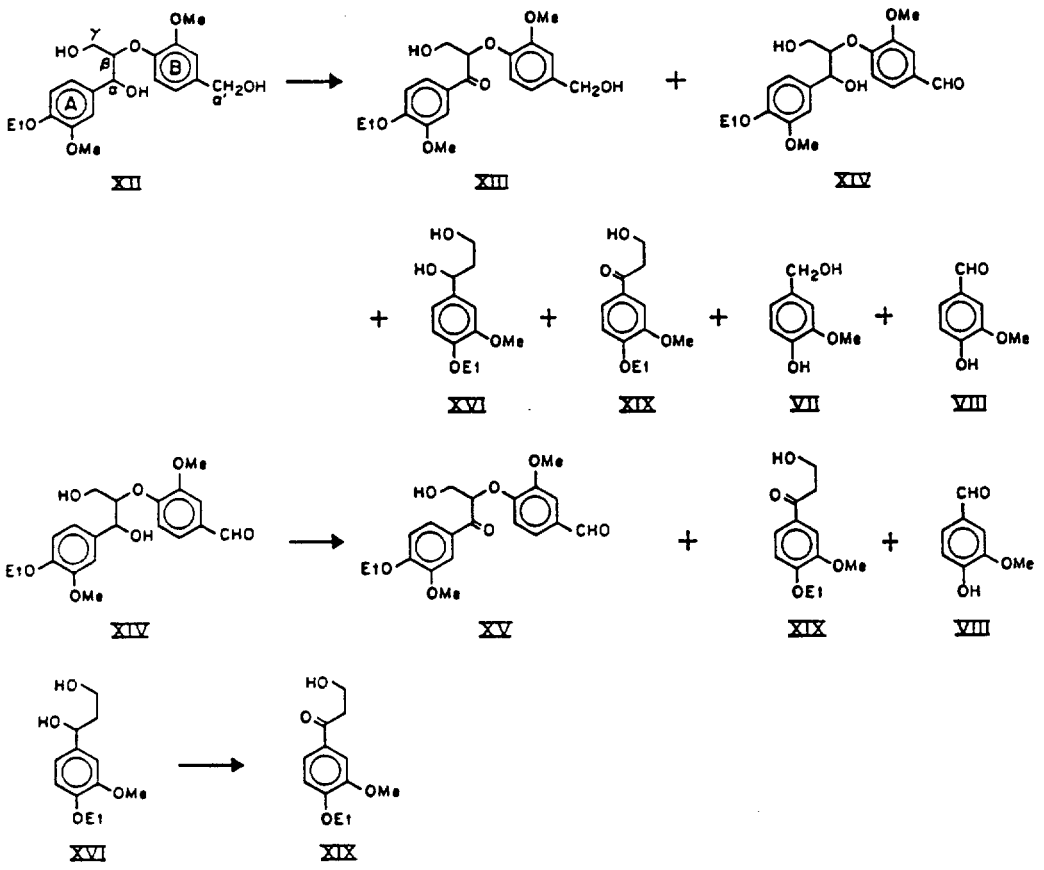

Fig. 5-3. **Products obtained from the oxidation of the nonphenolic substrates XII, XIV, and XVI by both the MnP/Mn^{II}/GSH and the γ-irradiation /GSH systems.** Reactions were conducted and analyzed as described in the text.

5-3). Finally, the phenylpropane-1,3-diol (**XVI**) was readily oxidized to the phenylpropane-1-oxo-3-ol (**XIX**) by the enzyme system. No products were obtained when the reactions were conducted in the absence of either GSH, Mn^{II}, H_2O_2, or enzyme.

When the substrates **XII**, **XIV**, and **XVI** were irradiated under anaerobic conditions in the presence of GSH, the same products were obtained as with the enzyme system (Fig. 5-3). In the absence of GSH, no products were obtained and substrate was recovered nearly quantitatively after irradiation for 6 hr.

5.3.4 Oxidation of Substrates under Aerobic Conditions

Product analysis revealed that with all of the substrates examined using each of the three systems (i. MnP/Mn^{II}/thiol; ii. Mn^{III}/thiol; iii. γ-irradiation/thiol), identical products were obtained under aerobic conditions but in reduced yield (~50% of anaerobic samples).

5.4 DISCUSSION

Spectral and kinetic studies have indicated that the principal function of MnP is the oxidation of Mn^{II} to Mn^{III} (104,108) via a typical peroxidase catalytic cycle (104,108,137,256,257). The enzymatically generated Mn^{III} in turn oxidizes a variety of organic

substrates (104,105,108,256-258). A number of organic acids are capable of forming complexes with Mn^{III} (104,256,257,275,289,294,303). For example, malonate and lactate chelate Mn^{III} to form distorted octahedral complexes, containing two water molecules (289). These complexes are relatively stable in aqueous solution but still possess a high redox potential (0.9-1.2 V) (275,289). We have recently demonstrated that chelation of Mn^{III} by organic acids also facilitates its release from the enzyme-Mn complex (257). Mn^{III}-organic acid complexes are well-studied one-electron oxidants which are capable of oxidizing numerous substrates including phenols and thiols (104,108, 275,294,303). We recently reported that MnP catalyzes C_α-C_β and alkylphenyl bond cleavage of a phenolic diarylpropane dimer and that these cleavage reactions are initiated by the oxidation of the dimer to a phenoxy radical by enzymatically generated Mn^{III} (258). Nonphenolic lignin models are not oxidized by either the MnP/ Mn^{II}-malonate system or by Mn^{III}-malonate complexes (258) under physiological conditions. In contrast, lignin peroxidase catalyzes the one-electron oxidation of non-phenolic lignin model compounds to form aryl cation radicals which subsequently undergo a variety of nonenzymatic reactions including C_α-C_β cleavage and ring cleavage (29-31,106,231, 232,241).

5.4.1 Role of Thiol as a Mediator

Recently, the oxidation of veratryl alcohol and nonphenolic β-aryl-ether-type lignin dimers by MnP in the presence of thiols has been reported (305). In that report (305) the authors claim that in

the presence of thiols the Mn^{III}-pyrophosphate complex is capable of oxidizing aromatic substrates to their corresponding aryl cation radicals, and that GSH stimulates the reaction by reducing oxygen to superoxide. We considered this to be an unlikely mechanism (305) for several reasons: (a) Aryl cation radicals of lignin models readily undergo C_α-C_β cleavage in reactions involving LiP or other single electron oxidizing agents (29-31,106); yet C_α-C_β cleavage was not observed in the MnP/Mn^{II}/thiol system (305). (b) Stimulation by thiol was attributed to the production of superoxide radical; however, superoxide dismutase did not significantly affect the reaction rate (305). (c) The redox potential of Mn^{III}-pyrophosphate (~0.6 V at pH 4.5) (312) is less than the redox potential of Mn^{III}-malonate or lactate (275,289). Therefore, the oxidation to aryl cation radicals of veratryl alcohol and other dimethoxy benzenes with higher redox potentials (313) by Mn^{III}-pyrophosphate is not energetically favorable.

To clarify the mechanism of the MnP-catalyzed thiol-mediated oxidation of nonphenolic lignin models, we have reexamined the reaction using spectroscopic, kinetic, and product analyses.

As shown in Tables 5-1 and 5-2, veratryl alcohol, anisyl alcohol, and benzyl alcohol were oxidized by (i) MnP/Mn^{II}/thiol; (ii) Mn^{III}-malonate/thiol; and (iii) γ-irradiation in the presence of thiol, to yield identical products. In each system the benzyl alcohols were oxidized to yield the corresponding aldehyde as the major product and a coupled dimer as a minor product. These reactions were absolutely

dependent on the presence of thiol. Initial rates of reactions conducted under anaerobic conditions were ~2x greater than the rates of reactions conducted under aerobic conditions. Table 5-1 shows that veratryl alcohol, anisyl alcohol and benzyl alcohol were oxidized with approximately equal efficiency by all three systems, indicating that aromatic methoxy groups do not influence these reactions. The addition of aromatic methoxy groups lowers the redox potential of methoxy benzenes (313); for example, the redox potentials of mono-methoxy and dimethoxy benzenes have been determined to be ~1.76 and 1.34-1.45 V, respectively (313). Thus, the oxidation of methoxy benzenes to aryl cation radicals by peroxidases is facilitated by the addition of methoxy groups (241,314). For example, lignin peroxidase easily oxidizes veratryl alcohol, but oxidizes anisyl alcohol slowly, and is not capable of oxidizing benzyl alcohol (K. Valli, H. Wariishi, M. H. Gold, manuscript in preparation). It is therefore unlikely that the reactions reported herein proceed through a cation radical intermediate.

The results in Fig. 5-1A indicate that Mn^{III} is rapidly reduced to Mn^{II} in the presence of GSH. Furthermore, accumulation of Mn^{III} in the enzyme system is suppressed in the presence of GSH (Fig. 5-1B). Finally, reduction of Mn^{III} with DTT yields an intramolecular disulfide product. All of these results indicate that the Mn^{III} oxidizes the thiol to a thiyl radical which undergoes radical coupling to form the disulfide. The oxidation of thiols to thiyl radicals by Mn^{III} and other transition metals has been reported previously

(289,294,303,304,315). The existence of free thiyl radicals has been confirmed by electron spin resonance spectroscopy (316,317).

As further proof of the involvement of thiyl radicals, we utilized γ-irradiation in the presence of thiols as a source of these radicals. Generation of thiyl radicals from thiols by γ-irradiation via ·OH mediation has been well established (310,311,318). Table 5-1 shows that the thiol/γ-irradiation system oxidizes all of the benzyl alcohols to yield the same products as the MnP/Mn^{II}/thiol system. None of the reactions occurred in the absence of thiol. These results also suggest that the enzyme-generated Mn^{III} oxidizes thiols to thiyl radicals which, in turn, mediate the dehydrogenation of the substituted benzyl alcohols. Hydrogen abstraction from active hydrogen donors by thiyl radicals to yield carbon-centered radicals has been previously reported (319,320).

The initial rate of the reactions conducted under anaerobic conditions is twice the reaction rate under aerobic conditions (Table 5-2). As described previously (304), molecular oxygen reacts with thiyl radicals to form superoxide anion, thereby lowering the effective concentration of the reactive thiyl radicals. These results contradict the proposal by Forrester et al. (305) that thiols stimulate the oxidation by forming superoxide radical. In addition, in contrast to the results reported by Forrester et al. (305), Table 5-2 shows that malonate and lactate stimulate the oxidation of veratryl alcohol in these systems more effectively than either oxalate

or pyrophosphate. The results in Fig. 5-2, demonstrating that activity increases with increasing pH, suggest that protonation of the thiol inhibits its oxidation (304).

5.4.2 Mechanism of Benzyl Alcohol Oxidation

Oxidation of thiol by Mn^{III} generates a thiyl radical, which in turn can abstract a benzylic hydrogen from benzyl alcohol (319,320) to form a benzylic radical. Under anaerobic conditions, the benzylic radical probably couples with another thiyl radical to produce an unstable thiohemiacetal (Fig. 5-4). The latter would decompose to form a free thiol and a benzaldehyde. The formation of stable GSH conjugates from thiyl radicals has been reported previously (317,321). Radical coupling of two benzylic radicals would yield the coupled dimers **IX**, **X**, and **XI**, which were observed in this study. Although these coupled dimers are obtained in only trace amounts, their formation strongly supports this mechanism. Under aerobic conditions the benzylic radical could be scavenged by molecular oxygen or a hydroperoxy radical to yield a peroxy intermediate which would decompose to yield the benzaldehyde product (322). Formation of the dimeric α-carbonyl (**XIII**) and the β-vanillin ether (**XIV**) from the β-vanillyl alcohol ether (**XII**) (Fig. 5-3) and the benzylic oxidation of **XIV** and **XVI** to yield **XV** and **XIX**, respectively (Fig. 5-3) can be explained in a similar manner.

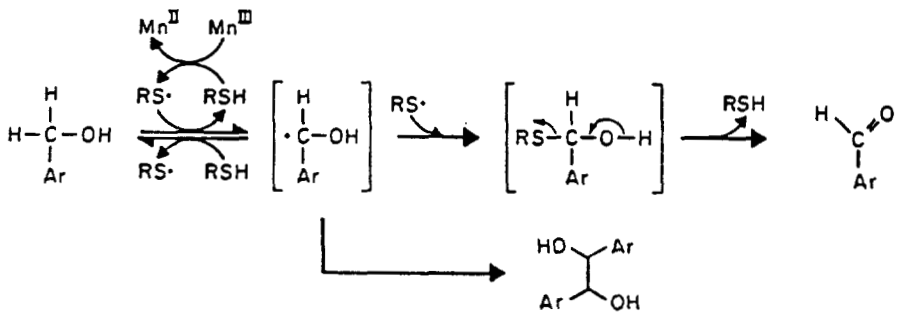

Fig. 5-4. Proposed mechanism for benzyl alcohol oxidation by the MnP /Mn^{II}/thiol (RSH) and Mn^{III}/thiol systems. Ar = aromatic.

5.4.3 Mechanism of β-Ether Cleavage

The β-vanillyl alcohol ether dimer (**XII**) has two benzylic hydrogens available for abstraction by thiyl radicals. Abstraction of the C_α (A ring) hydrogen yields a benzylic radical, leading to C_β-oxygen ether bond cleavage. This results in the formation of the unstable phenylpropene and phenoxy radical intermediates (Fig. 5-5, pathway A). The phenylpropene would be converted to the phenylpropane-1-oxo-3-ol (**XIX**). The phenoxy radical could abstract a hydrogen from GSH as previously proposed (315) to yield vanillyl alcohol (**VII**) and another thiyl radical (Fig. 5-5). When the reaction was conducted in D_2O, no deuterium was incorporated into the vanillyl alcohol (data not shown), suggesting that the phenolic hydrogen derived from GSH. The phenoxy radical of vanillyl alcohol may also be oxidized to vanillin via the transient formation of a quinone methide intermediate (86,258).

Alternatively, when the benzylic radical is formed at the C_α' (ring B) (Fig. 5-5, pathway B), the ensuing radical cleavage yields a quinone methide and a C_β radical intermediate. The quinone methide spontaneously rearranges to vanillin. The C_β radical may abstract a proton from GSH to generate the phenylpropane-1,3-diol (**XVI**). The fact that when the reaction was conducted in D_2O, no deuterium was incorporated into the diol (**XVI**) supports this mechanism. Exogenous phenylpropane-1,3-diol was oxidized to the corresponding ketone (**XIX**) by the enzyme system (Figs. 5-3 and 5-5).

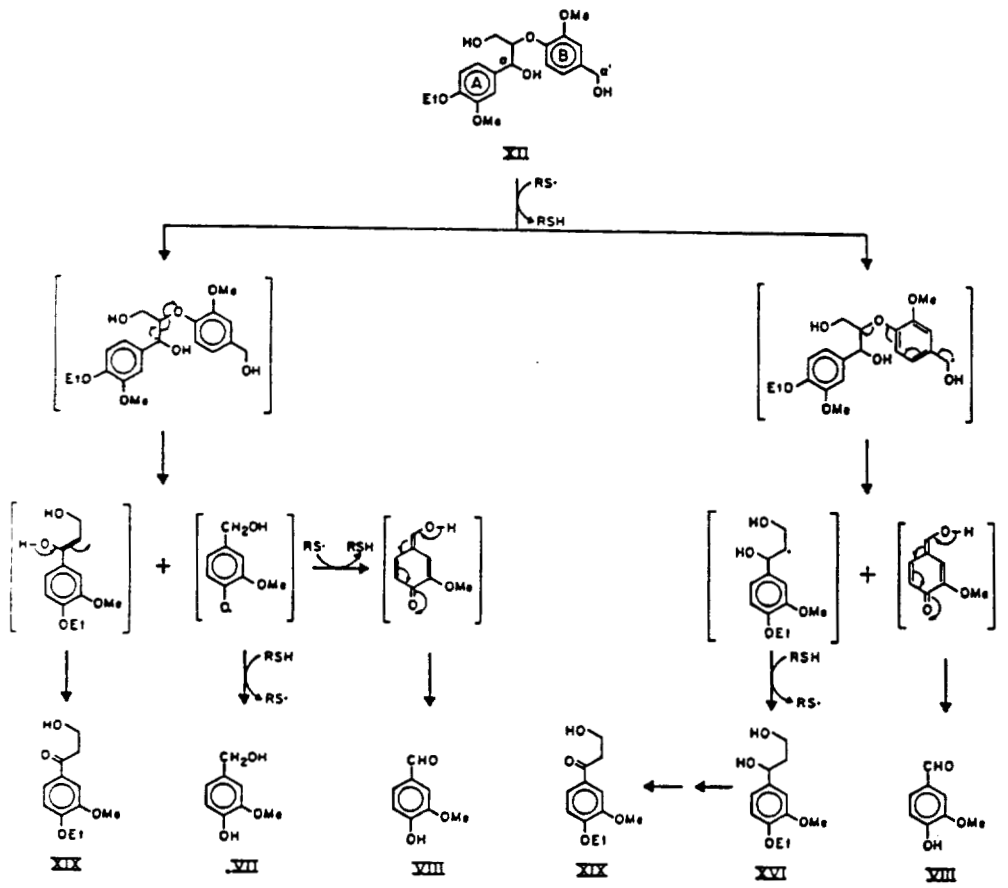

Fig. 5-5. Proposed mechanisms for β-aryl ether cleavage of the non phenolic β-aryl ether dimer (XII) by MnP/Mn^{II}/thiol.

The results reported here and previously can be summarized in the following reactions:

$$Mn^{III} + RSH \rightarrow Mn^{II} + RS\cdot + H^{+} \quad [5\text{-}1]$$

$$RS\cdot + AH \rightleftarrows A\cdot + RSH \quad [5\text{-}2]$$

$$A\cdot \rightarrow \text{further nonenzymic reactions} \quad [5\text{-}3]$$

$$2RS\cdot \rightarrow RSSR \quad [5\text{-}4]$$

where RSH and AH represent thiol and nonphenolic aromatic substrates, respectively. The key steps in the system are the oxidation of thiols to thiyl radicals by enzymically generated Mn^{III} (reaction 5-1) and hydrogen abstraction at the α carbon by thiyl radicals to form a benzylic radical (reaction 5-2). These results preclude formation of an aryl cation radical as proposed by Forrester et al. (305).

Product and kinetic analyses (Tables 5-1 and 5-2) demonstrate that molecular oxygen is not required for these reactions. Indeed, oxygen probably inhibits the reaction by competing for the thiyl radical (304) (reactions 5-5 and 5-6):

$$RS\cdot + O_2 \rightarrow RSO_2\cdot \quad [5\text{-}5]$$

$$RSO_2\cdot + RSH \rightarrow RSSR + H^{+} + O_2^{-}\cdot \quad [5\text{-}6]$$

Although nonphenolic β-aryl ether lignin dimers were effectively cleaved at the C_β-O bond subsequent to the thiol-mediated formation of benzylic radicals, it seems unlikely that extracellular thiols could

play a significant role in the process of lignin degradation by white-rot fungi since: (a) lignin degradation is greatly stimulated by aerobic conditions, and (b) there is no evidence for free thiols in the extracellular culture media of several white rot fungi (M. H. Gold et al., unpublished results). Nevertheless, the effective thiol-mediated degradation of dimeric model compounds and of polymeric lignin (305) by MnP suggests that this system may have potential applications in the degradation of industrial lignins.

CHAPTER 6

SPECTROSCOPIC AND KINETIC PROPERTIES OF THE OXIDIZED INTERMEDIATES OF LIGNIN PEROXIDASE[*1]

6.1 INTRODUCTION

Under secondary metabolic conditions the wood-rotting basidiomycete Phanerochaete chrysosporium secretes two extracellular heme peroxidases which are involved in the degradation of lignin (29-31). These enzymes, manganese peroxidase and lignin peroxidase (LiP),[*2] have been purified and characterized (98-101,104). LiP, a glycoprotein with a molecular weight of 41,000 and a single iron protoporphyrin IX prosthetic group (99-101), catalyzes the H_2O_2-dependent oxidation of lignin model compounds via the initial formation of a substrate aryl cation radical with subsequent nonenzymatic reactions to yield the

---

*1 The contents of this chapter have been published; Spectroscopic and Kinetic Properties of the Oxidized Intermediates of Lignin Peroxidase from Phanerochaete chrysosporium. L. Marquez, H. Wariishi, H. B. Dunford, and M. H. Gold (1988) J. Biol. Chem. 263, 10549-10553 (Ref. 260)

final products (29-31,67,106,231,241,248,249). Our initial characterization of the oxidized intermediates LiPI, LiPII and LiPIII has been reported (232). Herein, we have utilized rapid-scan spectrophotometry to determine the spectra ofthe oxidized intermediates of LiP generated both at the pH optimum (3.0) and at pH 6.0 under pseudo-first-order conditions with excess H_2O_2. We have also investigated the pH dependence of LiPI formation and the rate of reduction of LiPI and LiPII using VAlc as the reducing substrate.

6.2 EXPERIMENTAL PROCEDURES

6.2.1 Enzyme Preparation

The major isozyme of LiP was purified from cultures of P. chrysosporium as previously described (99,101). The purified protein was homogeneous and had an RZ value (A_{408}/A_{280}) of ~5.0. Enzyme concentrations were determined at 407.6 nm using a molar absorptivity of 133 mM^{-1} cm^{-1} (99,101). The enzyme was dialyzed exhaustively against triply-distilled water before use (232). The concentration of

---

*2 Abbreviations:
LiP, lignin peroxidase; LiPI, LiPII, LiPIII, compounds I, II, and III of lignin peroxidase; HRPI, HRPII, HRPIII, compounds I, II, and III of horseradish peroxidase; VAlc, veratryl alcohol.

H_2O_2 (BDH Chemicals) was determined as reported (280).

6.2.2 Rapid Scan Spectrometry

Rapid scan spectra were recorded with the Photal (formerly Union Giken) RA601 Rapid Reaction Analyzer equipped with a 1-cm cell. The absorption spectra were measured by means of a multichannel photodiode array and memorized in a digital computer system (Sord M200 Mark III). The analogue replica was plotted on an X-Y recorder. Spectral regions of 96 nm were scanned from 360 to 700 nm.

6.2.3 Kinetic Analysis

Kinetic measurements were conducted using the Photal RA601 in the stopped-flow mode. One of the drive syringes contained native LiP or LiPI in deionized water while the other syringe contained the substrate (H_2O_2 or VAlc) and buffer. All experiments were performed at (25.0±0.5) °C in 0.1 M sodium citrate buffer $\leq$ pH 4.5 and in 0.1 M sodium phosphate > pH 4.5.

LiPI formation was followed at 407.6 nm using a final enzyme concentration of 1.5 μM and various concentrations of excess H_2O_2 (20 to 200 μM) to maintain pseudo-first-order conditions. The reaction was observed from pH 3.06 to 7.39. LiPII formation and decay were followed at 426 nm. LiPI (1.5 μM) was freshly prepared for each experiment. Various concentrations of VAlc or cresol were buffered at the pH indicated.

6.3 RESULTS

6.3.1 Spectral Characteristics of LiP Compound I

The pH optimum for LiP is ~3.0 (101,236,237); thus, where possible, spectral measurements were made at this pH. Measurements were also made at pH 6.0 where LiPI and LiPII are more stable (232). The spectrum of native LiP has maxima at 407, 496 and 632 nm (98,101, 232) (Fig. 6-1). Within 0.2 seconds after addition of excess H_2O_2 (30 equivalents) to the native enzyme at pH 3.06, the Soret peak height was reduced by ~60% and a new peak appeared at 650 nm, suggesting the formation of LiPI (232). Isosbestic points between native LiP and LiPI occur at 426 and 540 nm.

6.3.2 Spectral Characteristics of LiP Compounds II and III

Upon addition of 30 equivalents of H_2O_2 to the native enzyme at pH 3.06, a sequence of spectral changes were recorded over a 10-second time span. During the first 0.2 seconds, LiPI formation was observed (Fig. 6-1); subsequently the Soret maximum red-shifted to 419 nm and new peaks appeared in the visible region at 545 and 579 nm indicating the formation of compound III (Fig. 6-2A) (232). A spectrum for LiPII could not be observed under these conditions. In contrast, within 2 seconds after the addition of 30 equivalents of H_2O_2 to the native enzyme at pH 6.21, the transient formation of LiPII (visible maxima at 525 and 555 nm) (232) was observed (Fig. 6-2B). Within 10 seconds, LiPII was converted to LiPIII (maxima at 419, 543 and 579 nm) (232).

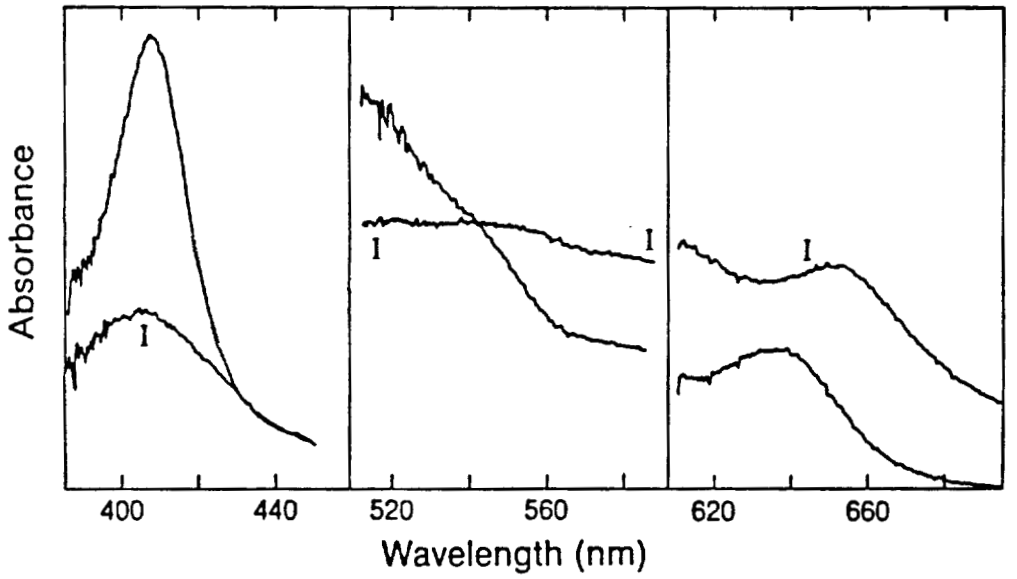

Fig. 6-1. **Reaction between LiP and hydrogen peroxide. Formation of LiPI at pH 3.06.** Concentrations after mixing: LiP, 1.5 μM; H_2O_2, 50 μM for the Soret spectrum and 10μM LiP, 300 μM H_2O_2 for the visible spectrum. Spectrum of LiPI was obtained 0.2 s after mixing. The reference spectrum is that of native LiP.

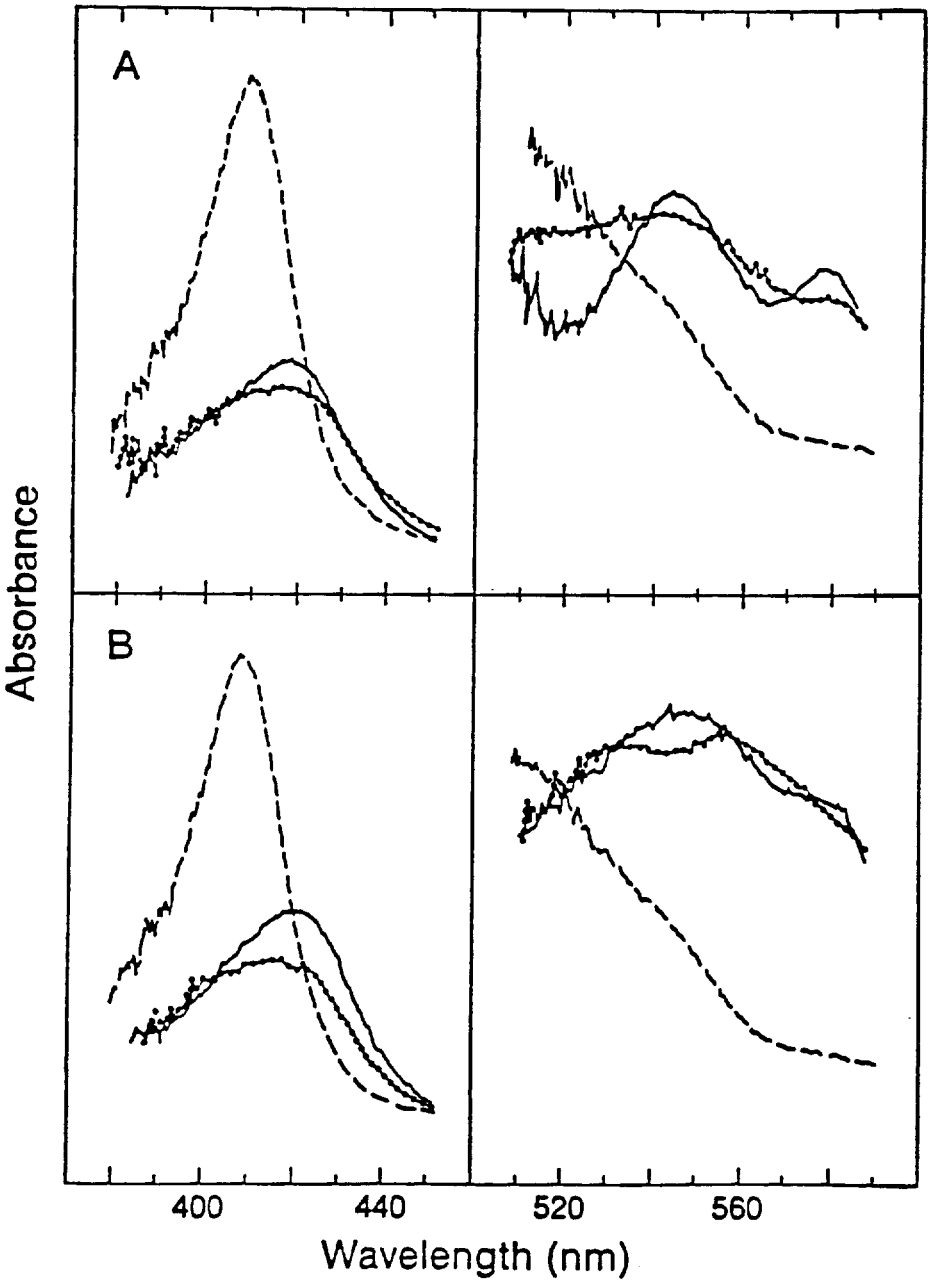

Fig. 6-2. **Reaction between LiP and hydrogen peroxide. Formation of LiPII and LiPIII.** A: Experimental conditions as in Fig. 6-1. Spectra recorded 2 (·–·) and 10 (——) s after mixing. B: Experimental conditions as in Fig. 6-1, except pH is 6.21. Spectra obtained 2 and 10 s after mixing. The dashed lines are the spectrum of native LiP.

6.3.3 Compound II Formation in the Steady State

In the previous work (232) LiPII was prepared by adding two equivalents of H_2O_2 to the native enzyme at pH 6.0. In order to prepare LiPII under pseudo-first-order conditions with excess H_2O_2, steady-state conditions were applied. If the rate constant for the reduction of LiPI (k_2) is larger than that for the reduction of LiPII (k_3), and if sufficient H_2O_2 is present so that LiPI formation is not rate limiting, then the accumulation of LiPII can be expected in the steady state (Appendix C). With HRP, k_2 is ~10 times k_3 (137).

Rapid scan spectra of LiP were recorded in the steady state in the presence of either p-cresol or VAlc at pH 6.21. When the concentrations of H_2O_2, p-cresol and LiP were 60, 15 and 1.5 μM, respectively, a spectrum for the Soret region of LiPII was obtained (Fig. 6-3). The Soret of LiPII had ~85% of the molar absorptivity of the native enzyme. A steady-state spectrum for LiPII could also be obtained at pH 3.0 with VAlc as the reducing substrate (data not shown).

6.3.4 Kinetic Analysis on Compound I Formation

All kinetic traces were of a single exponential character. The observed rate constants were linearly proportional to the H_2O_2 concentration in the range used. The formation of LiPI exhibited no pH dependency from pH 3.06 to 7.39 (data not shown). The mean rate constant was $(6.5 \pm 0.2) \times 10^5$ $M^{-1}s^{-1}$.

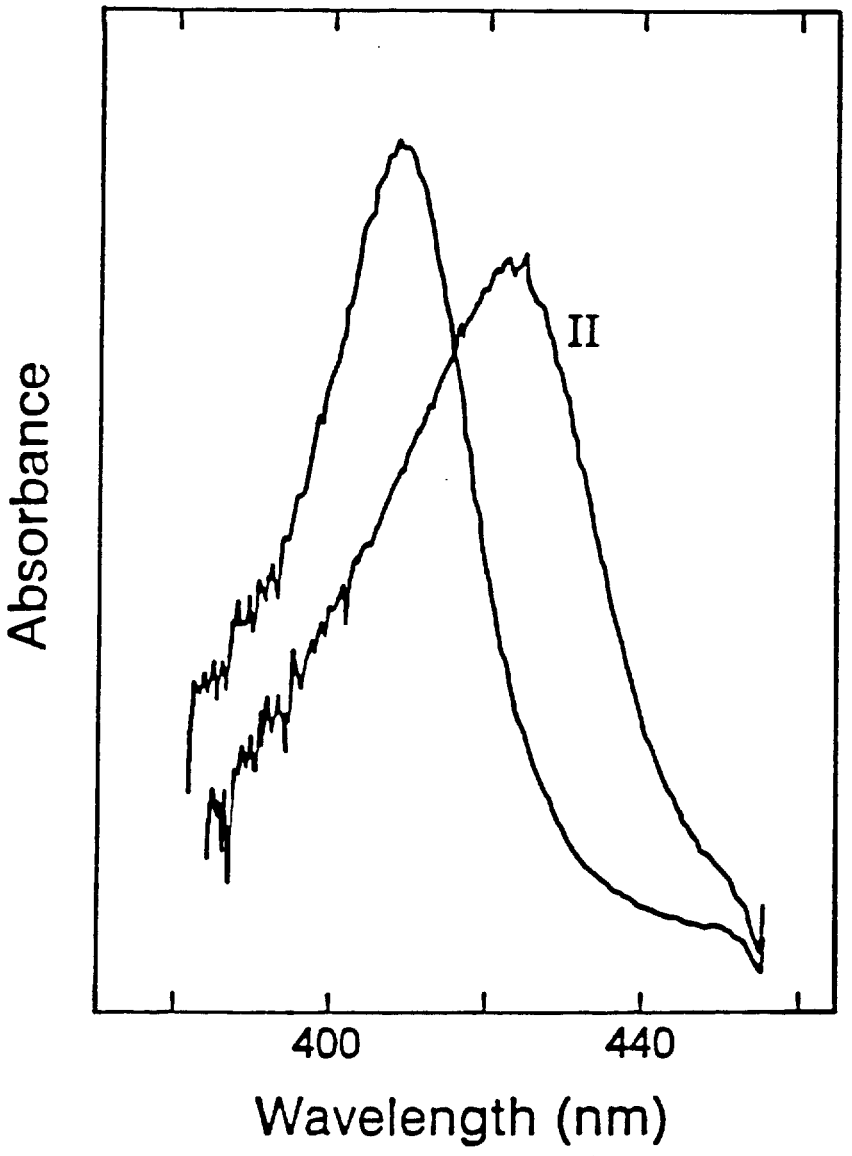

Fig. 6-3. **Formation of compound II in the steady state.** Reaction mixtures contained LiP (1.5 μM), H_2O_2 (60 μM), and p-cresol (15 μM) and were buffered at pH 6.2. Spectrum of LiPII obtained 7.2 s after mixing.

6.3.5 Reduction of LiPI by Veratryl Alcohol

The formation of LiPII and its subsequent conversion to the native enzyme in the presence of VAlc was followed at 426 nm, the isosbestic point between native LiP and LiPI. At this wavelength the absorptivity of LiPII is >2 times that of native LiP and LiPI (232).

Fig. 6-4 shows a typical time course trace of the changes in absorbance. The biphasic curve shows an initial increase in absorbance (formation of LiPII) which is completed in less than 20 ms (shown on the expanded scale) followed by a decline (reduction of LiPII). The traces were exponential in character when followed for sufficiently short intervals. The rate of formation of LiPII was followed at different pH values ranging from 3.06 to 7.39. Fig. 6-5A shows the pH dependence of the reaction of LiPI with VAlc. The rate decreased dramatically with increasing pH, from 2.5×10^6 $M^{-1}s^{-1}$ at pH 3.06 to 4.1×10^3 $M^{-1}s^{-1}$ at pH 7.39. This result is consistent with published findings (236,237) that the activity of LiP increases to a maximum near pH 2.5 and approaches zero at pH values above 6.

The second portion of the biphasic curve (Fig. 6-4) corresponds to the slower one-electron reduction of LiPII to the native enzyme. Fig. 6-5B shows the pH dependence of this reaction. Again, a striking decrease in rate constant is observed as the pH is increased from 3.06 (1.6×10^5 $M^{-1}s^{-1}$) to 5.16 (2.3×10^3 $M^{-1}s^{-1}$).

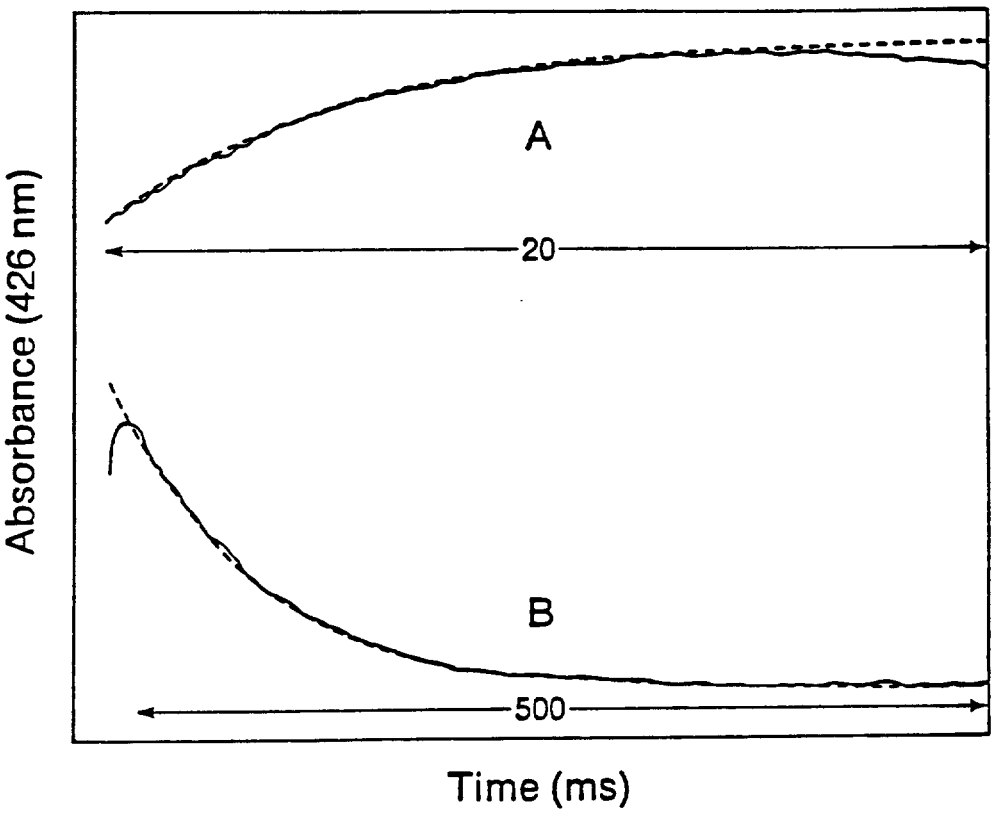

Fig. 6-4. **Time course of the reaction of compound I with VAlc.** LiPI (~1.5 μM) was prepared as rapidly as possible. VAlc (final concentration 100 μM) was buffered at pH 3.06. Sampling period: A: 20 ms; B: 500 ms. The broken lines are the computer-fit exponential curves.

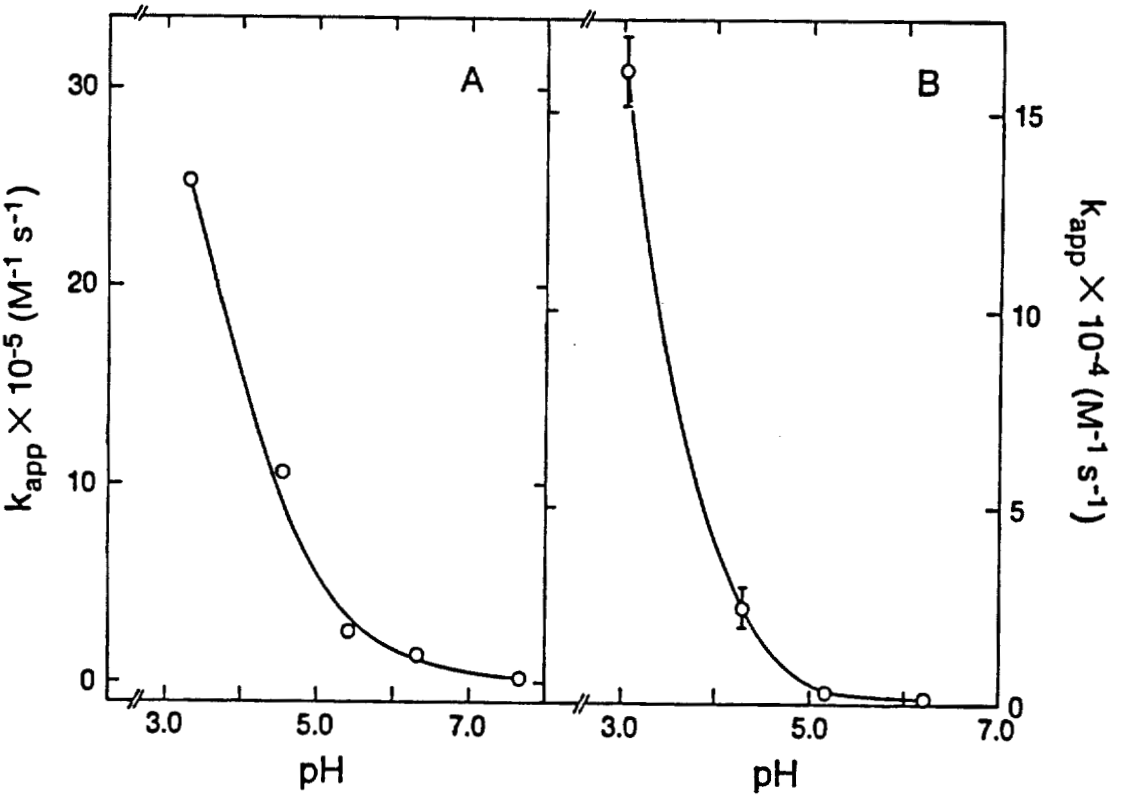

Fig. 6-5. **A. pH dependence of LiPII formation from LiPI.** Experimental conditions as in Fig. 6-4. At each pH the VAlc concentration was varied from 20 to 200 μM. Sampling period ranged from 20 ms to 3 s. **B. pH dependence of native LiP formation from LiPII.** Experimental conditions as in Fig. 6-4. Sampling period ranged from 300 ms to 30 s.

6.4 DISCUSSION

Recently, the oxidized intermediates of the enzyme, LiPI, LiPII, and LiPIII, were prepared at pH 6.0 in the presence of stoichiometric amounts of H_2O_2 (232). Each of these intermediates has spectral characteristics similar to those of the corresponding intermediates of HRP (137). These results suggest that the catalytic cycle of LiP is similar to that of other peroxidases as shown in reactions 6-1 through 6-3:

$$\text{Native LiP} + H_2O_2 \rightarrow \text{LiPI} + H_2O \qquad [6\text{-}1]$$

$$\text{LiPI} + \text{AH} \rightarrow \text{LiPII} + \text{A}\cdot \qquad [6\text{-}2]$$

$$\text{LiPII} + \text{AH} \rightarrow \text{Native LiP} + \text{A}\cdot + H_2O \qquad [6\text{-}3]$$

However, the pH optimum of the enzyme is unusually low for a peroxidase (pH 3.0) (101,236,237) and the K_m of the enzyme for H_2O_2 is ~30 μM (101,236). Therefore, in order to study the oxidized intermediates of LiP at the pH optimum and under pseudo-first-order conditions with H_2O_2 in excess, stopped-flow rapid scan techniques were utilized.

6.4.1 LiP Compound I

The spectrum of LiPI obtained at pH 3.06 with 30 equivalents of H_2O_2 (Fig. 6-1) is very similar to that obtained previously at pH 6.0 (232) and to those obtained for HRP (137), and indicate that this LiPI

preparation is >95% pure. This is the first spectrum of a reasonably pure LiPI at the pH optimum. A recently published spectrum of LiPI, limited to the Soret region, clearly shows contamination by native LiP (Soret intensity ~82% of native LiP) rather than, as the authors claim, an unusually high Soret intensity (261). The reduced absorption of the Soret region of LiPI compared to native LiP and the characteristic absorption band at 650 nm suggests that, like HRPI (137,176,184), LiPI contains two oxidizing equivalents over the native enzyme (232). The first oxidizing equivalent apparently is contained in the ferryl state of the iron (137) as recently confirmed by the resonance Raman experiments (277); the second equivalent is contained as a porphyrin π-cation radical (176,184).

Our kinetic results (data not shown) for LiPI formation demonstrate no pH dependence over a pH range of 3.06 to 7.39, confirming previous results (261). Formation of compound I for other peroxidases is pH-dependent and the distal ionizable group has a low pKa value: for HRP and chloroperoxidase, pKa $\leq$3.0 (193,282) and for yeast cytochrome c peroxidase, pKa $\leq$4.5 (323). Presumably this ionizable group plays a role in the heterolytic cleavage of H_2O_2. The unique lack of pH dependence for LiPI formation suggests that such an ionization may not occur in this system. This may account for the decreased rate of LiPI formation compared to that found for other peroxidases (193,282,323).

6.4.2. LiP Compounds II and III

At pH 3.0 in the presence of excess H_2O_2 and the absence of a reducing substrate, LiP is rapidly oxidized to LiPIII. Within 2 seconds after addition of 30 equivalents of H_2O_2 to native LiP at pH 3.0, a spectrum with characteristic peaks at 545 and 579 nm is observed (Fig. 6-2). Apparently, at this pH in the presence of 30 equivalents of H_2O_2, the half-life of LiPII is too short to obtain its spectrum on this time scale. Even at pH 6.0, the addition of only 25 equivalents of H_2O_2 to native LiP results in its conversion to LiPIII (232) whereas 250 equivalents of H_2O_2 are required to convert native HRP to HRPIII at that pH. Our observation of the rapid formation of LiPIII at pH 3.0 is in contrast to a recent report (261) which claims the detection of LiPII 30 seconds after addition of 20 equivalents of H_2O_2 to native LiP at pH 3.5. However, in that report only the Soret region was scanned and in that region LiPII and LiPIII cannot be readily differentiated.

Evidence for the transient formation of LiPII in the presence of excess H_2O_2 at pH 6.0 is shown in Fig. 6-2B. Possibly, at low pH in the absence of another reducing substrate, H_2O_2 is readily oxidized by LiPII to form $HO_2\cdot$ and native LiP. $HO_2\cdot$ may then complex with the FeIII in native LiP to form the $Fe^{III}O_2^{-}\cdot$ structure of LiPIII (137,223,232). The formation of HRPIII from HRPII and H_2O_2 has been reported (137,223).

6.4.3 Formation of Compound II in the Steady State

In order to prepare a relatively pure preparation of LiPII under pseudo-first-order conditions with H_2O_2 in excess, steady state conditions were applied. Under these steady state conditions a Soret spectrum for LiPII was obtained (Fig. 6-3). The molar absorptivity of the Soret of LiPII was 20% higher than the value we obtained previously (232). These results suggest that, as for HRP (193,282), LiPI has a higher reactivity than LiPII for the reducing substrate.

6.4.4 Reduction of LiPI and LiPII

Our earlier work suggested that the oxidation of VAlc by LiPI proceeds via two single-electron steps (232) with the intermediate formation of a VAlc cation radical (101,248,249) rather than by a single two-electron step (236). The results in Fig. 6-4 show this directly. The initial conversion of LiPI to LiPII takes place in 20 msec. This is followed by a slower conversion of LiPII to the native enzyme over 500 msec. Thus, at pH 3.0 in the presence of excess reducing substrate (VAlc), the normal catalytic cycle is completed via two single-electron steps as shown in reactions 6-1,6-2, and 6-3. This result also demonstrates that LiPII is capable of efficiently oxidizing VAlc.

The pH dependence of the conversion of LiPI to LiPII (k_2) and LiPII to native LiP (k_3) is shown in Fig. 6-5. These results demonstrate directly for the first time that the rate of these conversions is strongly dependent on pH with optimum activity at a low

pH. Apparently, it is the pH dependence of the reduction of LiPI and LiPII rather than the formation of LiPI which dictates the unusually low pH optimum for this enzyme (236,237). These results suggest that an ionizable group(s) with a pK <5.0 controls either the binding and/or oxidation of the reducing substrate by these oxidized enzyme intermediates. Preliminary results (data not shown) indicate that the binding VAlc to the native enzyme has a similar dependence. The low pH optimum of the enzyme may facilitate the formation and stabilization of the aryl cation radical (101,248,249).

CHAPTER 7

LIGNIN PEROXIDASE COMPOUND III: FORMATION, INACTIVATION, AND CONVERSION TO THE NATIVE ENZYME[*1]

7.1 INTRODUCTION

Lignin peroxidase (LiP),[*2] a heme-containing glycoprotein, has been purified from the extracellular medium of the white-rot basidiomycete Phanerochaete chrysosporium (98-101). The H_2O_2-oxidized states of LiP (232,260,261) are similar to those of HRP (137). The enzyme has an unusually low pH optimum (<3.0) (236,237) and catalyzes the H_2O_2-dependent oxidation of a variety of lignin model compounds (30,31,98-101,106). At pH 3.0 in the presence of 20 equiv. of H_2O_2 and in the absence of a reducing substrate, LiP compound III (LiPIII)

[*1] The contents of this chapter have been published;
Lignin Peroxidase Compound III: Formation, Inactivation, and Conversion to the Native Enzyme.
H. Wariishi and M. H. Gold (1989) FEBS Lett. **243**, 165-168 (Ref. 262)

is formed readily (232). In this chapter, we demonstrate that the formation of LiPIII, an oxidized intermediate not involved in the normal peroxidase catalytic cycle (137,232) can lead to inactivation of the enzyme. We also demonstrate that the conversion of LiPIII back to the native enzyme is dependent on veratryl alcohol (VAlc).

7.2 EXPERIMENTAL PROCEDURES

7.2.1 Enzyme Preparation

The major isozyme of LiP was purified from cultures of P. chrysosporium as previously described (98,101), and dialyzed against deionized water. The H_2O_2 concentration was determined as described (280).

7.2.2 Spectral and Kinetic Experiments

Electronic absorption spectra and TNM reduction kinetics were recorded on a Shimadzu UV-260 spectrophotometer equipped with an SEA-11 stopped-flow apparatus (Hi-Tech Scientific). Rapid scan spectra

---

*2 Abbreviations:
HRP, horseradish peroxidase; LiP, lignin peroxidase; TNM, tetranitromethane; VAlc, veratryl alcohol (3,4-dimethoxybenzyl alcohol).

were recorded with a Photol RA601 reaction analyzer as previously described (260). LiP-catalyzed VAlc oxidation products were analyzed by HPLC and GCMS (VG Analytical 7070E) after extraction and derivatization as previously described (98,101). Experiments were performed in 20 mM sodium succinate, pH 3.0. VAlc and TNM were obtained from Aldrich. Tetranitromethane (TNM) was dissolved in ethanol (20 μl), and diluted to 1 mM with water immediately before use (324).

7.3 RESULTS

7.3.1 Formation and irreversible inactivation of LiPIII

Addition of excess H_2O_2 (>20 equiv.) to native LiP at pH 3.0 resulted in its rapid conversion to LiPIII with absorption maxima at 419, 543 and 578 nm (Fig. 7-1A) (232,260). More than 20 equiv. of H_2O_2 was required to form spectrally pure LiPIII. When >30 equiv. of H_2O_2 was used, the formation of LiPIII was followed by the complete disappearance of the Soret and α and β bands within 60 min. (Fig. 7-1A). The spectrally featureless form of the enzyme was inactive when assayed with VAlc. During the enzyme inactivation, LiPIII absorption bands were not shifted, suggesting that LiPIII was converted directly to the inactive form.

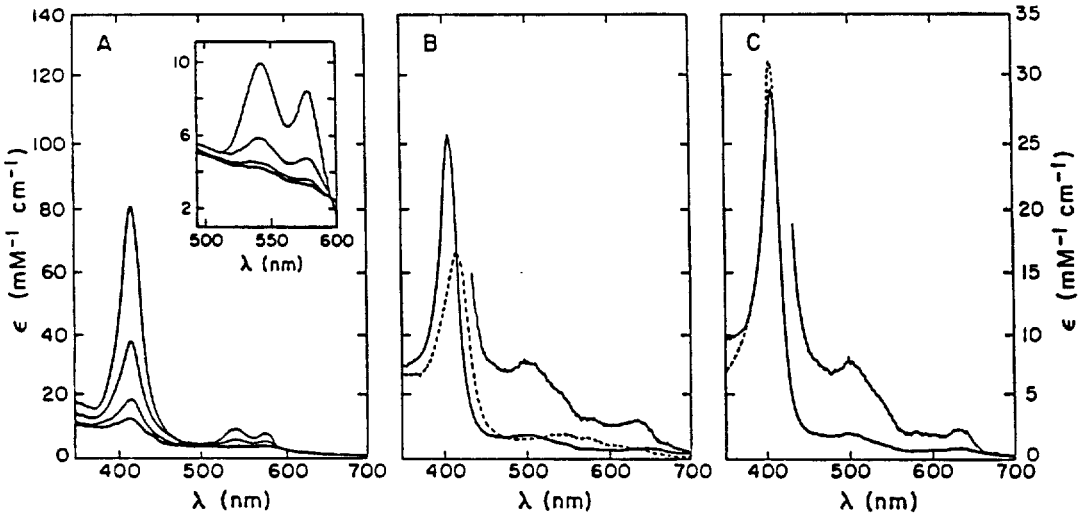

Fig. 7-1. **Formation, inactivation and conversion of LiPIII.** A. H_2O_2 (30 equiv.) was added to 1.5 μM LiP (inset 5.0 μM LiP) at pH 3.0. Spectral scans (20 min. intervals) monitored the inactivation of LiPIII. B. LiPIII (- - -) was prepared by adding 20 equiv. of H_2O_2 to 1.5 μM native LiP. VAlc (40 equiv.) was then added and the conversion to native LiP (———) was observed. C. 40 equiv. of VAlc was added to 1.5 μM native LiP (- - -), after which 20 equiv. of H_2O_2 was added. The resulting spectrum (———) is that of native LiP.

7.3.2 Effect of VAlc on the conversion of LiPIII to native LiP

Addition of 40 equiv. of VAlc to LiPIII resulted in its rapid conversion to native LiP (absorption bands at 408, 500 and 632 nm) (232,260) (Fig. 7-1B). When VAlc was added prior to the addition of H_2O_2, recovery of native LiP was near-quantitative (Fig. 7-1C). Fig. 7-2 shows the rapid scan Soret spectrum of the VAlc-stimulated conversion of LiPIII. The Soret peak shifted from 419 nm to 408 nm over a 0.2-sec. time span. The isosbestic point at 413 nm between LiPIII and native LiP suggests that LiPIII was converted directly to the native enzyme.

To determine whether VAlc was oxidized during the conversion of LiPIII to native LiP, 2 ml of LiPIII (20 μM) was prepared using 40 equiv. of H_2O_2; 15 units of catalase (Sigma) were added to the LiPIII preparation to remove excess H_2O_2, assuring a single turnover event. After 5 min., VAlc (0.2 mM) was added and the conversion of LiPIII was monitored. At the end of the reaction no veratryl aldehyde was detected and the starting VAlc was still present in the reaction mixture. VAlc was also added to LiPI (20 μM) prepared as previously described (232). In this case, oxidation of VAlc to veratryl aldehyde was confirmed by HPLC and GC retention times and by the mass fragmentation pattern of the product, which were identical to the standard.

TNM is efficiently reduced by superoxide anion/hydroperoxide radical ($pK_a \simeq 4.5$) to yield the trinitromethane anion (325) which has

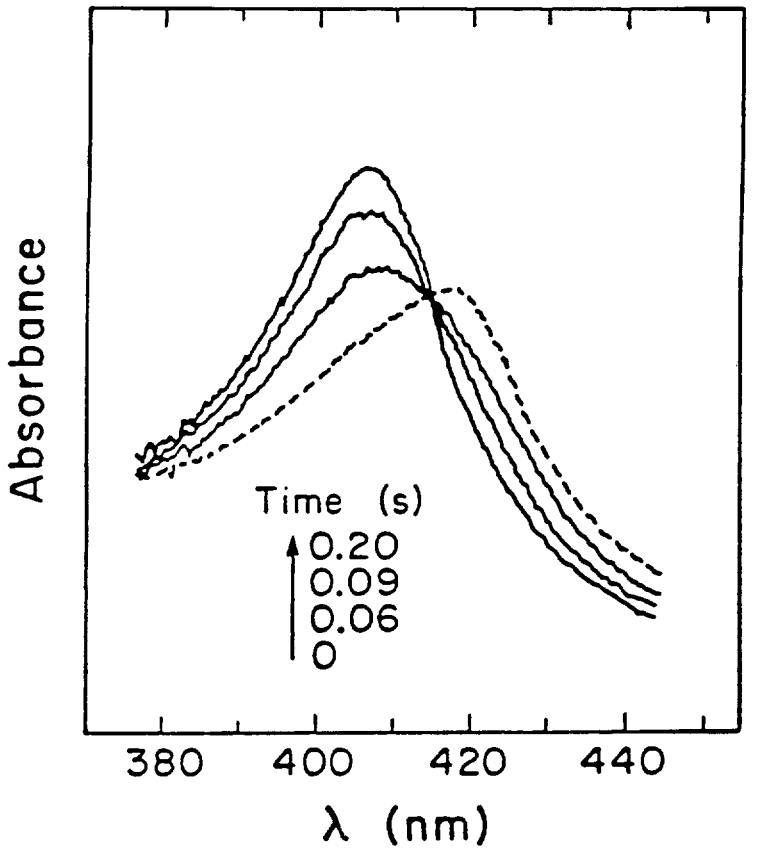

Fig. 7-2. **Rapid scan spectra of LiPIII conversion to native LiP.** LiPIII (- - -) was prepared as in Fig. 7-1A after which 40 equiv. of VAlc was added and rapid scan Soret spectra were taken at the intervals indicated.

a strong absorbance at 350 nm. Fig. 7-3 shows that TNM was rapidly reduced during the conversion of LiPIII. TNM reduction was dependent on the presence of LiPIII and the time course of TNM reduction corresponded closely to that of LiPIII conversion, suggesting that $HO_2\cdot/O_2^{-}\cdot$ was released.

7.4 DISCUSSION

7.4.1 Formation and Inactivation of LiPIII

In the presence of excess H_2O_2 and the absence of a reducing substrate, heme peroxidases are converted from compound II to the compound III state which is either a [$Fe^{III}O_2^{-}\cdot$] complex or [$Fe^{II}O_2$] complex (137,223) (Fig. 7-4). Transient state kinetic studies with H_2O_2 in excess have demonstrated the formation of LiPI (Fe^{IV}=O,$P^{+}\cdot$) and LiPII (Fe^{IV}=O) prior to LiPIII under pseudo-first-order conditions with H_2O_2 in excess (260) (Fig. 7-4). LiP is unusual in that only 20-30 equiv. of H_2O_2 are required for LiPIII formation and inactivation (Fig. 7-1A). In contrast, ~500 equiv. of H_2O_2 are required to form HRPIII (223) which is also followed by its inactivation (326). Since the formation of LiPIII leads to enzyme inactivation (Fig. 7-4), the mechanism of LiPIII conversion back to the native enzyme was of interest.

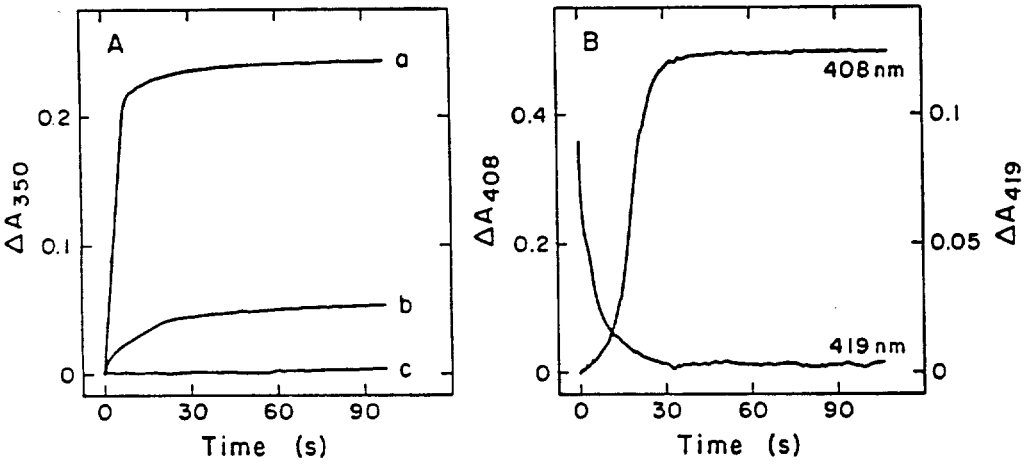

Fig. 7-3. **Reduction of TNM during the conversion of LiPIII.** LiPIII was prepared by adding 40 equiv. of H_2O_2 to native LiP (5.5 μM). A. (a) Reaction mixture contained LiPIII, EDTA (0.1 mM), TNM (0.1 mM) in sodium succinate, pH 3.0; reaction was initiated by adding VAlc (0.23 mM). (b) As in (a) without TNM. (c) As in (a) without LiPIII but with H_2O_2. B. Reaction mixture as in A(a). Formation of native LiP and decrease of LiPIII were followed at 408 and 419 nm, respectively.

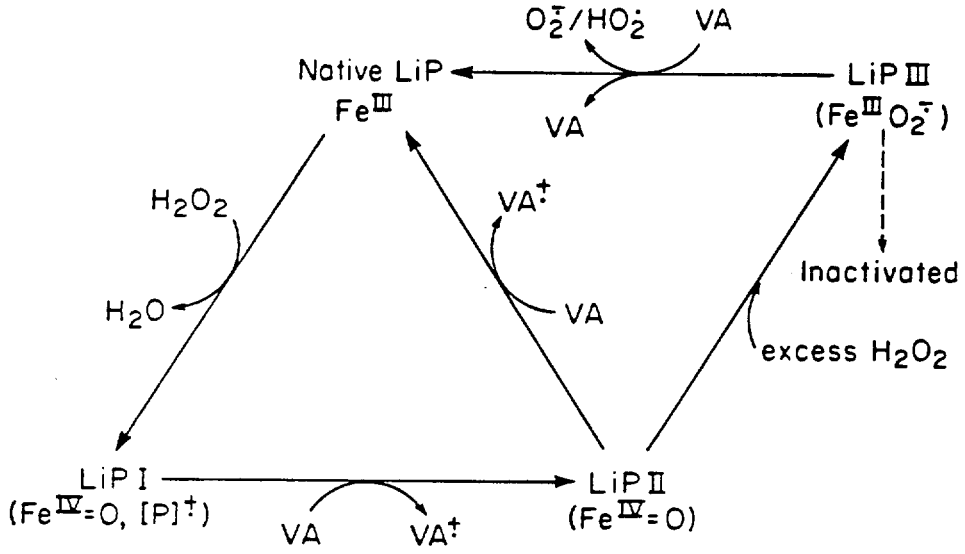

Fig. 7-4. **Interrelationships between the four oxidation states of LiP.** The reaction path, Native LiP → LiPI → LiPII → Native LiP, indicates the catalytic cycle. VA = veratryl alcohol. $VA^{\cdot+}$ = veratryl alcohol cation radical.

7.4.2 Conversion of LiPIII to the Native Enzyme

The reversion of HRPIII to the native enzyme is stimulated by phenolic substrates (127,128). Preliminary evidence also indicated that VAlc stimulates the conversion of LiPIII to native LiP (327). The addition of VAlc to LiPIII caused the rapid conversion of this oxidized intermediate to native LiP (Fig. 7-1B). A single isosbestic point at 413 nm in the Soret region between LiPIII and native LiP indicates that the conversion of LiPIII to native LiP is direct and without intermediates. Ferrous-LiP (absorption maxima 435, 556 nm) (98,232) was not detected during the conversion, suggesting that the LiPIII produced in this study exists as the [$Fe^{III}O_2^{-\cdot}$] complex rather than the [$Fe^{II}O_2$] complex. This was confirmed by measuring the release of $O_2^{-\cdot}/HO_2\cdot$ during the conversion using the $O_2^{-\cdot}$ reduction of TNM as an assay. The release of $O_2^{-\cdot}/HO_2\cdot$ and the total recovery of the added VAlc indicate that oxidation of the substrate did not occur. These results can best be explained by a displacement mechanism (Fig. 7-4) in which the binding of VAlc to the Fe^{III}-$O_2^{-\cdot}$ enzyme complex leads to the release of $HO_2\cdot/O_2^{-\cdot}$ and the formation of the native enzyme. Native LiP binds VAlc at pH 3.0 with an apparent dissociation constant of 4.7 mM (H. Wariishi, unpublished data). Superoxide is also released during the conversion of myeloperoxidase compound III and HRPIII to their native states (226). It is also conceivable that through the release of superoxide which could react with cation radicals, LiPIII may play a role in lignin degradation.

7.4.3 Possible Role of Veratryl Alcohol in LiP Catalytic Action

Since VAlc is a substrate for the enzyme (98-101), its presence also helps ensure that LiPII will be reduced to the native enzyme rather than react with excess H_2O_2 to form LiPIII (Figs. 7-1C and 7-4). VAlc formation coincides with the onset of ligninolytic activity (102,115-117). Recent work has shown that VAlc enhances LiP activity in culture by protecting LiP against inactivation by H_2O_2 (328). A unique feature of LiP is its ready formation of compound III under relatively low concentrations of H_2O_2 (137,232,260). This study demonstrates that LiPIII is rapidly inactivated at its pH optimum. Furthermore, we have also demonstrated that VAlc protects the enzyme against LiPIII formation by reducing LiPII back to the native enzyme, and against inactivaiton by stimulating the conversion of LiPIII to the native enzyme.

Acknowledgements are due to Professor H. B. Dunford for the use of his rapid reaction analyzer.

CHAPTER 8

MECHANISM OF FORMATION AND DECOMPOSITION OF LIGNIN PEROXIDASE COMPOUND III[*1]

8.1 INTRODUCTION

White-rot basidiomycetous fungi are primarily responsible for the initiation of the decomposition of lignin in wood (18,29-31). When cultured under ligninolytic conditions, the white-rot fungus Phanerochaete chrysosporium secretes two extracellular heme enzymes, lignin peroxidase (LiP)[*2] and manganese peroxidase, which, along with an H_2O_2-generating system, are the major components of its lignin degradative system (30,31,106). LiP has been purified to homogeneity and partially characterized. The enzyme is a glycoprotein with a molecular weight of ~41,000, contains one mole of Fe protoporphyrin

---

[*1] The contents of this chapter have been published;
Lignin Peroxidase Compound III: Mechanism of Formation and Decomposition.
H. Wariishi and M. H. Gold (1990) J. Biol. Chem. **265**, 2070-2077 (Ref. 263).

IX, and exists as a series of isozymes (pI 3.2-4.0) (30,31,98-101, 103,106).

The enzyme catalyzes the H_2O_2-dependent oxidation of a variety of nonphenolic lignin model compounds via the initial formation of a substrate aryl cation radical, with subsequent nonenzymatic reactions yielding the final products (29-31,67,106,329). Electronic absorption (31,99), EPR, and resonance Raman (227-229) spectroscopic studies indicate that the heme iron in the native resting enzyme is in the high-spin, predominantly pentacoordinate, ferric state with histidine coordinated as the fifth ligand. The nucleotide sequences of several LiP cDNAs indicate that the proximal histidine and the distal histidine are conserved (233-235).

Initial characterization of the formation and the reactions of the oxidized intermediates LiPI, LiPII, and LiPIII indicate that the oxidation states and catalytic cycle of LiP are similar to horseradish peroxidase (HRP) (31,137,232,260,261). LiP has a typical peroxidase catalytic cycle, but with several unique features. Although LiP has an unusually low pH optimum, ~3.0 (137,236,237), the rate of formation of LiPI is independent of pH from 3.0-8.0 (260,261). In addition, the

---

*2 Abbreviations:
FPLC, fast protein liquid chromatography; HPLC, high-pressure liquid chromatography; HRP, horseradish peroxidase; LiP, lignin peroxidase; LiPI, LiPII, LiPIII, lignin peroxidase compounds I, II, III; TNM, tetranitromethane; VAlc, veratryl alcohol.

ready formation of a LiPIII-like species occurs with considerably less H_2O_2 than is required with other peroxidases (232,260,262). Since this compound III-like species is irreversibly inactivated in the presence of excess H_2O_2, yet can be converted to the native enzyme by addition of the P. chrysosporium secondary metabolite veratryl alcohol (VAlc) (262),we decided to study the mechanisms of the formation and decomposition of LiPIII in greater detail. We have prepared LiPIII via three different pathways (137,156), and have studied its reversion to the native enzyme as well as its reaction with H_2O_2 and subsequent inactivation.

8.2 EXPERIMENTAL PROCEDURES

8.2.1 Enzyme Preparation

P. chrysosporium strain OGC 101 (290) was grown in agitated, acetate-buffered cultures as previously described (99,101), except that the medium contained 0.1% Tween 80 and 6-fold concentrated trace elements. VAlc (3 mM) was added on day 3 (279). Cultures were harvested when maximal LiP activity was observed (day 6 or 7). The enzyme was purified by DEAE-Sepharose chromatography (99,101) and FPLC (mono Q) (102). The purified protein was electrophoretically homogeneous and had an RZ ($A_{408/280}$) value of ~5.0. Enzyme concentrations were determined at 407.6 nm using an extinction coefficient of 133 mM^{-1} cm^{-1} (99). The enzyme was dialyzed exhaustively against deionized water before use.

8.2.2 Preparation of LiPIIIa (ferrous oxy complex)

The addition of a large excess of dithionite during the reduction of HRP adversely affects the subsequent yield of the ferrous oxy complex (220). For this reason, ferrous LiP was prepared by adding only 50 equiv. of sodium dithionite to the native enzyme under anaerobic conditions. Dithionite was dissolved in N_2-saturated H_2O to prepare a 1-mM stock solution immediately prior to use. LiPIIIa was generated by purging the ferrous enzyme with O_2 gas.

8.2.3 Preparation of LiPIIIb (ferric superoxide complex)

LiPIII was also prepared from native LiP by the addition of superoxide anion generated from the xanthine/xanthine oxidase system at pH 6.0 (137,156,330). Superoxide anion was monitored by measuring its capacity to reduce ascorbate to dehydroascorbate at 249.6 nm (330).

8.2.4 Preparation of LiPIII* and LiPIIIc from LiPII

LiP compound II was prepared by the successive addition of stoichiometric amounts of ferrocyanide and H_2O_2 to the native enzyme, followed by dilution with buffer to obtain the desired pH and ionic strength. LiPIII* was prepared by adding 40 equiv. of H_2O_2 (buffered at pH 3.0) to LiPII (6.25 μM). Addition of catalase (0.01 equiv.) to LiPIII* at pH 3.0 to remove excess peroxide resulted in its conversion to LiPIIIc. LiPIIIc was also prepared by separating the LiPIII* from H_2O_2 on a Sephadex G-25 column equilibrated with 50 mM sodium succinate, pH 4.5.

8.2.5 Spectral and Kinetic Experiments

Electronic absorption spectra and rate measurements were recorded on a Shimadzu UV-260 spectrophotometer with a spectral bandwidth of 1.0 nm and cuvettes of 1-cm light path. Reactions were carried out at room temperature in 20 mM sodium succinate, pH 3.0, or as indicated in the text. Some kinetic data were obtained with the spectrophotometer equipped with an SEA-11 stopped-flow apparatus (Hi-Tech Scientific). Possible veratryl alcohol oxidation products were separated by HPLC as described (262).

8.2.6 Chemicals

H_2O_2 (30%), xanthine oxidase, cytochrome c, and catalase were obtained from Sigma. The concentration of H_2O_2 was determined by the HRP assay (280) or spectrophotometrically (331). VAlc and tetranitromethane (TNM) were purchased from Aldrich. TNM was dissolved in ethanol, then diluted with H_2O to prepare a 10-mM stock solution immediately prior to use (262,324).

8.3 RESULTS

8.3.1 Formation and Decomposition of LiPIIIa

Addition of molecular oxygen to ferrous LiP resulted in the immediate formation of LiPIIIa (ferrous oxy complex) (232), with absorption maxima at 414, 543, and 578 nm (Fig. 8-1, Table 8-1).

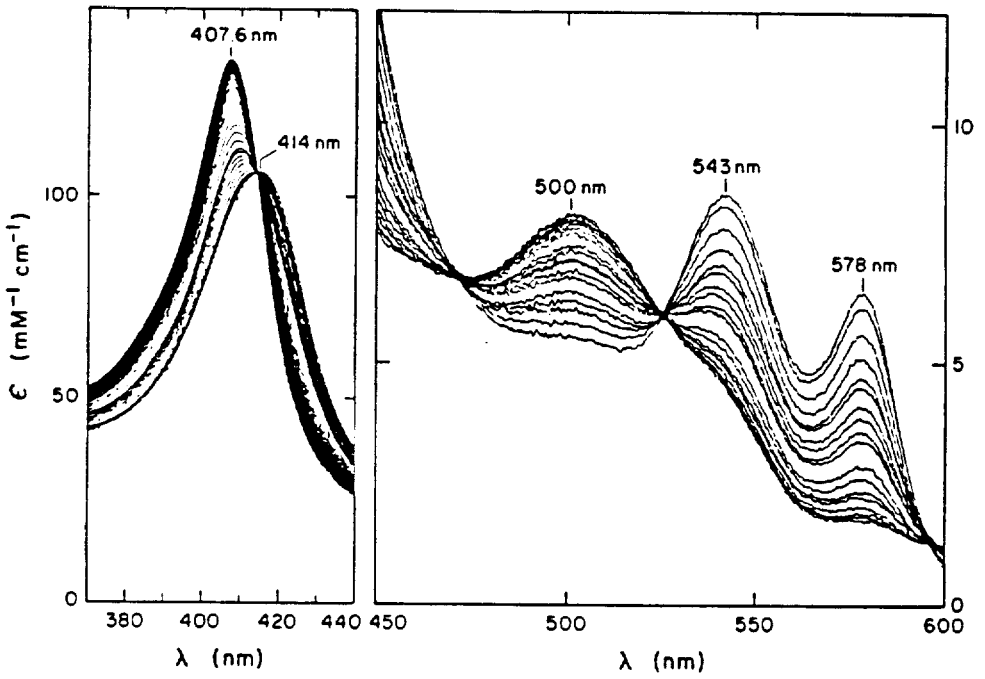

Fig. 8-1. **Spontaneous decomposition of LiPIIIa (ferrous LiP + O_2).** LiPIIIa was prepared by the addition of O_2 to ferrous LiP (5.0 μM). In the Soret region, spectra were taken at intervals of 1 minute (0-6 min); 2 minutes (6-20 min) and 5 minutes (20-120 min). In the visible region, spectra were taken at intervals of 2 minutes (0-18 min) and 5 minutes (25-60 min).

Table 8-1. Spectral characteristics of oxidized intermediates of lignin peroxidase (LiP)

Enzyme intermediates	Absorption maxima (nm) [ε, mM^{-1}, cm^{-1}]				Ref.
Ferric LiP	407.6[133]	500[8.1]		632 [2.7]	98
LiPI	408 [55]	550	608 [sh]	650 [4.5]	232
LiPII	420 [108]	525[7.5]	556 [7.5]		232, this work
LiPIII:					
LiPIIIa[a]	414 [106]	543[8.8]	578 [7.6]		23, this work
LiPIIIb[b]	412 [115]	543[7.1]	578 [6.0]		this work
LiPIIIc[c]	414 [105]	543[8.9]	578 [7.8]		this work
LiPIII*	419 [90]	543[9.0]	578 [7.9]		232, 262, this work
LiP-CN^-	360 [35]	425[76]	540 [10.4]		8
LiPIII* + KCN + VAlc	360 [31]	425[65]	540 [7.6]		this work

[a] Ferrous LiP + O_2

[b] Ferric LiP + $O_2^{\cdot-}$, ~80% purity, contaminated by ferric LiP

[c] LiPII + H_2O_2 + catalase

At pH 3.0, LiP IIIa spontaneously reverted to the native enzyme with a half-life of ~20 minutes. The spectrum displayed isosbestic points at 413, 470, 525, and 597 nm (Fig. 8-1), suggesting a direct conversion without intermediates. To study the kinetics of the spontaneous reversion of LiPIIIa, its disappearance was followed at 543 and 578 nm and the appearance of native LiP was followed at 407.6 and 500 nm (Fig. 8-2A). Fig. 8-2B shows the natural log of the absorbance plotted against time according to

$$\ln|A_t - A_\infty| = -kt + \ln|A_o - A_\infty| \qquad [8\text{-}1]$$

where A_o, A_t, and A_∞ are the absorbances at times 0, t, and 120 minutes. The replotted lines (Fig. 8-2B) for each wavelength were linear and parallel, indicating that the conversion of LiPIIIa to ferric LiP followed first-order kinetics. The rate constant (k_1) determined from the slope of the line was $(1.1 \pm 0.1) \times 10^{-3}$ s^{-1} (Table 8-2).

8.3.2 Formation and Decomposition of LiPIIIb

The oxidation of native HRP to HRPIII in the presence of superoxide has been reported (137,156). Superoxide anion was generated in the presence of LiP with xanthine/xanthine oxidase (330) at pH 6.0. Catalase was added to eliminate H_2O_2 formed via the dismutation of $O_2^{\cdot-}$. Approximately 50 μM $O_2^{\cdot-}$ was generated in 20 minutes under the conditions described in the legend to Fig. 8-3.

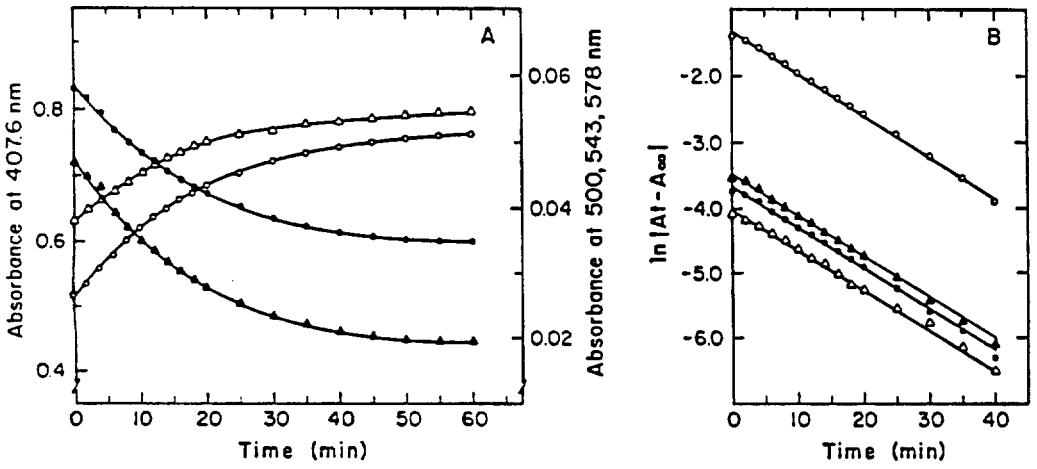

Fig. 8-2. **Time course for the spontaneous decomposition of LiPIIIa (ferrous LiP + O_2).** (A) Appearance of native LiP was monitored at 407.6 (○) and 500 (△) nm. Disappearance of LiPIIIa was followed at 543 (●) and 578 (▲) nm. (B) First-order plot for the decomposition of LiPIIIa. LiPIIIa (5.0 μM) was prepared as described in the text.

Table 8-2. Kinetic parameters for the reactions of LiPIII and LiPIII*

Compound III species	Conditions	First order rate constant (s^{-1})	Second order rate constant ($M^{-1}s^{-1}$)
Conversion to ferric LiP:			
LiPIIIa (ferrous LiP + O_2)	Spontaneous	1.1×10^{-3} (k_1)	----
	+ VAlc[a]	1.3×10^{-3} (k_1VAlc)	----
	+ TNM[b]	2.1×10^{-3} (k_1TNM)	----
LiPIIIb (ferric LiP + $O_2^{\cdot-}$)	Spontaneous	1.0×10^{-3} (k_2)	----
LiPIIIc (LiPII + H_2O_2 + catalase)	Spontaneous	1.0×10^{-3} (k_3)	----
	+ VAlc[a]	1.3×10^{-3} (k_3VAlc)	----
LiPIII* (LiPII + H_2O_2)	+ VAlc (excess)	----	3.5×10^{1} ($k_6$app)
Inactivation:			
LiPIII* (LiPII + H_2O_2)	+ H_2O_2 (excess)		
Fast[c]		----	1.7×10^{1} ($k_4$app)
Slow[c]		$(5.0\text{-}6.5) \times 10^{-4}$ (k_5)	----

[a] The rate was measured under pseudo-first-order conditions with VAlc in excess (100 equiv.).

[b] The rate was measured under pseudo-first-order conditions with TNM in excess (100 equiv.).

[c] The reaction is biphasic (Fig. 8-7).

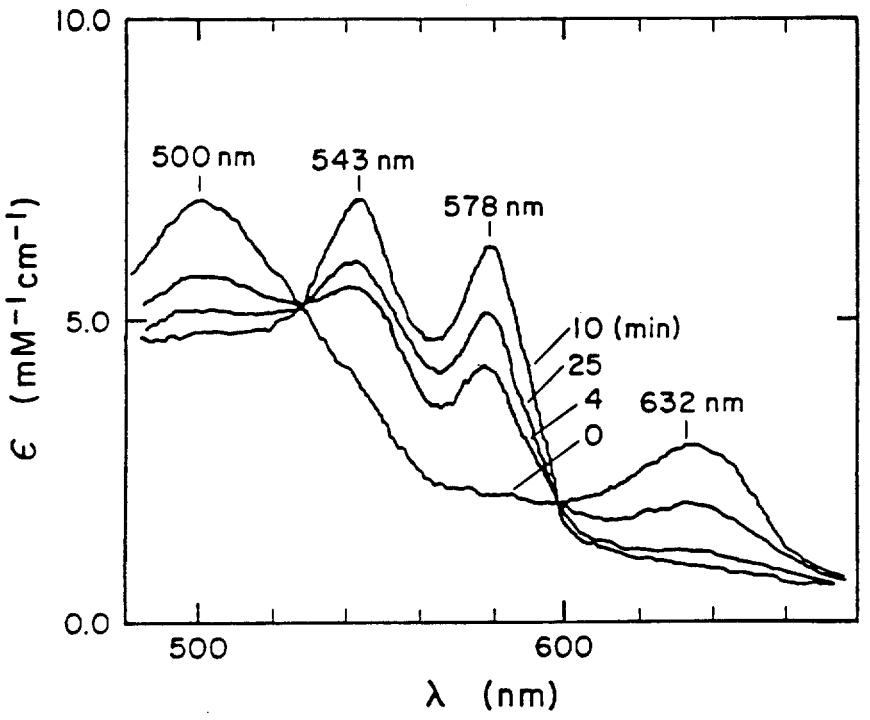

Fig. 8-3. **Formation and spontaneous decomposition of LiPIIIb (ferric LiP + $O_2^{\cdot-}$).** Reaction mixtures (1 ml) contained xanthine (0.2 mM), xanthine oxidase (50 μg), EDTA (70 μM), catalase (22 μg), and LiP (2.1 μM) in 20 mM succinate, pH 6.0. The reference cuvette contained the same mixture, minus LiP. Spectra were taken at 0, 4, 10, and 25 minutes. The reaction was initiated by the addition of xanthine oxidase.

When the reaction was initiated by the addition of xanthine oxidase, ferric LiP was converted to LiPIIIb (Fe^{III}-$O_2^{\cdot-}$ complex). Under these conditions, LiPIIIb started to revert to the native enzyme after ~18 minutes. The spectral changes for the formation and reversion of LiPIIIb showed the same isosbestic points in the visible region at 525 and 597 nm (Fig. 8-3), suggesting that both the forward and reverse reactions occurred in a single reversible step. The kinetics of the reversion of LiPIIIb at pH 3.08 were measured by following the absorbance at 407.6, 500, 543, and 578 (as described in Fig. 8-2) using the pH jump method in which LiPIIIb was prepared at pH 6.0 (5 mM succinate), then buffer (35 mM succinate, pH 3.0) was added to obtain the final pH (data not shown). A plot of ln A vs. time according to eq. 8-1 yielded a first-order rate constant (k_2) for the reversion of LiPIIIb of $(1.0 \pm 0.2) \times 10^{-3}$ s^{-1} (Table 8-2).

8.3.3 Reaction of LiPII with H_2O_2

Previously we prepared a LiPIII species by adding excess H_2O_2 to the native enzyme (232,262). In the present study, this LiPIII species was prepared by the reaction of LiP compound II with H_2O_2. At pH 6.0, LiPII, prepared as described above, was stable for several minutes. In contrast, as described previously, at pH 3.0 LiPII was unstable with a $t_{1/2}$ of less than 1 second (232,260). Addition of 5 equiv. of ferrocyanide to LiPII (pH 6.0) resulted in its rapid reduction to ferric LiP, with isosbestic points at 417.5, 462, and 518 nm.

The addition of excess H_2O_2, buffered at pH 3.0, to LiPII prepared in aqueous solution resulted in the formation of a LiPIII-like species with absorption maxima at 419, 543, and 578 nm (Fig. 8-4, Table 8-1). This spectrum was identical to those reported earlier (232,262). The dependence of the conversion of LiPII to this LiPIII species on H_2O_2 concentration is shown in Fig. 8-4. The spectra displayed isosbestic points at 497, 529, 556, 565, and 588 nm. The LiPIII species derived from LiPII and excess H_2O_2 had properties which distinguished it from LiPIIIa and LiPIIIb. Although the visible spectra of all LiPIII species were identical, the Soret of LiPIII derived from LiPII and H_2O_2 was red-shifted from 412-414 nm to 419 nm (Table 8-1). Also, in contrast to the LiPIIIa and LiPIIIb which spontaneously reverted to the native enzyme, the LiPIII prepared from ferryl LiP and excess H_2O_2 was irreversibly inactivated over time. Previously we reported that this inactivation also followed the addition of excess H_2O_2 to native LiP (262). These observations indicate that LiPIII derived from LiPII and excess H_2O_2 is a different species from LiPIIIa and LiPIIIb and thus is referred to as LiPIII*.

8.3.4 Addition of Catalase to LiPIII*

Although catalase activity was not optimal at pH 3.0, it was found that 6.25×10^{-2} μM catalase (1:100 catalase:LiP) was capable of removing >95% of the H_2O_2 (250 μM) within 3 minutes at pH 3.0, as detected by two independent assays (280,331). During the first two minutes following addition of catalase to LiPIII* (Fig. 8-5A), the

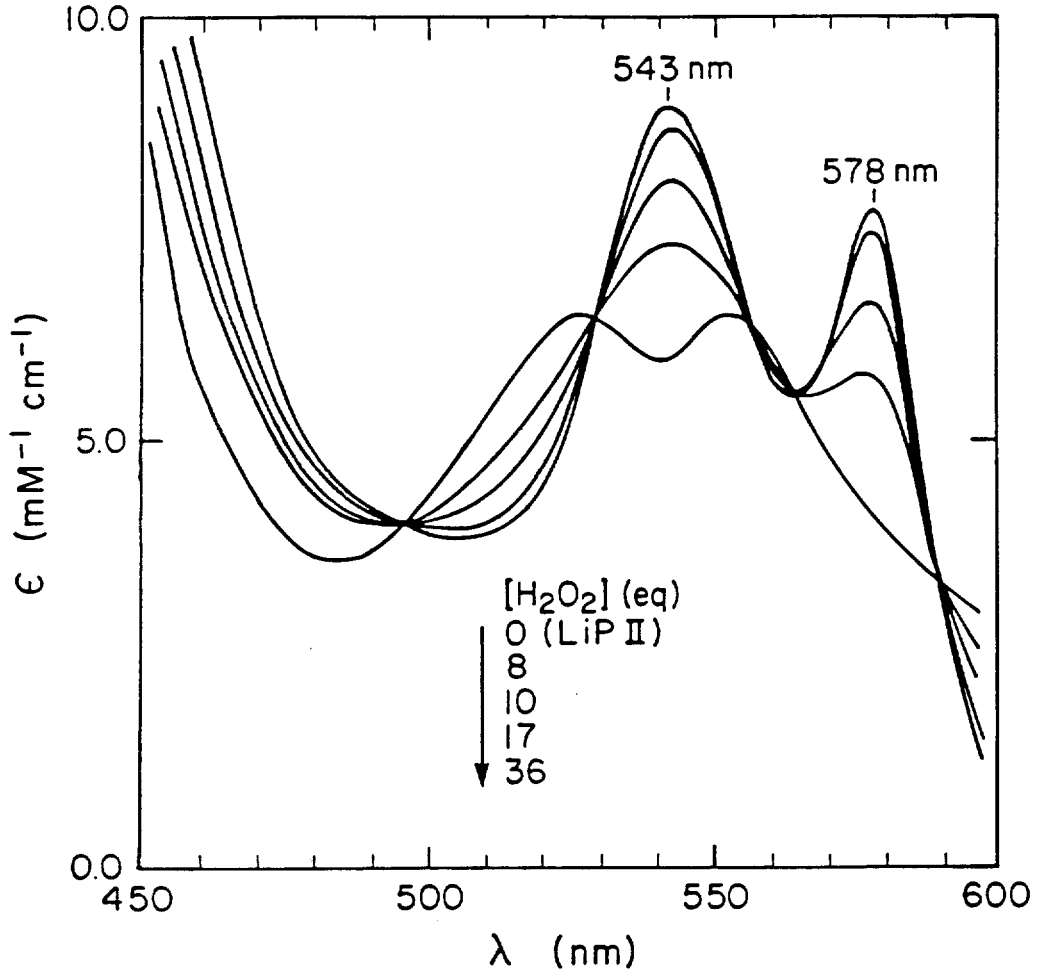

Fig. 8-4. **Preparation of LiPIII* from LiPII and H_2O_2.** LiPII was prepared in H_2O by the successive addition of stoichiometric amounts of ferrocyanide and H_2O_2 to ferric LiP (5 μM). The indicated amounts of H_2O_2 buffered at pH 3.0 were added and the spectra were recorded when the spectral change was maximal (~ 0.5 min.).

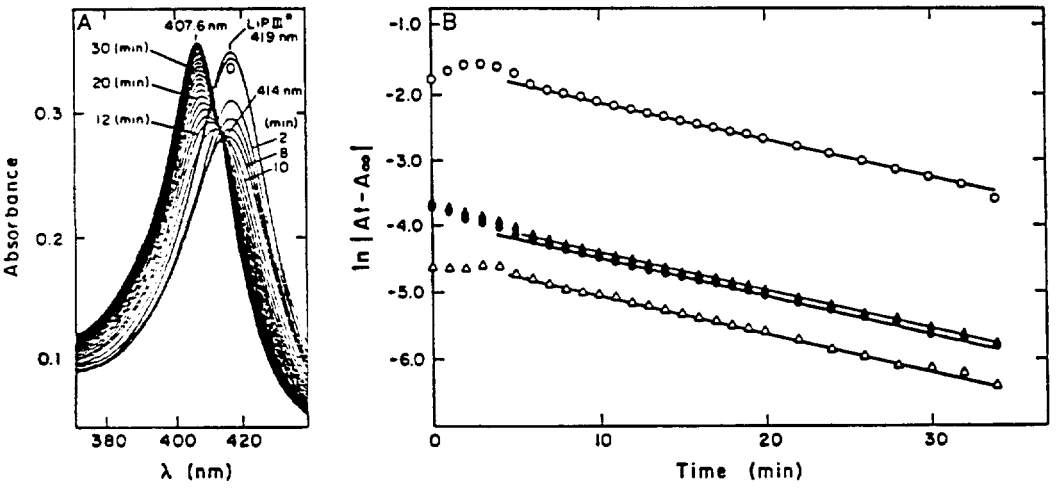

Fig. 8-5. **Effect of catalase on LiPIII*.** (A) LiPIII* was prepared by adding 40 equiv. of H_2O_2 buffered at pH 3.0 to LiPII (6.25 μM) in H_2O. Catalase (6.25×10^{-2} μM final concentration) was then added and spectra were recorded at 2-minute intervals. (B) A time course of the conversion was followed at 407.6 (○), 500 (△) 543 (●), and 578 (▲) nm, and the absorption ($\ln|A_t-A_\infty|$) was plotted against time according to eq. 8-1 in the text.

Soret intensity decreased but the wavelength maximum did not shift. From 2-10 minutes after addition of catalase, the Soret decreased further and shifted to 414 nm. After the first Soret shift was complete, the Soret increased slowly and shifted to 407.6 nm, the wavelength characteristic of native LiP, with isosbestic points at ~413 nm (Fig. 8-5A) and at 470, 525, and 597 nm (data not shown). The time course for spectral changes at 543 and 578 nm (disappearance of LiPIII* or LiPIIIc) and at 407.6 and 500 nm (appearance of ferric LiP) was measured. Replotting ln A vs. time yielded straight lines in the time frame 7-20 minutes after initiation of the reaction. These lines fit eq. 8-1 with first-order rate constant (k_3) of $(1.0 \pm 0.1) \times 10^{-3}$ s^{-1} which is essentially identical to k_1 and k_2 (Table 8-2). These results suggest that the addition of catalase to LiPIII* converts it to LiPIIIc by reacting with bound H_2O_2 and that the resultant LiPIIIc reverts to native LiP through a first-order process.

8.3.5 Involvement of H_2O_2 in LiPIII* formation and inactivation

The results in Fig. 8-5 suggested that LiPIII* might be a LiPIII-H_2O_2 complex. In order to investigate this further, the spectra of LiP III* prepared from different precursors were compared. Fig. 8-6A shows the spectrum of the product of the reaction of LiPIIIa with excess H_2O_2. Fig. 8-6B shows the spectrum of the reaction of LiPIIIb with excess H_2O_2. Finally, LiPII was reacted with H_2O_2 to yield

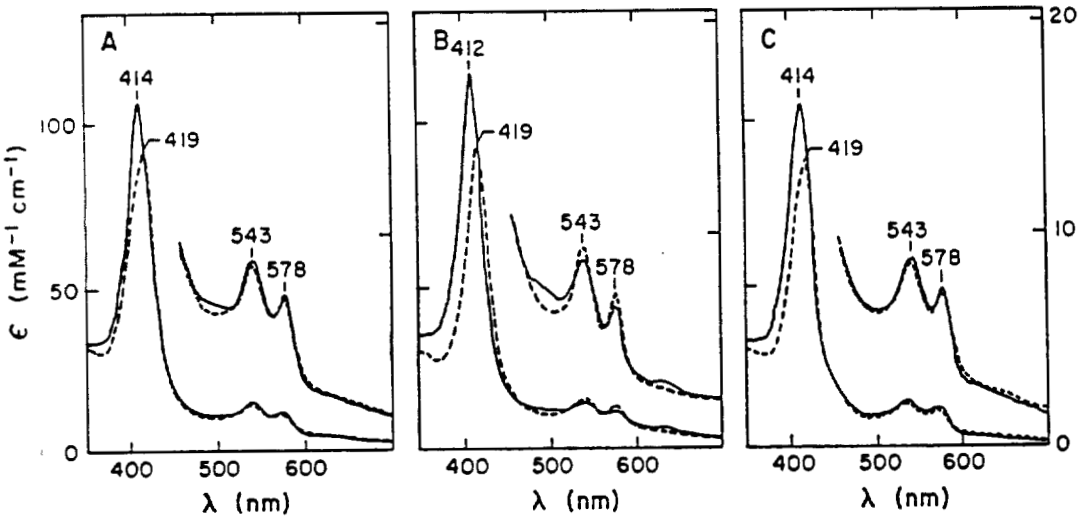

Fig. 8-6. **Effect of excess H_2O_2 on LiPIII.** (A) H_2O_2 (30 equiv.) was added to LiPIIIa (ferrous LiP + O_2) (2.0 μM). (B) H_2O_2 (30 equiv.) was added to LiPIIIb (ferric LiP + $O_2^{-\cdot}$) (2.0 μM), prepared via the pH jump method described in the text. (C) H_2O_2 (40 equiv.) was added to LiPIIIc [LiPII (2.0 μM) + H_2O_2 + catalase (0.02 μM)]. In each case the spectrum of LiPIII was recorded (solid line); H_2O_2 was then added and the resultant LiPIII* spectrum was recorded (dashed line).

LiPIII*, followed by a 4-minute incubation with catalase to generate LiPIIIc. Subsequent addition of excess H_2O_2 to the LiPIIIc yielded the spectrum shown in Fig. 8-6C. LiPIIIa, b, and c had Soret maxima at 412-414 nm, and visible maxima at 543 and 578 nm (Fig. 8-6). Addition of excess H_2O_2 to either LiPIIIa, b, or c resulted in a reproducible 5-nm red shift in the Soret from ~414 to 419 nm, and ~15-20% decrease in Soret intensity. Very little change was observed in the visible maxima. In each case, conversion of LiPIII to LiPIII* in the presence of excess H_2O_2 was followed by inactivation (262) (data not shown). Addition of excess H_2O_2 buffered at pH 3.0 to LiPII also led to the formation of LiPIII* and subsequent inactivation (Fig. 8-7). The semi-log plot of the change in absorbance at 419 nm vs. time at various H_2O_2 concentrations yielded a set of biphasic curves. The k_{4obs} for the first reaction (fast reaction) varied with the amount of H_2O_2 added. In contrast, the rate constant for the second reaction (slow reaction) appeared to be independent of the H_2O_2 concentration. For the fast reaction, a replot of k_{obs} vs. H_2O_2 concentration was linear and passed through the origin (Fig. 8-7, inset), indicating that the fast reaction obeys second-order kinetics and the reaction is irreversible. The second-order rate constant (k_{4app}) determined from the slope of the replot, was $(1.7 \pm 0.1) \times 10^1$ $M^{-1}s^{-1}$. The first-order rate constant (k_5) for the slow reaction was determined to be $(5.0\text{-}6.8) \times 10^{-1}$ s^{-1} (Table 8-2).

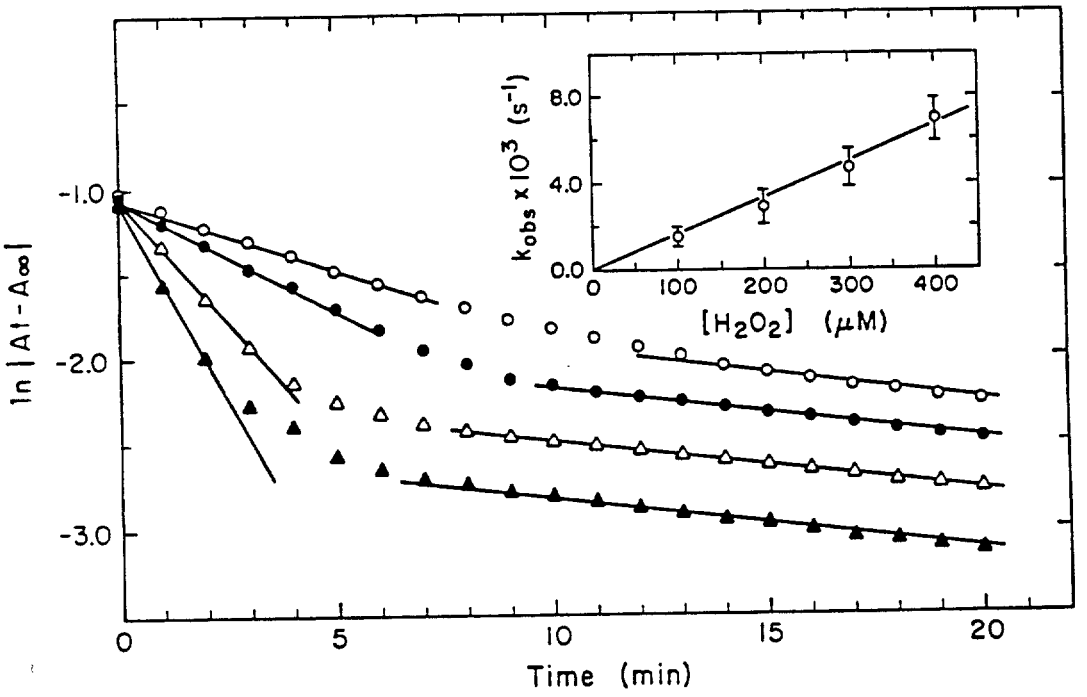

Fig. 8-7. **Reaction of LiPIII* with H_2O_2.** LiPIII* (3.0 μM) was prepared as described in the legend to Fig. 8-4 at pH 3.0 with excess H_2O_2 (100-400 μM). Kinetic traces were obtained at 419 nm and plotted according to eq. 8-1. The concentrations of H_2O_2 used were 100 (○), 200 (●), 300 (△), and 400 (▲) μM. Inset: The slopes of the first phase of the reaction were replotted against [H_2O_2]. Each determination of k_{obs} is the mean of 5 traces.

8.3.6 Release of superoxide from LiPIII

LiPIIIa, b, and c each slowly reverted to the native state via first-order reactions (Table 8-2) with no apparent intermediate involved. Thus, the mechanism of reversion of LiPIII to native LiP is likely to involve the dissociation of a ferric-superoxide complex to ferric LiP + $O_2^{-\cdot}$. In order to examine the reaction, we used the TNM assay method (262,324) to detect released $O_2^{-\cdot}$. Fig. 8-8A shows the time course for the reduction of TNM to trinitromethane (ε_{350} = 14,600 M^{-1} cm^{-1}) (325,332) during the conversion of the LiPIIIc formed by the addition of catalase to LiPIII*. Using the ε for trinitromethane, the amount of $O_2^{-\cdot}$ released from LiPIIIc (6.0 μM) over 10 minutes was found to be 5.6 μM (93% conversion). $O_2^{-\cdot}$ generation was also detected with the cytochrome c reduction assay. Reduced cytochrome c has intense maxima at 520 and 550 nm. Spectra obtained during the conversion of LiP IIIc (55 μM) to ferric LiP, in the presence of cytochrome c, displayed two new maxima at 520 and 550 nm (data not shown). Fig. 8-8B shows the time course of TNM reduction during the conversion of LiP IIIa. The kinetics of TNM reduction corresponded to the disappearance of LiPIIIa and the appearance of ferric LiP. During the reversion of 2.9 μM of LiPIIIa, 2.4 μM of $O_2^{-\cdot}$ was generated (83% efficiency) as measured by TNM reduction. Furthermore, TNM appeared to stimulate this reversion.

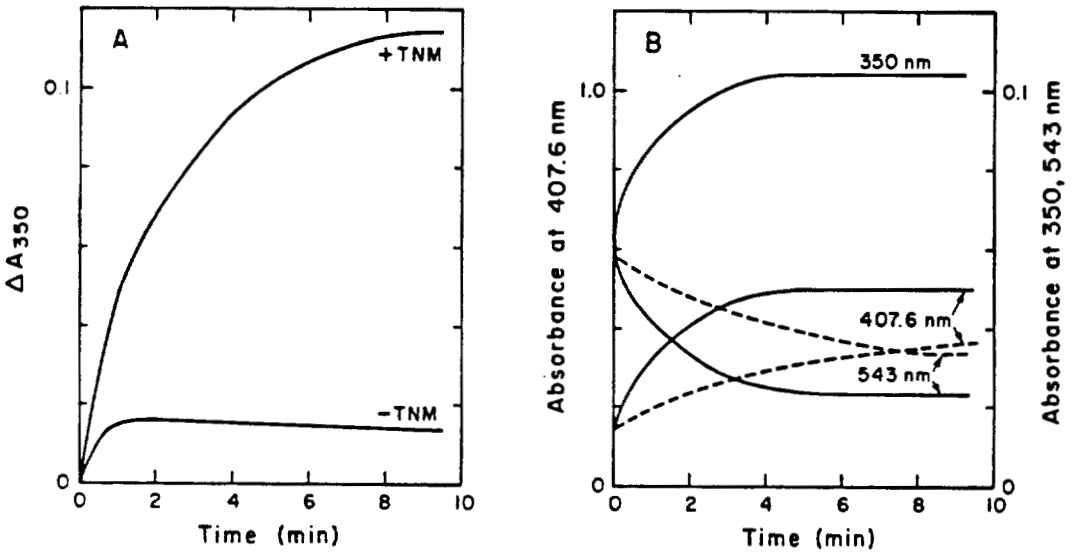

Fig. 8-8. **Release of superoxide during the decomposition of LiPIII.** (A) LiPIIIc (6.0 μM) was prepared from ferryl LiP, H_2O_2 (40 equiv.), followed by catalase (0.06 μM). The time course of the spontaneous release of $O_2^{-\cdot}$ from LiPIIIc was followed at 350 nm using TNM (0.1 mM). (B) LiPIIIa (2.9 μM) was prepared from ferrous LiP + O_2. TNM (0.1 mM) was added and the release of $O_2^{-\cdot}$ was followed at 350 nm (solid line). Formation of native LiP (407.6 nm) and disappearance of LiPIIIc (543 nm) were also monitored. Dashed lines: Spontaneous conversion of LiPIIIc to ferric LiP in the absence of TNM.

8.3.7 Reactions of LiPIII* and LiPIII with Veratryl Alcohol

Because the oxidized species formed in the presence of excess H_2O_2 is actually LiPIII* which may be a LiPIII-H_2O_2 complex, we reinvestigated the reactions of LiPIII* and LiPIII with VAlc (262). Fig. 8-9 (inset) shows the conversion of LiPIII* to ferric LiP ($A_{407.6}$) under pseudo-first-order conditions with VAlc in excess. A linear dependence of k_{obs} vs. VAlc concentration was observed between 0-500 μM VAlc (Fig. 8-9). The second-order rate constant (k_{6app}) calculated from the slope of the line was $(3.5 \pm 0.1) \times 10^1$ $M^{-1}s^{-1}$ (Table 8-2). Since this suggested that VAlc is involved in the reaction, we reinvestigated the possible oxidation of VAlc during this reaction (262). The VAlc-stimulated conversion of LiPIII* to ferric LiP was carried out in the presence of excess KCN. Binding of this strong ligand to native ferric LiP results in the formation of an inactive ferric, low-spin-cyanide complex (99,227). Addition of KCN to LiPIII* or to LiPIIIa alone did not result in a change in the optical spectrum. However, addition of KCN followed by the addition of VAlc to LiPIII* resulted in a spectrum identical to that of the CN-LiP low-spin spectrum previously observed (Fig. 8-10, Table 8-1) (99). Furthermore, addition of VAlc to a TNM-LiPIII*-KCN reaction mixture resulted in an increase in absorbance at 350 nm, indicating the release of $O_2^{\cdot-}$. Finally, the LiPIII*-KCN-VAlc reaction mixture was assayed for veratraldehyde by HPLC. No veratraldehyde was detected and VAlc was recovered quantitatively. In the absence of KCN, however, veratraldehyde was observed. In this case the LiPIII*

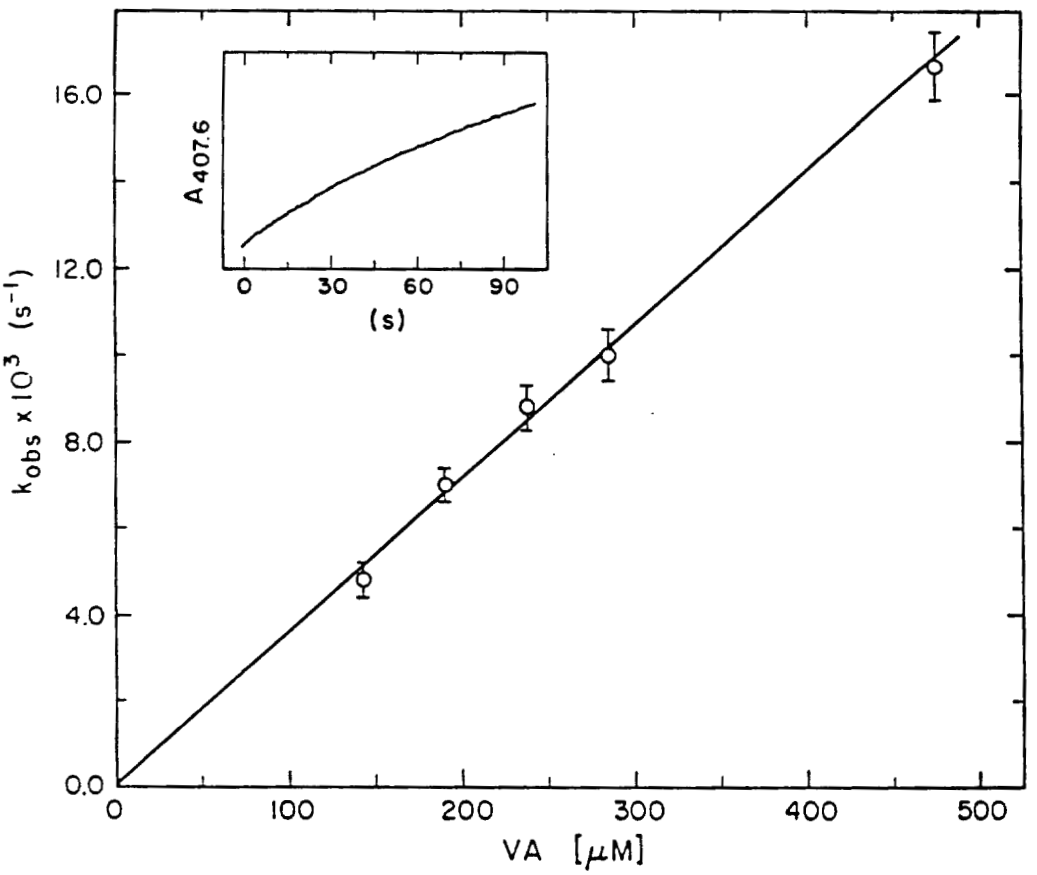

Fig. 8-9. **Plot of k_{obs} vs. VAlc concentration for the reaction of LiP III* with VAlc.** Inset: Typical exponential trace (VAlc, 190 μM and LiPIII*, 9.5 μM) from which k_{obs} was calculated. The linear plot of k_{obs} vs. VAlc concentration indicates that any complex between LiPIII* and VAlc is too short-lived to detect under these conditions.

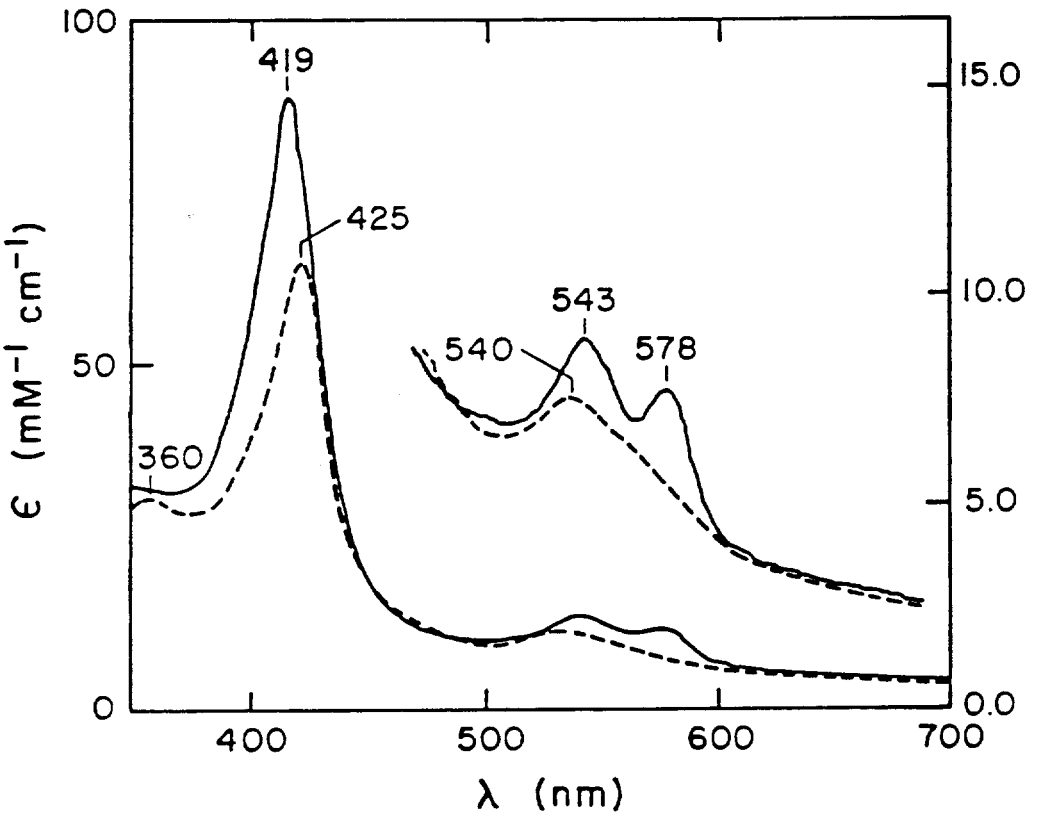

Fig. 8-10. **Reaction of LiPIII* with VAlc in the presence of KCN.** LiPIII* (12 μM) was prepared as described for Fig. 8-4. KCN (80 mM) was added and the spectrum (solid line) was recorded. Finally, VAlc (400 μM) was added and the resultant spectrum (dashed line) was recorded after 3 minutes.

preparation containing excess H_2O_2 was converted to native LiP and the latter reacted with H_2O_2 to initiate another catalytic cycle. In contrast, adding VAlc (100 equiv.) to LiPIIIa or to LiPIIIc did not result in a stimulation of their conversion to native LiP. The rate constants for these processes were calculated to be $(1.3 \pm 0.1) \times 10^{-3}$ s^{-1} (k_1VAlc and k_3VAlc), which are comparable to the rates in the absence of VAlc (Table 8-2).

8.4 DISCUSSION

Although LiP has a typical peroxidase catalytic cycle (31,137,232,260), several features of this enzyme distinguish it from other plant peroxidases. LiP oxidizes methoxy benzenes to aryl cation radicals (29-31,67,106,329). It has an unusually low pH optimum, ~3.0 (236,237), and at its pH optimum, LiP is easily oxidized to a LiPIII-like species (LiP III*) with H_2O_2 concentrations that are considerably less than those required for other peroxidases (260,262). LiPIII*, which was previously referred to as LiPIII (262), is irreversibly inactivated in the presence of excess H_2O_2 (262,333), and can be converted to the native enzyme by the addition of VAlc (262). These unusual properties of LiP encouraged us to study the formation and reactions of LiPIII and LiPIII* in greater detail. Peroxidase compound III-like species can be prepared via three different pathways

(137,156) as described below for LiP. These compound III species have been characterized as $Fe^{II}-O_2$ or as $Fe^{III}-O_2^{-\cdot}$ complexes (137,156). Since compound III is not involved in the peroxidatic cycle, the reversibility of its formation has been investigated (137,156,220,223,226,334).

LiPIII was prepared via three reaction paths: (a) ferrous LiP + O_2 (Fig. 8-1, Table 8-1) (LiPIIIa); (b) ferric LiP + $O_2^{-\cdot}$ (Fig. 8-3, Table 8-1) (LiPIIIb); and (c) LiPII + H_2O_2 + catalase (Fig. 8-5A, Table 8-1) (LiPIIIc). In the latter case, excess H_2O_2 was removed by catalase or by gel filtration to form pure LiPIIIc from LiPIII*. The spectral features of LiPIIIa, b, and c are almost identical (Table 8-1) with spectral maxima at ~414, 543, and 578 nm. LiPIIIb had a Soret maximum at 412 nm, but the visible spectrum indicated that it was only ~80% pure. Thus, this 2-nm shift from 414 to 412 nm is probably due to contamination with native ferric LiP (Soret maximum at 407.6 nm). The addition of H_2O_2 to LiPIIIa, b, or c or to LiPII results in the formation of LiP III* (Fig. 8-6, Table 8-1), which has visible maxima identical to those of LiPIII at 543 and 578 nm, but which has a red-shifted Soret maximum at 419 nm (Table 8-1) (232,260,262). Removal of excess H_2O_2 from LiP III* by catalase (Fig. 8-5A) or by gel filtration (data not shown) converts this intermediate to LiPIII (Soret maximum at 414 nm). This suggests that LiPIII* may be a complex of LiPIII and one or more molecules of bound H_2O_2.

8.4.1 Decomposition of LiPIII

In the absence of H_2O_2, LiPIIIa, b, and c all slowly revert to native LiP via first-order processes. The similarity of the first-order rate constants for these reversions (~1.0×10^{-3} s^{-1}) (Table 8-2) and the identical isosbestic points at 413, 470, and 525 nm (Figs. 8-1, 8-3, 8-5A) suggest that these reversions all occur via the same single step mechanism. Furthermore, during the spontaneous decomposition of LiPIIIa and c, stoichiometric amounts of $O_2^{-\cdot}$ are released (Fig. 8-8) and the conversion of LiPIII to native LiP is accelerated in the presence of an $O_2^{-\cdot}$ scavenger, in a manner similar to that reported for the conversion of HRPIII (226). All of these results strongly suggest that LiPIIIa, b, and c have the identical Fe^{III}–$O_2^{-\cdot}$ structure. Resonance Raman spectroscopic evidence for LiPIIIa and c is consistent with a ferric oxidation state (M. Mylrajan K. Valli, H. Wariishi, T. M. Loehr, and M. H. Gold, manuscript in preparation).

8.4.2 Mechanism of LiPIII Formation

It has been proposed that upon the binding of O_2 to the ferrous heme, electron density migrates from the iron to the oxygen (334). Thus the predominant structure of the ferrous-oxygen adduct of peroxidases is probably a ferric-superoxide complex as shown:

$$Fe^{II} + O_2 + H^+ \rightarrow Fe^{II}\text{–}O_2 \cdots H^+ \leftrightarrow Fe^{III}\text{–}O_2^{-\cdot} \cdots H^+ \qquad [8\text{-}2]$$

The ferric-superoxide complex would release $O_2^{-\cdot}$ during its conversion to native LiP as observed.

Ferric LiP reacts with enzymatically generated $O_2^{-\cdot}$ to form LiPIII directly (Fig. 8-3) as shown:

$$Fe^{III} + O_2^{-\cdot} + H^+ \leftrightarrow Fe^{III}\text{-}O_2^{-\cdot} \cdots H^+ \qquad [8\text{-}3]$$

This reaction is inhibited in the presence of superoxide dismutase (1 μM) at pH 6 (data not shown). Identical isosbestic points for the forward and reverse reactions indicate that the reaction is reversible (Fig. 8-3).

In the absence of a reducing substrate, excess H_2O_2 reacts with compound II to form LiPIII* (Fig. 8-4) and LiPIII is probably an intermediate in this process (Fig. 8-6). The formation of LiPIII* from LiP II and H_2O_2 is not inhibited by TNM (data not shown), a strong $O_2^{-\cdot}$ scavenger (223,325,332), suggesting that the mechanism probably does not involve the reduction of LiPII to the native enzyme and the reaction of the latter with $O_2^{-\cdot}$ (223). Instead, the mechanism of LiPII conversion to LiPIII may involve a ligand-exchange reaction as described in ref. 223, and as shown:

$$Fe^{IV}{=}O + H^+ \leftrightarrow Fe^{IV}{=}O \cdots H^+ \rightarrow Fe^{IV} + OH^- \qquad [8\text{-}4]$$

$$Fe^{IV} + H_2O_2 \rightarrow Fe^{III}\text{-}O_2^{-\cdot} \cdots H^+ + H^+ \qquad [8\text{-}5]$$

Unlike HRP, LiP is oxidized to LiPIII in the presence of a relatively

low concentration of H_2O_2 (137,156,223,232,262). This may reflect the relative strengths of the iron-oxygen bond in the two Fe^{IV}=O enzyme species.

The addition of H_2O_2 to LiPIII results in the formation of LiPIII* (Fig. 8-6) which is followed by enzyme inactivation and bleaching of the heme (data not shown) (262). Removal of excess H_2O_2 from LiPIII* by the addition of catalase or by gel filtration converts it back to LiPIII (Fig. 8-5), indicating that the formation of LiPIII* is reversible. Previous work has demonstrated the formation of an HRP oxidized intermediate compound IV upon exposure of that enzyme to excess H_2O_2 (137,335). The formation of HRP compound IV is also followed by its inactivation (326,335). Two types of bromoperoxidase compound III species with identical visible maxima but a small difference in the Soret maxima have also been reported (284). The exact structure of LiPIII* remains unclear, although its ready conversion to LiPIII upon removal of H_2O_2 suggests that it is a LiPIII-H_2O_2 adduct. A major ligand substitution or spin-state change is unlikely since LiPIII and LiPIII* share almost identical α and β visible absorption bands (Table 8-1).

8.4.3 Mechanism of Enzyme Inactivation

In the presence of excess H_2O_2, LiPIII*, which we previously referred to as LiPIII, is irreversibly inactivated and the heme is bleached (262,333). The kinetics of bleaching appear to be biphasic (Fig. 8-7). The fast first phase obeys second-order kinetics,

suggesting that LiPIII* reacts with H_2O_2. The second (slower) phase obeys first-order kinetics. When 100 equiv. of H_2O_2 are present, >80% of the bleaching occurs during the first phase, suggesting that inactivation is due to the reaction of H_2O_2 with the enzyme. The rate of bleaching increases as the pH is lowered (data not shown). A similar pH dependence has been observed for the bleaching of lactoperoxidase (336). Bleaching of the heme may be due to ·OH formed via the reaction of $O_2^{\cdot-}$ with H_2O_2. The formation of ·OH has been detected during the irreversible inactivation of lactoperoxidase in the presence of excess H_2O_2 (337).

8.4.4 Veratryl Alcohol-Induced Conversion of LiPIII* to Native LiP

Recently we reported that the addition of VAlc to LiPIII, prepared by the addition of excess H_2O_2 to the native enzyme, leads to the rapid single-step conversion of this LiPIII species back to the native enzyme (262). Herein we have recharacterized the LiPIII species prepared from native LiP or from LiPII with excess H_2O_2 as LiPIII* and have reexamined the reaction of VAlc with LiPIII* and with LiPIII. Addition of excess VAlc to LiPIII* results in its rapid conversion to the native enzyme via a second-order process (Fig. 8-9). The apparent second-order rate constant for this process is 3.5×10^1 $M^{-1}s^{-1}$. The ferric LiP produced by this reaction can be trapped with KCN to form a stable ferric-CN complex (Fig. 8-10) (31,99), thus preventing subsequent catalytic cycles. HPLC analysis of the reaction products formed under these conditions indicates that VAlc is not

oxidized during this reaction. In the absence of KCN, VAlc is oxidized to veratraldehyde since in the presence of excess H_2O_2, the recovered native enzyme begins a new catalytic cycle. We have previously shown that the reversion of LiPIII* to native LiP probably occurs in a single step (isosbestic point in the Soret region at 413 nm) and that $O_2^{-\cdot}$ is released during this reaction (262). Taken together, these results suggest that the binding of VAlc to LiPIII* leads to the displacement of $O_2^{-\cdot}$, resulting in the conversion of the $Fe^{III}-O_2^{-\cdot}$ enzyme to the ferric enzyme. The effect of VAlc on the spontaneous reversion of LiPIIIa and LiPIIIc has also been examined. In each case the first-order rate constant is not accelerated (Table 8-2). This contrasts with conclusions implied in our previous paper (262). It also suggests that conversion of LiPIII* to ferric LiP occurs via a single step, and that LiPIII is probably not an intermediate in this process.

All of these results indicate that LiP undergoes the reactions shown in Fig. 8-11. Three different pathways for LiPIII formation have been established and these are similar to pathways previously described for HRP (137,156). LiPIIIa, b, and c spontaneously revert to the native enzyme, releasing a stoichiometric amount of $O_2^{-\cdot}$ in the process, suggesting an $Fe^{III}-O_2^{-\cdot}$ structure for LiPIII. VAlc does not accelerate the rates of reversion of LiPIIIa, b, or c. In the presence of excess H_2O_2, LiPIII is converted to LiPIII* which is subsequently bleached and inactivated via a second-order process.

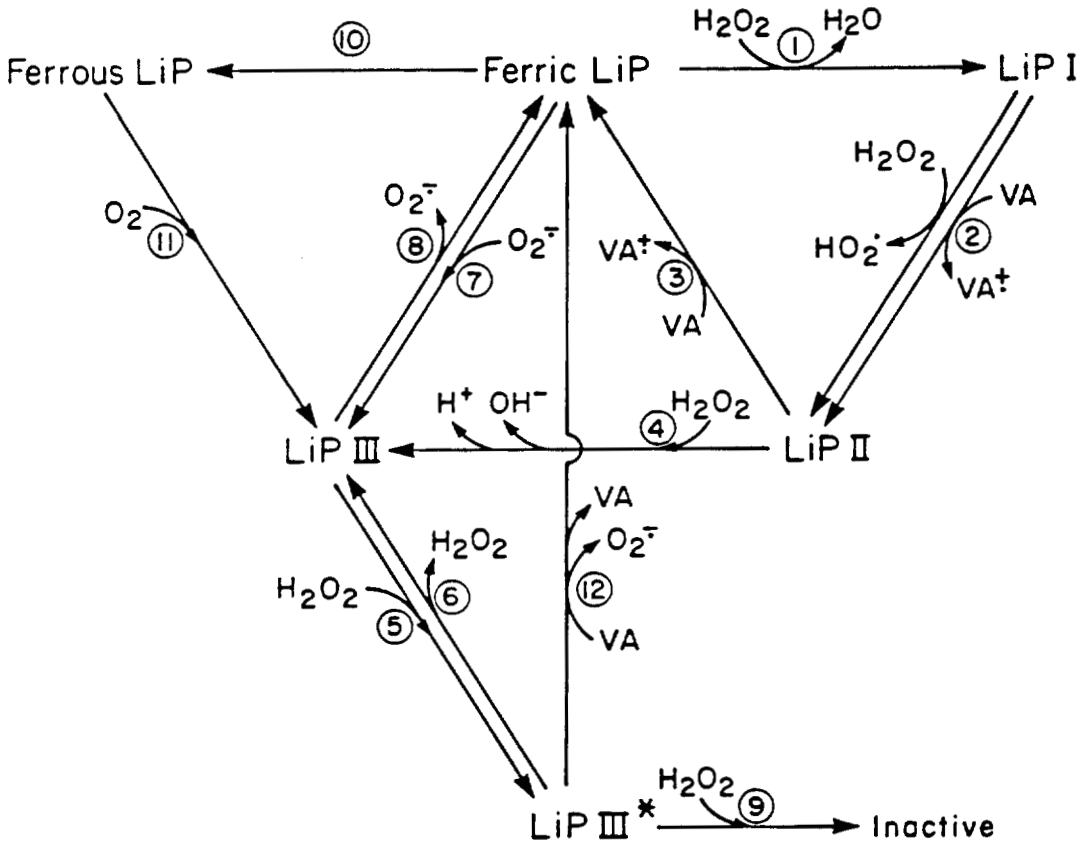

Fig. 8-11. **Interrelationships between the oxidized intermediates of lignin peroxidase.** Reactions 1, 2, and 3 denote the catalytic cycle. VA = veratryl alcohol. $VA^{+\cdot}$ = veratryl alcohol cation radical. Reactions 5 and 6 suggest that LiPIII* is a LiPIII-H_2O_2 complex.

In contrast to the negligible effect of VAlc on LiPIII, addition of VAlc to LiPIII* results in its rapid conversion to native LiP with the release of $O_2^{-\cdot}$ (262). VAlc is not oxidized in this reaction, suggesting a mechanism whereby the binding of VAlc displaces $O_2^{-\cdot}$. Thus, an important role for VAlc, a secondary metabolite of the fungus, appears to be in the protection of LiP from inactivation by H_2O_2 (262,328).

Recent work has demonstrated that superoxide scavengers such as Mn^{II} suppress the occurrence of ring-opening and quinone-forming reactions of LiP (338). Since LiPIII, like HRP (335), spontaneously releases $O_2^{-\cdot}$, and LiPIII* releases $O_2^{-\cdot}$ upon binding VAlc, these reactions may have an indirect role in the oxidation of lignin. Thus, the ready formation of LiPIII and LiPIII* may be a factor in the biodegradation of this polymer by P. chrysosporium.

CHAPTER 9

REACTIONS OF COMPOUNDS II AND III OF LIGNIN PEROXIDASE WITH PEROXIDES[*1]

9.1 INTRODUCTION

White-rot basidiomycetes are primarily responsible for the initiation of the decomposition of lignin in wood, playing a key role in the earth's carbon cycle (18,29-31). Under secondary metabolic conditions, the white-rot fungus Phanerochaete chrysosporium produces two extracellular heme enzymes, lignin peroxidase (LiP)[*2] and manganese peroxidase which, along with a H_2O_2-generating system, are the major components of its lignin degradative system (30,31,106,329). LiP is a glycoprotein with a molecular weight of ~41,000. It contains one mole of ferriprotoporphyrin IX, and exist as a series of acidic

---

[*1] The contents of this chapter will be submitted to J. Biol. Chem. Lignin Peroxidase Compounds II and III: Spectral and Kinetic Characterization of Reactions with Peroxides.
H. Wariishi, L. Marquez, H. B. Dunford, and M. H. Gold

isozymes (pI, 3.2-4.0) (30,31,103,106). The enzyme catalyzes the H_2O_2-dependent, one-electron oxidation of nonphenolic lignin related compounds to form aryl cation radicals (29-31,67,106,329). Spectral studies on the native ferric enzyme indicate that its heme environment is very similar to that of HRP (31,99,101,137,227-229,232). The occurrence of a proximal and distal histidine at the active site was also confirmed by nucleotide sequence analysis of several LiP cDNAs (233-235). Spectral and kinetic characterization of the interrelationships among the oxidized intermediates, LiPI, LiPII, and LiPIII, indicate that the oxidation states and the catalytic cycle of LiP are similar to those of HRP (137,232,260,261).

Although LiP has a typical peroxidative cycle via compounds I and II, it has several unique features. The enzyme has an unusually low pH optimum (pH ~3.0) (236,237); however, the rate of LiPI formation is independent of pH from 2.0-7.5 (260,261). The substrate specificity of LiP is totally different from that of HRP. Methoxybenzenes are preferred substrates for LiP (29-31,106,137,239), suggesting higher redox potentials for LiPI and LiPII. In addition, LiPIII formation from LiP II occurs readily. Considerably less H_2O_2 is required to

---

*2 Abbreviations:
LiP, lignin peroxidase; LiPI, LiPII, and LiPIII, Compounds I, II, and III of LiP; HRP, horseradish peroxidase; HRPI, HRPII, and HRP III, compounds I, II, and III of HRP; mCPBA, m-chloroperoxy benzoic acid; p-nitroperoxybenzoic acid; t-BuOOH, t-butyl hydro peroxide; AcOOH, peroxyacetic acid; DHF, dihydroxyfumaric acid.

convert LiPII to LiPIII than for the comparable conversion with other peroxidases (232,260,262).

Recently, two types of compound III were characterized spectroscopically, designated as LiPIII and LIPIII*. LiPIII is essentially identical to the typical compounds III obtained from other peroxidases. The addition of H_2O_2 to LiPIII caused the reversible formation of LiPIII*, thus LiPIII* was suggested to be a H_2O_2 adduct of LiPIII (263).

There are three reaction paths to form LiP III (263). Among these, the reaction of LiPII with H_2O_2 is the most important path for the formation of LiPIII species under physiological conditions. Furthermore, enzyme inactivation resulted from the reaction of LiPIII* with H_2O_2 (262,263,333). Herein, we utilized rapid-scan spectrometry and transient kinetic techniques to characterize the reaction of LiPII and LiP III with H_2O_2.

9.2 EXPERIMENTAL PROCEDURES

9.2.1 Enzyme Preparation

LiP isozyme 2 was isolated and purified from the extracellular medium of acetate-buffered, agitated cultures of P. chrysosporium OGC 101 (290) as previously described (263). The purified enzyme was electrophoretically homogeneous and had RZ (A_{408}/A_{280}) value of ≈5.0. Enzyme concentrations were determined at 407.6 nm using an extinction

coefficient of 133 $mM^{-1}cm^{-1}$ (99). The purified enzyme was dialyzed exhaustively against deionized water before use.

9.2.2 Preparation of Enzyme Intermediates

LiPII was freshly prepared for each experiment by adding a stoichiometric amount of ferrocyanide and m-chloroperoxybenzoic acid (mCPBA) to native LiP in 1 mM sodium succinate (pH 6.0). The visible spectrum of the preparation showed >95% purity and no spectral change for several minutes.

LiPIII was prepared by successive addition of 20 equiv. of dihydroxyfumaric acid (DHF) and 1 equiv. of H_2O_2 to the native enzyme (220). DHF was dissolved in N_2-saturated H_2O immediately prior to use.

9.2.3 Rapid-Scan Spectrometric and Kinetic Measurements

Rapid-scan spectra were recorded using a Photal RA601 Rapid Reaction Analyzer equipped with a 1-cm observation cell. The absorption spectra were measured by means of a multichannel photodiode array and memorized in a digital computer system (Sord M200 Mark III). The analog replica was plotted on an X-Y recorder. Spectral regions of 96 nm were scanned from 360 to 600 nm.

Kinetic measurements were conducted using the Photal RA601 in the stopped-flow mode. One reservoir contained LiPII or LiPIII in a weakly buffered (1 mM Na-succinate) solution at pH 6.0. The other reservoir contained buffer (39 mM Na-succinate, pH 3.0) and H_2O_2 in

excess (40-300 equiv.) to maintain pseudo-first order conditions. LiPIII formation was followed at 417.5 nm, the isosbestic point between LiPII and native LiP. Pseudo-first order rate constants were determined by a nonlinear least squares computer analysis of exponential traces. In all kinetic experiments, except for those in which the pH dependence of LiPIII and LiPIII* formation was studied, several different substrate concentrations were used for otherwise identical experimental conditions. Thus, plots of pseudo-first order rate constants versus substrate concentration were obtained. For pH-dependent studies, single experiments were performed at each pH using 400 μM H_2O_2.

All experiments were performed at 25 $\pm$ 0.5 °C in 20 mM sodium succinate buffer after mixing except as otherwise indicated. The temperature dependence of LiPIII formation was studied from 15.0 to 30.8 °C. The final pH was determined using a Fisher microprobe electrode and Fisher digital pH meter. Electronic absorption spectra were recorded on a Shimadzu UV-260 as previously reported (256,257).

9.2.4 Chemicals

H_2O_2 (30% solution) and peroxyacetic acid (AcOOH) (40% solution) were obtained from BDH Chemicals and FMC Corporation, respectively. t-Butyl hydroperoxide (t-BuOOH), p-nitroperoxybenzoic acid (pNPBA), and mCPBA were obtained from Aldrich. DHF was obtained from Sigma. All other chemicals were reagent grade and used without further

purification. The concentrations of peroxides were determined using the HRP assay method (280). Solutions were prepared in deionized water obtained from the Milli Q system (Millipore).

9.3 RESULTS

9.3.1 Reaction of LiPII with H_2O_2

The spectrum of LiPII has absorption maxima at 420, 525, and 556 nm (Fig. 9-1A, B) (232,263). Upon the addition of excess H_2O_2 (40 equiv.) to LiPII, the Soret peak was reduced (~20%) and shifted to ~414 nm within 2.3 s. Approximately 3 s after mixing, the peak shifted to 419 nm and its intensity increased with an isosbestic at ~400 nm (Fig. 9-1A). The spectral change in the Soret region clearly showed that the reaction of LiPII with H_2O_2 occurred in two steps: the transient formation of LiP III (Soret peak at 414 nm) (263) and the reaction of LiPIII with H_2O_2 to form LiPIII* (Soret peak at 419 nm) (263).

Under the same conditions (addition of 40 equiv. H_2O_2 to LiPII), the visible region showed the occurrence of the isosbestic point between LiPII and LiPIII species at 558 nm in the time range 0.26-7.8 s after mixing, suggesting the single step conversion of LiPII to LiPIII. This observation is in agreement with the previous result that the visible spectra of LiPIII and LIPIII* are essentially

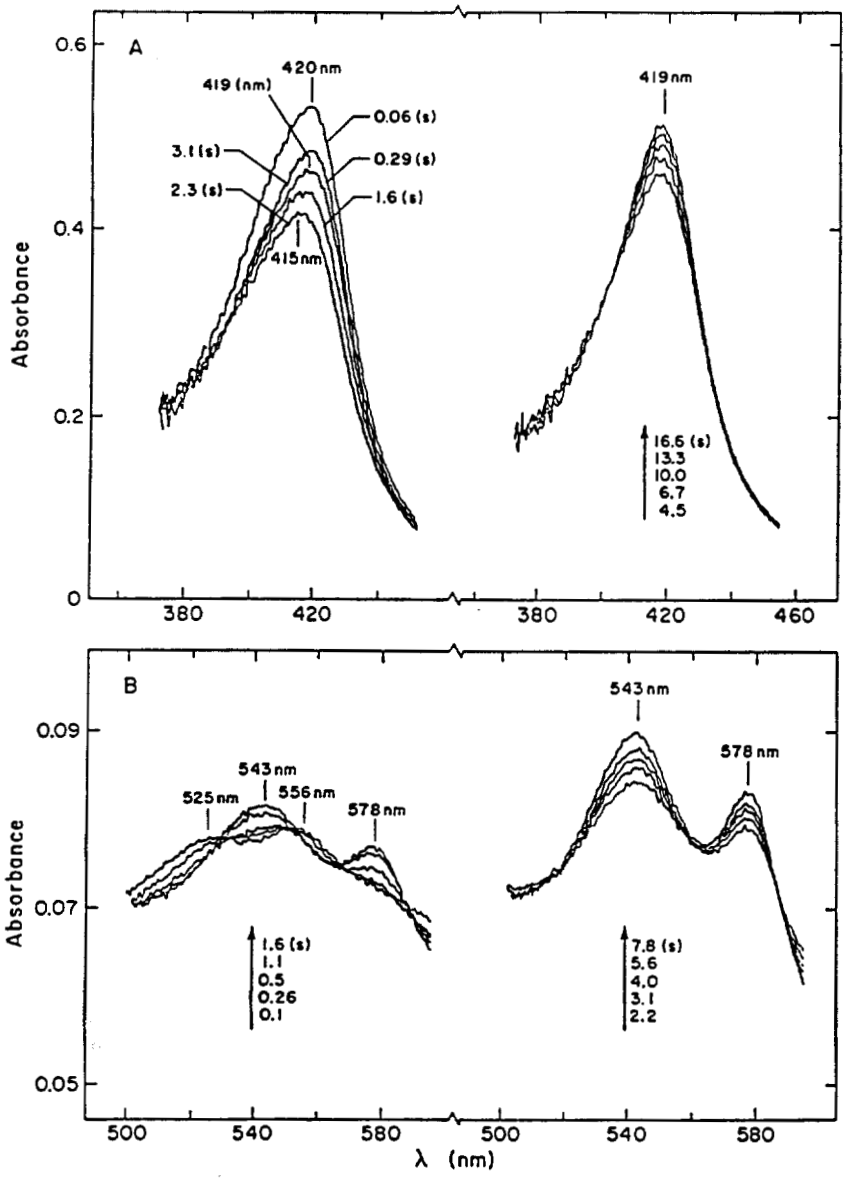

Fig. 9-1. **Reaction of LiPII with H_2O_2.** Spectra were recorded in 20 mM Na-succinate, pH 3.3 at 25°C. (A) Soret region spectra taken at 0.06-3.1 s (left) and at 4.5-16.6 s (right) after mixing. Final reactant concentrations: LiPII, 5 μM; H_2O_2, 200 μM. (B) Visible region spectra taken at 0.1-1.6 s (left) and at 2.2-7.8 s (right) after mixing. Final reactant concentrations: LiPII, 10 μM; H_2O_2, 400 μM. The numbers indicated are the wavelength maxima of the peaks (nm) and time (s) after mixing.

identical, although the Soret peak appear at different wavelengths (263). Therefore, we studied the kinetics of the biphasic reaction of LiPII with H_2O_2 by monitoring spectral changes in the Soret region.

Fig. 9-2 shows a typical time course of the change in absorbance at 417.5 nm, the isosbestic point between LiPII and native LiP. Therefore, the possible conversion of LiPII back to native LiP would not contribute any error to the rate constant determination for LiPIII formation. When 40 equiv. of H_2O_2 was used (same as in Fig. 9-1), the biphasic curve showed an initial decrease in absorbance in ~2.4 s (Fig. 9-2A) which corresponds to the formation of LiPIII shown in Fig. 9-1A. This transient formation of LiPIII was then followed by an increase in absorbance up to ~17 s after mixing, indicating the formation of LiPIII* (Fig. 9-1A, -2B). Both the initial decrease in absorbance and the following increase were of simple exponential character, from which the pseudo-first order rate constants for LiPIII formation (k_{1obs}) and for LiPIII* formation (k_{2obs}) were obtained. After 17 s, a slow decrease in absorbance was observed (Fig. 9-2B), which corresponds to enzyme inactivation (262,263).

9.3.2 Rate of LiPIII Formation

The plot of k_{1obs} versus $[H_2O_2]$ conforms to a rectangular hyperbola; the plot levels off at high H_2O_2 concentration (Fig. 9-3A). This behavior can be described by a simple binding interaction between reactants according to eq. 9-1:

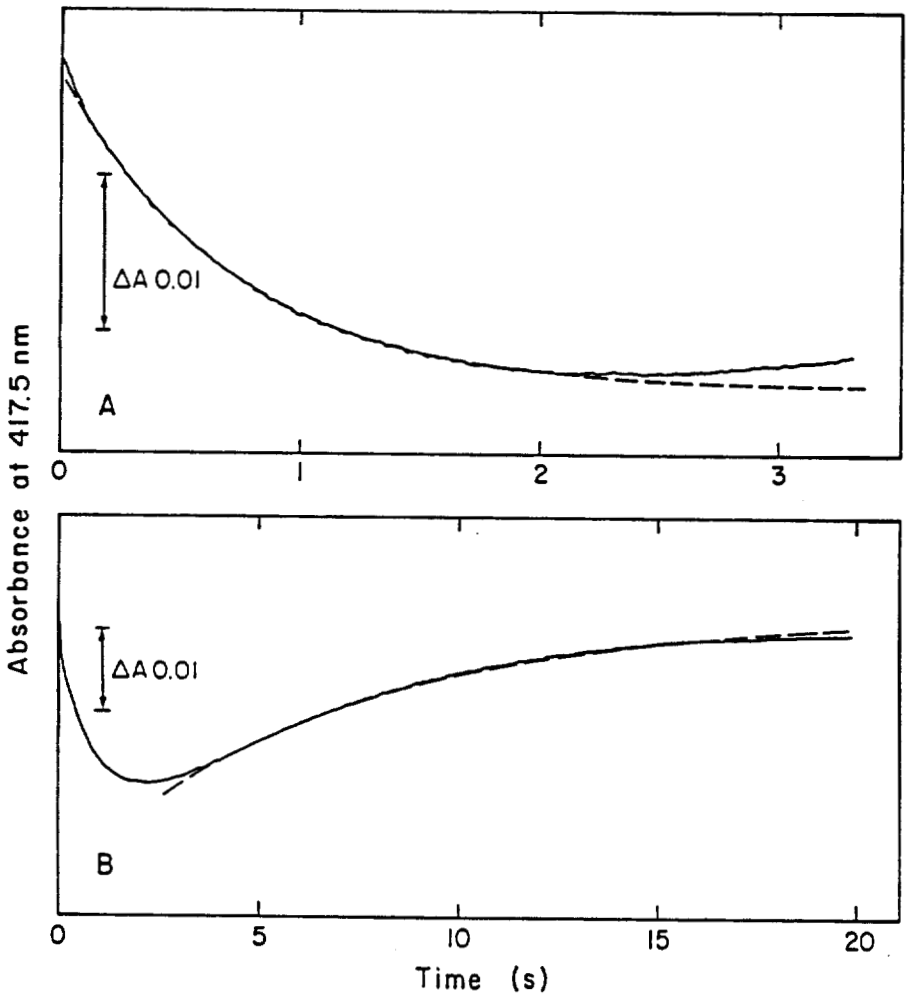

Fig. 9-2. **Time course of the reaction between LiPII and H_2O_2.** Reactions were followed at 417.5 nm. One syringe contained LiPII (2 μM after mixing) in Na-succinate, pH 6.0 and the other contained H_2O_2 (80 μM after mixing) in Na-succinate, pH 3.0. The pH after mixing was 3.3 (20 mM). Sampling period: (A) 3.2 s; (B) 20 s. The broken lines are the computer-fit exponential curves for (A), the first phase reaction, LiPIII formation and (B), the second phase reaction, LiPIII* formation.

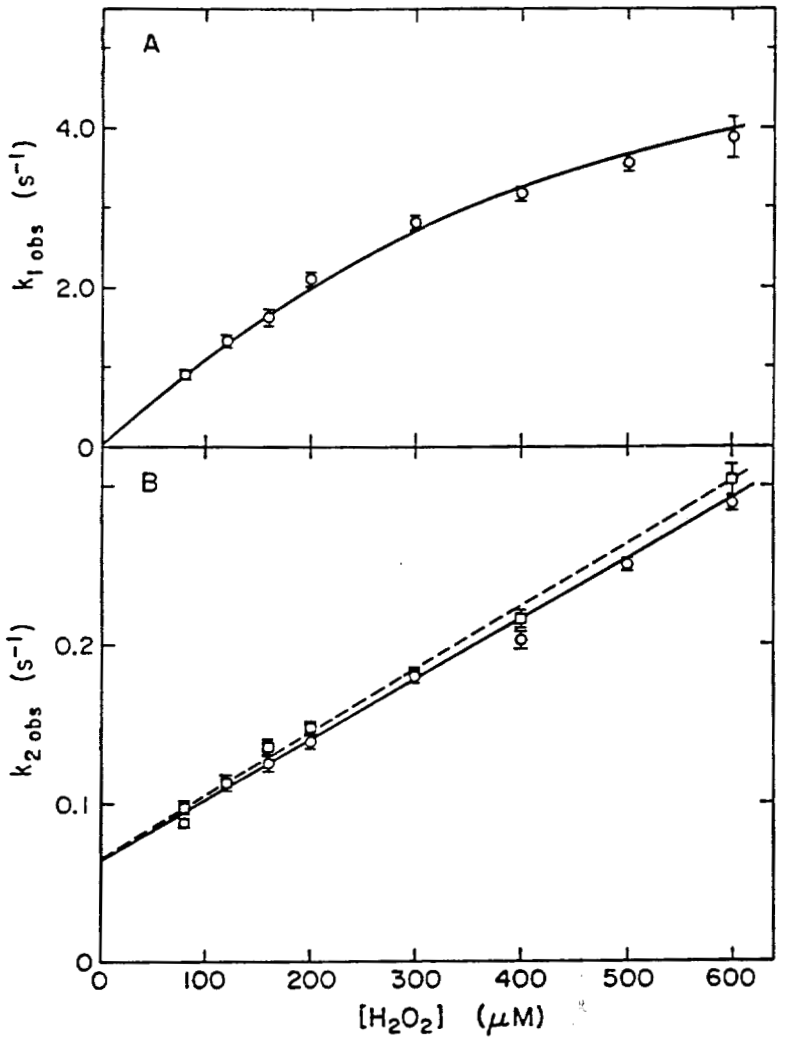

Fig. 9-3. **Plot of k_{obs} versus H_2O_2 concentration for the formation of (A) LiPIII (k_{1obs}) and (B) LiPIII* (k_{2obs}).** Experiments were conducted as described in Fig. 9-2 with various $[H_2O_2]$. k_{1obs} and k_{2obs} were obtained from the exponential change in absorbance at 417.5 nm of the first phase (○) (Fig. 9-2A) and the second phase (○) (Fig. 9-2B), respectively. (□), data obtained using exogenously prepared pure LiPIII. Each determination of k_{obs} is the mean of 5 traces. Lines are (A) a nonlinear least squares fit and (B) a linear least squares fit of the data, using eq. 9-2 and 9-5 in the text, respectively.

$$\text{LiPII} + H_2O_2 \underset{}{\overset{K_1}{\rightleftharpoons}} \text{LiPII-}H_2O_2 \xrightarrow{k_1} \text{LiPIII} + H_2O \qquad [9\text{-}1]$$

which leads to eq. 9-2 (Appendix D):

$$k_{1obs} = \frac{k_1}{1 + \frac{K_1}{[H_2O_2]}} \qquad [9\text{-}2]$$

where k_1 is a first-order rate constant (s^{-1}) and K_1 is an apparent dissociation constant (M) given by eq. 9-3:

$$K_1 = \frac{[\text{LiPII}][H_2O_2]}{[\text{LiPII-}H_2O_2]} \qquad [9\text{-}3]$$

The constants k_1 and K_1 were calculated from eq. 9-2 using a nonlinear least squares fit to the data. The experimental points and the calculated curve are shown in Fig. 9-3A; k_1 and K_1 were determined to be $(7.9 \pm 0.5)\ s^{-1}$ and $(5.8 \pm 0.6) \times 10^{-4}$ M (Table 9-1).

9.3.3 Rate of LiPIII* Formation

A linear dependence of k_{2obs} on $[H_2O_2]$ was observed between 0-600 μM $[H_2O_2]$ with a clearly defined ordinate intercept (Fig. 9-3B). Since no spontaneous conversion of LiPIII to LiPIII* in the absence of H_2O_2 appears to occur (263), the intercept indicates that the formation of LiPIII* is reversible:

Table 9-1. Kinetic parameters for the reactions of LiPII and LiPIII

Oxidized enzyme	Substrate	LiPIII Formation		LiPIII* Formation (forward)	LiPIII* Formation (reverse)
		First order rate constant (s^{-1})	Apparent dissociation constant (M)	Second order rate constant ($M^{-1}s^{-1}$)	First order rate constant (s^{-1})
LiPII	H_2O_2	7.9±0.5 (k_1)	$(5.8\pm0.6)\times10^{-4}$ (K_1)		
	AcOOH	4.9±0.6 (k_3)	$(1.1\pm0.6)\times10^{-4}$ (K_3)		
LiPIII	H_2O_2			$(3.7\pm0.2)\times10^{2}$ (k_{2app})	$(6.6\pm0.6)\times10^{-2}$ (k_{-2})
				$(4.0\pm0.1)\times10^{2}$ (k_{2app})[a]	$(6.7\pm0.4)\times10^{-2}$ (k_{-2})[a]
	AcOOH			$(2.9\pm0.2)\times10^{2}$ (k_{4app})	$(6.4\pm0.6)\times10^{-2}$ (k_{-4})

[a] Values obtained using exogenously prepared pure LiPIII.

$$\text{LiPIII} + H_2O_2 \underset{k_{-2}}{\overset{k_{2app}}{\rightleftarrows}} \text{LiPIII}^* \qquad [9\text{-}4]$$

$$k_{2obs} = k_{2app}[H_2O_2] + k_{-2} \qquad [9\text{-}5]$$

where k_{2app} is an apparent second order rate constant ($M^{-1}s^{-1}$) and k_{-2} is a first-order rate constant (s^{-1}). The values of k_{2app} and k_{-2} were found to be $(3.7 \pm 0.2) \times 10^2$ $M^{-1}s^{-1}$ and $(6.6 \pm 0.6) \times 10^{-2}$ s^{-1} using a linear least squares fit to the data (Table 9-1).

In order to confirm the rate constant for LiPIII* formation, an alternative stable preparation of LiPIII was used. During the oxidation of DHF to diketosuccinate by HRP, the generation of superoxide has been reported. Superoxide in turn reacts with native HRP to form HRPIII (128,220). Fig. 9-4 shows the formation of LiPIII from native LiP in the presence of DHF. Isosbestic points at 413, 470, 525, and 597 nm between native LiP and LiPIII suggest the reaction occurs by a single step (263). Upon adding 20 equiv. DHF to native LiP, no enhanced peak shift from 414 to 419 nm was detectable, suggesting that H_2O_2 formation from dismutation of superoxide was not complicating the reaction. The addition of 100 equiv. DHF caused the formation of LiPIII*.

A reasonable yield of LiPIII could be obtained from native LiP using DHF only. However, it was found that LiPIII formation could be accelerated by adding 1 equiv. H_2O_2 to the reaction system, consisting of native LiP and 20 equiv. DHF at pH 6.0 (Fig. 9-4, inset). LiPIII

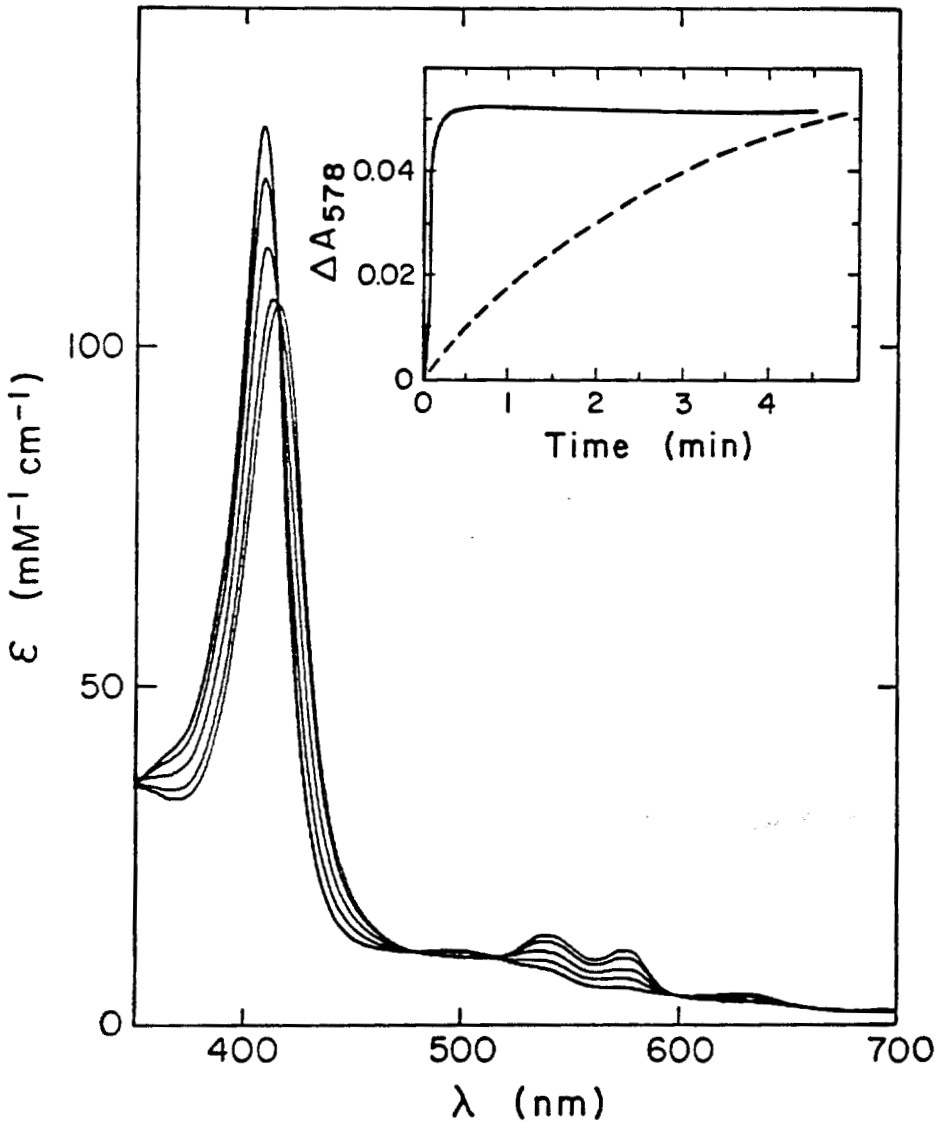

Fig. 9-4. **Conversion of native LiP to LiPIII in the presence of DHF.** 80 μM DHF was added to native LiP (4 μM) in 1 mM Na-succinate, pH 6.0. Spectra were recorded at 1.5 min interval. inset: Formation of LiPIII was followed at 578 nm. LiP, 10 μM; DHF, 200 μM (– – –). By adding 10 μM H_2O_2 to the LiP/DHF system, the formation of LiPIII was completed within 20 s (———).

was formed and was stable for 2-3 min, followed by its slow spontaneous conversion to native LiP. For kinetic measurements, LiPIII was prepared freshly for each trace using 20 equiv. DHF and 1 equiv. H_2O_2.

When excess H_2O_2 was added to pure LiPIII, LiPIII* formation occurred as indicated by the Soret peak shift to 419 nm as previously reported (263). The kinetic traces obtained at 419 nm showed a single exponential feature (data not shown) from which the pseudo-first order rate constant (k_{2obs}) was calculated. The plot of k_{2obs} versus [H_2O_2] indicates a linear relationship from 0-600 μM $H_2O_2$with a finite ordinate intercept (Fig. 9-3B). A linear least squares fit was applied to the data according to eq. 9-5; k_{2app} and k_{-2} were found to be $(4.0 \pm 0.1) \times 10^2$ $M^{-1}s^{-1}$ and $(6.7 \pm 0.4) \times 10^{-2}$ s^{-1} (Table 9-1). Therefore, these results obtained for pure LiPIII preparation confirm the accuracy of the transient state results obtained when stable LiPII was reacted with excess H_2O_2.

9.3.4 Activation Energy for LiPIII Formation

Using H_2O_2 the rate of LiPIII formation was measured over the temperature range of 15.0-30.8°C. The temperature dependence of the first order rate constant (k_1) is presented as an Arrhenius plot (Fig. 9-5); k_1 was calculated as shown in Fig. 9-3 for each temperature. The activation energy calculated from the slope of the plot was 22.9 $\pm$ 1.3 kJ mol^{-1} or 5.5 $\pm$ 0.3 kcal mol^{-1}.

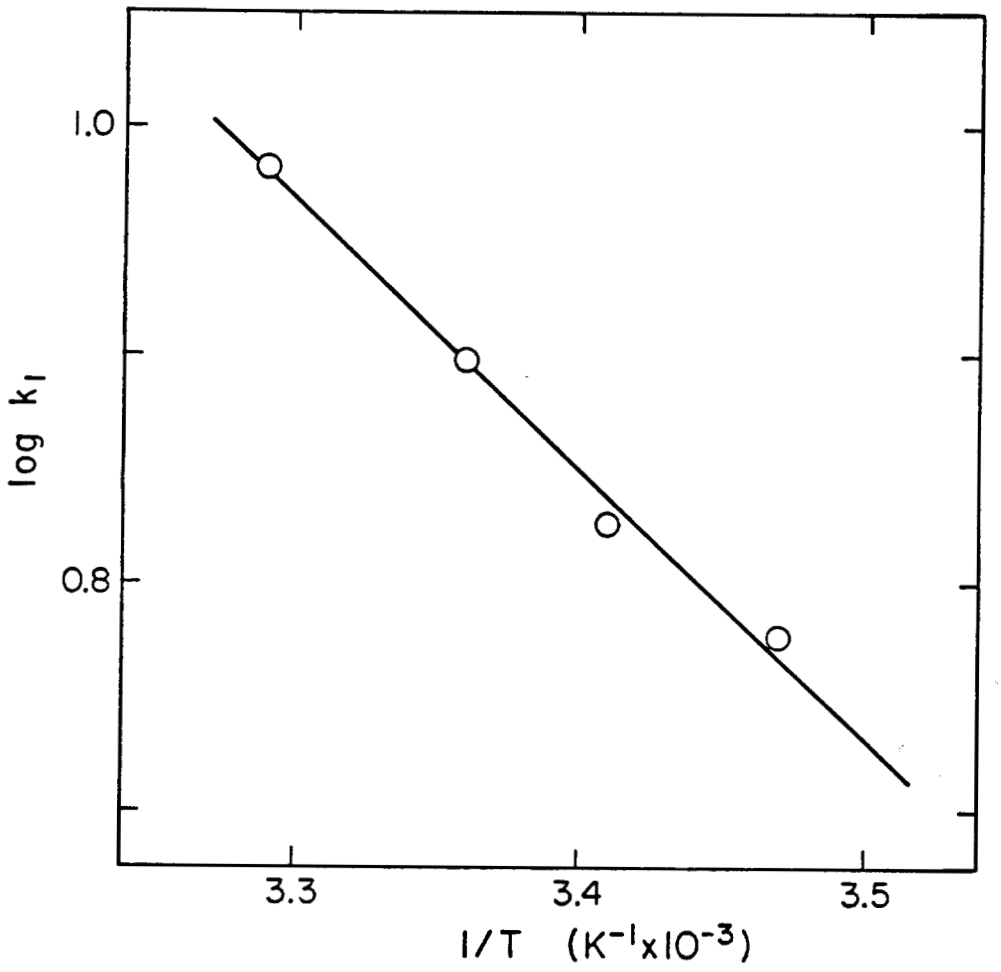

Fig. 9-5. **Arrhenius plot for LiPIII formation.** Values for k_1 were obtained as in Fig. 9-3A. The temperature was varied from 15.0 to 30.8°C. All other experimental conditions are the same in Fig. 9-3.

9.3.5 pH Dependence of LiPIII and LiPIII* Formation

Upon addition of 200 equiv. H_2O_2 to LiPII, k_{1obs} and k_{2obs} were calculated from the biphasic traces over the pH range of 3.0-5.1. Plots of $\log k_{1obs}$ and $\log k_{2obs}$ against pH are shown in Fig. 9-6. Above pH 4.0 both k_{1obs} and k_{2obs} decreased with increasing pH. An apparent pKa value of ~4.2 was found to influence the reaction rates.

9.3.6 LiPIII and LiPIII* Formation by Organic Peroxides

Reactions of LiPII with organic peroxides were also investigated. When excess peroxyacetic acid (AcOOH) was added to LiPII, it was biphasically converted to LiPIII*. The appropriate constants were calculated according to the following equations 9-6 through 9-10 which are analogous to equations 9-1 through 9-5:

$$\text{LiPII} + \text{AcOOH} \underset{}{\overset{K_3}{\rightleftarrows}} \text{LiPII-AcOOH} \xrightarrow{k_3} \text{LiPIII} + \text{AcOH} \qquad [9\text{-}6]$$

$$k_{3obs} = \frac{k_3}{1 + \dfrac{K_3}{[\text{AcOOH}]}} \qquad [9\text{-}7]$$

$$K_3 = \frac{[\text{LiPII}][\text{AcOOH}]}{[\text{LiPII-AcOOH}]} \qquad [9\text{-}8]$$

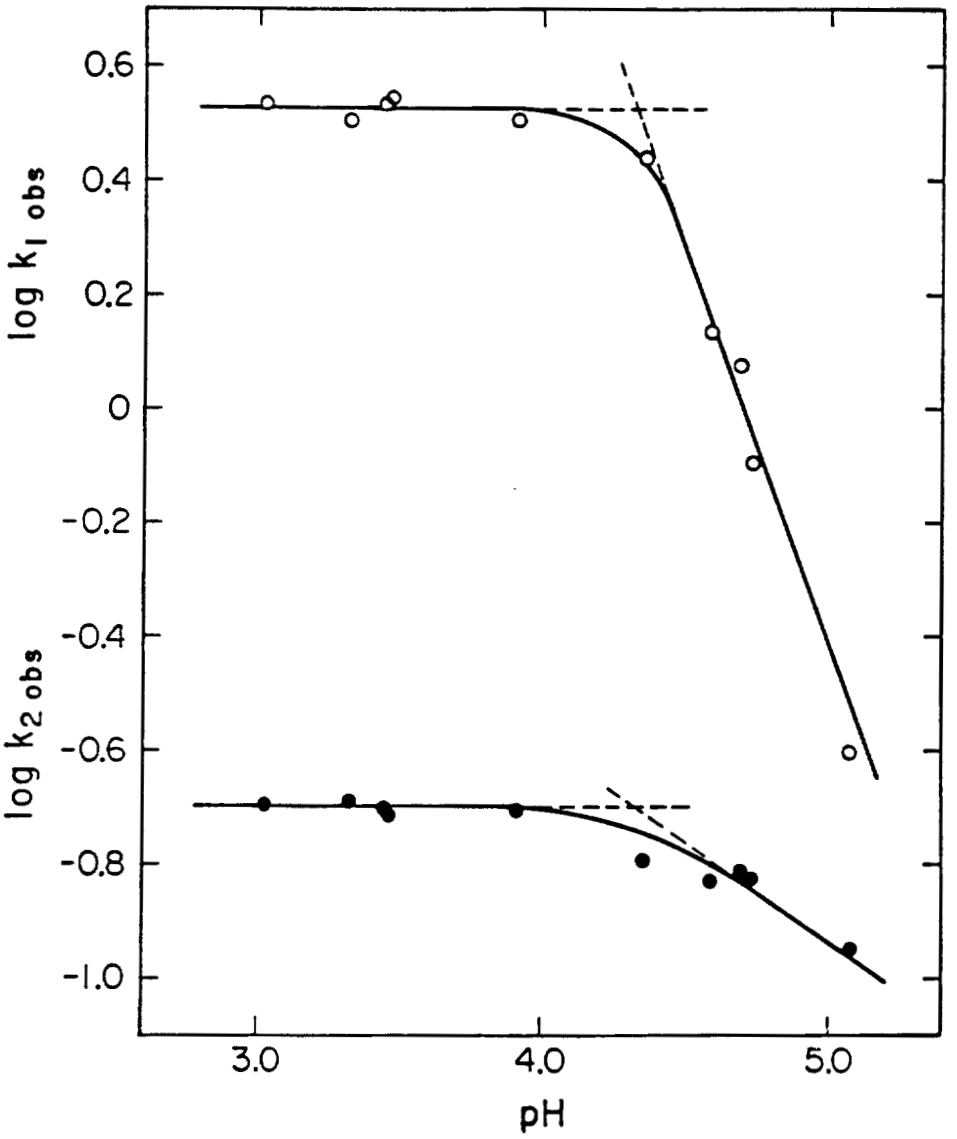

Fig. 9-6. **pH Dependence of LiPIII and LiPIII* formation.** The pH was varied from 3.0 to 5.1. Concentrations after mixing: LiPII, 2 μM; H_2O_2, 400 μM and ionic strength is 0.02 M due to Na-succinate.

$$\text{LiPIII} + \text{AcOOH} \underset{k_{-4}}{\overset{k_{4app}}{\rightleftarrows}} \text{LiPIII}^{*} \qquad [9\text{-}9]$$

$$k_{4obs} = k_{4app}[\text{AcOOH}] + k_{-4} \qquad [9\text{-}10]$$

When k_{3obs} is plotted against [AcOOH] (Fig. 9-7), the formation of LiPIII shows saturation kinetics similar to the reaction of LiPII with AcOOH. A straight line with a finite intercept is obtained when k_{4obs} is plotted versus [AcOOH], indicating that the formation of LiPIII* is a reversible reaction (Fig. 9-7). The values are summarized in Table 9-1. The first order rate constant (k_{-4}) is almost the same as the comparable value obtained with H_2O_2 (k_{-2}).

No occurrence of LiPIII formation was found with the addition of t-BuOOH, mCPBA, and pNPBA to LiPII. Moreover, when these bulky organic peroxides were added to LiPIII prepared from native LiP and DHF, no peak shift from 414 nm to 419 nm was observed (data not shown).

9.4 DISCUSSION

In previous work (263), LiPIII was prepared via three different reaction paths; ferrous LiP + O_2, ferric LiP + $O_2^{\cdot-}$, and LiPII + H_2O_2 followed by removal of excess H_2O_2. The stability and reactivity of these LiPIII preparations were examined using spectral and kinetic

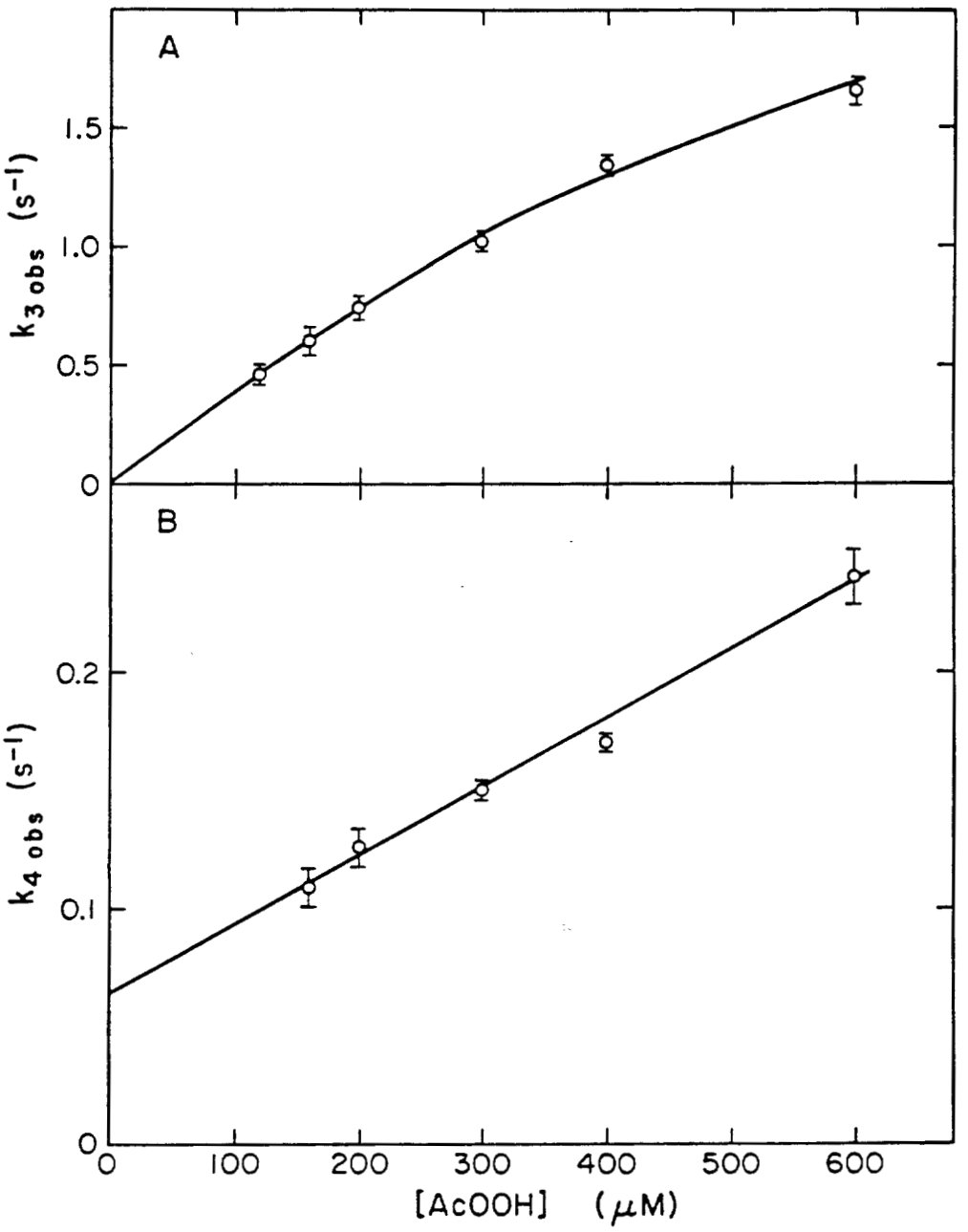

Fig. 9-7. **Plot of k_{obs} versus peroxyacetic acid concentration for the formation of (A) LiPIII (k_{3obs}) and (B) LiPIII* (k_{4obs}).** Experiments were conducted as in Fig. 9-3 except that peroxyacetic acid was used instead of H_2O_2. Lines are (A) a nonlinear least squares fit and (B) a linear squares fit to the data, using eq. 9-7 and 9-10 in the text, respectively.

techniques, demonstrating that although, at the catalytic pH LiPIII is more stable than other oxidized intermediates, it spontaneously converts to native ferric LiP with the release of superoxide (263). LiPIII reacts with H_2O_2 to form an unique intermediate, LiPIII*. This intermediate subsequently reacts with H_2O_2 and is inactivated (262,263). By removal of excess H_2O_2, LiPIII* is converted to LiPIII, suggesting that the conversion of LiPIII to LiPIII* is reversible and that LiPIII* may be a complex of LiPIII and H_2O_2 (262). In the presence of excess H_2O_2, LiPII is rapidly converted to LiPIII* followed by inactivation (263). Thus, it was of interest to determine the relative rates of reactions of H_2O_2 and methoxybenzenes, such as veratryl alcohol, with LiPII. Furthermore, it was of interest to determine whether LiPIII* formation from LiPII with H_2O_2 occurs via an one-step or a two-step mechanism. To address these questions, the kinetics and mechanism of the conversion of LiPII to LiPIII* and of LiPIII to LiPIII* were studied utilizing stopped-flow and rapid scan spectral techniques. Kinetic analyses of the reactions of LiPII and LiPIII with peroxides were facilitated by the preparation of a more stable LiPII and a purer preparation of LiPIII. LiPII was prepared in the presence of mCPBA instead of H_2O_2. LiPIII was prepared using DHF as a superoxide generator (128,220).

The results clearly indicate that the reaction of LiPII with peroxide to form LiPIII* occurs via intermediate formation of LiPIII (Fig. 9-1 and 9-2). They also indicate that there is a kinetically detectable LiPII-peroxide complex (Fig. 9-3). Both H_2O_2 and AcOOH are

effective peroxides for the conversion of LiPII to LiPIII* but t-BuOOH, mCPBA, and PNPBA apparently are not.

9.4.1 Formation of LiPIII from LiPII and H_2O_2

The first phase of kinetic traces, in which saturation kinetics is observed, corresponds to the conversion of LiPII to LiPIII. A plot of the pseudo-first order rate constant for the conversion of LiPII to LiP III is sufficiently close to linear at low [H_2O_2] that the second order rate constant can be estimated from the initial slope (Fig. 9-3A). The values is ~10^4 $M^{-1}s^{-1}$ which is ~500 times larger than the comparable second order rate constant reported for HRP (223).

The activation energy for the formation of LiPIII was estimated from the Arrhenius plot of the logarithm of the first order dissociation constant (k_1) the reciprocal of the temperature, giving the value of ~23 kJ mol^{-1} (Fig. 9-5). An activation energy of ~29 kJ mol^{-1} has been reported for HRPIII formation from HRPII (223).

Why is LiPII so much more readily converted into LiPIII than the comparable HRP reaction? Also, why is excess peroxide required to convert compound II to compound III? The difference in rate between LiP and HRP for compound III formation from compound II and peroxide can be rationalized in terms of known structural and kinetic behavior of the peroxidase compounds. The ferryl oxygen atom of HRP II is known to undergo exchange with solvent oxygen (178-180,339). Therefore, the conversion can be explained by a ligand displacement in which the single oxygen atom bound to iron in HRPII (Fe^{IV}=O) is

displaced by a dioxygen species derived from H_2O_2 to form HRPIII ($Fe^{III}-O_2^{-\cdot} \leftrightarrow Fe^{II}-O_2$). The enhanced reactivity of LiPII toward H_2O_2 would imply that the ferryl oxygen atom of LiPII is more readily displaced and/or is more readily dissociated than in HRPII. The excess peroxide for the conversion of compound II to compound III is required because of the necessity to capture the transient dissociated ferryl species or to force the displacement of the ferryl oxygen atom.

As described above, at low [H_2O_2] the second order rate constant for the reaction of LiPII with H_2O_2 was estimated to be ~1.0 x 10^4 M^{-1} s^{-1} at 25°C. On the other hand, the second order rate constant for the reaction of LiPII with veratryl alcohol, one of the best organic reducing substrates, has been reported to be 1.6 x 10^5 $M^{-1}s^{-1}$ at 25°C, pH 3.1 (260). Therefore, in the reaction system consisting of LiP, H_2O_2, and veratryl alcohol, a little conversion of LiPII to LiPIII is to be expected.

9.4.2 Formation of LiPIII* from LiPIII and H_2O_2

The second phase of the kinetic trace corresponds to the formation of LiPIII* from LiPIII and H_2O_2 (Fig. 9-1A and -2B). Kinetic data analysis revealed that formation of LiPIII* from LiPIII and H_2O_2 occurs reversibly with the forward second order rate constant of 3.7 x 10^2 $M^{-1}s^{-1}$ and the first order rate constant of 6.6 x 10^{-2} s^{-1} for the reverse reaction (Fig. 9-3B, Table 9-1). In addition, the kinetic characterization of this reaction was performed with exogenously prepared LiPIII. In the present study, DHF was used to

form pure LiPIII. The formation of HRPIII using DHF has been extensively studied (178,220). Fig. 9-4 shows the direct conversion of LiPIII using DHF as shown by isosbestic points at 413, 470, 525, and 597 nm and by the peak shift from 407.6 to 414 nm. This conversion was stimulated by adding 1 equiv. H_2O_2 to the reaction system (Fig. 9-4, inset). According to the reported mechanism, HRPI and HRPII oxidize DHF to the corresponding carbon-centered radical intermediate which in turn reduces oxygen to superoxide (178,220). The formation of HRP and LiP compounds III through the reaction of ferric peroxidase and superoxide has been verified (178,220,221,263).

The LiPIII preparation obtained using DHF (>95% purity) was used for the kinetic study of the conversion of LiPIII to LiPIII*. The kinetic features were almost identical to those found in the second phase of the transient state reaction of LiPII with H_2O_2 (Fig. 9-3B, Table 9-1), confirming the accuracy of the transient state results. The occurrence of the reverse reaction explains the formation of LiPIII from LiP III* upon the removal of H_2O_2 (263). These data also suggest that the structure of LiPIII* is best described as a covalently bound LiPIII-H_2O_2 complex. Since Fig. 9-1A and 9-2B reconfirm the identical visible spectra for LiPIII and LiPIII* (263), a major oxidation or coordination state change is unlikely to have occurred upon LiPIII* formation. From the values of k_{2app} and k_{-2}, the apparent dissociation constant was calculated to be ~1.7 x 10^{-4} M.

Recently, the equilibrium between LiPII and LiPIII in the presence of H_2O_2 was proposed (333). It was also claimed that the rapid conversion of LiPIII back to native in the presence of both H_2O_2

and veratryl alcohol occurs via a two-step reaction, wherein the reaction of LiPIII with H_2O_2 converts it into LiPII. The latter in turn is reduced to ferric LiP by veratryl alcohol. However, a nonlinear least squares fit of the data suggested that the formation of LiPIII from LiPII occurs irreversibly, since the curve passed through the origin and that an equilibrium occurs only between LiPII and LiPII-H_2O_2 complex (Fig. 9-3A). Furthermore, the conversion of LiPIII to LiPIII* by adding H_2O_2 was clearly shown (Fig. 9-1 and 9-3B) (263). This indicates that the rapid conversion of LiPIII* to ferric LiP by the addition of veratryl alcohol occurs via single step displacement of superoxide from LiPIII* (263).

9.4.3 pH Dependence of LiPIII and LiPIII* Formation

The plot of k_{1obs} versus pH clearly showed the existence of heme-linked ionizable group with pKa of ~4.2 (Fig. 9-6). Most likely this ionizable group is involved in the reaction of the cleavage of H_2O_2 to generate the dioxygen species for LiPIII formation.

Interestingly, pH-rate profile for the reaction of LiPIII* shows the same pKa value, suggesting that probably the same ionizable group controls both LiPIII and LiPIII* formation. Since LiPIII* has been suggested to be a LiPIII-H_2O_2 complex, this pH dependence was assumed not to be caused by an amino acid residue directly involved in the catalytic action. A possible explanation is that the ionizable group might be located at the entrance of the active cavity enabling the orientation of the peroxide. The narrow active site cavity may

prohibit the reaction with more bulky peroxides, such as t-BuOOH, mCPBA, and pNPBA and reduce the reaction rate with AcOOH (Fig. 9-7, Table 9-1).

Since simple binding kinetics (eq. 9-2 and 9-6) fit well with the reaction of LiPII with either H_2O_2 or AcOOH (Fig. 9-3 and 9-7), an identical mechanism for LiPIII and LiPIII* formation with both peroxides is suggested without any more kinetic factors. Furthermore, tetranitromethane, a strong superoxide scavenger, did not inhibit the formation of LiPIII(*) from LiPII and H_2O_2 (263). These observations eliminate a mechanism for LiPIII formation whereby H_2O_2 reacts as a reducing substrate with LiPII to form hydroperoxyl radical and native LiP, then the hydroperoxyl radical reacts with native LiP to form LiPII (223). Rapid scan spectral analyses also demonstrated that no trace of native LiP appeared during the reaction of LiPII with peroxides (Fig. 9-1).

Compound I formation has been studied extensively with various peroxidases and the distal histidine has been implicated in the heterolytic cleavage of H_2O_2 (185,340). The formation of compound I is pH-dependent with many peroxidases and the distal group shows a low pKa value: for HRP and chloroperoxidase, pKa ~3.0 (193,282); for yeast cytochrome c peroxidase, pKa ~4.5 (323); for bromoperoxidase, pKa ~5.3 (284). In contrast, LiPI formation is pH-independent over a pH range of 2.0-7.5 (260,261), possibly suggesting a strong hydrophobicity of the active pocket or the involvement of another amino acid. Therefore, the pKa value of ~4.2 for the formation of LiPIII may not

be caused by the distal histidine, but may be due to a carboxylic residue such as Asp 42 (233,235) or the protoporphyrin IX.

LiPII reacts with H_2O_2 to form LiPIII* via the transient formation of LiPIII. The formation rate of LiPIII from LiPII and H_2O_2 was found to be much higher than that for HRPIII (Fig. 9-3A) (223). Thus, even in the presence of some preferred reducing substrate, LiPII may react with H_2O_2 to form LiPIII. LiPIII further reacts with H_2O_2 to form LiPIII*. Both LiPIII and LiPIII* can revert back to ferric native LiP with release of superoxide. The reversion of LiPIII* requires preferred substrate such as veratryl alcohol to rapidly displace superoxide (262,263). In contrast, LiPIII does not react with veratryl alcohol, and the slow reversion occurs spontaneously (263). Superoxide could be captured by the carbon-centered radicals formed through LiP's peroxidative catalytic action. The peroxyl- or hydroperoxyl-intermediates formed undergo further nonenzymatic cleavage yielding oxygenated products (30,31,67,106). Superoxide scavengers such as Mn^{II} suppress the occurrence of ring-opening and quinone-forming reactions of LiP (338). Therefore, LiPIII* may be involved in lignin degradation as a superoxide generator. The possible roles of veratryl alcohol, the secondary metabolite of the fungus, are (i) the protection of the enzyme against the formation of LiPIII by reducing LiPII, (ii) protection of the enzyme against the inactivation by reacting with LiPIII*, and (iii) the enhancement of the generation of superoxide during the reversion of LiPIII*.

In conclusion, we propose a mechanism in which LiPII and H_2O_2 form a complex which leads to LiPIII formation. The conversion to LiPIII is accompanied by substitution of a dioxygen species derived from H_2O_2 for the single oxygen atom of the ferryl oxy complex in LiPII. Details of this substitution (dissociative, associative, 5-, 6-, or 7-coordinate transition state) are not yet known. However, the reaction of native LiP with superoxide to form LiPIII was eliminated from the mechanism for LiPIII formation from LiPII and H_2O_2.

CHAPTER 10

FINAL COMMENTS

10.1 MANGANESE PEROXIDASE

MnP has been shown to share structural and mechanistic features with other plant and fungal peroxidases; yet it has several unique features. Mn^{II}, the real substrate for the enzyme, is oxidized to Mn^{III}. C_2 and C_3 dicarboxylic or α-hydroxyl acids such as malonate and lactate are required for the enzyme activity. The organic acids facilitate the dissociation of Mn^{III} from the enzyme-Mn complex to form a stable Mn^{III}-organic acid complex. Thus, the terminal substrates are oxidized by a freely diffusible Mn^{III} complex. This system is advantageous since the stable Mn^{III} complex can diffuse from the enzyme and oxidize the relatively inaccessible, insoluble lignin polymer. Phenolic lignin model dimers are oxidatively cleaved by either enzymatically or chemically generated Mn^{III} complex. Furthermore, nonphenolic lignin model dimers can be degraded by the MnP system in the presence of thiols. Therefore, MnP is an important ligninolytic enzyme rather than a H_2O_2-generating enzyme as previously proposed.

To characterize the MnP reaction mechanism further, the following should be considered:

A Spectroscopic Studies

Native MnP has been shown to bind Mn^{II} with a K_D 4.5 μM. Electron paramagnetic resonance (EPR) studies on the binding of Mn^{II} to native MnP may show the impact of Mn^{II} on the Fe signal. This might provide information on the distance between the heme Fe and the bound Mn^{II}. Similar studies could be done with nuclear magnetic resonance (NMR) spectroscopy.

If a metal ion which binds to the enzyme intermediates but is not oxidized, could be found, additional spectral studies could be undertaken. This might demonstrate the interaction between the substrate and enzyme intermediates, MnPI and MnPII.

Mössbauer spectroscopy could be used to determine the electronic configuration of the iron in native MnP, MnPI, MnPII, and MnPIII. We would predict that they would be similar to those of HRP and its intermediates.

NMR investigation could be utilized to determine the axial ligands bound to heme iron. It could also demonstrate how changes in quaternary structure may affect bond lengths and strengths, and what amino acid residues and hydrogen binding patterns are near the heme.

X-ray diffraction studies are being undertaken and will describe the similarities and differences between the structure of MnP and

cytochrome c peroxidase. MnP forms quite stable intermediates, MnPI and MnPII. Therefore, X-ray crystallography of these intermediates may be possible.

B Kinetic Studies

MnP has a pH optimum at 4.5, yet MnPI formation shows no pH dependence. pH dependency of the enzyme activity may be controlled by MnPI and MnPII reduction. Determination of pKa values for these reductions might suggest the amino acid residue involved in the catalytic action of MnP.

Binding of N_3^- to native HRP has been reported to mimic the formation of compound I (341). Determination of the pH dependency of apparent dissociation constants of MnP against N_3^- may indicate the possible amino acid residue involved in MnPI formation. Transient state kinetic techniques will be required for these studies.

If these studies demonstrate the amino acid residues implicated in the MnP catalytic action, site-directed mutagenesis studies could be undertaken to further clarify the role of the key amino acid residues.

C Biochemical Studies

The roles of chelators in MnP reaction are (i) facilitating the dissociation of Mn^{III} from MnP-Mn complex and (ii) stabilizing Mn^{III} in aqueous solution to maintain a relatively high redox potential. Many C_2 and C_3 acids have been reported to stimulate MnP catalytic

action. The Mn^{III}/Mn^{II} redox couple in aqueous solution has a redox potential of 1.56 V, which may be high enough to oxidize methoxybenzenes to aryl cation radicals. However, free Mn^{III} is extremely unstable and disproportionates to Mn^{II} and MnO_2. The latter is insoluble in aqueous solution. Acetate, a chelator for Mn^{III}, failed to stimulate MnP catalytic action, since acetate apparently does not facilitate the dissociation of Mn^{III} from the enzyme. Therefore, the search for a better chelator is essential. The ideal chelator might allow MnP to oxidize the nonphenolic rings of lignin.

Thiols have been shown to act as radical mediators in the MnP reaction. However, free thiols have not been found as extracellular products. The possibilities of membrane-bound or protein-bound thiol should be examined. Alternative radical mediators should also be sought in the ligninolytic culture medium of the fungus.

10.2 LIGNIN PEROXIDASE

LiP is another important and extensively studied ligninolytic enzyme as previously reviewed (29-31,106,329). LiP has a typical peroxidase catalytic cycle but with several unique features. LiP oxidizes methoxybenzenes to aryl cation radicals, suggesting that the redox potentials for LiPI and LiPII are higher than those for HRP intermediates. The enzyme has an unusually low pH optimum at ~3.0. This low pH may be required for facilitating the formation of aryl

cation radical. In addition, the ready formation of LiPIII species from LiPII and H_2O_2 has been described. Two types of LiPIII species have been characterized and designated as LiPIII and LiPIII*. LiPIII* is formed via the reaction of LiPIII with H_2O_2. LiPIII* reacts further with H_2O_2 and is inactivated. However, LiPIII* in the presence of veratryl alcohol reverts to native LiP via a single step. The possible roles of veratryl alcohol, a secondary metabolite of P. chrysosporium, have been proposed: (i) the protection of the enzyme against the formation of LiPIII by reducing LiPII; (ii) the protection of the enzyme against the inactivation by reacting with LiPIII*; and (iii) the enhancement of the generation of superoxide during the reversion of LiPIII*.

To characterize these unique features and to know why these features are required for lignin biodegradation, further studies are needed.

A Spectroscopic Studies

NMR studies would provide further information about the heme environment to determine the lengths and strengths of the bond between iron and the axial ligands in native LiP and LiPIII(*) and the amino acid residues near the iron. Furthermore, NMR spectroscopy can be a valuable tool for the elucidation of the ligand exchange mechanism. For example, it could provide kinetic information on the ligand exchange of native LiP during the formation of LiPI and of LiPIII* during its reversion to ferric LiP.

X-ray diffraction studies have been initiated and will provide the three-dimensional structure of LiP, which will aid the elucidation of the catalytic mechanism of the enzyme.

B Kinetic Studies

LiP has a pH optimum of ~3.0. However, LiPI formation shows no pH dependence. pH dependence of the reduction of LiPI and LiPII has been shown utilizing transient state kinetics. This work could be extended to reveal heme-linked pKa value(s), which may suggest an amino acid residue involved in the catalytic action.

The reduction of LiPI and LiPII should also be attempted utilizing transient state kinetics with various aromatic substrates, including di-and mono-methoxybenzenes. This may clarify the substrate specificity of the enzyme. Since in the presence of H_2O_2 and non-preferable reducing substrate LiPII might be converted to LiPIII, substrate specificity of the enzyme can be misestimated in the steady state.

As mentioned in the section 10.1, pH dependency of the apparent dissociation constant of LiP with N_3^- could be measured to determine the amino acid residue involved in the formation of LiPI.

If any amino acid residues or any sites on the porphyrin ring are suggested to be involved in the LiP catalytic mechanism, site-directed mutagenesis or heme modifications can be utilized to further elucidate the reaction mechanism.

Higher redox potentials for LiPI and LiPII have been suggested. This could be measured, based on the equilibrium data coupled with K_2IrCl_6/K_3IrCl_6 system.

C Biochemical Studies

Veratryl alcohol, the secondary metabolite of the fungus, plays an important role in the LiP system. A biosynthetic pathway of veratryl alcohol starting with phenylalanine has been proposed (57). The fungus synthesizes veratraldehyde, which is reduced to veratryl alcohol. The immediate precursor of veratraldehyde may be veratryl-glycerol, which might be formed from dimethoxycinnamyl alcohol (57). However, recently the oxygenase from Pseudomonas sp., which can directly cleave C=C bond in dimethoxycinnamyl alcohol to produce veratraldehyde, has been reported (342). In each pathway, the counterpart product of veratraldehyde might be glycolaldehyde. Interestingly, the latter is the substrate for glyoxal oxidase, the H_2O_2-generating enzyme from P. chrysosporium (129). The oxidation product from glycolaldehyde, hydroxyacetate, may act as a chelator for Mn^{III} generated by MnP.

Since many aspects of the ligninolytic system overlap with the biosynthesis of veratryl alcohol, the entire biosynthetic pathway should be clarified. The oxidations of dimethoxycinnamyl alcohol and veratrylglycerol can be catalyzed by LiP. However, there is no report which shows the appearance of LiP activity prior to veratryl alcohol synthesis. Moreover, this reaction probably occurs intracellularly.

cDNA sequence analysis shows that LiP is coded as an extracellular enzyme containing a signal peptide (235). Thus, the elucidation of the enzyme involved in veratryl alcohol synthesis will probably lead to the discovery of new enzyme, an intracellular LiP-like enzyme or a novel oxygenase.

Finally, enzymatic lignin degradation should be attempted. It has been reported that LiP can depolymerize methylated DHP (97). However, it does not represent natural lignin. Recently, LiP has been reported to oxidize isolated lignins such as spruce MWL or alkali straw lignin, but resulting mainly in further polymerization (343). These results are in keeping with the conventional understanding of peroxidase action on polymeric lignin — i.e., that the effect of peroxidase results only in internal rearrangement of the polymeric components (344). However, the degradation of lignin (DHP) by MnP has not been attempted and is of great interest since the freely diffusible Mn-complex is the real oxidant in this enzyme system. ^{14}C-DHP degradation by the MnP system should be attempted. Finally, ^{14}C-DHP degradation would be examined using combined LiP and MnP system, or crude culture media.

REFERENCES

1. Payen, A. (1838) Compt. Rend. 7, 1052-1056
2. Schulze, F. (1857) Chem. Center. 28, 321
3. Klason, P. (1897) Svensk. Kem. Tidskr. 9, 133-137
4. Freudenberg, K. (1939) Z. Angew. Chem. 52, 362-363
5. Mitchell, L., & Hibbert, H. (1944) J. Am. Chem. Soc. 66, 602-604
6. Harris, E.E., D'Ianni, J., & Adkins, H. (1938) J. Am. Chem. Soc. 60, 1467-1470
7. Lange, P.W. (1954) Svensk. Papperstidn. 57, 525-532
8. Freudenberg, K., & Hübner, H.H. (1952) Chem. Ber. 85, 1181-1191
9. Erdtman, H. (1933) Biochem. Z. 258, 172-180
10. Freudenberg, K., & Richtzinhain, H. (1943) Ber. 76B, 997-1006
11. Klason, P. (1923) Cellulosechem. 4, 81-84
12. Bjorkman, A. (1954) Nature 174, 1057-1058
13. Adler, E. (1977) Wood Sci. Technol. 11, 169-218
14. Sarkanen, K.V., & Ludnig, C. (1971) Lignins: Occurence, Formation, Structure, and Reactions, Wiley-Interscience, New York
15. Nimz, H. (1974) Angew. Chem. 86, 336-344
16. Freudenberg, K. (1964) Holzforschung 18, 3-9
17. Adler, E. (1964) Chim. Biochim. Lignine, Cellulose, Hemicellulose, Actes. Symp. Intern. pp 73-83, Grenoble, France

18. Crawford, R.L. (1981) Lignin Biodegradation and Transformation, Wiley-Interscience, New York

19. Freudenberg, K., Chen, C.L., & Cardinale, G. (1962) Chem. Ber. **95**, 2814-2828

20. Freudenberg, K. (1968) in Constitution and Biosynthesis of Lignin (Neish, A. C., & Freudenberg, K., Eds.) pp 47-122, Spring-Verlag, New York

21. Higuchi, T., Shimada, M., Nakatsubo, F., & Tanahashi, M. (1977) Wood Sci. Technol. **11**, 153-167

22. Schöning, A.G., & Johonsson, G. (1965) Svensk. Papperstidn. **68**, 607-613

23. Marth, D.E. (1959) Tappi **42**, 301-308

24. Musha, Y., & Goring, D.I.A. (1974) Wood Sci. **7**, 133-134

25. Effland, M.J. (1977) Tappi **60**, 143-144

26. Harkin, J.M., & Obst, J.R. (1973) Science **180**, 296-298

27. Vance, C.P., Kirk, T.K., & Sherwood, R.T. (1980) Annu. Rev. Phytopathol. **18**, 259-288

28. Wilson, C.L., Loomis, W.E., & Stevens, T.A. (1971) in Botany (5th Ed.) pp 62-64, Holt, Rinehart & Winston, New York

29. Buswell, J.A., & Odier, E. (1987) CRC Crit. Rev. Biotechnol. **6**, 1-60

30. Kirk, T.K., & Farrell, R.L. (1987) Annu. Rev. Microbiol. **41**, 465-505

31. Gold, M.H., Wariishi, H., & Valli, K. (1989) in Biocatalysis in Agricultural Biotechnology (Whitaker, J.R., & Sonnet, P., Eds.) pp 127-140, American Chemical Seciety, Washington D.C.

32. Norman, A.G. (1936) Sci. Progr. **30**, 442-456

33. Wise, L.E., & Ratliff, E.K. (1947) Anal. Chem. **19**, 459-462

34. Gottlieb, S., & Pelczar, M.J. (1951) Bacteriol. Rev. **15**, 55-76

35. Kirk, T.K. (1971) Annu. Rev. Phytopathol. **9**, 185-210

36. Ander, P., & Eriksson, K.-E. (1978) Prog. Ind. Microbiol. **14**, 1-58

37. Brown, W., Cowling, E.B., & Falkehag, W.I. (1968) Svensk. Papperstidn. **22**, 811-821

38. Kirk, T.K. (1975) Holzforschung **29**, 99-107

39. Savory, J.G., & Pinion, L.C. (1958) Holzforschung **12**, 99-103

40. Corbett, N.H. (1965) J. Inst. Wood Sci. **14**, 18-29

43. Haider, K., & Trojanowski, J. (1975) Arch. Microbiol., **105**, 33-42

44. Iwahara, S. (1983) in Recent Advances in Lignin Biodegradation Research (Higuchi, T., Chang, H.-m., & Kirk, T.K., Eds.) pp 96-111, Uni Ltd., Tokyo

45. Kaplan, D.L., & Hartenstein, R. (1980) Soil Biol. Biochem., **12**, 65-74

44. Kirk, T.K., Connors, W.J., & Zeikus, J.G. (1976) Appl. Environ. Microbiol. **32**, 192-194

45. Kirk, T.K., & Chang, H.-m. (1974) Holzforschung **28**, 217-222

46. Kirk, T.K., & Chang, H.-m. (1975) Holzforschung **29**, 56-64

47. Higuchi, T. (1971) Adv. Enzymol. **34**, 207-283

48. Hata, K. (1966) Holzforschung **20**, 142-147

49. Chen, C.-L., Miranda, G.S.C., Evans, J.E., Chang, H.-m., & Kirk, T.K. (1981) Int. Symp. Wood Pulping Chem. vol.3 pp.75-

50. Tai, D., Terazawa, M., Chen, C.-L., Chang, H.-m., & Kirk, T.K. (1983) in Recent Advances in Lignin Biodegradation (Higuchi, T., Chang, H.-m., & Kirk, T.K., Eds.) pp 44-63, Uni Ltd., Tokyo

51. Burdsall, H.H., & Eslyn, W.E. (1974) Mycotaxon. **109**, 123-133

52. Gold, M.H., & Cheng, T.M. (1978) Arch. Microbiol. **121**, 37-41

53. Jeffries, T.W., Choi, S., & Kirk, T.K. (1981) Appl. Environ. Microbiol. **42**, 290-296

54. Fenn, P., Choi, S., & Kirk, T.K. (1981) Arch. Microbiol. **130**, 66-71

55. MacDonald, M.J., Paterson, A., & Broda, P. (1984) J. Bacteriol. **160**, 470-472

56. Lundquist, K., & Kirk, T.K. (1978) Phytochem. **17**, 1676

57. Shimada, M., Nakatsubo, F., Kirk, T.K., & Higuchi, T. (1981) Arch. Microbiol. **129**, 321-324

58. Enoki, A., Goldsby, G.P., & Gold, M.H. (1981) Arch. Microbiol. **129**, 141-145

59. Enoki, A., & Gold, M.H. (1982) Arch. Microbiol. **132**, 123-130

60. Weinstein, D.A., Krisnangkura, K., Mayfield, M.B., & Gold, M.H. (1980) Appl. Environ. Microbiol. **39**, 535-540

61. Kirk, T.K., Schulz, E., Connors, W.J., Lorenz, L.F., & Zeikus, J.G. (1978) Arch. Microbiol. **117**, 277-285

62. Bar-Lev, S.S., & Kirk, T.K. (1981) Biochem. Biophys. Res. Commun. **99**, 373-378

63. Nakatsubo, F., Reid, I.D., & Kirk, T.K. (1982) Biochim. Biophys. Acta **719**, 284-291

64. Enoki, A., Goldsby, G.P., & Gold, M.H. (1980) Arch. Microbiol. **125**, 227-232

65. Goldsby, G.P., Enoki, A., & Gold, M.H. (1980) Arch. Microbiol. **128**, 190-195

66. Higuchi, T. (1984) Mokuzai Gakkaishi, **30**, 613-627

67. Higuchi, T. (1986) Wood Res. **73**, 58-81

68. Hall, P.L. (1980) Enz. Microbial. Technol. **2**, 170-176

69. Forney, L.J., Reddy, M., Tien, M., & Aust, S.D. (1982) J. Biol. Chem. **257**, 11455-11462

70. Kutsuki, H., & Gold, M.H. (1982) Biochem. Biophys. Res. Commun. **109**, 320-327

71. Gold, M.H., Kutsuki, H., & Morgan, M.A. (1983) Photochem. Photobiol. **38**, 647-651

72. Nakatsubo, F., Reid, I.D., & Kirk, T.K. (1981) Biochem. Biophys. Res. Commun. **102**, 484-491

73. Kutsuki, H., Enoki, A., & Gold, M.H. (1983) Photochem. Photobiol. **37**, 1-7

74. Kirk, T.K., Nakatsubo, F., & Reid, I.D. (1983) Biochem. Biophys. Res. Commun. **111**, 200-204

75. Kirk, T.K., Mozuch, M.D., & Tien, M. (1985) Biochem. J. **226**, 455-460

76. Faison, B.D., & Kirk, T.K. (1983) Appl. Environ. Microbiol. **46**, 1140-1145

77. Bavendamm, W. (1928) Z. Pflanzenkr. **38**, 257-276

78. Kirk, T.K., & Kelman, A. (1965) Phytopathol. **55**, 739-745

79. Sundman, V., & Näse, L. (1971) Pap. Puu. **53**, 67-71

80. Ander, P., & Eriksson, K.-E. (1976) Arch. Microbiol. **109**, 1-8

81. Gold, M.H., Mayfield, M.B., Cheng, T.M., Krinsnangkura, K., Shimada, M., Enoki, A., & Glenn, J.K. (1982) Arch. Microbiol. **132**, 115-122

82. Wood, D.A. (1985) in Developmental Biology of Higher Fungi (Moore, D., Casselton, L.A., Woodand, D.A., & Frankland, J.C., Eds.) pp 375-387, Cambridge Univ. Press, Cambridge, U.K.

83. Kirk, T.K., Harkin, J.M., & Cowling, E.B. (1968) Biochim. Biophys. Acta **165**, 134-144

84. Morohoshi, M., & Haraguchi, T. (1987) Mokuzai Gakkaishi **33**, 495-502

85. Wariishi, H., Morohoshi, N., & Haraguchi, T. (1987) Mokuzai Gakkaishi **33**, 892-898

86. Kawai, S., Umezawa, T., & Higuchi, T. (1988) Arch. Biochem. Biophys. **262**, 99-110

87. Leonowicz, A., Edgehill, R.U., & Bollag, J.-M. (1984) Arch. Microbiol. **137**, 89-96

88. Ishihara, T., & Miyazaki, M. (1972) Mokuzai Gakkaishi **18**, 415-419

89. Morohoshi, N., Fujita, K., Wariishi, H., & Haraguchi, T. (1987) Mokuzai Gakkaishi **33**, 310-315

90. Gierer, J., & Opara, A.E. (1973) Acta Chem. Scand. **27**, 2909-2922

91. Kaplan, D. (1979) Phytochem. **18**, 1917-1920

92. Trojanowski, J., & Leonowicz, A. (1969) Microbios. **3**, 247-251

93. Harkin, J.M., & Obst, J.R. (1973) Experimentia **29**, 381-387

94. Gold, M.H., Glenn, J.K., Mayfield, M.B., Morgan, M.A., Kutsuki, H. (1983) in Recent Advances in Lignin Biodegradation Research (Higuchi, T., Chang, H.-m., & Kirk, T.K., Eds.) pp219-232, Uni Ltd., Tokyo

95. Kirk, T.K., & Tien, M. (1983) in Recent Advances in Lignin Biodegradation Research (Higuchi, T., Chang, H.-m., & Kirk, T.K., Eds.) pp 233-245, Uni Ltd., Tokyo

96. Glenn, J.K., Morgan, M.A., Mayfield, M.B., Kuwahara, M., & Gold, M.H. (1983) Biochem. Biophys. Res. Commun. **114**, 1077-1083

97. Tien, M., & Kirk, T.K. (1983) Science **221**, 661-663

98. Kuwahara, M., Glenn, J.K., Morgan M.A., & Gold, M.H. (1984) FEBS Lett. **169**, 247-250

99. Gold, M.H., Kuwahara, M., Chiu, A.A., & Glenn, J.K. (1984) Arch. Biochem. Biophys. **234**, 353-362

100. Tien, M., & Kirk, T.K. (1984) Proc. Natl. Acad. Sci. U.S.A. **81**, 2280-2284

101. Renganahtan, V., Miki, K., & Gold, M.H. (1985) Arch. Biochem. Biophys. **241**, 304-314

102. Kirk, T.K., Croan, S., Tien, M., Murtagh, K.E., & Farrell, R.L. (1986) Enz. Microbiol. Technol. **8**, 27-32

103. Leisola, M.S.A., Kozulic, B., Meussdoerffer, F., & Fiechter, A. (1987) J. Biol. Chem. **262**, 419-424

104. Glenn, J.K., & Gold, M.H. (1985) Arch. Biochem. Biophys. **242**, 329-341

105. Paszczynski, A., Huynh, V.-B., & Crawford, R.L. (1986) Arch. Biochem. Biophys. **244**, 750-765

106. Tien, M. (1987) CRC Crit. Rev. Microbiol. **15**, 141-168

107. Glenn, J.K., & Gold, M.H. (1983) Appl. Environ. Microbiol. **45**, 1741-1747

108. Glenn, J.K., Akileswaran, L., & Gold, M.H. (1986) Arch. Biochem. Biophys. **251**, 688-696

109. Hattaka, A., & Tervilä-wilo, A. (1986) in Proc. Sov. Finn. Sem. Microb. Degradation Lignocellulose Raw Mater. pp 65-74, Tbilisi, Georgia, USSR

110. Maltseva, O.V., Myasoedowa, N.M., Leontievsky, A.A., & Golovleva, L.A. (1986) in Proc. Sov. Finn. Sem. Microb. Degradation Lignocellulose Raw Mater. pp 74-82, Tbilisi, Georgia, USSR

111. Dodson, A.P.J., Evans, C.S., Harvey, P.J., & Palmer, J.M. (1987) FEMS Microbiol. Lett. **42**, 17-22

112. Johansson, T., & Nyman, P.O. (1987) Acta Chem. Scand. **Ser. B41**, 762-765

113. Leatham, G.F. (1986) Appl. Microbiol. Biotechnol. **24**, 51-58

114. Kawai, S., Umezawa, T., & Higuchi, T. (1987) Wood Res. **73**, 18-21

115. Leisola, M.S.A., Ulmer, D.C., Waldner, R., & Fiechter, A. (1984) J. Biotechnol. **1**, 331-339

116. Faison, B.D., & Kirk, T.K. (1985) Appl. Environ. Microbiol. **49**, 299-304

117. Leisola, M.S.A., Thanei-Wyss, U., & Fiechter, A. (1985) J. Biotechnol. **3**, 97-107

118. Ulmer, D.C., Leisola, M.S.A., & Fiechter, A. (1984) J. Biotechnol. **1**, 13-24

119. Chua, M.G.S., Choi, S., & Kirk, T.K. (1983) Holzforschung **37**, 55-61

120. Greene, R.V., & Gould, J.M. (1984) Biochem. Biophys. Res. Commun. **118**, 437-443

121. Kelley, R.L., & Reddy, C.A. (1986) J. Bacteriol. **166**, 269-274

122. Eriksson, K.-E., Pettersson, B., Volc, J., & Musiek., V. (1986) Appl. Microbiol. Biotechnol. **23**, 257-262

123. Molskness, T.A., Pankow, K.S.M., & Gold, M.H. (in preparation)

124. Greene, R.V., & Gould, J.M. (1983) Biochem. Biophys. Res. Commun. **117**, 275-281

125. Asada, Y., Miyabe, M., Kikkawa, M., & Kuwahara, M. (1986) Agric. Biol. Chem. **50**, 525-529

126. Kuwahara, M., Ishida, Y., Miyagawa, Y., & Kawakami, C. (1984) J. Ferment. Technol. **62**, 237-242

127. Gross, G.G., Janse, C., & Elstner, E.F. (1977) Planta **136**, 271-276

128. Halliwell, B. (1978) Planta **140**, 81-88

129. Kersten, P.J., & Kirk, T.K. (1987) J. Biotechnol. **169**, 2195-2201

130. Bourbonnais, R., & Paice, M.G. (1988) Biochem. J. **255**, 445-450

131. Farmer, V.C., Henderson, M.E.K., & Russell, J.D. (1960) Biochem. J. **74**, 257-262

132. Iwahara, S., Nishihara, T., Jomori, T., Kuwahara, M., & Higuchi, T. (1980) J. Ferment. Technol. **58**, 183-188

133. Fåhraeus, G., & Reinhammer, B. (1967) Acta Chem. Scand. **21**, 2367-2378

134. Ishihara, T., & Miyazaki, M. (1970) Mokuzai Gakkaishi **16**, 181-184

135. Sanders, B.C., Holmes-Siedle, A.G., & Stark, B.P. (1964) Peroxidase, Butterworths, London

136. Paul, K.G. (1986) in Molecular and Physiological Aspects of Plant Peroxidases, (Greppin, H., Penel, C., & GAsper, Th., Eds.) pp 1-14, Univ. Geneva, Switzerland

137. Dunford, H.B., & Stillman, J.S. (1976) Coord. Chem. Rev. **19**, 187-251

138. Hultquist, D.E., & Morrison, M. (1963) J. Biol. Chem. **238**, 2843-2846

139. Agner, K. (1958) Acta Chem. Scand. **12**, 89-94

140. Ehrenberg, A., & Agner, K. (1958) Acta Chem. Scand. **12**, 95-100

141. Taurog, A., Lothrop, M.L., & Estabrook, R.W. (1970) Achiv. Biochem. Biophys. **139**, 221-229

142. Morris, D.R., & Hager, L.P. (1966) J. Biol. Chem. **241**, 1763-1768

143. Hager, L.P., Morris, D.R., Brown, F.S., & Eberwein, H. (1966) J. Biol. Chem. **241**, 1769-1777

144. Manthey, J.A., & Hager, L.P. (1981) J. Biol. Chem. **256**, 11232-11238

145. Abrams, R., Altschul, A.M., & Hogness, T.R. (1942) J. Biol. Chem. **142**, 303-316

146. Yonetani, T., & Ray, G.S. (1965) J. Biol. Chem. **240**, 4503-4508

147. Flohè, L., Günzler, W.A., & Schock, H.H. (1973) FEBS Lett. **32**, 132-134

148. Klebanoff, S.J., & Clark, R.A. (1978) The Neutrophil: Function and Clinical disorders, North-Holland, Amsterdam

149. Taurog, A (1979) Endocrinology **1**, 331-342

150. Magnusson, R.P., Taurog, A., & Dorris, M.L. (1984) J. Biol. Chem. **259**, 13783-13790

151. Ohtaki, S., Nakagawa, H., Nakamura, S., Nakamura, M., & Yamazaki, I. (1985) J. Biol. Chem. **260**, 441-448

152. Ohki, S., Ogino, N., Yamamoto, S., & Hayaishi, O (1979) J. Biol. Chem. **254**, 829-836

153. Van der Ouderaa, F.J., Buytenhek, M., Slikkerveer, F.J., & Van Droop, D.A. (1979) Biochim. Biophys. Acta **572**, 29-42

154. Lambeir, A.-M., Markey, C.M., Dunford, H.B., & Marnette, L.J. (1985) J. Biol. Chem. **260**, 14894-14896

155. Dunford, H.B. (1982) Adv. Inorg. Biochem. **4**, 41-68

156. Yamazaki, I. (1974) in Molecular Mechanism of Oxygen Activation (Hayaishi, O., Ed.) pp 535-558, Academic, New York

157. Felton, R.H., & Yu, N.-T. (1978) in The Porphyrin (Dolphin, D., Ed.) Vol. III, Academic Press, New York

158. La Mar, G.N., & deRopp, J.S. (1979) Biochem. Biophys. Res. Commun. **90**, 36-41

159. Kobayashi, K., Tamura, M., Hayashi, K., Hori, H., & Morimoto, H. (1980) J. Biol. Chem. **225**, 2239-2242

160. Reed, C.A., Mashiko, T., Bentley, S.P., Kastner, M.E., Sheidt, W.R., Spartalian, K., & Lang, G. (1979) J. Am. Chem. Soc. **101**, 2948-2965

161. Maltempo, M.M., Ohlsson, P,-I., Paul, K.G., Petersson, L., & Ehrenberg, A. (1979) Biochemistry **18**, 2935-2941

162. La Mar, G.N., deRopp, J.S., Smith, K.M., & Langry, K.C. (1980) J. Biol. Chem. **255**, 6646-6652

163. Evangelista-Kirkup, R., Crisati, M., Poulos, T.L., & Spiro, T.G. (1985) FEBS Lett. **190**, 221-226

164. Welinder, K.G. (1976) FEBS Lett. **72**, 19-23

165. Mauk, M.R., & Girotti, A.W. (1974) Biochemistry **13**, 1757-1763

166. Kaput, J., Goltz, S., & Blobel, G. (1982) J. Biol. Chem. **257**, 15054-15058

167. Welinder, K.G., & Mazza, G. (1977) Eur. J. Biochem. **73**, 353-358

168. Sono, M., & Dawson, J.H. (1982) J. Biol. Chem. **257**, 5496-5502

169. Ozols, J., & Strittmatte, P. (1964) J. Biol. Chem. **239**, 1018-1023

170. Loehr, T.M., Keyes, W.E., & Pincus, P.A. (1979) Anal. Biochem. **96**, 456-463

171. Theorell, H. (1941) Enzymologia **10**, 250-252

172. Chance, B. (1952) Arch. Biochem. Biophys. **41**, 404-415

173. Theorell, H., Ehrenberg, A., & Chance, B. (1952) Arch. Biochem. Biophys. **37**, 237-239

174. Theorell, H., & Ehrenberg, A. (1952) Arch. Biochem. Biophys. **41**, 442-461

175. Keilin, D., & Mann, T. (1937) Proc. Roy. Soc. London **Ser. B122**, 119-133

176. Schultz, C.E., Rutter, R., Sage, J.T., Debrunner, P.G., & Hager, L.P. (1984) Biochemistry **23**, 4743-4754

177. La Mar, G.N., deRopp, J.S., Latos-Grazynski, L., Balch, A.L., Johnson, R.B., Smith, K.M., Parish, D.W., & Chang, R. (1983) J. Am. Chem. Soc. **105**, 782-787

178. Hashimoto, S., Tatsuno, Y., & Kitagawa, T. (1984) Proc. Jpn. Acad. **Ser. B60**, 345-348

179. Terner, J., Sitter, A.J., & Reczek, C.M. (1985) Biochim. Biophys. Acta **828**, 73-80

180. Sitter, A.J., Reczek, C.M., & Terner, J. (1985) Biochim. Biophys. Acta **828**, 229-235

181. Brill, A.S., & Williams, R.J.P. (1961) Biochem. J. **78**, 246-253

182. Morita, Y., & Mason, H.S. (1965) J. Biol. Chem. **240**, 2654-2659

183. Aasa, R., Vänngard, T., & Dunford, H.B. (1975) Biochim. Biophys. Acta **391**, 259-264

184. Dolphin, D.H., Forman, A., Borg, D.C., Fajer, J., & Felton, R.H. (1971) Proc. Natl. Acad. Sci. U.S.A. **68**, 614-618

185. Dolphin, D.H., & Felton, R.H. (1974) Accts. Chem. Res. **7**, 26-32

186. DiNello, R.K., & Dolphin, D.H. (1981) J. Biol. Chem. **256**, 6903-6912

187. Penner-Hahn, J.E., Eble, K.S., McMurry, T.J., Renner, M., Balch, A.L., Groves, J.T., Dawson, J.H., & Hodgson, K.O. (1986) J. Am. Chem. Soc. **108**, 7819-7825

188. Yonetani, T., & Asakura, T. (1968) J. Biol. Chem. **243**, 3996-3998

189. Yonetani, T., & Asakura, T. (1986) J. Biol. Chem. **243**, 4715-4721

190. Loach, P.A., & Calvin, M. (1963) Biochemistry **2**, 361-371

191. Poulos, T.L. (1987) Adv. Inorg. Biochem. **7**, 1-36

192. Dawson, J.H. (1988) Science **240**, 433-439

193. Araiso, T., & Dunford, H.B. (1980) Biochem. Biophys. Res. Commun. **94**, 1177-1182

194. Araiso, T., & Dunford, H.B. (1981) J. Biol. Chem. **256**, 10099-10104

195. Hayashi, Y., & Yamazaki, I. (1978) Arch. Biochem. Biophys. **190**, 446-453

196. Hewson, W.D., & Dunford, H.B. (1975) Can. J. Chem. **53**, 1928-1932

197. Chance, B. (1952) Arch. Biochem. Biophys. **41**, 416-424

198. Cormier, M.J., & Prichard, P.M. (1968) J. Biol. Chem. **243**, 4706-4714

199. Dunford, H.B., & Hasinoff, B.B. (1970) Biochemistry **9**, 4930-4939

200. Hewson, W.D., & Dunford, H.B. (1976) J. Biol. Chem. **251**, 6036-6042

201. Critchlow, J.E., & Dunford, H.B. (1972) J. Biol. Chem. **247**, 3703-3713

202. Dunford, H.B., & Cotton, M.L. (1975) J. Biol. Chem. **250**, 2920-2932

203. Hayashi, Y., & Yamazaki, I. (1979) J. Biol. Chem. **254**, 9101-9106

204. Ator, M.A., & Ortiz de Montellano, P.R. (1987) J. Biol. Chem. **262**, 1542-1551

205. Ator, M.A., David, S.K., & Ortiz de Montellano, P.R. (1987) J. Biol. Chem. **262**, 14954-14960

206. Ortiz de Montellano, P.R., David, S.K., Ator, M.A., & Tew, D. (1988) Biochemistry **27**, 5470-5476

207. Ortiz de Montellano, P.R., Choe, Y.S., DePillis, G., & Catalano, C.E. (1987) J. Biol. Chem. **262**, 11641-11646

208. Ortiz de Montellano, P.R. (1987) Acc. Chem. Res. **20**, 289-294

209. Job, D., & Dunford, H.B. (1976) Eur. J. Biochem. **66**, 607-614

210. Bohne, C., MacDonald, I.D., & Dunford, H.B. (1987) J. Biol. Chem. **262**, 3572-3578

211. Yamada, H., & Yamazaki, I. (1974) Arch. Biochem. Biophys. **165**, 728-738

212. Colleta, M., Ascoli, F., Brunori, M., & Traylor, T.G. (1986) J. Biol. Chem. **261**, 9811-9814

213. George, P. (1952) Adv. Catal. Relat. Sub. **4**, 367-428

214. Harbury, H.A. (1957) J. Biol. Chem. **225**, 1009-1024

215. Chance, B. (1965) in Oxidases and Related Redox System (King, T.E., Mason, H.S., & Morrison, M., Eds.) pp 504-526, Willey, New York

216. Wittenberg, J.B., Nobel, R.W., Wittenberg, B.A., Antonini, E., Brunori, M., & Wyman, J. (1967) J. Biol. Chem. **242**, 626-634

217. Blumberg, W.E., Peisach, J., Wittenberg, B.A., & Wittenberg, J.B. (1968) J. Biol. Chem. **243**, 1854-1862

218. Tamura, M., & Yamazaki, I. (1972) J. Biochem. **71**, 311-319

219. Yamazaki, I., Yamazaki, H., Tamura, M., Ohnishi, T., Nakamura, S., & Iyanagi, T. (1968) Adv. Chem. Ser. 77, 290-306

220. Yamazaki, I., & Piette, L.H. (1963) Biochim. Biophys. Acta 77, 47-64

221. Metodiewa, D., & Dunford, H.B. (1989) Arch. Biochem. Biophys. 272, 245-253

222. George, P. (1953) J. Biol. Chem. 201, 427-434

223. Nakajima, R., & Yamazaki, I. (1987) J. Biol. Chem. 262, 2576-2581

224. Ricard, J., & Job, D. (1974) Eur. J. Biochem. 44, 359-374

225. Smith, A.M., Morrison, W.L., & Milham, P.J. (1982) Biochemistry 21, 4414-4419

226. Rotilio, G., Falcioni, G., Fioretti, E., & Brunori, M. (1975) Biochem. J. 145, 405-407

227. Andersson, L.A., Renganathan, V., Chiu, A.A., Loehr, T.M., & Gold, M.H. (1985) J. Biol. Chem. 263, 7029-7036

228. Kuila, D., Tien, M., Fee, J.A., & Ondrias, M.R. (1985) Biochemistry 24, 3394-3397

229. Andersson, L.A., Renganathan, V., Loehr, T.M., & Gold M.H. (1987) Biochemistry, 26, 2258-2263

230. Hammel, K.E., Tien, M., Kalyanaraman, B., & Kirk, T.K. (1985) J. Biol. Chem. 260, 8348-8353

231. Renganathan, V., Miki, K., & Gold M.H. (1986) Arch. Biochem. Biophys. 246, 155-161

232. Renganathan, V., & Gold, M.H. (1986) Biochemistry 25, 1626-1631

233. Tien, M., & Tu, C.-P.D. (1987) Nature 326, 520-523

234. de Boer, H.A., Zhang, Y.Z., Collins, C., & Reddy, C.A. (1987) Gene (Amst.) **60**, 93-102

235. Ritch, T.G., Nipper, V.J., Akileswaran, L., Pribnow, D., & Gold, M.H. (1989) (submitted)

236. Tien, M., Kirk, T.K., Bull, C., & Fee, J.A. (1986) J. Biol. Chem. **261**, 1687-1693

237. Renganathan, V., Miki, K., & Gold, M.H. (1987) Biochemistry **26**, 5127-5132

238. Harvey, P.J., Schoemaker, H.E., & Palmer, J.M. (1986) FEBS Lett. **195**, 242-246

239. Haemmerli, S.D., Leisola, M.S.A., Sangland, D., & Fiechter, A. (1986) J. Biol. Chem. **261**, 6900-6903

240. Hammel, K.E., Kalyanaraman, B., & Kirk, T.K. (1986) Proc. Natl. Acad. Sci. U.S.A. **83**, 3708-3712

241. Miki, K., Renganathan, V., & Gold, M.H. (1986) Biochemistry **25**, 4790-4796

242. Miki, K., Renganathan, V., & Gold, M.H. (1986) FEBS Lett. **203**, 235-238

243. Miki, K., Renganathan, V., Mayfield, M.B., & Gold, M.H. (1987) FEBS Lett. **210**, 199-238

244. Miki, K., Kondo, R., Renganathan, V., Mayfield, M.B., & Gold, M.H. (1988) Biochemistry **27**, 4787-4794

245. Kirk, T.K., Tien, M., Kerstein, P.J. & Kalyanaraman, B. (1986) Biochem. J. **236**, 279-292

246. Umezawa, T., Shimada, M., Higuchi, T., & Kusai, K. (1986) FEBS Lett. **250**, 287-292

247. Umezawa, T., & Higuchi, T. (1987) FEBS Lett. **218**, 255-260

248. Schoemaker, H.E., Harvey, P.J., Bowen, R.M., & Palmer, J.M. (1985) FEBS Lett. **183**, 7-12

249. Kersten, P.J., Tien, M., Kalyanaraman, B., & Kirk, T.K. (1985) J. Biol. Chem. **260**, 2609-2612

250. Umezawa, T., & Higuchi, T. (1985) FEBS Lett. **182**, 257-259

251. Leisola, M.S.A., Schmidt, B., Thanei-Wyss, U., & Fiechter, A. (1985) FEBS Lett. **189**, 267-270

252. Mino, Y., Wariishi, H., Blackburn, N.J., Loehr, T.M., & Gold, M.H. (1988) J. Biol. Chem. **263**, 7029-7036

253. Yonetani, T., Yamamoto, H., Erman, J.E., Leigh, J.S.,Jr., & Reed, G.H. (1972) J. Biol. Chem. **247**, 2447-2455

254. Pribnow, D., Mayfield, M.B., Nipper, V.J., Brown, J.A., & Gold, M.H. (1989) J. Biol. Chem. **264**, 5036-5040

255. Elizabeth, A.P., Andrawis, A., & Tien, M. (1989) J. Biol. Chem. **264**, 13531-13535

256. Wariishi, H., Akileswaran, L., & Gold, M.H. (1988) Biochemistry **27**, 5365-5370

257. Wariishi, H., Dunford, H.B., MacDonald, I.D., & Gold, M.H. (1989) J. Biol. Chem. **264**, 3335-3340

258. Wariishi, H., Valli, K., & Gold, M.H. (1989) Biochemistry **28**, 6017-6023

259. Wariishi, H., Valli, K., Renganathan, V., & Gold, M.H. (1989) J. Biol. Chem. **264**, 14185-14191

260. Marquez, L., Wariishi, H., Dunford, H.B., & Gold, M.H. (1988) J. Biol. Chem. **263**, 10549-10552

261. Andrawis, A., Johnson, K.A., & Tien, M. (1988) J. Biol. Chem. **263**, 1195-1198

262. Wariishi, H., & Gold, M.H. (1989) FEBS Lett. **243**, 165-168

263. Wariishi, H., & Gold, M.H. (1990) J. Biol. Chem. **264**, 7070-7078

264. Hewson, W.D., & Hager, L.P. (1979) in The Porphyrins (Dolphin, D., Ed.) Vol. VII, pp 295-333, Academic Press, New York

265. Rutter, R., Valentine, M., Hendrich, M.P., Hager, L.P., & Debrunner, P.G. (1983) Biochemistry **22**, 4769-4774

266. Roberts, J.E., Hoffman, B.M., Rutter, R., & Hager, L.P. (1983) J. Am. Chem. Soc. **103**, 7654-7656

267. Palcic, M.M., Rutter, R., Araiso, T., Hager, L.P., & Dunford, H.B. (1980) Biochem. Biophys. Res. Commun. **94**, 1123-1127

268. Rakhit, G., Spiro, T.G., & Uyeda, M. (1976) Biochem. Biophys. Res. Commun. **71**, 803-808

269. Felton, R.H., Romans, A.Y., Yu, N.-T., & Schonbaum, R. (1976) Biochim. Biophys. Acta **434**, 82-89

270. Terner, J., & Reed, D.E. (1984) Biochim. Biophys. Acta **789**, 80-86

271. Schonbaum, G.R., & Lo, S. (1972) J. Biol. Chem. **247**, 3353-3360

272. Yamazaki, I., & Yokota, K. (1965) Biochem. Biophys. Res. Commun. **19**, 249-254

273. Latimer, W.M. (1952) The Oxidation States of the Elements and their Potentials in Aqueous Solutions, Prentice-Hall, Englewood Cliffs, NJ

274. Ogawa, H. (1985) Kagaku Gijutsu Kenkyusho Hokoku **80**, 31-36

275. Waters, W.A., & Littler, J.S. (1965) in Oxidation in Organic Chemistry (Wiberg, K.B., Ed.) Vol. 5a, pp 186-241, Academic Press, New York

276. Archibald, F.S., & Fridovich, I. (1983) Arch. Biochem. Biophys. **214**, 452-463

277. Nakajima, R.,Yamazaki, I., & Griffin, B.W. (1985) Biochem. Biophys. Res. Commun. **128**, 1-6

278. Kimura, S., & Yamazaki, I. (1979) Arch. Biochem. Biophys. **198**, 580-588

279. Jager, A., Croan, S., & Kirk, T.K. (1985) Appl. Environ. Microbiol. **50**, 1274-1278

280. Cotton, M.L., & Dunford, H.B. (1973) Can. J. Chem. **51**, 582-587

281. Job, D., Ricard, J., & Dunford, H.B. (1978) Can. J. Biochem. **56**, 702-707

282. Lambeir, A.-M., Dunford, H.B., & Pickard, M.A. (1983) J. Inorg. Biochem. **19**, 291-300

283. Maguire, R.J., Dunford, H.B., & Morrison, M. (1971) Can. J. biochem. **49**, 1165-1171

284. Manthey, J.A., & Hager, L.P. (1985) J. Biol. Chem. **260**, 9654-9659

285. Poulos, T.L., & Kraut, J. (1980) J. Biol. Chem. **255**, 8199-8205

286. Loo, S., & Erman, J.E. (1975) Biochemistry **14**, 3467-3470

289. Demmber, H., Hinz, I., Keller-Rudek, H., Koeber, K., Köttelwesch, H., & Schneider, D. (1980) in Coordination Compounds of Manganese, Gmelin Handbook for Inorganic Chemistry (Schleitzer-Rust, E., Ed.) 8th ed., Vol. 56, pp 85-185, Springer-Verlag, New York

290. Alic, M., Letzring, C., & Gold, M.H. (1987) Appl. Environ. Microbiol. **53**, 1464-1469

291. Nakatsubo, F., & Higuchi, T. (1975) Holzforschung **29**, 193-198

292. Feiser, M.F. (1982) in Feiser's Reagents for Organic Synthesis (Feiser, M.F., Ed.) Vol. 10, pp 135-136, Wiley-International, New York

293. Baker, W. (1941) J. Chem. Soc., 662-670

294. Arndt, D. (1981) Manganese Compounds as Oxidizing Agents in Organic Chemistry, Open Court Publishing, La Salle, IL

295. Heiba, E.I., Dessau, R.M., & Koehl, W.J. (1969) J. Am. Chem. Soc. **91**, 138-145

296. Ingold, K.U. (1969) Acc. Chem. Res. **2**, 1-9

297. Bridge, N.K., & Porter, G. (1958) Proc. R. Soc. London **A244**, 259-288

298. Kawai, S., Umezawa, T., Shimada, M., Higuchi, T., Koide, K., Nishida, T., Morohoshi, N., & Haraguchi, T. (1987) Mokuzai Gakkaishi **33**, 792-797

299. Zonis, S.A., & Kornilova, Y.I. (1950) J. Gen. Chem. USSR (Engl. Transl.) **20**, 1301-1310

300. Zonis, S.A. (1954) J. Gen. Chem. USSR (Engl. Transl.) **24**, 815-816

301. Bush, J.B., & Finkbeiner, H. (1968) J. Am. Chem. Soc. **90**, 5903-5904

302. Heiba, E.I., Dessau, R.M., & Koehl, W.J. (1968) J. Am. Chem. Soc. **90**, 5905-5906

303. Benson, D. (1976) Mechanisms of Oxidation by Metal Ions, Elsevier, New York

304. Misra, H.P. (1974) J. Biol. Chem. **249**, 2151-2155

305. Forrester, I.T., Grabski, A.C., Burgess, R.R., & Leatham, G.F. (1988) Biochem. Biophys. Res. Commun. **157**, 992-999

306. Adams, R., & Marvel, C.S. (1941) Org. Syn. Coll. Vol. I, 94-95

307. Shimada, M., & Gold, M.H. (1983) Arch. Microbiol. **134**, 299-302

308. Katayama, T., Nakatsubo, F., & Higuchi, T. (1981) Mokuzai Gakkaishi **27**, 223-230

309. Hauser, C.R., & Breslow, D.S. (1955) Org. Syn. Coll. Vol. III, 408-410

310. Bielski, B.H.J., & Gebicki, J.M. (1977) in Free Radicals in Biology (Pryor, W.A., Ed.), Vol. III, pp 1-51

311. Adams, G.E., & Wardman, P. (1977) in Free Radicals in Biology (Pryor, W.A., Ed.) Vol. III, pp 53-95

312. Waters, J., & Kolthoff, I.M. (1948) J. Am. Chem. Soc. **70**, 2455-2460

313. Zweig, A., Hodson, W.G., & Jura, W.H. (1964) J. Am. Chem. Soc. **86**, 4124-4129

314. Kersten, P.-J., Kalyanaraman, B., Hammel, K.E., & Kirk, T.K. (1987) in Lignin Enzymic and Microbial Degradation pp 75-79, INRA, Paris

315. Mason, R.P. (1982) in Free Radicals in Biology (Pryor, W.A., Ed.) Vol. V, pp 161-222

316. Ross, D., Norbeck, K., & Moldeus, P. (1985) J. Biol. Chem. **260**, 15028-15032

317. Foureman, G.L., & Eling, T.E. (1989) Arch. Biochem. Biophys. **269**, 55-68

318. Lin, W.S., Clement, J.R., Gaucher, G.M., & Armstrong, D.A. (1975) Radiat. Res. **62**, 438-455

319. Kosower, N.S., & Kosower, E.M. (1976) in Free Radicals in Biology (Pryor, W.A., Ed.), Vol. II, pp 55-84

320. Pryor, W.A., Gojon, G., & Stanley, J.P. (1973) J. Am. Chem. Soc. **95**, 945-946

321. Stock, B.H., Schreiber, J., Guenat, C., Mason, R.P., Bend, J.R., & Eling, T.E. (1986) J. Biol. Chem. **261**, 15915-15922

322. Haemmerli, S.D., Schoemaker, H.E., Schmidt, H.W.H., & Leisola, M.S.A. (1987) FEBS Lett. **220**, 149-154

323. Balny, C., Anni, H., & Yonetani, T. (1987) FEBS Lett. **221**, 349-354

324. Green, M.J., & Hill, H.A.O. (1984) Methods Enzymol. **105**, 3-22

325. McCord, J.M., & Fridovich, I. (1969) J. Biol. Chem. **244**, 6049-6055

326. Weinryb, I. (1966) Biochemistry 5, 2003-2008

327. Harvey, P.J., Schoemaker, H.E., & Palmer, J.M. (1987) in Lignin Enzymic and Microbial Degradation pp 145-150, JNRA, Paris

328. Tonon, F., & Odier E. (1988) Appl. Environ. Microbiol. **54**, 466-472

329. Palmer, J.M., Harvey, P.J., & Schoemaker, H.E. (1987) Philos. Trans. R. Soc. London Ser. A **321**, 495-502

330. Nishikimi, M. (1975) Biochem. Biophys. Res. Commun. **63**, 463-468

331. Nelson, D.P., & Kiesaw, L.A. (1972) Anal. Biochem. **49**, 474-478

332. Rabani, J., Mulac, W.A., & Matheson, M.S. (1965) J. Phys. Chem. **69**, 53-70

333. Cai, D., & Tien, M. (1989) Biochem. Biophys. Res. Commun. **162**, 464-469

334. Peisach, J., Blumberg, W.E., Wittenberg, B.A., & Wittenberg, J.B. (1968) J. Biol. Chem. **243**, 1871-1880

335. Bagger, S., & Williams, R.J.P. (1971) Acta Chem. Scand. **25**, 976-982

336. Jenzer, H., Jones, W., & Kohler, H. (1986) J. Biol. Chem. **261**, 15550-15556

337. Jenzer, H., Kohler, H., & Broger, C. (1987) Arch. Biochem.Biophys. **258**,381-390

338. Schmidt, H.W., Haemmerli, S.D., Schoemaker, H.E., & Leisola, M.S.A. (1989) Biochemistry **28**, 1776-1783

339. Hashimoto, S., Tatsuno, Y., & Kitagawa, T. (1986) Proc. Natl. Acad. Sci. U.S.A. **83**, 2417-2421

340. Bolscher, B.G.J.M., & Wever, R. (1984) Biochim. Biophys. Acta **778**, 8199-8205

341. Holzwarth, J.F., Meyer, F., Pickard, M., & Dunford, H.B. (1988) Biochemistry **27**, 6628-6633

342. Samejima, M., Habu, N., Kamoda, S., & Yoshimoto, T. (1989) Proc. 4th Intern. Conf. Biotech. Pulp & Paper Indust. pp 123-124, Raleigh, NC

343. Haemmerli, S.D., Leisola, M.S.A., & Fiechter, A. (1986) FEMS Microb. Lett. **35**, 33-36

344. Lewis, N.G., Razal, R.A., & Yamamoto, E. (1987) Proc. Natl. Acad. Sci. U.S.A. **84**, 7925-7927

APPENDIX

A BINDING INTERACTION BETWEEN MnPI AND MANGANESE

For a productive enzyme-substrate complex formation and an enzyme-catalyzed reaction, the simplest model is

$$\mathrm{MnPI} + \mathrm{Mn^{II}} \underset{}{\overset{K_1}{\rightleftarrows}} \mathrm{MnPI\text{-}Mn^{II}} \xrightarrow{k_5} \mathrm{Products} \qquad [A.1]$$

where K_1 is an apparent dissociation constant and k_5 is a first order rate constant.

Under the pseudo-first-order condition with Mn^{II} in excess, the disappearance rate of MnPI is given by

$$-\frac{d[\mathrm{MnPI}]_{tot}}{dt} = k_{obs}[\mathrm{MnPI}]_{tot} \qquad [A.2]$$

where $[MnPI]_{tot}$ is the total concentration of MnPI in the reaction system, and k_{obs} is an observed rate constant.

From the model (Eq. A.1),

$$[MnPI]_{tot} = [MnPI] + [MnPI\text{-}Mn^{II}] \qquad [A.3]$$

$$-\frac{d[MnPI]_{tot}}{dt} = k_5[MnPI\text{-}Mn^{II}] \qquad [A.4]$$

$$K_1 = \frac{[MnPI][Mn^{II}]}{[MnPI\text{-}Mn^{II}]} \qquad [A.5]$$

From A.5,

$$[MnPI] = \frac{K_1[MnPI\text{-}Mn^{II}]}{[Mn^{II}]} \qquad [A.6]$$

From A.3 and A.6

$$[MnPI]_{tot} = \frac{K_1[MnPI\text{-}Mn^{II}]}{[Mn^{II}]} + [MnPI\text{-}Mn^{II}]$$

Therefore,

$$[MnPI\text{-}Mn^{II}] = \frac{[MnPI]_{tot}}{1 + \frac{K_1}{[Mn^{II}]}} \qquad [A.7]$$

From A.4 and A.7,

$$-\frac{d[MnPI]_{tot}}{dt} = \left(\frac{k_5}{1 + \frac{K_1}{[Mn^{II}]}}\right)[MnPI]_{tot} \qquad [A.8]$$

From A.2 and A.8, k_{obs} is given by

$$k_{obs} = \frac{k_5}{1 + \frac{K_1}{[Mn^{II}]}} \qquad [A.9]$$

B BINDING INTERACTION BETWEEN MnPII AND MANGANESE

For a productive enzyme-substrate complex formation and an enzymecatalyzed reaction, the simplest model is

$$MnPII + Mn^{II} \underset{}{\overset{K_2}{\rightleftarrows}} MnPII\text{-}Mn^{II} \overset{k_8}{\rightarrow} \text{Products} \qquad [B.1]$$

Then the same derivation is made as shown in appendix A.

$$-\frac{d[MnPII]_{tot}}{dt} = k_{obs}[MnPII]_{tot} \qquad [B.2]$$

$$[MnPII]_{tot} = [MnPII] + [MnPII\text{-}Mn^{II}] \qquad [B.3]$$

$$-\frac{d[MnPII]_{tot}}{dt} = k_8[MnPII\text{-}Mn^{II}] \qquad [B.4]$$

$$K_2 = \frac{[MnPII][Mn^{II}]}{[MnPII\text{-}Mn^{II}]} \qquad [B.5]$$

From these equations, k_{obs} is given by

$$k_{obs} = \frac{k_8}{1 + \frac{K_2}{[Mn^{II}]}} \qquad [B.6]$$

C FORMATION OF COMPOUND II IN THE STEADY STATE

LiP has a typical peroxidative catalytic cycle shown below.

$$LiP + H_2O_2 \xrightarrow{k_1} LiPI + H_2O$$

$$LiPI + AH \xrightarrow{k_2} LiPII + A\cdot$$

$$LiPII + AH \xrightarrow{k_3} LiP + A\cdot$$

where AH is a reducing substrate such as VAlc or p-cresol. The fate of A· can be ignored since products of VAlc and p-cresol have no effect on absorptivity in the Soret region.

The following assumptions are made based on the theory that in the steady state the rates of the formation and disappearance of enzyme intermediates are equal.

$$[LiP]_{tot} = [LiP] + [LiPI] + [LiPII] \qquad \text{(Enzyme Conservation)}$$

$$-\frac{d[LiP]}{dt} = 0 = k_1[LiP][H_2O_2] - k_3[LiPII][AH] \qquad \text{(Steady State Assumptions)}$$

$$\frac{d[LiPI]}{dt} = 0 = k_1[LiP][H_2O_2] - k_2[LiPI][AH]$$

$$\frac{d[LiPII]}{dt} = 0 = k_2[LiPI][AH] - k_3[LiPII][AH]$$

From the steady state assumptions,

$$k_1[LiP][H_2O_2] = k_2[LiPI][AH] = k_3[LiPII][AH] \qquad [C.1]$$

Therefore,

$$[LiP] = \frac{k_3[LiPII][AH]}{k_1[H_2O_2]} \qquad [C.2]$$

and

$$[LiPI] = \frac{k_3}{k_2}[LiPII] \qquad [C.3]$$

From the conservation formula and C.2 and C.3,

$$[LiP]_{tot} = \frac{k_3[LiPII][AH]}{k_1[H_2O_2]} + \frac{k_3}{k_2}[LiPII] + [LiPII]$$

$$= [LiPII]\left(\frac{k_3[AH]}{k_1[H_2O_2]} + \frac{k_3}{k_2} + 1 \right) \qquad [C.4]$$

If $[AH] \rightarrow 0$ and $[H_2O_2] \rightarrow \infty$,

$$[LiP]_{tot} = [LiPII]\left(\frac{k_3}{k_2} + 1 \right) \qquad [C.5]$$

Then, if $k_2 >> k_3$,

$$[LiP]_{tot} \simeq [LiPII]$$

Usually, k_2 is more than 10 times larger than k_3 as in the case of HRP. Furthermore, in the case of LiP k_2 is ~15 times larger than k_3 with VAlc as a reducing substrate. So, with large $[H_2O_2]$ and low [AH], the high concentration of LiPII can be expected in the steady state. The purity of LiPII is roughly estimated to be ~ 90%.

D BINDING INTERACTION BETWEEN LiPII AND HYDROGEN PEROXIDE

For a productive enzyme-substrate complex formation and a enzyme-catalyzed reaction, the simplest model is

$$\text{LiPII} + H_2O_2 \underset{}{\overset{K_1}{\rightleftarrows}} \text{LiPII-}H_2O_2 \xrightarrow{k_1} \text{LiPIII} + H_2O \qquad [D.1]$$

where K_1 is an apparent dissociation constant and k_1 is a first order rate constant.

Under pseudo-first-order conditions with H_2O_2 in excess, the disappearance rate of LiPII is given by

$$-\frac{d[\text{LiPII}]_{tot}}{dt} = k_{1obs}[\text{LiPII}]_{tot} \qquad [D.2]$$

where $[\text{LiPII}]_{tot}$ is the total concentration of LiPII in the reaction system, and k_{1obs} is an observed rate constant.

From the model (eq. D.1),

$$[LiPII]_{tot} = [LiPII] + [LiPII\text{-}H_2O_2] \qquad [D.3]$$

$$-\frac{d[LiPII]_{tot}}{dt} = k_1[LiPII\text{-}H_2O_2] \qquad [D.4]$$

$$K_1 = \frac{[LiPII][H_2O_2]}{[LiPII\text{-}H_2O_2]} \qquad [D.5]$$

From D.5,

$$[LiPII] = \frac{K_1[LiPII\text{-}H_2O_2]}{[H_2O_2]} \qquad [D.6]$$

From D.3 and D.6

$$[LiPII]_{tot} = \frac{K_1[LiPII\text{-}H_2O_2]}{[H_2O_2]} + [LiPII\text{-}H_2O_2]$$

Therefore,

$$[\text{LiPII-}H_2O_2] = \frac{[\text{LiPII}]_{tot}}{1 + \frac{K_1}{[H_2O_2]}} \qquad [D.7]$$

From D.4 and D.7,

$$-\frac{d[\text{LiPII}]_{tot}}{dt} = \left(\frac{k_1}{1 + \frac{K_1}{[H_2O_2]}}\right)[\text{LiPII}]_{tot} \qquad [D.8]$$

From D.2 and D.8, k_{1obs} is given by

$$k_{1obs} = \frac{k_1}{1 + \frac{K_1}{[H_2O_2]}} \qquad [D.9]$$

VITA

Hiroyuki Wariishi was born in Tokushima, Japan on January 5, 1958. He received his Bachelor of Science degree from Tokyo Noko University, Japan in March, 1983. He immediately entered the Agricultural Sciences program at Tokyo Noko University, and received his Master of Science degree in March, 1985.

In September, 1985 the author began his studies at the Oregon Graduate Institute of Science and Technology where he completed the requirements for the degree of Doctor of Philosophy in February, 1990.